

DEPARTAMENTO DE ASTROFÍSICA

Universidad de La Laguna

*Pushing the surface brightness limits of  
optical integrated photometry*

Memoria que presenta D. Javier Román García para optar al grado de  
Doctor en astrofísica por la Universidad de La Laguna



Instituto de Astrofísica de Canarias  
San Cristóbal de La Laguna, Septiembre 2019

Este documento incorpora firma electrónica, y es copia auténtica de un documento electrónico archivado por la ULL según la Ley 39/2015.  
Su autenticidad puede ser contrastada en la siguiente dirección <https://sede.ull.es/validacion/>

Identificador del documento: 2260218 Código de verificación: Sm21pjYh

Firmado por: JAVIER ROMAN GARCIA  
UNIVERSIDAD DE LA LAGUNA

Fecha: 02/11/2019 16:23:59

IGNACIO TRUJILLO CABRERA  
UNIVERSIDAD DE LA LAGUNA

02/11/2019 17:39:19

Examination date: December 10th, 2019  
Thesis director: Ignacio Trujillo Cabrera  
© Javier Román García 2019

Este documento incorpora firma electrónica, y es copia auténtica de un documento electrónico archivado por la ULL según la Ley 39/2015.  
*Su autenticidad puede ser contrastada en la siguiente dirección <https://sede.ull.es/validacion/>*

Identificador del documento: 2260218 Código de verificación: Sm21pjYh

Firmado por: JAVIER ROMAN GARCIA  
UNIVERSIDAD DE LA LAGUNA

Fecha: 02/11/2019 16:23:59

IGNACIO TRUJILLO CABRERA  
UNIVERSIDAD DE LA LAGUNA

02/11/2019 17:39:19

*Dedicado a mi ángel, Nastia, esta tesis es también tuya  
A mi padre, por darme la oportunidad de ser quien soy  
A mi madre, por enseñarme que todo es posible  
A mi hermana, mi compañera en esta vida  
A mi abuelo, por mostrarme lo que hay allí arriba  
A toda mi familia, por darme todo  
A Kurco, por su cariño en tantas y tantas horas de trabajo*

Este documento incorpora firma electrónica, y es copia auténtica de un documento electrónico archivado por la ULL según la Ley 39/2015.  
Su autenticidad puede ser contrastada en la siguiente dirección <https://sede.ull.es/validacion/>

Identificador del documento: 2260218 Código de verificación: Sm21pjYh

Firmado por: JAVIER ROMAN GARCIA  
UNIVERSIDAD DE LA LAGUNA

Fecha: 02/11/2019 16:23:59

IGNACIO TRUJILLO CABRERA  
UNIVERSIDAD DE LA LAGUNA

02/11/2019 17:39:19



Este documento incorpora firma electrónica, y es copia auténtica de un documento electrónico archivado por la ULL según la Ley 39/2015.  
*Su autenticidad puede ser contrastada en la siguiente dirección <https://sede.ull.es/validacion/>*

Identificador del documento: 2260218      Código de verificación: Sm21pjYh

Firmado por: JAVIER ROMAN GARCIA  
UNIVERSIDAD DE LA LAGUNA

Fecha: 02/11/2019 16:23:59

IGNACIO TRUJILLO CABRERA  
UNIVERSIDAD DE LA LAGUNA

02/11/2019 17:39:19

# 0

## Summary

In this thesis, an extensive exploration of the low surface brightness Universe has been undertaken. A special emphasis has been placed on reducing the limitations arising from the use of integrated photometry, such as the residuals due to the observation and reduction of astronomical data, the effects of the point spread function and the presence of Galactic cirri. With this goal, numerous techniques have been developed and successfully applied to a large number of different data sets. In particular, an improvement in the image quality of the IAC Stripe82 Legacy Survey has been carried out, a data set that has been widely used in this thesis. Some complementary limitations such as big data analysis and the estimation of astronomical distances are also addressed. A comprehensive study has also been carried out of the so-called ultra-diffuse galaxies with significant results about its currently debated nature. Through the direct use of several astronomical facilities it has been possible to obtain a wealth experience in data processing, achieving great efficiency in the production of high quality images at low surface brightness. Some of the images produced are the deepest and highest quality in selected objects, such as intracluster light in galaxy clusters or galactic stellar halos, results that are currently under analysis. In general, this thesis has achieved a thorough study of the low surface brightness Universe and its observational limitations.

IV

Este documento incorpora firma electrónica, y es copia auténtica de un documento electrónico archivado por la ULL según la Ley 39/2015.  
Su autenticidad puede ser contrastada en la siguiente dirección <https://sede.ull.es/validacion/>

Identificador del documento: 2260218 Código de verificación: Sm21pjYh

Firmado por: JAVIER ROMAN GARCIA  
UNIVERSIDAD DE LA LAGUNA

Fecha: 02/11/2019 16:23:59

IGNACIO TRUJILLO CABRERA  
UNIVERSIDAD DE LA LAGUNA

02/11/2019 17:39:19



Este documento incorpora firma electrónica, y es copia auténtica de un documento electrónico archivado por la ULL según la Ley 39/2015.  
*Su autenticidad puede ser contrastada en la siguiente dirección <https://sede.ull.es/validacion/>*

Identificador del documento: 2260218      Código de verificación: Sm21pjYh

Firmado por: JAVIER ROMAN GARCIA  
UNIVERSIDAD DE LA LAGUNA

Fecha: 02/11/2019 16:23:59

IGNACIO TRUJILLO CABRERA  
UNIVERSIDAD DE LA LAGUNA

02/11/2019 17:39:19

## Contents

<b>1 Introduction</b>	<b>VII</b>
1.1 Pioneering studies . . . . .	VII
1.2 Motivation in the pursuit of the low surface brightness Universe through integrated photometry . . . . .	XII
1.3 Surface brightness limitations in integrated photometry . . . . .	XVI
1.3.1 Poisson noise . . . . .	XVI
1.3.2 Observational and processing of data . . . . .	XIX
1.3.3 Point Spread Function . . . . .	XXV
1.3.4 Galactic cirri . . . . .	XXVII
1.4 Current approaches in the pursuit of the low surface brightness . . . . .	XXX
<b>2 Methods</b>	<b>XXXIV</b>
2.1 The IAC Stripe82 Legacy Survey . . . . .	XXXIV
2.2 Data reduction and processing . . . . .	XXXIV
2.3 Correction of gradients in adverse circumstances . . . . .	XXXIX
2.4 PSF characterization and removal of the stars . . . . .	XXXIX
2.5 Big data analysis of astronomical surveys . . . . .	XLIV
<b>3 Compendium of articles</b>	<b>XLV</b>
3.1 Paper I: <i>The IAC Stripe82 Legacy Survey: Improved Sky-rectified Images</i> . . . . .	XLV
3.2 Paper II: <i>Spatial distribution of ultra-diffuse galaxies within large-scale structures</i> . . . . .	XLIX
3.3 Paper III: <i>Ultra-diffuse galaxies outside clusters: clues to their formation and evolution</i> . . . . .	LXIV
3.4 Paper IV: <i>The Nearest Ultra Diffuse Galaxy: UGC 2162</i> . . . . .	LXXIV
3.5 Paper V: <i>Discovery of a red ultra-diffuse galaxy in a nearby void based on its globular cluster luminosity function</i> . . . . .	LXXXI
3.6 Paper VI: <i>Galactic cirri in deep optical imaging</i> . . . . .	XCIV
<b>4 Additional results and ongoing work</b>	<b>CXIX</b>
4.1 Testing the OGS telescope for low surface brightness science . . . . .	CXIX
4.1.1 IC 1101 the "largest galaxy in the Universe" . . . . .	CXIX
4.1.2 A new ultra-faint satellite candidate around the nearby NGC 4565 galaxy . . . . .	CXXII
4.1.3 Identifying ultra-diffuse galaxies in the Coma cluster . . . . .	CXXII
4.1.4 Ultra-deep observations of the Abell 2199 galaxy cluster . . . . .	CXXV
4.2 Deep imaging with the Javalambre T80 telescope . . . . .	CXXIX
4.2.1 Ultra-deep observations of the M101 galaxy . . . . .	CXXIX

Este documento incorpora firma electrónica, y es copia auténtica de un documento electrónico archivado por la ULL según la Ley 39/2015.  
 Su autenticidad puede ser contrastada en la siguiente dirección <https://sede.ull.es/validacion/>

Identificador del documento: 2260218 Código de verificación: Sm21pjYh

Firmado por: JAVIER ROMAN GARCIA  
 UNIVERSIDAD DE LA LAGUNA

Fecha: 02/11/2019 16:23:59

IGNACIO TRUJILLO CABRERA  
 UNIVERSIDAD DE LA LAGUNA

02/11/2019 17:39:19

VI

BIBLIOGRAPHY

4.2.2	Deep observations of the Perseus galaxy cluster . . . . .	CXXXI
4.3	Deep imaging with the Jeanne Rich telescope . . . . .	CXXXII
4.3.1	Detection of several stellar streams in the environment of the NGC 1052 galaxy . . . . .	CXXXIII
4.3.2	Unveiling the intracluster light halo of the Coma galaxy cluster . . . . .	CXXXIII
<b>5</b>	<b>Summary and conclusions</b>	<b>CXXXVI</b>
	<b>Bibliography</b>	<b>CXXXIX</b>

Este documento incorpora firma electrónica, y es copia auténtica de un documento electrónico archivado por la ULL según la Ley 39/2015.  
Su autenticidad puede ser contrastada en la siguiente dirección <https://sede.ull.es/validacion/>

Identificador del documento: 2260218 Código de verificación: Sm21pjYh

Firmado por: JAVIER ROMAN GARCIA  
UNIVERSIDAD DE LA LAGUNA

Fecha: 02/11/2019 16:23:59

IGNACIO TRUJILLO CABRERA  
UNIVERSIDAD DE LA LAGUNA

02/11/2019 17:39:19

# 1

## Introduction

### 1.1 Pioneering studies

#### Galactic stellar halos

Due to its close proximity and high density of galaxies in any mass range, the Virgo galaxy cluster is often the site of pioneer discoveries. For the case of low surface brightness, this is no exception. Simultaneous works by de Vaucouleurs (1969) using a photoelectric photometer attached to the McDonald Observatory 36-inch telescope and Arp & Bertola (1969) using the 48-inch Palomar Schmidt telescope, showed the existence of an envelope or "outer corona" of extreme low surface brightness and surprising large extension (300 kpc) surrounding the giant M87 elliptical galaxy. This was possible by the application of new techniques such as photoelectric scanning or new emulsions for photographic plates, which allowed a higher efficiency in the detection of sources with very low surface brightness.

*"A faint outer corona surrounding the main body of M87 ... has been traced out to a minimum diameter in excess of one degree at a brightness level of 1 per cent of the night sky,  $\mu_B \approx 27.3 \text{ mag arcsec}^{-2}$ ".*

(Gerard de Vaucouleurs, 1969)

This is, in fact, the most common definition for low surface brightness sources: those astronomical sources whose surface brightness is only a small fraction of that of the night sky ( $\mu \approx 22 \text{ mag arcsec}^{-2}$ ). Although the value reported by de Vaucouleurs in 1969 of  $27.3 \text{ mag arcsec}^{-2}$  in the B band could be debatable considering the absence of error bars and the relatively high dispersion of the M87 galaxy flux profile at large radius (see Figures 1 and 3 by de Vaucouleurs 1969), the fact is that it was possible to detect a source of extreme low surface brightness (of the order of a small fraction of the surface brightness of the night sky) back in 1969. Moreover, de Vaucouleurs observed a color gradient in the M87 halo, becoming bluer as the radial distance increases. This color gradient was confirmed many years later by Rudick et al. (2010), showing the reliability of this early finding. It is really remarkable the low surface brightness achieved and the success of these results in such early times.

After these pioneering studies in the M87 galaxy, later works, such as Arp & Bertola (1971) analyzing a set of nearby elliptical galaxies or Kormendy & Bahcall (1974) analyzing groups of galaxies and isolated galaxies of varied morphology, showed the systematic presence of an

VII

Este documento incorpora firma electrónica, y es copia auténtica de un documento electrónico archivado por la ULL según la Ley 39/2015.  
Su autenticidad puede ser contrastada en la siguiente dirección <https://sede.ull.es/validacion/>

Identificador del documento: 2260218 Código de verificación: Sm21pjYh

Firmado por: JAVIER ROMAN GARCIA  
UNIVERSIDAD DE LA LAGUNA

Fecha: 02/11/2019 16:23:59

IGNACIO TRUJILLO CABRERA  
UNIVERSIDAD DE LA LAGUNA

02/11/2019 17:39:19

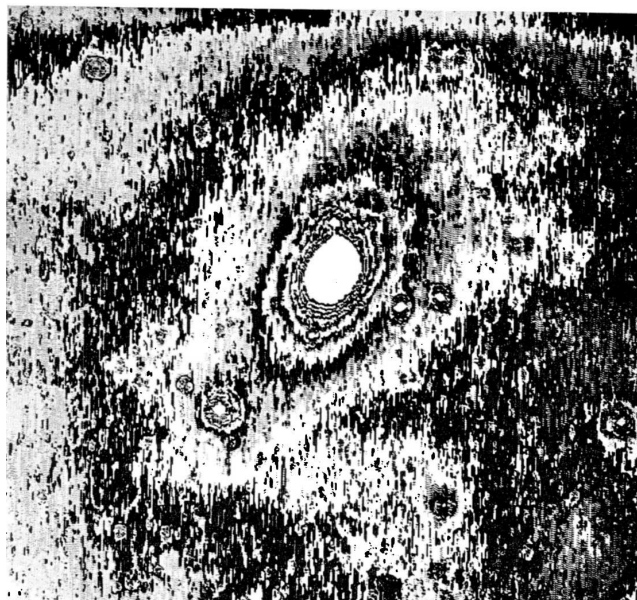


Figure 1.1: First image of a galactic stellar halo. Messier 87 in the Virgo galaxy cluster observed by Arp & Bertola (1969). The image size covers approximately 1.2 by 1 degrees.

envelope or stellar halo with very low surface brightness around any galaxy. This was found with a greater extent generally in the case of elliptical galaxies and with a more abrupt cutoff for the case of spiral galaxies. This diffuse material, sometimes, involved not only individual galaxies, but a set of these, what is now known as intragroup or intracluster light respectively. These results showed the systematic presence of an envelope or halo of diffuse material around all the galaxies, suggesting the existence of hidden material, only detectable in very deep observations.

#### Galactic cirri

Interestingly, one of the first low surface brightness objects detected was our own Galaxy, in particular, the dust clouds of the Milky Way galactic disk, the so-called Galactic cirri. Work by Sandage (1976) reported the detection of a diffuse emission, sometimes filamentary, of great extension whose origin was the reflection of the starlight in these clouds of the Galactic plane.

*“Extended regions of faint nebulosity have been found at high galactic latitudes from a survey in progress with the Palomar 1.2-m Schmidt telescope. The surface brightness of some of the nebulosities is as high as  $\mu \approx 25 \text{ mag arcsec}^{-2}$  in V, with many more at fainter levels. Some of the nebulosities are diffuse, while others are filamentary with widths on scales of  $\approx 30 \text{ arcsec}$  that extend in connective patterns over scales of degrees ... Special plates taken in continuum radiation show the regions to be*

Este documento incorpora firma electrónica, y es copia auténtica de un documento electrónico archivado por la ULL según la Ley 39/2015.  
Su autenticidad puede ser contrastada en la siguiente dirección <https://sede.ull.es/validacion/>

Identificador del documento: 2260218 Código de verificación: Sm21pjYh

Firmado por: JAVIER ROMAN GARCIA  
UNIVERSIDAD DE LA LAGUNA

Fecha: 02/11/2019 16:23:19

IGNACIO TRUJILLO CABRERA  
UNIVERSIDAD DE LA LAGUNA

02/11/2019 17:39:19

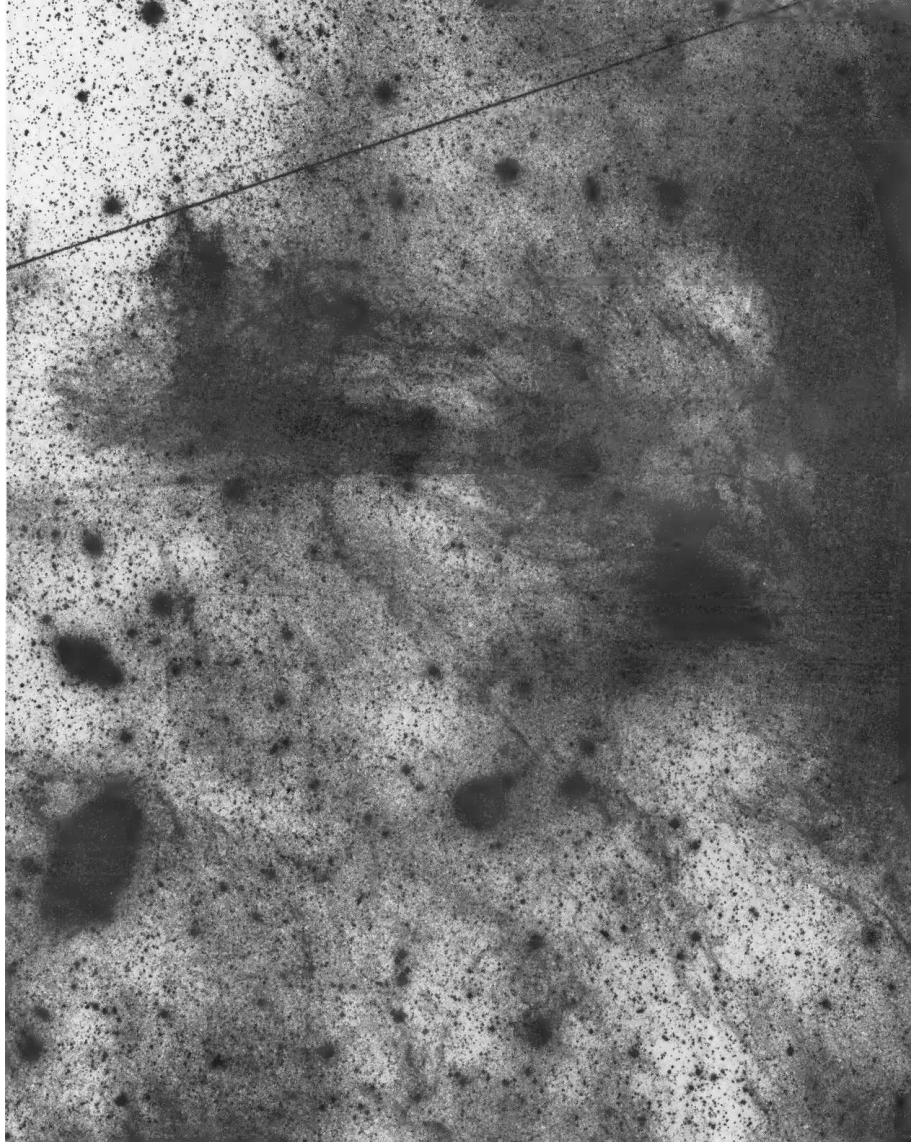


Figure 1.2: Galactic cirri in the field of the M81 and M82 galaxies by Sandage (1976). Even in 1976, satellite tracks appeared in astronomical images.

Este documento incorpora firma electrónica, y es copia auténtica de un documento electrónico archivado por la ULL según la Ley 39/2015.  
Su autenticidad puede ser contrastada en la siguiente dirección <https://sede.ull.es/validacion/>

Identificador del documento: 2260218 Código de verificación: Sm21pjYh

Firmado por: JAVIER ROMAN GARCIA  
UNIVERSIDAD DE LA LAGUNA

Fecha: 02/11/2019 16:23:59

IGNACIO TRUJILLO CABRERA  
UNIVERSIDAD DE LA LAGUNA

02/11/2019 17:39:19

*reflection nebulae. Calculations suggest that the source of the illumination at these high latitudes is the flux of the total galactic plane”.*

(Allan Sandage, 1976)

Although the work by Allan Sandage is considered the first to report the presence of Galactic cirri in photographic plates, the existence of emission due to the interstellar material of our Galaxy was already known almost 40 years before through the use of photometers covering large areas of the sky (Elvey & Roach 1937; Henyey & Greenstein 1941).

*“An analysis of the light associated with the galactic system shows that after the effect of the stars has been removed there is an excess of light, which we shall call the galactic light, and which is probably produced by the scattering of starlight by interstellar matter”*

(Elvey & Roach, 1937)

This would put our own Galaxy, specifically the Milky Way Galactic Cirri, as the first source of low surface brightness discovered. There is something ironic about it, because Galactic cirri are in fact one of the biggest problems in the study of the low surface brightness Universe nowadays, and presumably, the toughest obstacle that the community will have to face in the future.

#### Low surface brightness galaxies

Due to the large angular extent of nearby galaxies or the interstellar dust clouds of our own Galaxy, it is possible to spatially average the flux of these extended sources and therefore to reach remarkably low surface brightness. However, if there were galaxies with a maximum surface brightness below the surface brightness of the night sky, they would be impossible to detect according to the observational techniques at that time. It was Disney (1976) who warned that astronomical observations could be strongly biased by the limit imposed by the brightness of the night sky. Therefore, it was expected that if this galactic population of low surface brightness existed, it would be hidden.

*“It is well known that our counts of galaxies could be seriously biased by selection effects, largely determined by the brightness of the night sky. To illustrate this, suppose the Earth were situated near the centre of a giant elliptical galaxy, then the mean surface brightness of the sky would appear some 8–9 mag brighter than is observed from our position in the Galaxy  $\mu_V \approx 23 \text{ mag arcsec}^{-2}$  looking toward the galactic pole, discounting atmospheric and zodiacal contributions. Optical astronomers would then find extragalactic space an empty void; spiral and irregular galaxies would be quite invisible and all they would easily detect of galaxies would be the core regions of ellipticals very similar to their own. They would be blinded to much of the Universe by the surface brightness of their parent galaxy. But this blinding is clearly a relative matter and we should ask to what extent we are blinded by the spiral galaxy in which we exist, faint as it may appear by comparison. I will argue that strong indirect evidence already exists that our knowledge of galaxies is heavily biased by the sky background,*

Este documento incorpora firma electrónica, y es copia auténtica de un documento electrónico archivado por la ULL según la Ley 39/2015.  
Su autenticidad puede ser contrastada en la siguiente dirección <https://sede.ull.es/validacion/>

Identificador del documento: 2260218 Código de verificación: Sm21pjYh

Firmado por: JAVIER ROMAN GARCIA  
UNIVERSIDAD DE LA LAGUNA

Fecha: 02/11/2019 16:23:59

IGNACIO TRUJILLO CABRERA  
UNIVERSIDAD DE LA LAGUNA

02/11/2019 17:39:19

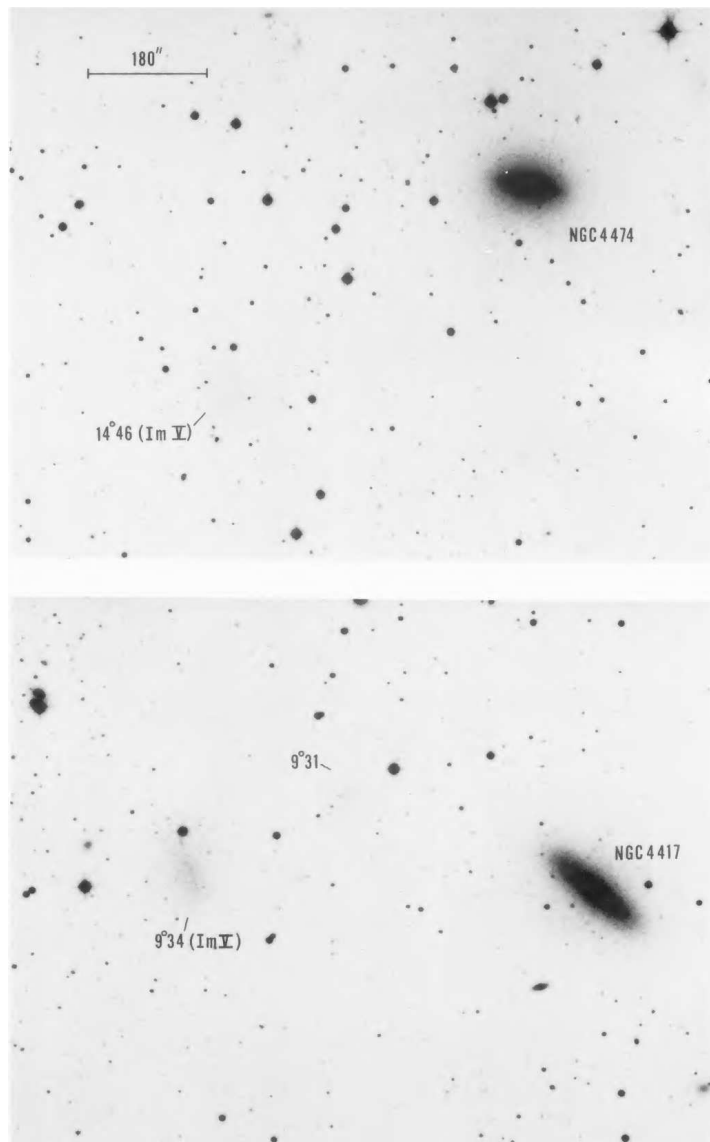


Figure 1.3: Examples of low surface brightness galaxies detected in the Virgo cluster by Sandage & Binggeli (1984) barely visible on photographic plates.

Este documento incorpora firma electrónica, y es copia auténtica de un documento electrónico archivado por la ULL según la Ley 39/2015.  
Su autenticidad puede ser contrastada en la siguiente dirección <https://sede.ull.es/validacion/>

Identificador del documento: 2260218 Código de verificación: Sm21pjYh

Firmado por: JAVIER ROMAN GARCIA  
UNIVERSIDAD DE LA LAGUNA

Fecha: 02/11/2019 16:23:59

IGNACIO TRUJILLO CABRERA  
UNIVERSIDAD DE LA LAGUNA

02/11/2019 17:39:19

*and that the true population of extra-galactic space may be very different from the one we can see."*

(Michael Disney, 1976)

Some years later, the detection of dwarf galaxies of extreme low surface brightness in the Virgo cluster by Sandage & Binggeli (1984) and the discovery of the iconic Malin I galaxy by David Malin in 1986, firstly discussed by Bothun et al. (1987), considered the first galaxy detected with low surface brightness, confirmed the existence of a population of galaxies whose surface brightness was lower than that of the night sky, as predicted by Michael Disney. In the immediately following years, a huge amount of low surface brightness galaxies were reported (e.g. Schombert, & Bothun 1988; Ferguson & Sandage 1988; Impey et al. 1988; Bothun et al. 1991). The brightness of the night sky was no longer a limit, the era of the low surface brightness Universe began.

## 1.2 Motivation in the pursuit of the low surface brightness Universe through integrated photometry

The information provided by the low surface brightness Universe is extremely relevant in revealing aspects of galaxy's hierarchical evolution. One of the most important is the information contained in the halos of galaxies. By the construction of simulations based on the current ingredients of the  $\Lambda$ -CDM cosmological paradigm, it is possible to reproduce the stellar content of galactic halos with a depth in surface brightness, in principle, unlimited. These simulations show a systematic accretion of material from satellites that is located mainly in the outer regions of galaxies. This accretion is hierarchized and these halos of material are produced both in the case of individual galaxies (see Figure 1.4) and in groups and clusters of galaxies (see Figure 1.5). This faint light is known as intragroup or intracluster light respectively.

Importantly, the amount of accreted material in galactic halos or galaxy clusters is strongly dependent on the cosmology used. Therefore, observational work in the exploration of the stellar content of galactic halos (e.g. Bullock & Johnston 2005; Abadi et al. 2006; Johnston et al. 2008; Martínez-Delgado et al. 2010; Duc et al. 2015; Trujillo & Fliri 2016) or intracluster light in galaxy clusters (e.g. Uson et al. 1991; Mihos et al. 2005; Rudick et al. 2010; Giallongo et al. 2014; Montes & Trujillo 2014, 2018) is a crucial observational pillar for the  $\Lambda$ -CDM cosmological paradigm.

In addition to the study of galactic stellar halos and the intracluster light, the number of low mass satellites in galaxies is a key aspect in the  $\Lambda$ -CDM cosmological paradigm. A much lower number of observed galactic satellites compared to those predicted by cosmological simulations in galactic analogs to the Milky Way is the so-called "missing satellite problem" (e.g. Moore et al. 1999; Klypin et al. 1999). While the satellite counts predicted in simulations (e.g. Springel et al. 2008; Madau et al. 2008) were systematically higher than those found observationally, the arrival of astronomical surveys with great depth has permitted to increase rapidly the detection rate of new ultra-faint satellites in the Local Group (e.g. Homma et al. 2018, 2019, and references therein). In fact, there is currently a debate in the community about whether this problem of the missing satellites still exists (e.g. Read, & Erkal 2019; Kim et al. 2019). The exploration of new extremely low surface brightness satellites, both in the Local Group and in external galactic associations, will be crucial in this important test of the cosmological paradigm.

Este documento incorpora firma electrónica, y es copia auténtica de un documento electrónico archivado por la ULL según la Ley 39/2015.  
Su autenticidad puede ser contrastada en la siguiente dirección <https://sede.ull.es/validacion/>

Identificador del documento: 2260218 Código de verificación: Sm21pjYh

Firmado por: JAVIER ROMAN GARCIA  
UNIVERSIDAD DE LA LAGUNA

Fecha: 02/11/2019 16:23:59

IGNACIO TRUJILLO CABRERA  
UNIVERSIDAD DE LA LAGUNA

02/11/2019 17:39:19

1.2 Motivation in the pursuit of the low surface brightness Universe through integrated photometry XIII

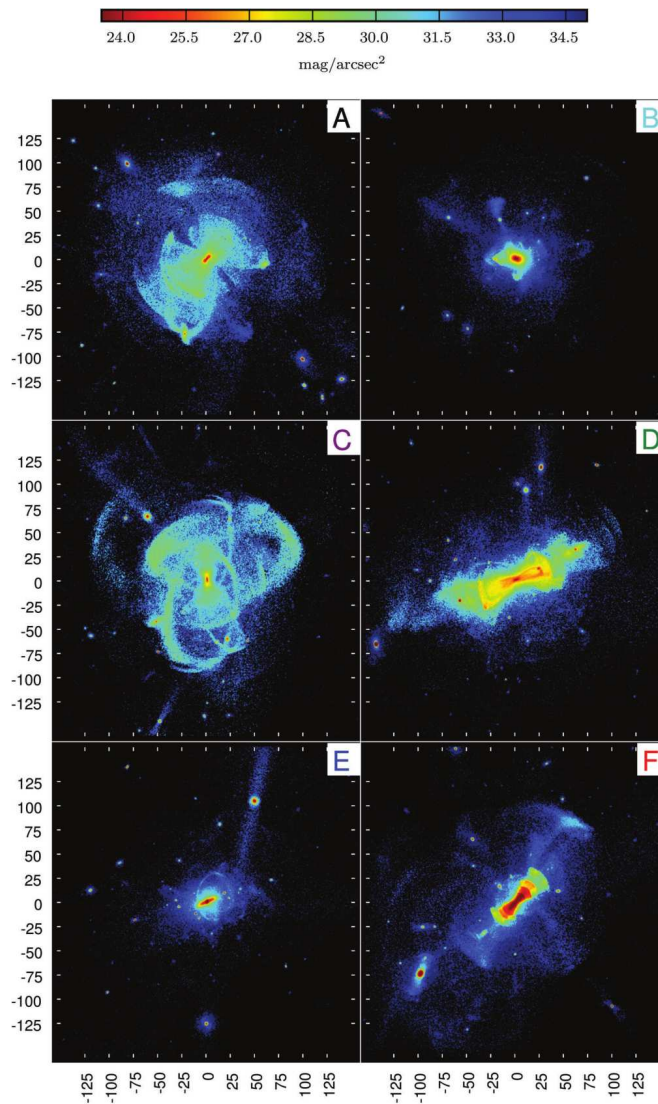


Figure 1.4: V-band surface brightness of stellar halos of Milky Way-like galaxies according to simulations (and surviving satellites). The images have a limiting depth of 35 mag arcsec<sup>-2</sup>. The axis scales are in kiloparsec. Only stars formed in satellites are present in this particle model; there is no contribution to these maps from a central galactic disc or bulge formed in situ. Figure and extracted caption obtained from Cooper et al. (2010).

Este documento incorpora firma electrónica, y es copia auténtica de un documento electrónico archivado por la ULL según la Ley 39/2015.  
 Su autenticidad puede ser contrastada en la siguiente dirección <https://sede.ull.es/validacion/>

Identificador del documento: 2260218 Código de verificación: Sm21pjYh

Firmado por: JAVIER ROMAN GARCIA  
 UNIVERSIDAD DE LA LAGUNA

Fecha: 02/11/2019 16:23:59

IGNACIO TRUJILLO CABRERA  
 UNIVERSIDAD DE LA LAGUNA

02/11/2019 17:39:19

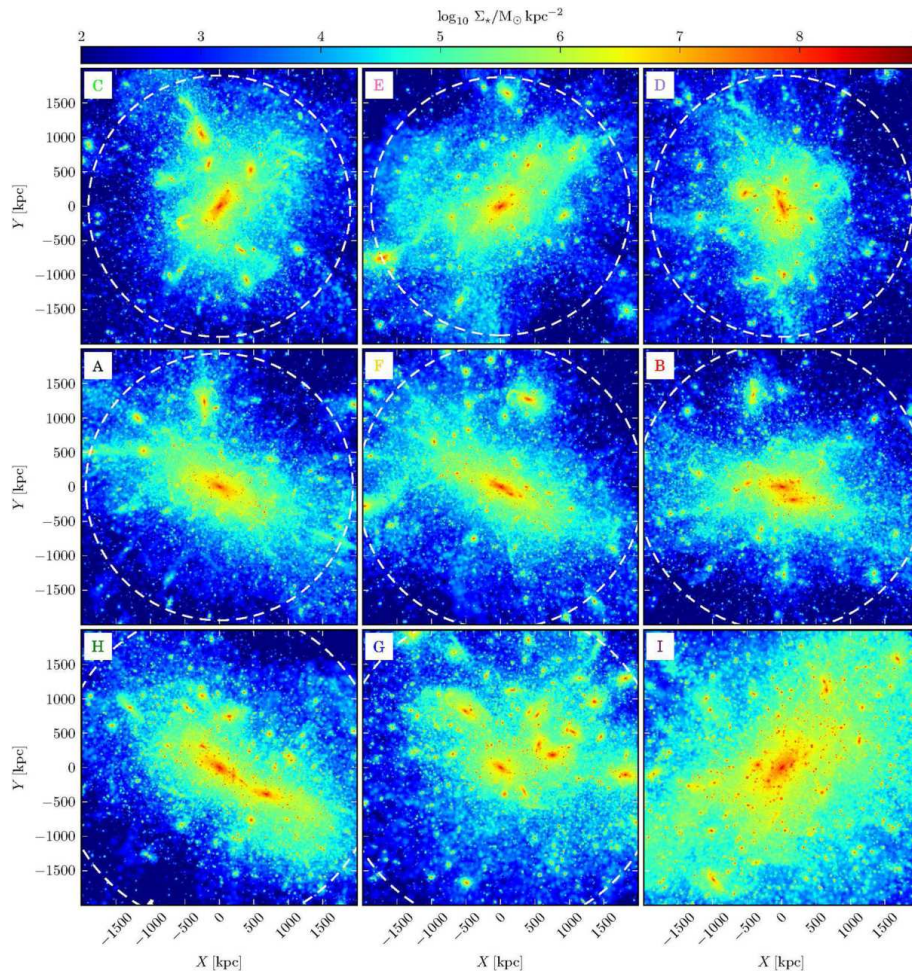


Figure 1.5: Projected 3 Mpc x 3 Mpc images of the Phoenix clusters centred on their Brighter Cluster Galaxies. The halo mass,  $M_{200}$ , increases from left to right and from top to bottom. The white dashed line shows the  $R_{200}$  radius (outside the image for Ph-I). The viewing angle is chosen randomly. Colours correspond to stellar mass surface density on a  $\log_{10}$  scale. Particles are smoothed by a cubic spline kernel scaled by the density of their 64 nearest neighbours. ‘Hot spots’ are individual cluster galaxies; only very small scale density fluctuations are due to shot noise. The brightest galaxies are surrounded by extensive diffuse envelopes of tidal debris. Figure and caption obtained from Cooper et al. (2015).

Este documento incorpora firma electrónica, y es copia auténtica de un documento electrónico archivado por la ULL según la Ley 39/2015.  
 Su autenticidad puede ser contrastada en la siguiente dirección <https://sede.ull.es/validacion/>

Identificador del documento: 2260218      Código de verificación: Sm21pjYh

Firmado por: JAVIER ROMAN GARCIA  
 UNIVERSIDAD DE LA LAGUNA

Fecha: 02/11/2019 16:23:59

IGNACIO TRUJILLO CABRERA  
 UNIVERSIDAD DE LA LAGUNA

02/11/2019 17:39:19

1.2 Motivation in the pursuit of the low surface brightness Universe through  
integrated photometry XV

Currently, the fainter limits in surface brightness are achieved by the star counting technique, reaching a surface brightness of  $32 \text{ mag arcsec}^{-2}$  ( $10 \times 10 \text{ arcsec}$  boxes) on galactic satellites within the Local Group (see a recent compilation in Figure 1.6) and extragalactic features as galactic halos of nearby galaxies (e.g. Ibata et al. 2009; Tanaka et al. 2011; Ibata et al. 2014; Martin et al. 2014; McConnachie et al. 2018). The star counting technique has important advantages over integrated photometry. First, it allows the observation of extremely low surface brightness structures by detecting sources that are intrinsically of high surface brightness, such as the stars. This avoids the important adverse systematic effects of integrated photometry. Moreover, by selecting sources only compatible with stellar populations expected of the source of interest based on color vs. magnitude diagrams, it is possible to filter the sources belonging to the structure, considerably reducing the spatial confusion of sources in the line of sight. Additionally, by using the technique of the tip of the red giant branch (e.g. Lee et al. 1993) it is possible to obtain a distance value from the source under study, which is of great importance in the case of low surface brightness sources due to the high observational cost of obtaining spectroscopic information with which to obtain its radial velocity, and therefore, an estimate of its distance<sup>1</sup>. However, the star counting technique has the obvious limitation of the resolution of the observations. This makes these studies currently limited to a maximum distance of 16 Mpc in the case of observations with the Hubble Space Telescope (Zackrisson et al. 2012) and few Mpc from ground observations with excellent seeing. Examples of state-of-the-art observations based on star counting are the works of the Pan-Andromeda Archaeological Survey (PAndAS; Martin et al. 2006; Ibata et al. 2007; McConnachie et al. 2008, and see Fig. 1.7) using data from the Canada France Hawaii Telescope (CFHT) in the Local Group environment around the M31 galaxy or observations of the M81 galaxy group with the Hyper-Suprime Cam of the Subaru Telescope (e.g. Okamoto et al. 2015). Another additional limitation of the star counting is that it is based on the observation of the brightest stars, mainly red-giant-branch (RGB) or asymptotic-giant-brach (AGB) stars. This causes a not straight forward comparison between the whole integrated flux of the studied structure and the counting of RGB and AGB stars because of its dependence on different models of stellar evolution, including initial-mass-function (IMF) and stochasticity (Willman 2010; Martin et al. 2014).

For the reasons discussed above, the study of low surface brightness sources through integrated photometry is necessary in order to study structures beyond the environment of the Local Group, allowing not only to increase the number of objects under study, but also to understand their evolution at different redshifts. There is currently a number of data sets of great depth in which it is potentially possible to study the low surface brightness Universe. However, the use of integrated photometry entails the presence of important systematic effects that hinders the study of the faintest galactic features. Moreover, the observational and astronomical data processing techniques that improve the study of low surface brightness features are not of common use, so most of the data available to the community lack of the necessary quality for their use at low surface brightness. Additionally, the characterization of the PSF and the modeling of stars, key point in low surface brightness, are also not a common tool, being few works at present day applying this technique. Other issues such as contamination by the presence of interstellar dust are basically unexplored, being a major problem for the next generations of ultra-deep observations.

<sup>1</sup>It is worth mentioning that obtaining radial velocities is not conclusive in measuring distances for nearby galaxies, due to the large departure from the Hubble flow caused by their peculiar velocities (see e.g. Trujillo et al. 2019).

Este documento incorpora firma electrónica, y es copia auténtica de un documento electrónico archivado por la ULL según la Ley 39/2015.  
Su autenticidad puede ser contrastada en la siguiente dirección <https://sede.ull.es/validacion/>

Identificador del documento: 2260218 Código de verificación: Sm21pjYh

Firmado por: JAVIER ROMAN GARCIA  
UNIVERSIDAD DE LA LAGUNA

Fecha: 02/11/2019 16:23:59

IGNACIO TRUJILLO CABRERA  
UNIVERSIDAD DE LA LAGUNA

02/11/2019 17:39:19

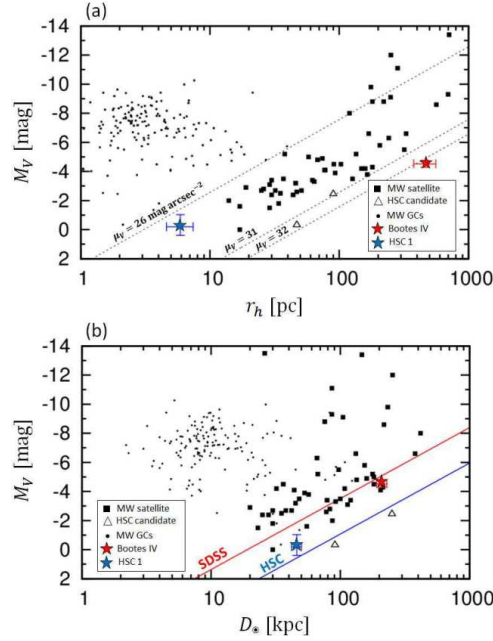


Figure 1.6: (a) The relation between  $M_V$  and  $r_h$  for MW globular clusters (dots) taken from Harris (1996) and MW dSphs (filled squares) from McConnachie (2012); Laevens et al. (2014); Bechtol et al. (2015); Koposov et al. (2015); Drlica-Wagner et al. (2015); Kim et al. (2015); Kim & Jerjen (2015); Laevens et al. (2015a,b); Torrealba et al. (2016, 2018). The empty triangles denote those found from the previous data release of the HSC-SSP Homma et al. (2016, 2018). The red and blue stars with error bars, respectively, denote Bootes IV and HSC 1. The dotted lines denote the loci of constant surface brightness,  $\mu_V = 26, 31, \text{ and } 32 \text{ mag arcsec}^{-2}$ . (b) The relation between  $M_V$  and heliocentric distance,  $D_\odot$ . The red and blue lines denote, respectively, the detection limits of the Sloan Digital Sky Survey (SDSS) and Hyper-Suprime Cam (HSC). Figure and caption obtained from Homma et al. (2019).

In what follows in this manuscript, only cases of integrated photometry will be discussed.

### 1.3 Surface brightness limitations in integrated photometry

#### 1.3.1 Poisson noise

The first limitation of astronomical observations, not only those focused on obtaining a low surface brightness but any in general, is the presence of Poisson noise. This is due to the discrete nature of the photon counts in CCD cameras along with the electronic noise of these devices. This limitation is imposed by the fraction between the flux received from the astronomical source and the artificial noise associated with the detector. In general terms, the flux in a resolution or pixel element of the CCD device ( $[x, y]$ ) will be given as follows:

Este documento incorpora firma electrónica, y es copia auténtica de un documento electrónico archivado por la ULL según la Ley 39/2015.  
 Su autenticidad puede ser contrastada en la siguiente dirección <https://sede.ull.es/validacion/>

Identificador del documento: 2260218 Código de verificación: Sm21pjYh

Firmado por: JAVIER ROMAN GARCIA  
 UNIVERSIDAD DE LA LAGUNA

Fecha: 02/11/2019 16:23:59

IGNACIO TRUJILLO CABRERA  
 UNIVERSIDAD DE LA LAGUNA

02/11/2019 17:39:19

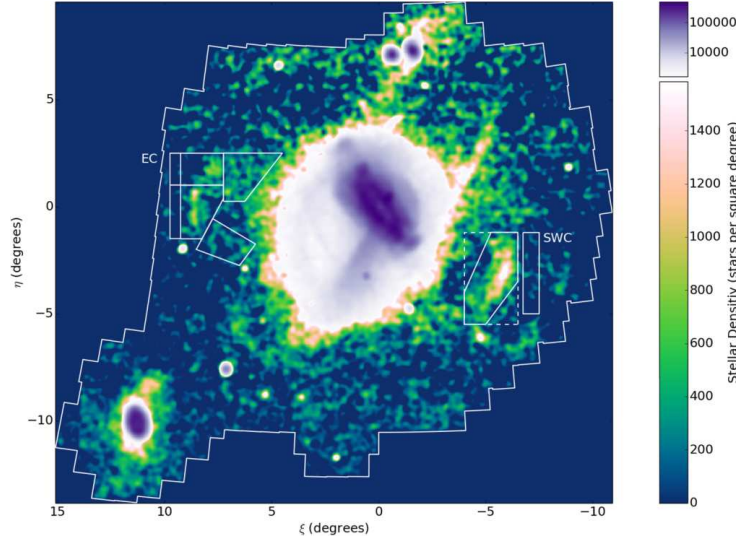


Figure 1.7: Stellar density map of PAndAS stars with dereddened colours and magnitudes consistent with metal-poor RGB populations at the distance of M31. Pixels are  $0.025 \times 0.025$  degrees, and the map has been smoothed using a Gaussian with a dispersion of  $\sigma = 0.1$  degrees. It is displayed in tangent-plane projection centred on M31, with scaling chosen to highlight the East Cloud and SWC. Figure and caption obtained from McMonigal et al. (2016)

$$I[x, y] = I[x, y]_{source} + I[x, y]_{noise} \quad (1.1)$$

where  $I[x, y]_{source}$  is the flux of astronomical sources present in the image and  $I[x, y]_{noise}$  is the artificial flux or Poisson noise in the resolution element  $[x, y]$  respectively. Due to the electronic nature of the CCD device, the term  $I[x, y]_{noise}$  is common to the entire image, in which each resolution element has a random flux characterized by a Gaussian probability distribution with width  $\sigma$ , this being the only parameter that characterizes this Poisson noise term (see Figure 1.8). Since, in principle, the Poisson noise does not depend on the spatial location of the resolution element, it can be characterized by a single parameter for the whole image. We can write:  $I[x, y]_{noise} = I_{noise}(\sigma)$ . We can define, therefore, a detection limit in flux for the image, for example at the  $3\sigma$  level, when it is fulfilled that:

$$I[x, y]_{source} > I_{noise}(3\sigma) \quad (1.2)$$

That is, there will be a limit defined by the Poisson noise of the image for which any astronomical source whose flux is below this limit will not be confidently detectable. This is the first and most important factor that limits observations in low surface brightness, because by definition, those sources are characterized by low values of  $I[x, y]_{source}$ . Given the discrete nature of photonic counts on CCD devices, the way to reduce this limiting factor ( $I_{noise}(3\sigma)$ ) is to

Este documento incorpora firma electrónica, y es copia auténtica de un documento electrónico archivado por la ULL según la Ley 39/2015.  
 Su autenticidad puede ser contrastada en la siguiente dirección <https://sede.ull.es/validacion/>

Identificador del documento: 2260218 Código de verificación: Sm21pjYh

Firmado por: JAVIER ROMAN GARCIA  
 UNIVERSIDAD DE LA LAGUNA

Fecha: 02/11/2019 16:23:59

IGNACIO TRUJILLO CABRERA  
 UNIVERSIDAD DE LA LAGUNA

02/11/2019 17:39:19

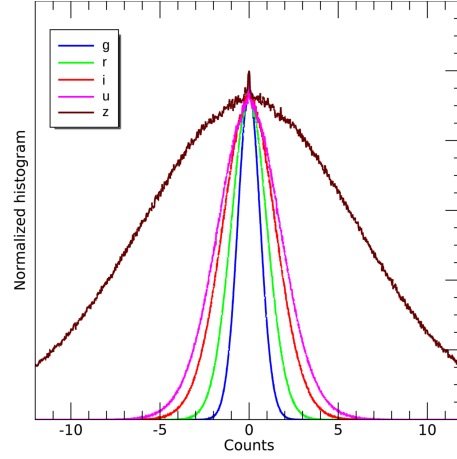


Figure 1.8: Distributions of counts for pixels purely dominated by Poisson noise (pixels without sources) for a 0.5x0.5 degrees image region of the IAC Stripe Legacy Survey in the five SDSS bands. The histograms in each band follow a normal distribution with a gaussian shape. Note the shallower z band evidenced by a wider distribution.

increase the photons received by the detector. Therefore, both the aperture of the telescope and the exposure time of the image are the factors to increase the detection threshold. In general, with a fixed exposure time, the Poisson noise will be reduced by the amount of photons that the detector receives, which is directly dependent on the telescope's aperture:

$$I_{noise}(3\sigma) \propto \frac{1}{\phi} \quad (1.3)$$

with  $\phi$  being the aperture (i.e. diameter) of the telescope. Additionally, by combining different exposures in a single coadd it is possible to reduce the Poisson noise of the image. That is, once the aperture is set for a given telescope, Poisson noise will be reduced in the form:

$$I_{noise}(3\sigma) \propto \frac{1}{\sqrt{t}} \quad (1.4)$$

with  $t$  being the total integration time of the coadd. Since a single astronomical facility is often used for obtaining an image, and therefore a telescope with a given aperture, the general way to reduce Poisson noise is to make larger exposures. This limit imposed by noise of the images is a first frontier that has to be overcome in order to observe sources with low flux, and only by integrating a sufficient number of photons it is possible to reach the desired surface brightness.

It is possible to define the surface brightness limit of the image imposed by the Poisson noise in the form:

Este documento incorpora firma electrónica, y es copia auténtica de un documento electrónico archivado por la ULL según la Ley 39/2015.  
 Su autenticidad puede ser contrastada en la siguiente dirección <https://sede.ull.es/validacion/>

Identificador del documento: 2260218 Código de verificación: Sm21pjYh

Firmado por: JAVIER ROMAN GARCIA  
 UNIVERSIDAD DE LA LAGUNA

Fecha: 02/11/2019 16:23:59

IGNACIO TRUJILLO CABRERA  
 UNIVERSIDAD DE LA LAGUNA

02/11/2019 17:39:19

$$\mu_{lim}(3\sigma) = -2.5 \times \log \left[ \frac{I_{noise}(3\sigma)}{pix^2} \right] + Zp \quad (1.5)$$

where  $pix$  is the angular size of the resolution element or pixel and  $Zp$  is the zero point of the photometric calibration. It is important to remark that this limit is defined on an angular scale fixed by the original resolution element or pixel of the camera. However, because most astronomical sources under study have an angular size that is much larger than the resolution element, it is possible to detect smaller surface brightness on larger angular scales by combining different resolution elements to create a larger one. This manages to average the random flux values in a set of pixels, reducing the width of the noise distribution allowing a higher depth at larger angular scales. The reduction of this noise, due to its Gaussian nature will be defined as:

$$I_{noise}(3\sigma; \Omega) = I_{noise}(3\sigma) \frac{pix}{\Omega} \quad (1.6)$$

where  $pix$  is the original resolution element and  $\Omega$  the angular scale of the combined resolution element. With this we can define the surface brightness limit for any angular scale as:

$$\mu_{lim}(3\sigma; \Omega) = -2.5 \times \log \left[ \frac{I_{noise}(3\sigma)}{pix \times \Omega} \right] + Zp \quad (1.7)$$

An angular scale of  $10'' \times 10''$  boxes has been used as representative of the typical extended source when exploring nearby galaxies (e.g. Fliri & Trujillo 2016), becoming the most common nominal definition of depth. It is also worth noting that the limiting depth is strongly dependent on the angular size or criteria to define it.

It is interesting to observe directly the effect of the limit imposed by the Poisson noise in real data. In the Figure 1.9, published by Trujillo & Fliri (2016) the UGC 180 galaxy is shown with different depth limits defined at  $3\sigma$  in  $10'' \times 10''$  boxes. As can be observed, the faintest structures in the halo of the galaxy can only be detected by reducing below a certain threshold (around 30 mag arcsec<sup>-2</sup>) the Poisson noise. This limiting factor is the first and most important limit in detecting low surface brightness sources, but it is not the only one. Next, we will describe different systematic effects that limit the detection in low surface brightness, obviating the Poisson noise factor that will always be taken into account as the main limitation of the images.

### 1.3.2 Observational and processing of data

The aim of photometric observations is to obtain an image in which in each position the flux value of the celestial source is obtained. Due to the optical instrumentation, the image obtained directly from the instrument has to be corrected or processed in order to get the true flux value. This processing of photometric data, commonly called data reduction, follows standard steps regardless of the astronomical facility, at least in optical observations. These steps are the bias correction due to the residual flux coming from the CCD electronics and the flat-fielding correction due to different sensitivities of the pixels, the presence of vignetting or other defects such as spots on the detector or mirrors. After this processing, the reduced image contains the actual flux of the astronomical sources in which the night sky flux is contained, but also the residuals of the reduction process that should be considered deviations from this ideal situation. Depending on how precise the reduction process is, these residuals will have a greater or lesser impact on the final reduced image. In general, the flux in a resolution element  $I[x, y]$  contains:

Este documento incorpora firma electrónica, y es copia auténtica de un documento electrónico archivado por la ULL según la Ley 39/2015.  
 Su autenticidad puede ser contrastada en la siguiente dirección <https://sede.ull.es/validacion/>

Identificador del documento: 2260218      Código de verificación: Sm21pjYh

Firmado por: JAVIER ROMAN GARCIA  
 UNIVERSIDAD DE LA LAGUNA

Fecha: 02/11/2019 16:23:59

IGNACIO TRUJILLO CABRERA  
 UNIVERSIDAD DE LA LAGUNA

02/11/2019 17:39:19

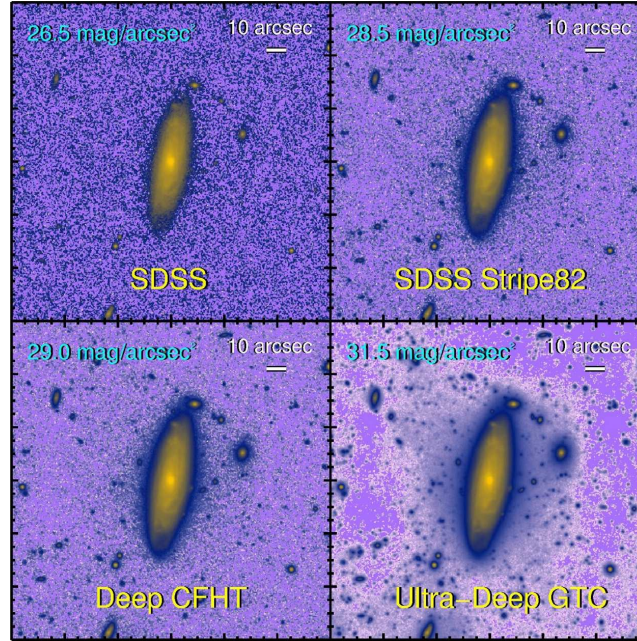


Figure 1.9: UGC 00180 as would be observed by different surveys: SDSS, SDSS Stripe82, Deep data with CFHT (i.e. Ferrarese et al. 2012; Duc et al. 2015) and the present work. Each surface brightness limiting magnitude has been estimated as a  $3\sigma$  surface brightness fluctuation in boxes of  $10'' \times 10''$ . Note how, for this galaxy, the emergence of a stellar halo requires reaching limiting surface brightness fainter than  $30 \text{ mag arcsec}^{-2}$  in the r-band. Figure and caption obtained from Trujillo & Fliri (2016).

$$I[x, y] = I[x, y]_{source} + I[x, y]_{sky} + \Gamma[x, y] \quad (1.8)$$

where  $I[x, y]_{source}$  is the flux value of the astronomical sources under analysis,  $I[x, y]_{sky}$  is the flux value of the night sky and  $\Gamma[x, y]$  is the residual flux due to the reduction process. Regarding the flux of the sky, this is approximately constant, however it also contains certain variations due to the fact that the brightness of the sky varies temporally and spatially during the course of the observations, the presence of moonlight, light pollution of the astronomical installation, airglow emission, etc. Therefore, we can express the flux of the sky as:

$$I[x, y]_{sky} = \overline{I_{sky}} + \delta[x, y]_{sky} \quad (1.9)$$

where  $\overline{I_{sky}}$  is the average value of the sky emission in the entire image<sup>2</sup>, commonly called the sky level and  $\delta[x, y]_{sky}$  are the spatial deviations of the sky flux with respect to its average

<sup>2</sup>The calculation of the average sky level itself is not a trivial process, see a discussion by Borlaff et al. (2019).

Este documento incorpora firma electrónica, y es copia auténtica de un documento electrónico archivado por la ULL según la Ley 39/2015.  
 Su autenticidad puede ser contrastada en la siguiente dirección <https://sede.ull.es/validacion/>

Identificador del documento: 2260218 Código de verificación: Sm21pjYh

Firmado por: JAVIER ROMAN GARCIA  
 UNIVERSIDAD DE LA LAGUNA

Fecha: 02/11/2019 16:23:59

IGNACIO TRUJILLO CABRERA  
 UNIVERSIDAD DE LA LAGUNA

02/11/2019 17:39:19

constant value over the course of the observations. Redefining the flux sources which vary spatially throughout the image and which do not belong to the astronomical sources, such as:

$$\nabla[x, y] = \delta[x, y]_{sky} + \Gamma[x, y] \quad (1.10)$$

We can finally express the flux in a resolution element of the image such as:

$$I[x, y] = I[x, y]_{source} + \overline{I_{sky}} + \nabla[x, y] \quad (1.11)$$

The factor  $\nabla[x, y]$  is commonly known as the gradients of the image, and this factor contains all the residuals of the reduction process, the contribution of light pollution in the observations and any source of parasitic light that has a spatial variation in the image. It is important to emphasize that  $\overline{I_{sky}}$  should not be considered exclusively the emission of the earth atmosphere at night, but the average level of any flux received outside the astronomical sources, although the brightness of the earth atmosphere at night will be dominant in this factor. Therefore, gradients in the image can be considered as the uncertainty factor in the calculation of the flux of astronomical sources under analysis in each resolution element. In the ideal case that the astronomical observatory is located in a place with ideal dark conditions, that the observational strategy manages to mitigate the effects of parasitic light, and that the reduction process is totally effective, null gradients would be obtained  $\nabla[x, y] \rightarrow 0$ . Assuming that the calculation of the sky level can be obtained accurately by measuring the flux in areas where no sources are detected, the flux of an astronomical source in a resolution element would be given uniquely as:  $I[x, y]_{source} = I[x, y] - \overline{I_{sky}}$ .

However, in practice, it is impossible to obtain total precision in the elimination of gradients from the image, being to a greater or lesser extent a limiting factor in the accuracy of obtaining the flux of astronomical sources. It is interesting to show what are the general characteristics of these gradients and their effects on the photometry of different types of astronomical sources. In the upper left panel of Figure 1.10 a reduced image of the M101 galaxy of a 300 second individual exposure with the OGS telescope is shown. As can be seen visually, there is a residual flux or gradient contribution with a maximum in the upper left side. In this particular case, the presence of this gradient is due to poor observational conditions at the time of data acquisition, such as the presence of the moon light and high clouds. As can be noticed, the gradient is defined by a flux surface whose variation throughout the image is only noticeable at large scales, its variation at small scales is negligible. It is interesting to note that for a given resolution element or pixel, it is impossible to know what are the different contributions in flux (see eq. 1.11) and thus be able to discern which is the flux of the astronomical source. Only by analyzing the image as a whole it is possible to appreciate the effects of the gradients, what are the sources located in the image and the appropriate areas for the estimation of the reference sky background level (areas with no astronomical sources).

The most common and "popular" way to correct these residual gradients is to fit a smooth surface (without strong variations at small scales) to the image. For this, it is necessary to calculate what are the regions of the image in which astronomical sources are found, in order to avoid them during the surface fitting to this flux, being able to fit exclusively the gradients present in the image. However, while for more conspicuous or smaller sources this differentiation is relatively immediate to perform, both visually and with common astronomical software, for larger sources, such as the M101 galaxy in this image, there is considerable confusion preventing

Este documento incorpora firma electrónica, y es copia auténtica de un documento electrónico archivado por la ULL según la Ley 39/2015.  
 Su autenticidad puede ser contrastada en la siguiente dirección <https://sede.ull.es/validacion/>

Identificador del documento: 2260218 Código de verificación: Sm21pjYh

Firmado por: JAVIER ROMAN GARCIA  
 UNIVERSIDAD DE LA LAGUNA

Fecha: 02/11/2019 16:23:59

IGNACIO TRUJILLO CABRERA  
 UNIVERSIDAD DE LA LAGUNA

02/11/2019 17:39:19

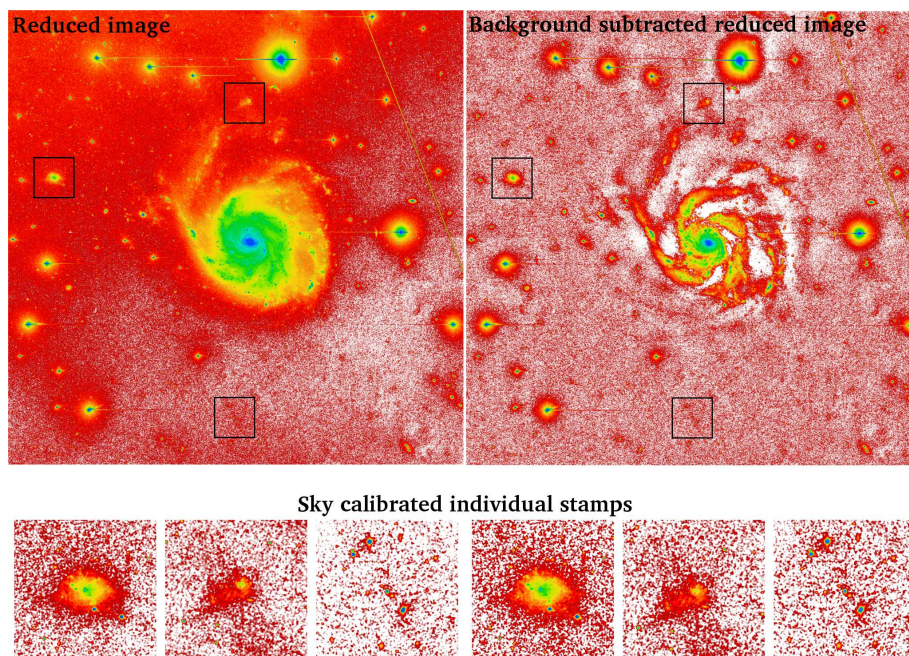


Figure 1.10: Reduced single exposure of 300 sec of the M101 galaxy field with the OGS telescope.

to discern between the gradient present in the image and the areas of the galaxy with a lower surface brightness, located mainly in the outskirts of the galaxy. The use of the software **SWarp** (Bertin et al. 2002) is of common use for the elimination of the gradients. This software makes a first estimate of the areas where astronomical sources are located. After ignoring these areas, a fitting of a smooth surface is performed to the light gradient that is subsequently subtracted from the image. The result of this procedure is shown in the upper right panel of Figure 1.10. As can be seen, this procedure is capable of correcting the overall gradient present in the image, producing an overall constant reference sky background level. However, regions of astronomical sources with greater extent and low surface brightness (external regions of the M101 galaxy and external regions of the brightest stars) are oversubtracted, being this flux irretrievably removed. The reason for this, among other factors, is due to the inefficiency of the software in assigning which areas contain flux from astronomical sources and which areas can be considered as pure sky emission (together with the residual gradients present in the image). In the lower surface brightness regions of the central M101 galaxy, this flux is misidentified by the software as sky regions, being fitted by the surface that tries to model the gradients, leaving these regions with strong oversubtraction, destroying the flux of the astronomical source. This is what is called an aggressive subtraction of the sky background. It is interesting to note that this aggressive sky subtraction procedure does not significantly affect astronomical sources of small extension

Este documento incorpora firma electrónica, y es copia auténtica de un documento electrónico archivado por la ULL según la Ley 39/2015.  
 Su autenticidad puede ser contrastada en la siguiente dirección <https://sede.ull.es/validacion/>

Identificador del documento: 2260218 Código de verificación: Sm21pjYh

Firmado por: JAVIER ROMAN GARCIA  
 UNIVERSIDAD DE LA LAGUNA

Fecha: 02/11/2019 16:23:59

IGNACIO TRUJILLO CABRERA  
 UNIVERSIDAD DE LA LAGUNA

02/11/2019 17:39:19

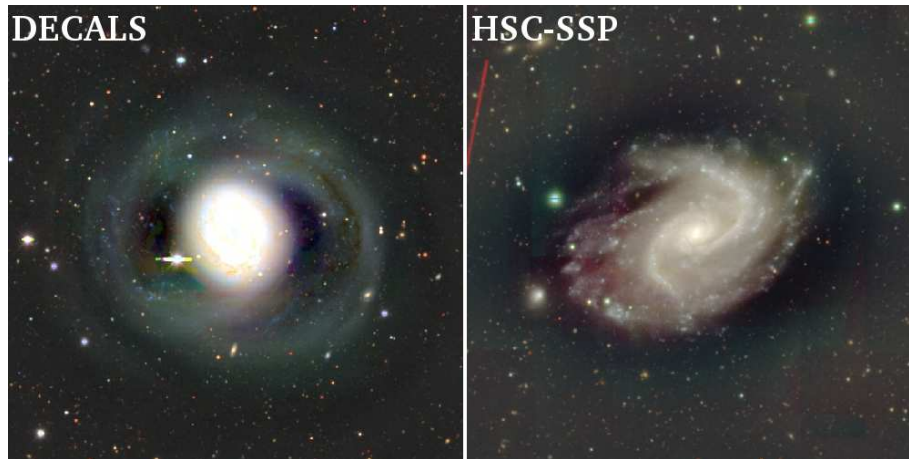


Figure 1.11: Example of aggressive sky subtraction in the Dark Energy Camera Legacy Survey (DECaLS) and Hyper Suprime-Cam Subaru Strategic Program (HSC-SSP)

and high brightness. This is due to its smaller size compared to the typical spatial variation of the surface that fits the sky background to eliminate such gradient. This can be checked in the lower panels of the Figure 1.10, corresponding to different areas of the image, both in the case of uncorrected gradients (lower left panels) and in the sky subtracted image (lower right panels). While the central galaxy (M101) and the brightest stars have undergone a process that destroy their lower surface brightness regions especially in the outer parts, the smaller sources have been reasonably preserved. However, with the increase in data depth, this over-subtraction process is harmful to any source of low surface brightness. In the case of astronomical sources only detectable after the stacking of several exposures in which this oversubtraction process has been applied, these sources will be corrupted or even eliminated in the final coadd image.

Although aggressive sky subtraction is a crucial loss of the low surface brightness information, it is commonly applied to the current generation of deep surveys such as the Dark Energy Camera Legacy Survey (DECaLS) (Dark Energy Survey Collaboration et al. 2016) or the Hyper Suprime-Cam Subaru Strategic Program (Aihara et al. 2018) (see Figure 1.11). The reason is that these surveys, intended to map large regions of the sky, contain an instrumentation based on CCD mosaics. These types of cameras carry enormous complexity in the data processing and reduction. Although these instruments are found in top-level astronomical facilities, and therefore with excellent darkness and seeing conditions, the classic reduction processes such as flat-fielding correction through the use of dome or twilight flats entail some considerable residuals. This means that although variations in image flux due to sky variations or parasitic light ( $\delta[x, y]_{sky}$ ) are relatively low, residuals due to the reduction process ( $\Gamma[x, y]$ ) are high. An added factor is the relative small size of the individual CCDs in the mosaic, which can be a problem if large sources occupies one of the individual CCDs completely, leaving no region for an accurate estimation of the average sky background flux ( $\overline{I_{sky}}$ ). An illustrative example of the level of complexity is shown

Este documento incorpora firma electrónica, y es copia auténtica de un documento electrónico archivado por la ULL según la Ley 39/2015.  
 Su autenticidad puede ser contrastada en la siguiente dirección <https://sede.ull.es/validacion/>

Identificador del documento: 2260218 Código de verificación: Sm21pjYh

Firmado por: JAVIER ROMAN GARCIA  
 UNIVERSIDAD DE LA LAGUNA

Fecha: 02/11/2019 16:23:59

IGNACIO TRUJILLO CABRERA  
 UNIVERSIDAD DE LA LAGUNA

02/11/2019 17:39:19

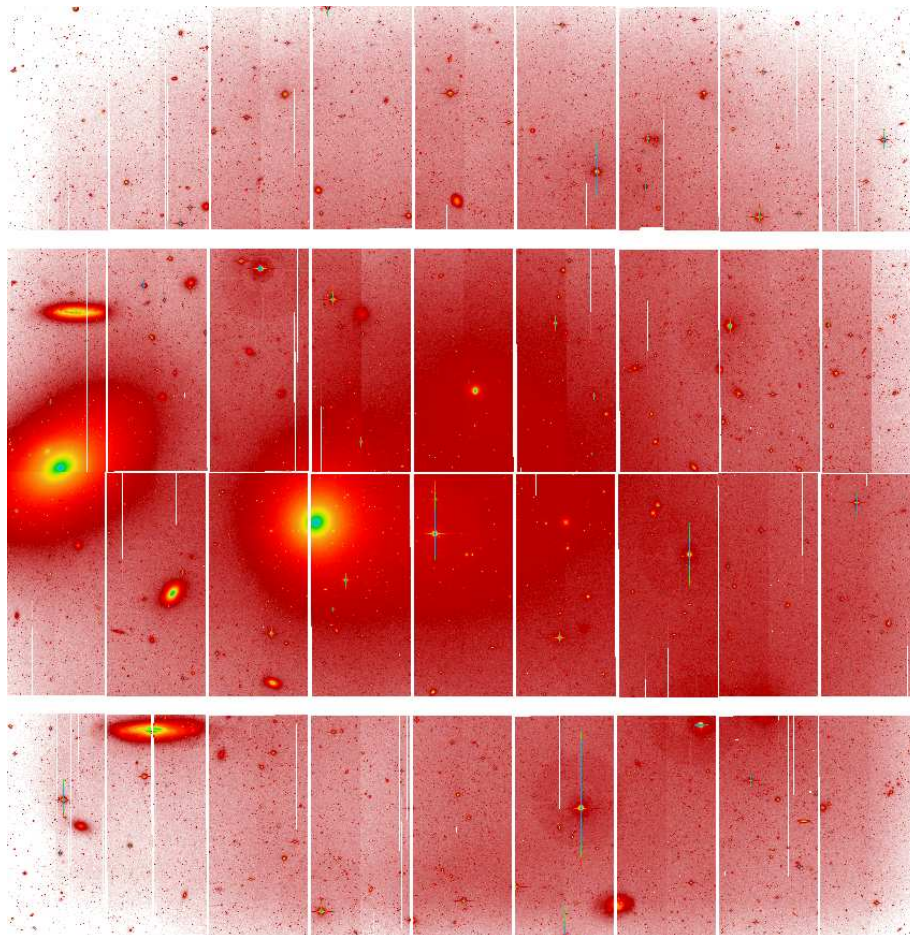


Figure 1.12: Reduced image of the center of the Virgo cluster with MegaCam on the Canada-France-Hawaii Telescope (CFHT) belonging to the Next Generation Virgo Survey.

Este documento incorpora firma electrónica, y es copia auténtica de un documento electrónico archivado por la ULL según la Ley 39/2015.  
Su autenticidad puede ser contrastada en la siguiente dirección <https://sede.ull.es/validacion/>

Identificador del documento: 2260218 Código de verificación: Sm21pjYh

Firmado por: JAVIER ROMAN GARCIA  
UNIVERSIDAD DE LA LAGUNA

Fecha: 02/11/2019 16:23:59

IGNACIO TRUJILLO CABRERA  
UNIVERSIDAD DE LA LAGUNA

02/11/2019 17:39:19

in Figure 1.12, showing a reduced image of the Next Generation Virgo Survey observed with the CFHT telescope. In this example, a clear gradient can be observed product of the inadequate correction by flat-fielding in which the areas furthest from the center of the mosaic contain a lower flux than the central parts. In turn, each region of the individual CCDs contains different background fluxes, consequence of a non-correct recalibration of the individual sky background of the chips to a common global sky background. Additionally, some of the astronomical sources present in the field-of-view have an extension of the same order as the size of the individual CCDs. Taking into account that this is only an individual exposure, it is assumed that the combination of multiple exposures in a final coadd will produce considerable residuals that are extremely problematic and in many cases unrecoverable. That is why an aggressive subtraction of the sky is usually common to minimize all the gradients and differences of relative sky background references between the different individual CCDs, creating a level of common sky between all the CCDs allowing a cleaner coadd and with a common sky background level reference. However, as discussed in the previous Section, the use of aggressive subtraction of the sky background is very harmful to the sources of extreme low surface brightness, losing their reliability. This case is a clarifying example of the serious problems that currently exist in preserving structures with low surface brightness in astronomical facilities with complex instrumentation.

### 1.3.3 Point Spread Function

Another limiting factor in the detection of low surface brightness sources is the Point Spread Function (PSF). The PSF is defined as the optical response of the instrumentation to the image of a point source. The net effect of the PSF is to blur the sources, bringing flux from the central to the outermost regions of the flux sources. Its most obvious effect is in the case of stars, creating artificial halos of light around them that create confusion with adjacent sources. However, its effect is also important in the study of galactic stellar halos, especially in very deep data.

Comprehensive works on the characterization of the PSF (e.g. de Jong 2008; Slater et al. 2009; Sandin 2014) show that the PSF has different characteristics in different telescopes or cameras, among different bands given the same instrumentation, varying even along the position on the CCD. Additionally, while the light profile of the PSF rapidly falls with radius, in the case of deep data the contribution of the scattered light by all the sources (mainly the stars) in regions of extremely low surface brightness is comparable, or even higher, than the surface brightness of the sources to be analyzed. A very illustrative example is shown in Figure 1.13. The upper panel shows SDSS data in the  $r$  band of the Abell 2199 galaxy cluster centered on its central dominant galaxy (NGC 6166). The SDSS data, being shallow (surface brightness limit of  $26.5 \text{ mag arcsec}^{-2}$  in the  $r$  band,  $3\sigma 10'' \times 10''$ ) due to their short integration time, do not show the regions of lower surface brightness, which are hidden under the Poisson noise of the image. In the lower panel, ultra-deep observations are shown using the 1 meter Optical Ground Station (OGS) telescope at Izaña Observatory, with a total integration time of 22 hours and with specific observational and processing techniques, allowing to reach a theoretical surface brightness limit of approximately  $29.5 \text{ mag arcsec}^{-2}$  in the  $R$  Johnson band,  $3\sigma 10'' \times 10''$ . Although the great depth of the image manages to show extremely low surface brightness features, the PSFs of the stars are the dominant source of flux against the faintest structures of the galaxies. Therefore, the PSF of the stars creates a considerable confusion imposing a strong limit on the analysis of low surface brightness sources.

Este documento incorpora firma electrónica, y es copia auténtica de un documento electrónico archivado por la ULL según la Ley 39/2015.  
 Su autenticidad puede ser contrastada en la siguiente dirección <https://sede.ull.es/validacion/>

Identificador del documento: 2260218      Código de verificación: Sm21pjYh

Firmado por: JAVIER ROMAN GARCIA  
 UNIVERSIDAD DE LA LAGUNA

Fecha: 02/11/2019 16:23:59

IGNACIO TRUJILLO CABRERA  
 UNIVERSIDAD DE LA LAGUNA

02/11/2019 17:39:19

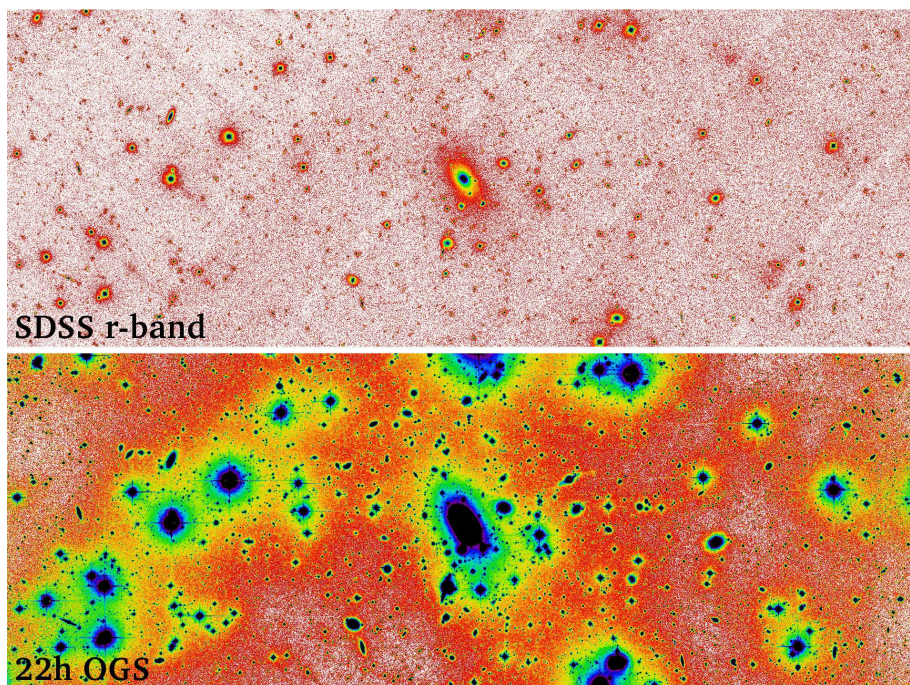


Figure 1.13: Center of the Abell 2199 galaxy cluster observed by the Sloan Digital Sky Survey (top panel) and the Optical Ground Station telescope at the Izaña Observatory (bottom panel). Note that the image on the lower panel has much higher depth than that of the top panel, revealing areas of lower surface brightness but being dominated by confusion by the scattered light by the stars due to the PSF.

It is worth emphasizing that the effect of PSF is completely independent of the gradients and residuals present in the images due to deficiencies in the observational and reduction techniques discussed in the previous Section. It means that although the image obtained would be completely free of gradients and with great depth or low Poisson noise, the effect of the PSF can be equally limiting, preventing the study of the low surface brightness sources. In Figure 1.14 an illustrative example regarding this issue is shown. The left panel shows what is the first evidence of diffuse (or intracluster light) material in the Coma cluster by Kormendy & Bahcall (1974) obtained on photographic plates with the 122 cm telescope of the Palomar Observatory. On the right panel it is shown a coadd image of the same field made with the OGS telescope with specific observational techniques to obtain a great image quality and free of gradients. It is noteworthy that although the image obtained with the OGS telescope, about 40 years later, with a considerably better image quality and depth, fails to reveal the true morphology of the intracluster light halo of the Coma cluster, being limited in an equivalent way to that of the Kormendy & Bahcall (1974) image by the bright stars present in adjacent regions. This limitation is exclusively due to the

Este documento incorpora firma electrónica, y es copia auténtica de un documento electrónico archivado por la ULL según la Ley 39/2015.  
 Su autenticidad puede ser contrastada en la siguiente dirección <https://sede.ull.es/validacion/>

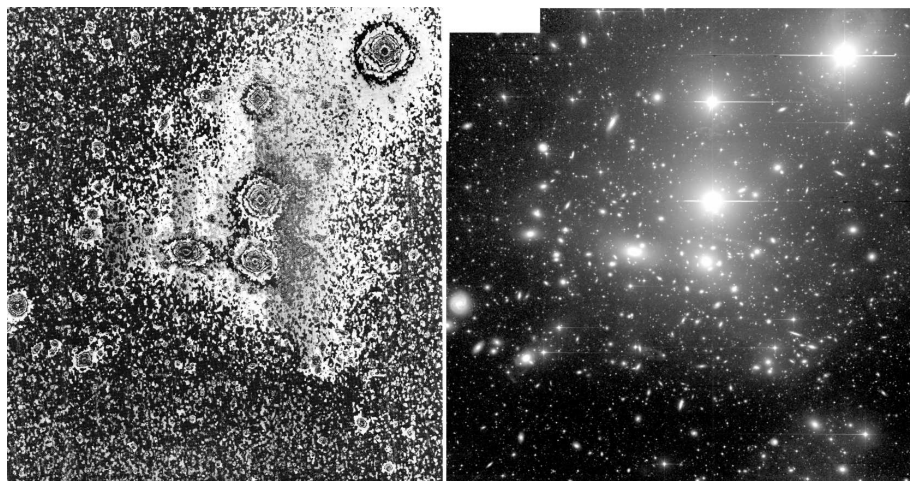
Identificador del documento: 2260218      Código de verificación: Sm21pjYh

Firmado por: JAVIER ROMAN GARCIA  
 UNIVERSIDAD DE LA LAGUNA

Fecha: 02/11/2019 16:23:59

IGNACIO TRUJILLO CABRERA  
 UNIVERSIDAD DE LA LAGUNA

02/11/2019 17:39:19



Kormendy & Bahcall (1974)

OGS telescope

Figure 1.14: Coma galaxy cluster observed by Kormendy & Bahcall (1974) and by the Optical Ground Station (OGS) telescope at Izaña observatory in 2017. Note that although the image of the OGS telescope has a much higher depth, better resolution and better quality in general, the study of diffuse light in Coma is limited by the light scattered from nearby bright stars, preventing its analysis in both cases.

confusion created by the stars due to the PSF. This example shows clearly the limitation imposed by the PSF on the low surface brightness and its independence from other factors such as image quality or depth.

In addition to the confusion created by the stars, the PSF has an impact on photometric measurements made in astronomical sources. Particularly significant are its effects on galaxy profiles of very deep data or when the PSF has poor quality (high scattered light). These effects have been detailed by different works (see a good summary on Sandin 2014) and are characterized by an artificial widening of the galaxy's halo (see Figure 1.15), in which the light itself from the core of the galaxy is transferred to the external parts of it. This effect has a strong impact in the particular case of disk galaxies with high inclination (e.g. Sandin 2015; Trujillo & Fliri 2016; Comerón et al. 2018) or images of high depth (Karabal et al. 2017). These circumstances require an analytical deconvolution of the source under study from the PSF, something unusual in the literature nowadays.

#### 1.3.4 Galactic cirri

In the previous Sections, the limitations imposed by instrumentation in achieving low surface brightness have been discussed. However, even ignoring these limitations and assuming that they are minimal, there is an additional limitation due to the place that we occupy in the Universe within the plane of the Milky Way. This limitation is due to the presence of clouds of dust in the interstellar medium, commonly called Galactic cirri. The abundance of interstellar dust is larger

Este documento incorpora firma electrónica, y es copia auténtica de un documento electrónico archivado por la ULL según la Ley 39/2015.  
 Su autenticidad puede ser contrastada en la siguiente dirección <https://sede.ull.es/validacion/>

Identificador del documento: 2260218 Código de verificación: Sm21pjYh

Firmado por: JAVIER ROMAN GARCIA  
 UNIVERSIDAD DE LA LAGUNA

Fecha: 02/11/2019 16:23:59

IGNACIO TRUJILLO CABRERA  
 UNIVERSIDAD DE LA LAGUNA

02/11/2019 17:39:19

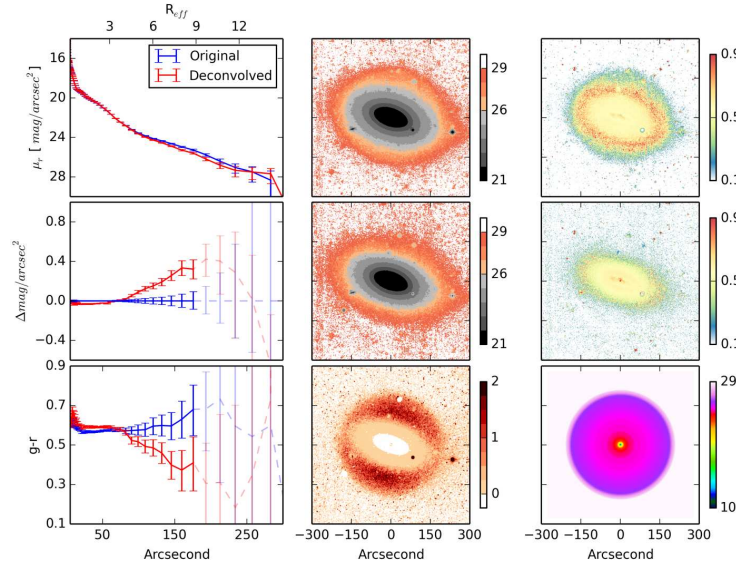


Figure 1.15: Deconvolution technique applied to NGC 3489. Left column: original and deconvolved galaxy profiles in r band (top), the difference between the profiles (middle) and original and deconvolved g - r color profiles (bottom) as a function of semi-major axis. Middle column: original (top) and deconvolved (middle) surface brightness maps in r band, and the difference between the maps (bottom). Right column: original (top) and deconvolved (middle) g - r color maps and the r-band surface brightness map of the PSF (bottom) that was used for the deconvolution. All maps, except PSF, were smoothed with a Gaussian kernel of sigma = 0.5500 to enhance the visibility of the faint regions. Figure and caption obtained from Karabal et al. (2017)

through the Galactic plane. In some occasions, the extinction can be as high to make optical observations opaque. Nonetheless, dust can be also found at high Galactic latitudes. These cirri usually appear with a filamentary morphology of very low surface brightness. In the case that cirri appear in the line of sight of observations, they create an important source of confusion being very hard to distinguish them from extragalactic sources or features.

An illustrative example is the Arp loop in the nearby M81 galaxy. First identified by Arp (1965) in what looked like a low surface brightness structure associated with the M81 galaxy. Its true nature has been extensively debated (e.g. Makarova et al. 2002; de Mello et al. 2008; Barker et al. 2009; Davidge 2009). Finally Sollima et al. (2010) using a multi band analysis in optical and far infrared (IR) data identified such structure as dust from our own Galaxy.

Because of the low temperature of these clouds of interstellar material, their peak emission is in the far infrared (IR) (e.g. Low et al. 1984; Veneziani et al. 2010), being its emission in optical (e.g. de Vries & Le Poole 1985; Laureijs et al. 1987; Witt et al. 2008) or ultraviolet (e.g. Witt et al. 1997; Boissier et al. 2015) bands due to the reflection of the surrounding starlight field. This is why it is usual to use surveys in the far IR or in sub-millimeters such as the IR Astronomical Satellite (IRAS) mission or the Planck Space Observatory as a counterpart to the

Este documento incorpora firma electrónica, y es copia auténtica de un documento electrónico archivado por la ULL según la Ley 39/2015.  
 Su autenticidad puede ser contrastada en la siguiente dirección <https://sede.ull.es/validacion/>

Identificador del documento: 2260218 Código de verificación: Sm21pjYh

Firmado por: JAVIER ROMAN GARCIA  
 UNIVERSIDAD DE LA LAGUNA

Fecha: 02/11/2019 16:23:59

IGNACIO TRUJILLO CABRERA  
 UNIVERSIDAD DE LA LAGUNA

02/11/2019 17:39:19

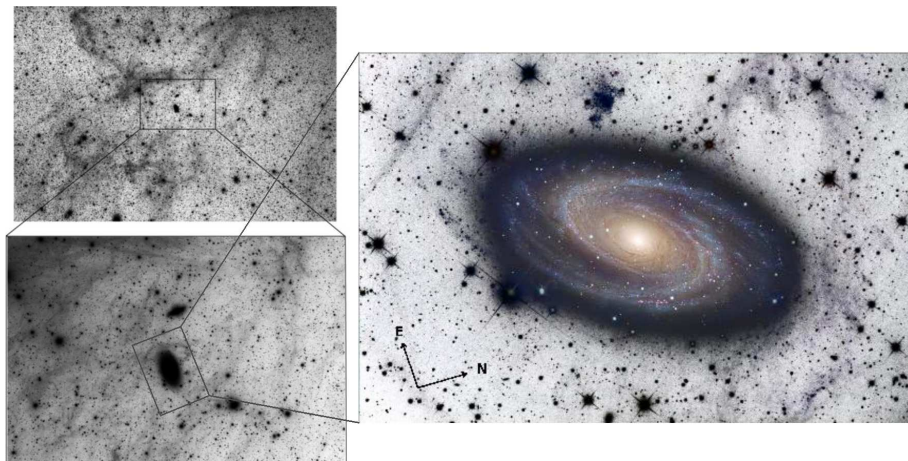


Figure 1.16: Sequence of zoom in images to the galaxy M81. Arp's loop is visible as the nebular ring crossing the disk of M81 on the right side of the image. Dust-absorption features are superimposed over and surround the disk of M81. Figure obtained from Sollima et al. (2010).

optical observations in order to elucidate the possible presence of cirri. However, the poor spatial resolution of these surveys ( $\text{FWHM} \approx 5$  arcmins; Miville-Deschênes & Lagache 2005; Lammare et al. 2003) makes them inefficient at low angular scales. Only with the availability of far IR data with better spatial resolution, such as the ESA Herschel Space Observatory (FWHM of 18 arcseconds in the  $250 \mu\text{m}$  band Pilbratt et al. 2010) it is possible to identify correctly, or even decontaminate, the presence of cirri in optical observations (see Mihos et al. 2017). Unfortunately, the Herschel Space Observatory data only cover a modest portion of the sky in selected fields, and the presence of dust is nowadays a major problem in extragalactic observations: There is currently no solution to distinguish between dust from our own galaxy and extragalactic sources (e.g. Chiboucas et al. 2009; Cortese et al. 2010; Rudick et al. 2010; Davies et al. 2010; Chiboucas et al. 2013; Hodges-Kluck & Bregman 2014; Besla et al. 2016; Duc et al. 2018; Barrera et al. 2018; Ramírez-Moreta et al. 2018).

The imminent arrival of the Large Synoptic Survey Telescope (LSST; LSST Science Collaboration et al. 2009) and the new generation of extremely large telescopes will reveal the presence of interstellar dust at any galactic latitude. An illustrative example of the expected scenario is the work by Trujillo & Fliri (2016) (see Fig. 1.17). This work provides an ultra-deep view of the UGC 180 galaxy, in which a diffuse structure of low surface brightness appears adjacent to the galaxy, being with a high probability due to a galactic cirrus. However, auxiliary observations in sub-millimeter bands only provide a guess to the possible presence of dust in the field due to its low resolution. In general, based on the observations by the Planck Space Observatory or IRAS, it is unfeasible to discern small-scale extragalactic features from dust emission. It is, therefore, a priority for the extragalactic community to urgently address this problem, being additionally crucial in other fields of astrophysics such as the study of the cosmic microwave background

Este documento incorpora firma electrónica, y es copia auténtica de un documento electrónico archivado por la ULL según la Ley 39/2015.  
 Su autenticidad puede ser contrastada en la siguiente dirección <https://sede.ull.es/validacion/>

Identificador del documento: 2260218 Código de verificación: Sm21pJYh

Firmado por: JAVIER ROMAN GARCIA  
 UNIVERSIDAD DE LA LAGUNA

Fecha: 02/11/2019 16:23:59

IGNACIO TRUJILLO CABRERA  
 UNIVERSIDAD DE LA LAGUNA

02/11/2019 17:39:19

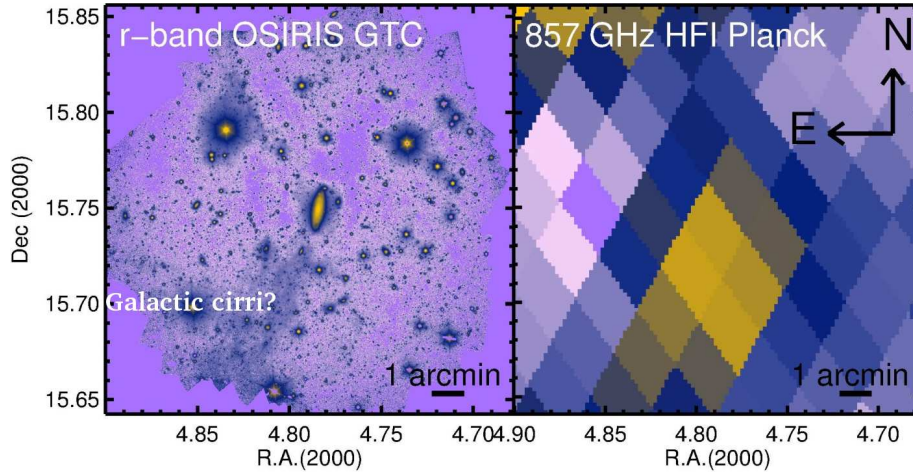


Figure 1.17: Field of view of 12.7'x12.7' around UGC00180 in optical (left panel) and submillimeter wevalenghts (right panel). The presence of an extended and filamentary emission in the bottom part of the image is also tentatively identified as a Galactic Cirrus of our own Galaxy. Figure and extracted caption obtained from Trujillo & Fliri (2016)

(Planck Collaboration et al. 2011) or the cosmic infrared background (Thacker et al. 2013).

#### 1.4 Current approaches in the pursuit of the low surface brightness

It is interesting to analyze from the point of view of the evolution of different works over time, what have been the key advances and limitations in the study of low surface brightness. For this, the comparison of different studies in the M87 galaxy, this being the first detection of a galactic stellar halo, is a good example. Some key observations of this galaxy are shown in Figure 1.18, such as the works by Arp & Bertola (1969), SDSS (York et al. 2000), Mihos et al. (2005) and the Next generation Virgo Survey (Ferrarese et al. 2012). Something that attracts attention first is that the work by Arp & Bertola (1969), the first observation of a galactic stellar halo, managed to reach a deeper detection than that of the SDSS despite having a considerably lower instrumental quality than SDSS. Analyzing the integration times of both works (1 hour with the Palomar Schmidt 1.2m telescope in the case of Arp & Bertola (1969) and 53 seconds with the 2.5m telescope of Apache point) it can be verified that the image by Arp & Bertola (1969) has a factor of approximately 15 times more integrated photons. It shows that integration times in deep images are a crucial factor. A very interesting comparison is that of the image by Mihos et al. (2005) with that of the Next generation Virgo Survey (Ferrarese et al. 2012). The first obtained with the 0.6m Burrell Schmidt telescope with about 18 hours of total integration and the second with the 3.5m CHFT telescope with approximately 1.2 hours of total integration. These telescope apertures and integration times imply that the image of the Next generation Virgo Survey has approximately twice as many integrated photons as the image of the Burrell

Este documento incorpora firma electrónica, y es copia auténtica de un documento electrónico archivado por la ULL según la Ley 39/2015.  
 Su autenticidad puede ser contrastada en la siguiente dirección <https://sede.ull.es/validacion/>

Identificador del documento: 2260218 Código de verificación: Sm21pjYh

Firmado por: JAVIER ROMAN GARCIA  
 UNIVERSIDAD DE LA LAGUNA

Fecha: 02/11/2019 16:23:59

IGNACIO TRUJILLO CABRERA  
 UNIVERSIDAD DE LA LAGUNA

02/11/2019 17:39:19

1.4 Current approaches in the pursuit of the low surface brightness XXXI

Schmidt telescope, which would imply a better signal to noise by about a factor  $\approx \sqrt{2}$  higher. However, what can be seen in Figure 1.18 is that in fact the Burrell Schmidt telescope is much more efficient in detecting low surface brightness sources. The reason is the exquisite processing of the data done by Mihos et al. (2005) together with the considerable complexity of the MegaCam camera for the reduction and processing of the data. It should be noted that the pure quality of the observations, both in darkness of the sky, seeing and sensitivity of the camera, are generally better for the case of the Next Generation Virgo Survey image, effectively impacting on a greater detection of objects with small angular scale, both dwarf galaxies with low surface brightness (e.g. Vollmer et al. 2013; Davies et al. 2016; Sánchez-Janssen et al. 2016; Prole et al. 2018) as for brighter objects or globular clusters (e.g. Durrell et al. 2014; Zhang et al. 2015; Liu et al. 2015), being the galactic stellar halos and tidal features of great extension (large angular objects and extreme low surface brightness) those sources better recovered in the image of the Burrell Schmidt telescope. This simple example of comparison shows the hard restrictions imposed by the limitations in low surface brightness.

The current efforts of the extragalactic community are focused on minimizing as far as possible the low surface brightness limitations discussed above. The first limitation is obviously that of Poisson noise. Therefore, any study in low surface brightness requires long exposure campaigns in order to obtain images with a sufficient signal to noise. In this sense, due to the great competitiveness for getting time on the large telescopes, the use of small aperture telescopes to have longer observational campaigns is becoming common.

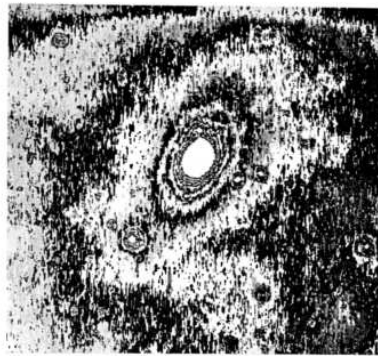
Regarding the minimization of gradients (see equation 1.10) there are different approaches. First, the improvement in the observational strategy is key in minimizing the factor  $\delta[x, y]_{sky}$ . For this, it is usual to make observations with wide offsets of individual exposures or "dithering", together with rotations in the case that the camera has a rotator. With this, it is possible to average the parasitic light producing a significant reduction of these effects. It is also possible to significantly reduce the gradients produced by the  $\Gamma[x, y]$  factor due to image processing, mainly due to flat-fielding. This type of gradient usually comes from the use of dome or twilight flats to perform the flat-fielding. Even though it is a very common procedure in all types of astronomical facilities, the use of dome or twilight flats is not optimal. The reason is the considerable deviation of the dome or twilight images from a true flatness. For this, the stacking of masked science images is an improvement, producing a high quality flat, whose main advantage is providing a minimal presence of gradients due to the reduction. However, to perform this procedure a perfect masking and the use of fields with low contamination by cirri are necessary. Related to this point, and also with the correction of possible residual gradients and even with the detection of low surface brightness sources, the need for software capable of dealing with these conditions of extreme precision is fundamental. New software specifically designed for the analysis of low surface brightness is currently being developed (e.g. Akhlaghi, & Ichikawa 2015; Borlaff et al. 2019) that are considerably more efficient than the classic use of **SExtractor** (Bertin & Arnouts 1996) or **SWarp** (Bertin et al. 2002).

Another crucial aspect is the characterization of the PSF up to radii of the order of many arc minutes. Works like the one by Slater et al. (2009) with the Burrell Schmidt telescope, Trujillo & Fliri (2016) with the Gran Telescopio Canarias (GTC) or Karabal et al. (2017) with the CFHT followed an approach based on an exquisite characterization of the PSF, with excellent results. There is no doubt that in the near future, any work in low surface brightness will require an excellent characterization of the PSF, both for the subtraction of stars, eliminating that element

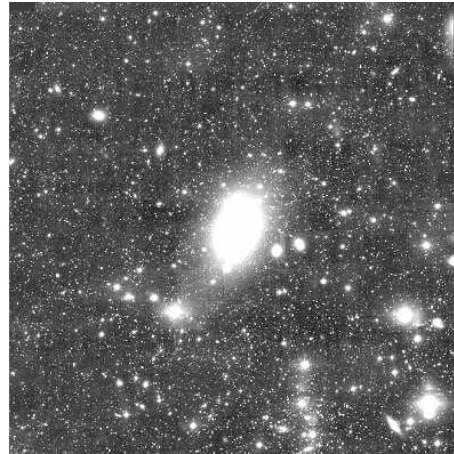
Este documento incorpora firma electrónica, y es copia auténtica de un documento electrónico archivado por la ULL según la Ley 39/2015.  
 Su autenticidad puede ser contrastada en la siguiente dirección <https://sede.ull.es/validacion/>

Identificador del documento: 2260218      Código de verificación: Sm21pjYh

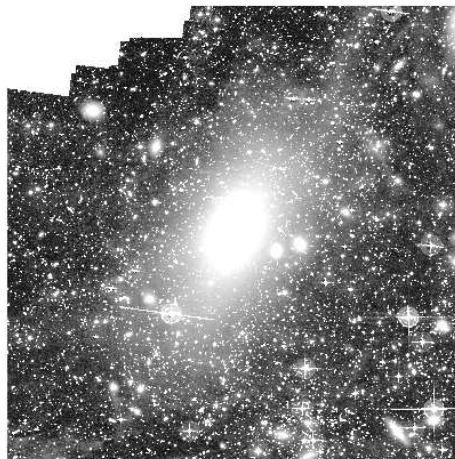
Firmado por: JAVIER ROMAN GARCIA UNIVERSIDAD DE LA LAGUNA	Fecha: 02/11/2019 16:23:59
IGNACIO TRUJILLO CABRERA UNIVERSIDAD DE LA LAGUNA	02/11/2019 17:39:19



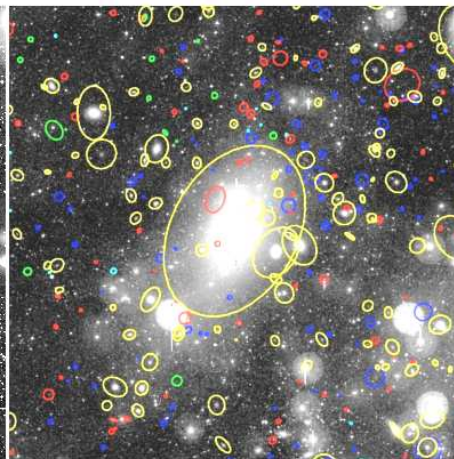
Arp & Bertola (1969)



Sloan Digital Sky Survey.  
York et al. (2000)



Burrell Schmidt Deep Virgo Survey.  
Mihos et al. (2005)



Next generation virgo cluster survey.  
Ferrarese et al. (2012)

Figure 1.18: Different observations of the M87 galaxy over time: Top-left panel (Arp & Bertola 1969), top-right panel (SDSS; York et al. 2000), bottom-left (Mihos et al. 2005) and bottom-right (Next Generation Virgo Survey; Ferrarese et al. 2012). The color scaling of the images is random and only useful for a visual taste in the detection.

Este documento incorpora firma electrónica, y es copia auténtica de un documento electrónico archivado por la ULL según la Ley 39/2015.  
Su autenticidad puede ser contrastada en la siguiente dirección <https://sede.ull.es/validacion/>

Identificador del documento: 2260218

Código de verificación: Sm21pjYh

Firmado por: JAVIER ROMAN GARCIA  
UNIVERSIDAD DE LA LAGUNA

Fecha: 02/11/2019 16:23:59

IGNACIO TRUJILLO CABRERA  
UNIVERSIDAD DE LA LAGUNA

02/11/2019 17:39:19

#### 1.4 Current approaches in the pursuit of the low surface brightness XXXIII

of confusion, and for the deconvolution of its effect on the photometry of galaxies. In this sense, while the characterization of the PSF and subsequent subtraction of the stars is applicable in deep observations, the effect of internal reflections is much more damaging, being extremely complex to remove (see work by Slater et al. (2009) and Karabal et al. (2017)), and sometimes its complete elimination is impossible. Thus, the use of small aperture telescopes with simple optics is very efficient in avoiding the presence of internal reflections, together with the characteristic of having high quality PSFs and monolithic CCDs that allow efficient data reduction. Some notable examples in the use of small-aperture amateur telescopes are those by (Martínez-Delgado et al. 2008; Martínez-Delgado et al. 2010; Martínez-Delgado et al. 2018) or the Dragonfly Telephoto Array (Abraham & van Dokkum 2014). In turn, future specific telescopes for the study of the low surface brightness Universe are also designed on the basis of simple optics with small aperture (e.g. Muslimov et al. 2017; Valls-Gabaud & MESSIER Collaboration 2017).

Regarding the problem of contamination by Galactic cirri, there is currently no effective approach to its solution. The only way explored currently is the comparison of the optical observations with the far infrared (e.g. Sollima et al. 2010; Mihos et al. 2017). However, as discussed above, the lousy spatial resolution of most instruments in the far IR makes features of small angular scale currently impossible to differentiate from dust clouds of our own galaxy. It is, the presence of Galactic cirri, probably the hardest limitation to resolve in the study of the low surface brightness Universe.

Based on these current approaches, this thesis starts with the aim of pushing the low surface brightness limits on integrated photometry.

Este documento incorpora firma electrónica, y es copia auténtica de un documento electrónico archivado por la ULL según la Ley 39/2015.  
Su autenticidad puede ser contrastada en la siguiente dirección <https://sede.ull.es/validacion/>

Identificador del documento: 2260218 Código de verificación: Sm21pjYh

Firmado por: JAVIER ROMAN GARCIA  
UNIVERSIDAD DE LA LAGUNA

Fecha: 02/11/2019 16:23:59

IGNACIO TRUJILLO CABRERA  
UNIVERSIDAD DE LA LAGUNA

02/11/2019 17:39:19

## 2

### Methods

#### 2.1 The IAC Stripe82 Legacy Survey

The Stripe82 region has an extension of 300 square degrees covering  $20\text{h} < \text{R.A.} < 4\text{h}$  and  $-1.25^\circ < \text{Decl.} < 1.25^\circ$  (Adelman-McCarthy et al. 2007). This region was observed repeatedly between the years 1998-2004 by the Sloan Digital Sky Survey (York et al. 2000) with the main goal of detecting transient objects. The potential use for the low surface brightness science of these multiple images was evident. The total exposure time per field was around 1 hour with the 2.5m Telescope at Apache Point Observatory (SDSS) in all the five SDSS filters ( $u$ ,  $g$ ,  $r$ ,  $i$  and  $z$ ) in excellent photometric conditions, with an average seeing of around 1 arcsec. Two versions of this coadd were produced by Annis et al. (2014) and Jiang et al. (2014) in order to obtain greater depth. However, the data processing of these works was not focused on the low surface brightness science, producing over-subtraction effects, partially removing the low surface brightness structures.

In order to produce a reliable data set for the study of the low surface brightness sources Fliri & Trujillo (2016) made a combination with special care in the stability of the sky, avoiding over-subtraction (see Figure 2.1). This processing provided a high quality data of great efficiency for the low surface brightness studies, preserving the most diffuse structures. The average surface brightness limits of this dataset are  $\mu_{lim}(3\sigma; 10'' \times 10'') = 28.0, 29.1, 28.6, 28.2$  and  $26.6 \text{ mag arcsec}^{-2}$  for the  $u, g, r, i$  and  $z$  bands respectively.

This survey is the main source of data in this thesis, not only in its use, but in its maintenance, updating and improvement. Webpage: <http://research.iac.es/proyecto/stripe82/>

#### 2.2 Data reduction and processing

A crucial point in the minimization of image gradients (see equation 1.10) is to carry out adequate processing or reduction of the data in order to obtain images optimized for the detection of low surface brightness structures within the limits of telescope aperture and exposure time. As part of this thesis, different astronomical data reduction pipelines have been created to produce high-quality reduced data. An appropriate observational strategy is also important in order to take full advantage of optimized data reduction procedures. In turn, given the hypothetical presence of gradients in the final images due to different uncontrollable factors such as the presence of light pollution, parasitic light or any other uncertainty that affects the presence of gradients,

XXXIV

Este documento incorpora firma electrónica, y es copia auténtica de un documento electrónico archivado por la ULL según la Ley 39/2015.  
Su autenticidad puede ser contrastada en la siguiente dirección <https://sede.ull.es/validacion/>

Identificador del documento: 2260218 Código de verificación: Sm21pjYh

Firmado por: JAVIER ROMAN GARCIA  
UNIVERSIDAD DE LA LAGUNA

Fecha: 02/11/2019 16:23:59

IGNACIO TRUJILLO CABRERA  
UNIVERSIDAD DE LA LAGUNA

02/11/2019 17:39:19

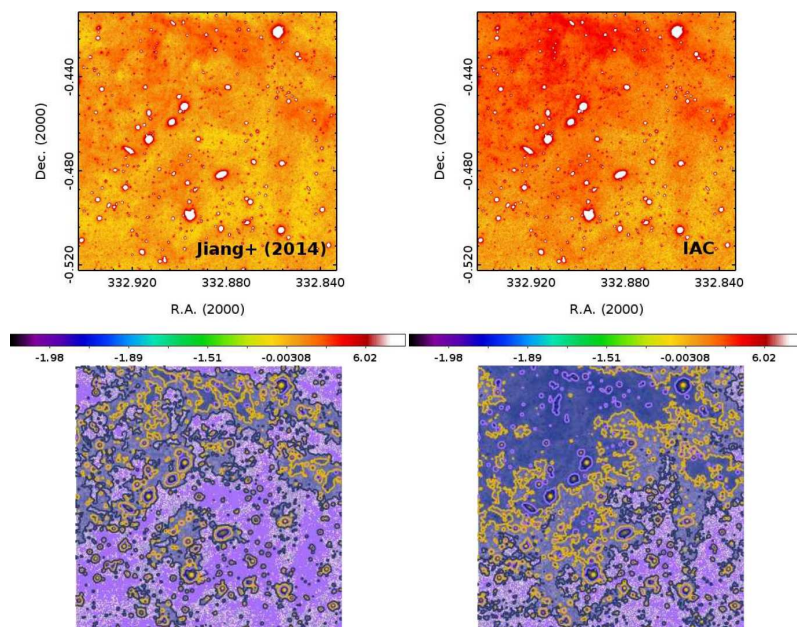


Figure 2.1: Comparison of a field showing intense emission of Galactic Cirrus in Jiang et al. (2014) (left-hand panels) and in Fliri & Trujillo (2016) (right-hand panels). The top panels show the coadds in the r-band in the same dynamic range. Both images were photometrically aligned to the same zeropoint. The bottom panels show the surface brightness distribution of the Galactic Cirri in both images. Contour values are 25, 26 and 27 mag arcsec<sup>-2</sup>. Compared to Fliri & Trujillo (2016), the cirrus emission is largely reduced in the Jiang et al. (2014) data, presumably due to differences in the background treatment in the reduction process. Figure and extracted caption obtained from Fliri & Trujillo (2016).

different techniques have been performed for the correction of these gradients without creating strong oversubtraction. The key points of the procedures developed are detailed below.

### Observational strategy

The observational strategy is based on, as far as possible, large dithering patterns in which each of the individual images in the observational campaign have different pointings, covering a wide field around the target of interest (see Figure 2.2). With this, the possible presence of parasitic light is not located in a fixed position, being more easily eliminated. However, the most important aspect of this dithering pattern is the use of the science images to create the flat-fielding.

Este documento incorpora firma electrónica, y es copia auténtica de un documento electrónico archivado por la ULL según la Ley 39/2015.  
 Su autenticidad puede ser contrastada en la siguiente dirección <https://sede.ull.es/validacion/>

Identificador del documento: 2260218 Código de verificación: Sm21pjYh

Firmado por: JAVIER ROMAN GARCIA  
 UNIVERSIDAD DE LA LAGUNA

Fecha: 02/11/2019 16:23:59

IGNACIO TRUJILLO CABRERA  
 UNIVERSIDAD DE LA LAGUNA

02/11/2019 17:39:19

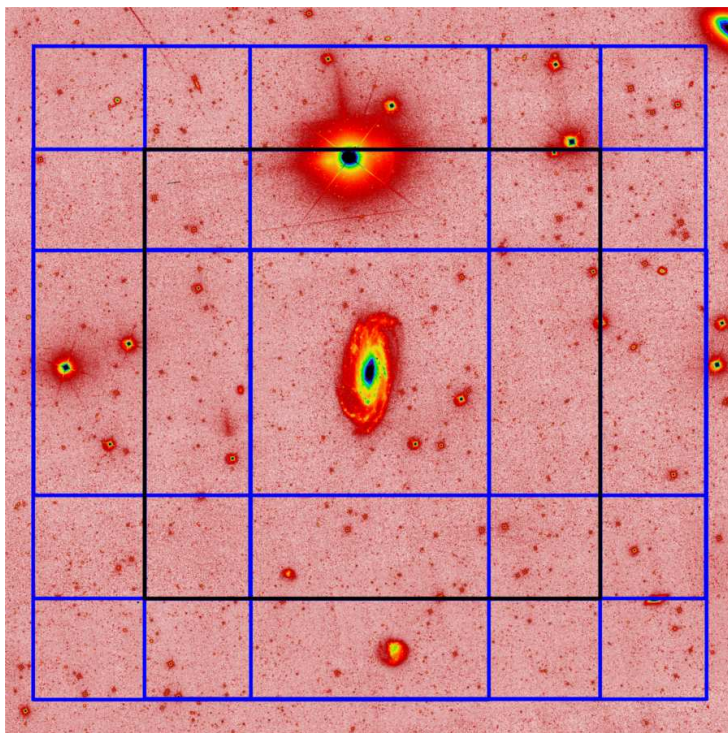


Figure 2.2: Schematic representation of the observation strategy applied with the goal of reducing the gradients. The black rectangle marks the field-of-view of the Space Debris Camera at the OGS telescope. The superimposed blue rectangles mark the different pointings of the dithering.

### Bias and dark corrections

Bias correction is a standard process. After the combination of the bias images, a master bias is obtained, that is subtracted from all the science images. Additionally, in the case that the camera has certain dark current, we perform a similar process, in this case to correct the dark current. The combination of bias and dark images to produce a master bias and master dark is performed with a resistant mean. We reject values beyond 3 times the standard deviation on each combined pixel. Additionally, when the camera has overscan regions, a recalibration of the overscan level to 0 counts is performed. This improves the normalization for the subsequent flat-fielding step of the science images.

Este documento incorpora firma electrónica, y es copia auténtica de un documento electrónico archivado por la ULL según la Ley 39/2015.  
 Su autenticidad puede ser contrastada en la siguiente dirección <https://sede.ull.es/validacion/>

Identificador del documento: 2260218 Código de verificación: Sm21pjYh

Firmado por: JAVIER ROMAN GARCIA  
 UNIVERSIDAD DE LA LAGUNA

Fecha: 02/11/2019 16:23:59

IGNACIO TRUJILLO CABRERA  
 UNIVERSIDAD DE LA LAGUNA

02/11/2019 17:39:19

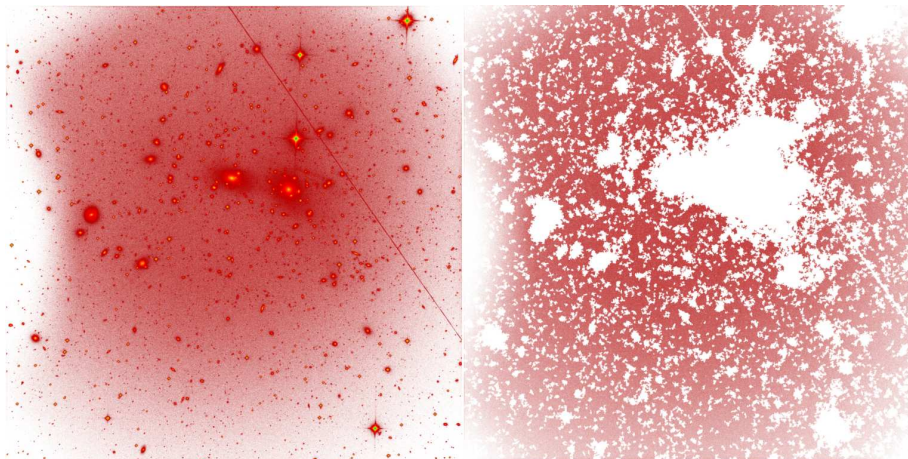


Figure 2.3: Image masking example.

### Flat-fielding

In most astronomical facilities it is usual to take dome or twilight flats for the correction of flat-fielding together with any imperfections such as sensitivity of individual pixels, spots in the optics, etc. However, these flats are not accurate enough. The reason is that the light screen received from both inside the dome and in twilight images, is not perfectly flat. Additionally, small deviations in the linearity of conversion between the number of photons received and counts produced can mean that for regions with fewer photons in science images (the brightness of the night sky), gradients can be generated by applying these dome or twilight flats, since the counts in these flats are usually high in order to produce a high signal to noise flat screen of light.

A different approach for the construction of the flat is to use the science images themselves. This procedure consists in accurate masking of the science images. It leaves the science images with only values of the sky unmasked. From these images, in principle, we can create the response of the CCD to flat illumination<sup>1</sup>. In this step, the dithering applied to the science images is crucial, since the sources will appear at different positions of the CCD in different exposures. Due to the relatively low brightness of the night sky ( $22 \text{ mag arcsec}^{-2}$ ,  $V$  band), a large number of masked science images have to be combined in order to obtain a flat with sufficient signal to noise per pixel, typically more than 50 individual exposures with large dithering.

A key point of this method is the normalization of the masked images. The normalization to one in mean flux of the flat image is common in dome or twilight flats. However, due to the vignetting of the camera and the masking of the images, especially with the presence of sources with large extent over the field of view, normalization can be problematic. The reason is that

<sup>1</sup>The perfect flatness of the night sky is, in turn, debatable because of the presence of light pollution, etc. However, if there are gradients due to light pollution or any type of external light source, these should be accounted for the final flat image. This will result in its correction when applied to science images.

Este documento incorpora firma electrónica, y es copia auténtica de un documento electrónico archivado por la ULL según la Ley 39/2015.  
 Su autenticidad puede ser contrastada en la siguiente dirección <https://sede.ull.es/validacion/>

Identificador del documento: 2260218 Código de verificación: Sm21pjYh

Firmado por: JAVIER ROMAN GARCIA  
 UNIVERSIDAD DE LA LAGUNA

Fecha: 02/11/2019 16:23:59

IGNACIO TRUJILLO CABRERA  
 UNIVERSIDAD DE LA LAGUNA

02/11/2019 17:39:19

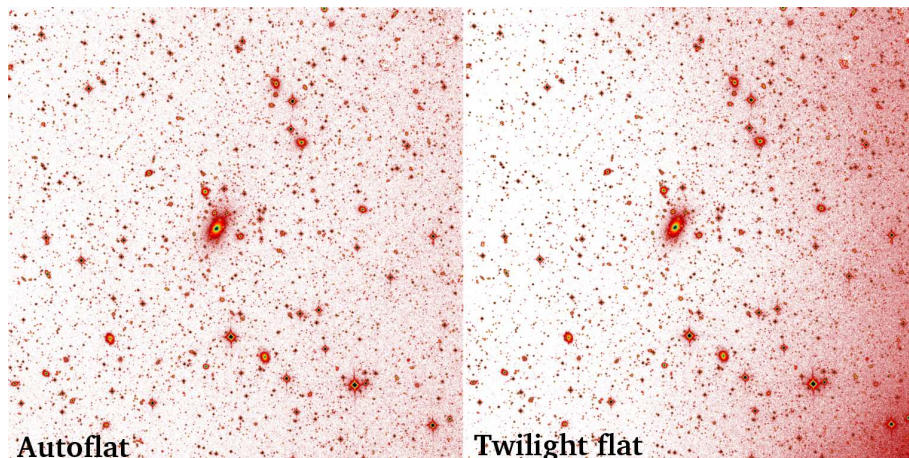


Figure 2.4: The same image processed with the autoflat technique (left panel) and with twilight flats (right panel).

depending on where the sources are randomly located, regions with greater or lesser vignetting will be masked. Therefore, the normalization of these masked images will be inaccurate if the total flux of the image is used as normalization factor. This can be better understood visually by checking Figure 2.3. In this image, there is a large structure (the Coma cluster) that occupies a considerable region of the field-of-view. Depending on where this source is located, pixels with different vignetting values will be masked, so the normalization value calculating the total flux of the whole image will vary depending on where the source is located. To take this into account, normalization is performed by calculating the fraction in flux between the image to be normalized and a reference image in those non masked pixels. Afterwards, the normalization will be given calculating the average of this flux fraction, which is made regardless of which regions of the image are masked, as only factors in flux between the same pixels are taken into account. With this it is possible to increase the precision in the normalization, which will later produce a better quality and better signal to noise in the final flat image. As a reference image, a provisional version of a flat or some masked science image with a low presence of sources in the field of view (a blank-field) can be used.

Finally, by combining the masked images the flat image is obtained. This flat obtained by using science images is commonly called "autoflat". For the combination, as in the case of the combination of bias images, a resistant mean is used, rejecting values beyond 3 times the standard deviation. This flat is applied to the images. In Figure 2.4 an example of an image processed with the autoflat technique (left) and the same image processed using twilight flats (right) is shown. As can be seen, there is an important appearance of gradients in the image that uses twilight flats, disappearing in the image processed with the discussed technique.

Este documento incorpora firma electrónica, y es copia auténtica de un documento electrónico archivado por la ULL según la Ley 39/2015.  
 Su autenticidad puede ser contrastada en la siguiente dirección <https://sede.ull.es/validacion/>

Identificador del documento: 2260218      Código de verificación: Sm21pjYh

Firmado por: JAVIER ROMAN GARCIA  
 UNIVERSIDAD DE LA LAGUNA

Fecha: 02/11/2019 16:23:59

IGNACIO TRUJILLO CABRERA  
 UNIVERSIDAD DE LA LAGUNA

02/11/2019 17:39:19

### 2.3 Correction of gradients in adverse circumstances

In the previous Section, the need to control all the steps was discussed, from observational data acquisition to reduction process, with the aim of minimizing gradients. However, since the data usually come from astronomical facilities with their own procedures for data acquisition and processing, it is not possible to have control over all these steps. When the images are taken without the required observational strategy, when the number of science images is insufficient to obtain a high-quality autoflat or for any other reason, the images may appear with gradients. In these occasions, it is sometimes possible to make a correction of the gradients present without reasonably damaging the information of the fainter regions, allowing to obtain competitive images in low surface brightness studies.

A possible correction, provided the gradients are not very strong, is to fit a smooth surface to the final coadd image. To do this, a precise masking of the sources is carried out, preferably with specialized software (`NoiseChisel`; Akhlaghi, & Ichikawa 2015). The aim is that the surface does not fit the outermost and faintest regions of the astronomical sources in the image. In other words, the fitted surface reproduces with great fidelity the true gradient structure, producing an image with great stability without gradients, reliable for low surface brightness science.

Another approach is to perform a secondary flat-fielding correction from the reduced final images, building a flat that contains information on the residual gradients in the images. This is possible when a reduction from scratch is not possible using the raw images and the gradients in the reduced images are predominantly by residuals in the reduction process. The flat obtained from this secondary flat-fielding correction is often called delta-flat. The delta-flat construction is totally equivalent to the autoflat procedure, with the only difference in that already reduced images are used for the construction of the flat instead of the raw images. The use of this secondary flat correction is sometimes very effective, producing gradient-free images.

In general, we can argue that the presence of gradients in the images can be always improved, however the nature of these gradients and the particular circumstances of each data set mean that there is no a general procedure for this correction. Each data set must be evaluated, applying different methodologies depending on their different characteristics.

### 2.4 PSF characterization and removal of the stars

An exquisite characterization of the PSF has become a fundamental requirement in extremely low surface brightness analysis. Both the removal of the scattered light by the stars and the deconvolution of the effect of PSF in galaxies are necessary to make precise photometric measurements in the low surface brightness regime. During this thesis, different techniques have been developed both for obtaining the PSF in any data set and for the removal of the stars. The procedures described below are based on data obtained with the OGS telescope, however this methodology can be applied to any data set in general.

#### Obtaining the PSF

One of the necessary characteristics for the PSF applicable in the low surface brightness regime is a high signal to noise up to far radii, typically several arcminutes. For this, the observation of very bright stars is a requirement. The high luminosity of these stars makes the light scattered

Este documento incorpora firma electrónica, y es copia auténtica de un documento electrónico archivado por la ULL según la Ley 39/2015.  
Su autenticidad puede ser contrastada en la siguiente dirección <https://sede.ull.es/validacion/>

Identificador del documento: 2260218 Código de verificación: Sm21pjYh

Firmado por: JAVIER ROMAN GARCIA  
UNIVERSIDAD DE LA LAGUNA

Fecha: 02/11/2019 16:23:59

IGNACIO TRUJILLO CABRERA  
UNIVERSIDAD DE LA LAGUNA

02/11/2019 17:39:19

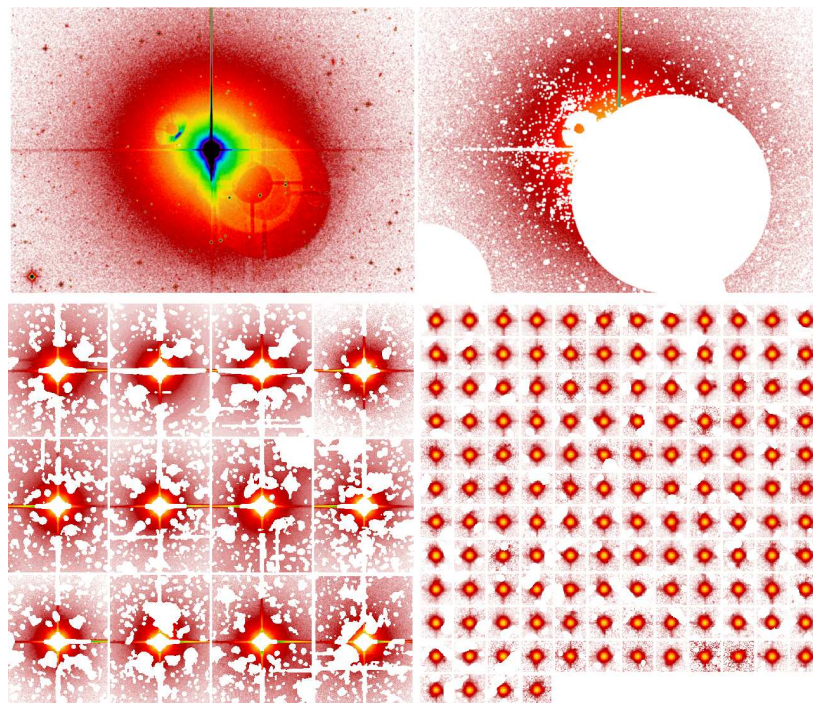


Figure 2.5: Examples of star masking and normalization for the construction of the PSF model. The upper panels show an unmasked magnitude 3 star in the  $R$  band (left panel) and the same image after masking the sources and internal reflections (right panel). The lower left panel shows masked and normalized intermediate magnitude stars used to obtain the PSF model in the aureole region. In the lower right panel, similar but with unsaturated low luminosity stars used for PSF model in the core region. The angular scale of all images is arbitrary, focused on providing detailed visual inspection.

by the PSF at large radii higher than the Poisson noise, and therefore detectable. The usual method to obtain that PSF model is the stacking of very bright stars. Eight stars of magnitude less than 5 were observed for the construction of the PSF in this example. These observations were made with a dithering pattern with the aim that the expected internal reflections, due to the high luminosity of the stars, were located at different positions. Typically, about 9 exposures for each star were made at different positions over the CCD (see Figure 2.2). Previously to perform the stacking of all the stars with the aim of obtaining a PSF model, all the internal reflections must be masked (see Figure 2.5 upper panel). This ensures to consider only for the PSF model the flux by the PSF (light coming from the main optical path without internal reflections due to the optics of the instrumentation). Additionally, all external sources have to be masked. Once the stars are masked, the flux normalization is performed, so that all stars contain a common flux profile prior to the stacking. For this, an aperture radius is selected and the flux of each star

Este documento incorpora firma electrónica, y es copia auténtica de un documento electrónico archivado por la ULL según la Ley 39/2015.  
 Su autenticidad puede ser contrastada en la siguiente dirección <https://sede.ull.es/validacion/>

Identificador del documento: 2260218 Código de verificación: Sm21pjYh

Firmado por: JAVIER ROMAN GARCIA  
 UNIVERSIDAD DE LA LAGUNA

Fecha: 02/11/2019 16:23:59

IGNACIO TRUJILLO CABRERA  
 UNIVERSIDAD DE LA LAGUNA

02/11/2019 17:39:19

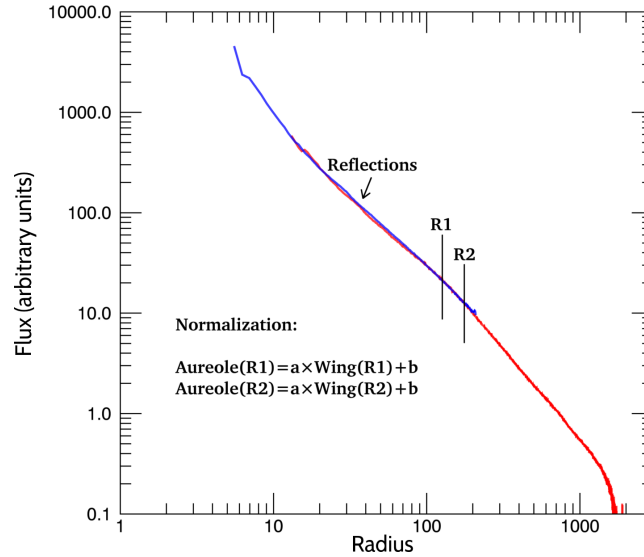


Figure 2.6: Illustrative example of normalization between PSF wing (red profile) and PSF aureole (blue profile). R1 and R2 are the two radii selected for the construction of the system of equations.

to that radius is calculated by means of a surface brightness profile, normalizing the complete image to that value. The specific value of that radius depends on the characteristics of the PSF on the given telescope. In general, a radius should be used where there are no problems due to the presence of artifacts, typically far from the regions affected by bleeding due to saturation, and in a region with high signal to noise in all observed stars. This normalization allows all the stars to have a common profile. Finally, all the stars are combined by a resistant mean statistic, producing the PSF model. However, due to the presence of saturation, the centers of the bright stars do not represent the true PSF. To deal with this issue, the same procedure is carried out with stars of fainter brightness. In this specific case, due to the high saturation of stars of such high luminosity, stars of intermediate magnitude are selected to provide a model covering these saturated regions with enough signal to noise. However, stars able to cover such a wide area are still saturated in the very center. To complete the innermost region, low luminosity and unsaturated stars are selected (see Figure 2.5 lower panels). With this, 3 different PSF models representative of different regions of the global PSF model are obtained: wing, aureole and core region, representing the outermost, intermediate and innermost regions respectively.

A key point to address is the junction of the different regions of the PSF to obtain the global PSF model. First, a precise calibration of the sky of the PSF wing is performed. However, for PSFs representing the aureole and core regions, it is not possible to obtain a sky reference level, since by definition any sky obtained in regions near these stars will not be zero but the flux of the PSF wing at this radii. That makes 2 parameters necessary to combine the PSF models at different regions: the flux normalization value ( $a$ ) and the reference sky background

Este documento incorpora firma electrónica, y es copia auténtica de un documento electrónico archivado por la ULL según la Ley 39/2015.  
 Su autenticidad puede ser contrastada en la siguiente dirección <https://sede.ull.es/validacion/>

Identificador del documento: 2260218 Código de verificación: Sm21pjYh

Firmado por: JAVIER ROMAN GARCIA  
 UNIVERSIDAD DE LA LAGUNA

Fecha: 02/11/2019 16:23:59

IGNACIO TRUJILLO CABRERA  
 UNIVERSIDAD DE LA LAGUNA

02/11/2019 17:39:19

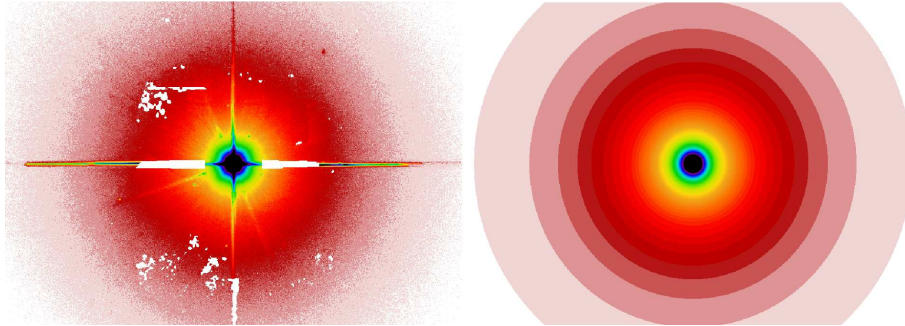


Figure 2.7: Example of PSF symmetrization. Left panel: PSF model obtained for the OGS telescope. Right panel: Symmetric PSF.

value ( $b$ ) such that their profiles match perfectly. We solve a system of equations to obtain the values  $a$  and  $b$ .  $R_1$  and  $R_2$  (see Figure 2.6) are 2 radii where the flux values in the profile of the PSF wing and aureole are reliable. Solving the system of equations gives the values  $a$  and  $b$  that are applied to the PSF aureole. Finally, the junction of both is done by assigning the flux value of the PSF aureole to the PSF wing in the regions where saturation is present. Performing this procedure between the combined PSF wing + aureole with the PSF core, the complete PSF model is obtained. It is worth mentioning that the number of PSFs models in different regions depends on the characteristics of the stars used for the construction of the final PSF according with reflections and saturations. Therefore any number of different models can be used to complete different regions of the PSF.

The final PSF model is shown in Figure 2.7 (left panel). As can be seen, there are different regions that still remain masked due to the lack of pixels during the combination (due to sources or internal reflections in those regions). There are also bleeding lines, different reflections of stray-light and also the spike lines due to the structure that holds the secondary mirror. To obtain a complete model and with the aim of increasing the signal to noise of the PSF is usual to proceed with the symmetrization of the PSF model in those cases where the PSF is circularly symmetric. For this, the average flux value on a photometric profile of the PSF model is constructed. Subsequently, for each pixel of the 2-dimensional symmetric PSF model, the corresponding flux value is assigned from the profile according to its radius from the center of the PSF. Figure 2.7 (right panel) shows the result of the symmetrization of the PSF model. Cases as PSFs in drift-scan mode, such as SDSS data, in which the PSF is elongated along the drift direction, are not symmetrizable (see Section 3.6). All procedures for obtaining the PSF model were performed with a set of subroutines specifically created in this thesis for PSF modeling, and can be used for any data set of different characteristics.

#### Removal of the scattered light produced by the stars

The removal of the stars using the PSF model is a procedure that is becoming common in the analysis of deep images. For instance, Slater et al. (2009) modeled the internal reflections

Este documento incorpora firma electrónica, y es copia auténtica de un documento electrónico archivado por la ULL según la Ley 39/2015.  
 Su autenticidad puede ser contrastada en la siguiente dirección <https://sede.ull.es/validacion/>

Identificador del documento: 2260218 Código de verificación: Sm21pjYh

Firmado por: JAVIER ROMAN GARCIA  
 UNIVERSIDAD DE LA LAGUNA

Fecha: 02/11/2019 16:23:59

IGNACIO TRUJILLO CABRERA  
 UNIVERSIDAD DE LA LAGUNA

02/11/2019 17:39:19

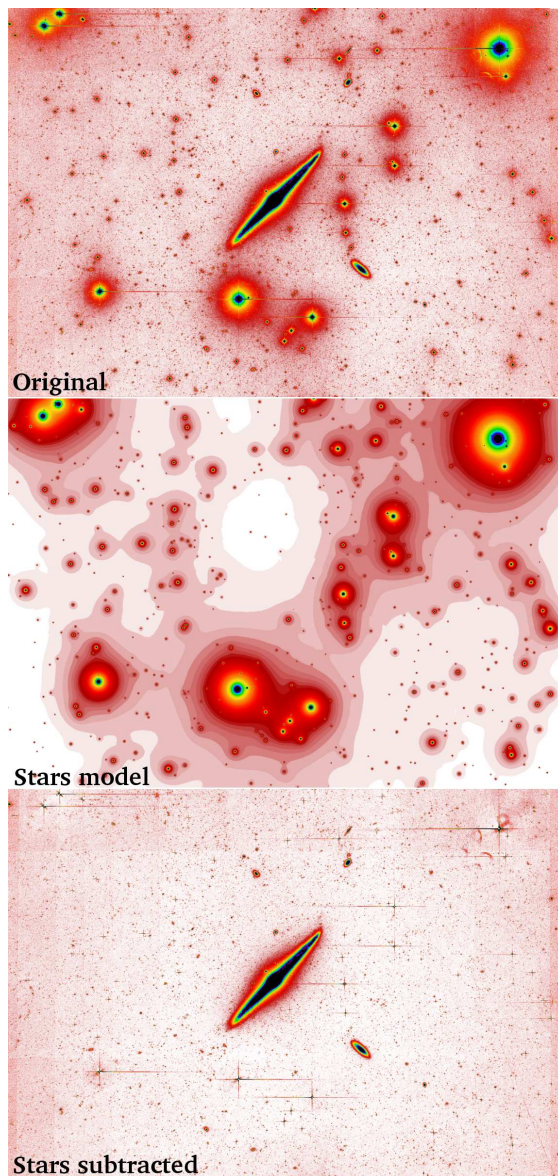


Figure 2.8: Example of the removal of the scattered light produced by the stars in the NGC 4565 galaxy field.

Este documento incorpora firma electrónica, y es copia auténtica de un documento electrónico archivado por la ULL según la Ley 39/2015.  
Su autenticidad puede ser contrastada en la siguiente dirección <https://sede.ull.es/validacion/>

Identificador del documento: 2260218 Código de verificación: Sm21pjYh

Firmado por: JAVIER ROMAN GARCIA  
UNIVERSIDAD DE LA LAGUNA

Fecha: 02/11/2019 16:23:59

IGNACIO TRUJILLO CABRERA  
UNIVERSIDAD DE LA LAGUNA

02/11/2019 17:39:19

produced by the stars with the Burrell Schmidt telescope (Rudick et al. 2010; Watkins et al. 2014, 2015, 2016, 2017; Mihos et al. 2017; Watkins et al. 2018). Trujillo & Fliri (2016) modeled the scattered light produced by stars in very deep observations of the UGC 00180 galaxy using a PSF characterization of the 10.4m GTC telescope and Karabal et al. (2017) modeled the internal reflections and PSF using images of the Canada France Hawaii Telescope (CFHT) to provide reliable deep photometry of galaxies.

During the course of this thesis, an automatic pipeline has been made for the removal of the scattered light produced by the stars in any data set, subsequent to the characterization of the PSF. Specific details of the operation of this pipeline can be found in Section 3.6. Figure 2.8 shows an example of the removal of the stars by characterizing the PSF of the OGS telescope in the field of the NGC 4565 galaxy.

## 2.5 Big data analysis of astronomical surveys

One of the fundamental aspects in deep imaging is the search for new sources of extreme low surface brightness. It requires automatic tools to detect these new sources. Data processing in a massive and unsupervised way is one of the main problems facing the new generation of ultra-deep surveys. The need to obtain a large number of parameters for the huge number of astronomical sources requires specific tools of great reliability with which to be able to extract useful information and with great efficiency in computational time. Although the identification of these sources is possible through visual inspection, due to the large volume of data, human supervision is not feasible. Additionally, just visually it is not possible to obtain specific parameters such as effective radii, surface brightness or any other parameter of interest.

In this thesis, a fully automatic pipeline has been developed for the search of objects with extreme low surface brightness, specifically the detection of the so-called ultra-diffuse galaxies (e.g. van Dokkum et al. 2015; Koda et al. 2015). The goal of this pipeline is the filtering of the hundreds of thousands of sources present in the data, obtaining those sources with the required characteristics as surface brightness, effective radius or colors among other parameters. This pipeline has been very effective producing important results, and specific details about its operation can be found in Sections 3.2 and 3.3.

Este documento incorpora firma electrónica, y es copia auténtica de un documento electrónico archivado por la ULL según la Ley 39/2015.  
Su autenticidad puede ser contrastada en la siguiente dirección <https://sede.ull.es/validacion/>

Identificador del documento: 2260218 Código de verificación: Sm21pjYh

Firmado por: JAVIER ROMAN GARCIA  
UNIVERSIDAD DE LA LAGUNA

Fecha: 02/11/2019 16:23:59

IGNACIO TRUJILLO CABRERA  
UNIVERSIDAD DE LA LAGUNA

02/11/2019 17:39:19

## 3

### Compendium of articles

#### 3.1 Paper I: *The IAC Stripe82 Legacy Survey: Improved Sky-rectified Images*

During the combination process of the final coadded images of the IAC Stripe82 Legacy Survey, some residuals perpendicular to the drift scan direction were still present. These residuals were partially removed in a first rectified version presented by Trujillo & Fliri (2016). In the following contribution, a specific pipeline was developed for the Stripe82 data in which the removal of these residuals was almost complete. This pipeline was run for the full IAC Stripe82 Legacy Survey data set, updating the rectified version by the one developed in this work. This new rectified version allows the use of Stripe82 data for the study of extremely faint diffuse sources, such as Galactic cirri, which require great stability of the sky background.

Along with the creation and publication of this new data set, an update of the project's website was made: <http://research.iac.es/proyecto/stripe82/>, including different advanced data products such as galaxy group catalogs, and up-to-date information.

XLV

Este documento incorpora firma electrónica, y es copia auténtica de un documento electrónico archivado por la ULL según la Ley 39/2015.  
Su autenticidad puede ser contrastada en la siguiente dirección <https://sede.ull.es/validacion/>

Identificador del documento: 2260218 Código de verificación: Sm21pjYh

Firmado por: JAVIER ROMAN GARCIA  
UNIVERSIDAD DE LA LAGUNA

Fecha: 02/11/2019 16:23:59

IGNACIO TRUJILLO CABRERA  
UNIVERSIDAD DE LA LAGUNA

02/11/2019 17:39:19

DRAFT VERSION AUGUST 9, 2018  
 Typeset using L<sup>A</sup>T<sub>E</sub>X RNAAS style in AASTeX62

THE IAC STRIPE82 LEGACY SURVEY: IMPROVED SKY-RECTIFIED IMAGES

Javier Román<sup>1,2</sup> and Ignacio Trujillo<sup>1,2</sup>

<sup>1</sup>Instituto de Astrofísica de Canarias, c/ Vía Láctea s/n, E-38205, La Laguna, Tenerife, Spain

<sup>2</sup>Departamento de Astrofísica, Universidad de La Laguna, E-38205 La Laguna, Tenerife, Spain

*Keywords:* atlases – catalogs – surveys – stars: general – galaxies: general

THE IAC STRIPE82 LEGACY SURVEY

The combination of better observational strategies and new instrumentation has allowed the building of large imaging surveys one order of magnitude deeper than current popular datasets such as the Sloan Digital Sky Survey (SDSS). Such advances have opened up the possibility of exploring the low surface brightness Universe with unprecedented precision (see e.g. Trujillo & Fliri 2016) allowing detailed studies of very low surface brightness galaxies, intra-cluster light and galactic Cirri (among other topics). Amid this new set of deep imaging surveys, the IAC Stripe 82 Legacy Survey (Fliri & Trujillo 2016) is playing a significant role (see e.g. Meusinger et al. 2017; Trujillo et al. 2017; Román & Trujillo 2017a,b; Peters et al. 2017).

The IAC Stripe 82 Legacy Survey is a new co-addition of the SDSS Stripe 82 data (Abazajian et al. 2009), especially reduced to preserve the faintest surface brightness features of this data set. The survey maps a 2.5 degree wide stripe along the Celestial Equator in the Southern Galactic Cap ( $-50^\circ < \text{R.A.} < 60^\circ$ ,  $-1.25^\circ < \text{Dec.} < 1.25^\circ$ ) with a total of 275 square degrees in all the five SDSS filters ( $u, g, r, i, z$ ). The new reduction includes an additional (deeper) band ( $r_{\text{deep}}$ ), which is a combination of  $g$ ,  $r$  and  $i$  bands. The average seeing of the Stripe82 dataset is around 1 arcsec. The mean surface brightness limits are  $\mu_{\text{lim}}[3\sigma, 10 \times 10 \text{ arcsec}^2] = 27.9, 29.1, 28.6, 28.1$  and  $26.7 \text{ mag arcsec}^{-2}$  for the  $u, g, r, i$  and  $z$  bands respectively. The significant depth of the data and the emphasis on preserving the characteristics of the background (sky + diffuse light) through a non-aggressive sky subtraction strategy make this dataset suitable for the study of the low surface brightness Universe. In this research note we present a new data release with improved sky-rectified images. This new data-set is published on the survey webpage (<http://www.iac.es/proyecto/stripe82/>) and is publicly available for the community.

THE NEW SKY-RECTIFIED CO-ADDS

Although the coadded images of the IAC Stripe 82 Legacy Survey were carefully reduced, they still contain some residuals along the direction of the drift-scan which is along the Right Ascension. These residuals are illustrated in Fig. 1 and are the result of the different sky brightness in individual exposures that compose the final co-addition. Due to the careful treatment of the sky in the co-adding, the different sky brightness are preserved in the final stacked images showing residuals that can present brightness (in the worst case) as bright as  $26 \text{ mag arcsec}^2$ . A correction of these residuals was already presented in the published version of the survey two years ago (Fliri & Trujillo 2016). Here we present a new version of the sky-rectified images of the IAC Stripe82 Legacy Survey, improving over the previous correction.

The procedure we have followed for producing better sky-rectified images is as follows. To create the masks we use our deepest dataset (i.e. the  $r_{\text{deep}}$  images). Masks of all the sources are obtained using SExtractor (Bertin & Arnouts 1996) on the original coadded images. Later, the masks are enlarged using a Gaussian kernel (with a width of 5 pixels) to include the missing flux beyond the masks provided by SExtractor. Additionally, to account for the diffuse light on the images (as the ones produced by the scattered light of the sources and the Galactic cirri emission) we create an extra mask using SExtractor in background mode, masking the areas above a certain threshold. Once the final mask in the  $r_{\text{deep}}$  band is created, we apply such mask to the rest of the bands. With this treatment the masked images

Corresponding author: Javier Román  
[jroman@iac.es](mailto:jroman@iac.es)

arXiv:1808.02499v1 [astro-ph.GA] 7 Aug 2018

Este documento incorpora firma electrónica, y es copia auténtica de un documento electrónico archivado por la ULL según la Ley 39/2015.  
 Su autenticidad puede ser contrastada en la siguiente dirección <https://sede.ull.es/validacion/>

Identificador del documento: 2260218 Código de verificación: Sm21pjYh

Firmado por: JAVIER ROMAN GARCIA  
 UNIVERSIDAD DE LA LAGUNA

Fecha: 02/11/2019 16:23:59

IGNACIO TRUJILLO CABRERA  
 UNIVERSIDAD DE LA LAGUNA

02/11/2019 17:39:19

3.1 Paper I: *The IAC Stripe82 Legacy Survey: Improved Sky-rectified Images*

2

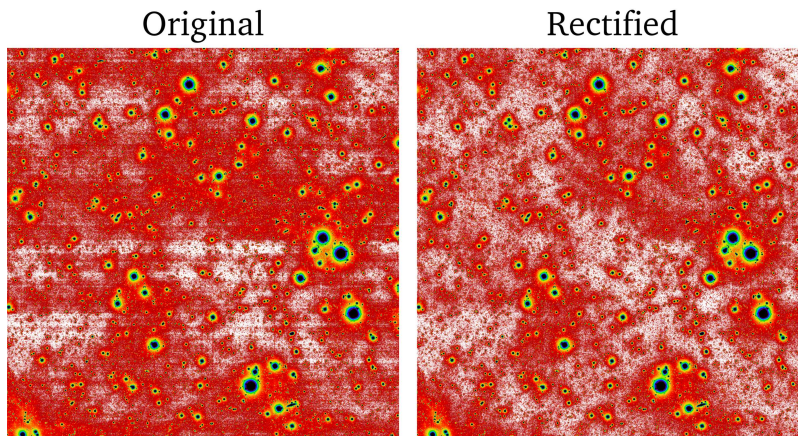


**Figure 1.** Example of the new sky-rectified images of the IAC Stripe82 Legacy Survey. The images are  $0.5^\circ \times 0.5^\circ$  wide. In the left panel the original image (after sky subtraction) is shown. In the right panel, we show the result of the new sky rectification. Both images are produced using the *rdeep* band (i.e. the combination of *g*, *r* and *i* bands). The images have been convolved with a Gaussian kernel of width of 3 pixels to enhance the contrast. This field, centered at R.A. =  $315.25^\circ$  and Dec =  $0.50^\circ$  shows a high contamination by Galactic cirri. The cirri are identified with great clarity in the new sky-rectified image.

only contain pixels which are mainly pure sky, or in the worst case, regions with a very weak contamination by diffuse light. The masked images are then used to estimate the global sky value. We associate such a value to each image as a reference to the sky in that image. In addition, the sky is measured along each pixel row of the image so as to follow the symmetry of the sky residuals (i.e. horizontal lines). We evaluate the difference between such sky row value and the global value and we remove/add such difference to every row. These differences, which are measured in the masked images, are applied to the images without masking, resulting in the sky-rectified images shown in Fig. 1.

The result of the sky rectification is a significant improvement in the quality of the images, showing now a homogeneous sky. The new sky-rectified data allows an accurate photometry of extremely low (fainter than  $26 \text{ mag arcsec}^{-2}$ ) surface brightness structures, such as the emission by Galactic dust clouds in the Stripe82 area. The sky-rectified images are systematically deeper than the original sky subtracted ones. The improvement in the depth of the images can reach up to  $0.1 \text{ mag arcsec}^{-2}$  in the case of fields heavily contaminated by diffuse emission.

We thank Juergen Fliri for his excellent work on the construction of the IAC Stripe82 Legacy Survey. We also thank Nushkia Chamba for her comments.

Este documento incorpora firma electrónica, y es copia auténtica de un documento electrónico archivado por la ULL según la Ley 39/2015.  
 Su autenticidad puede ser contrastada en la siguiente dirección <https://sede.ull.es/validacion/>

Identificador del documento: 2260218 Código de verificación: Sm21pjYh

Firmado por: JAVIER ROMAN GARCIA  
 UNIVERSIDAD DE LA LAGUNA

Fecha: 02/11/2019 16:23:59

IGNACIO TRUJILLO CABRERA  
 UNIVERSIDAD DE LA LAGUNA

02/11/2019 17:39:19

REFERENCES

- Abazajian, K. N., Adelman-McCarthy, J. K., Agüeros, M. A., et al. 2009, ApJS, 182, 543-558  
Bertin, E., & Arnouts, S. 1996, A&AS, 117, 393  
Fliri, J., & Trujillo, I. 2016, MNRAS, 456, 1359  
Meusinger, H., Brünecke, J., Schalldach, P., & in der Au, A. 2017, A&A, 597, A134  
Peters, S. P. C., van der Kruit, P. C., Knapen, J. H., et al. 2017, MNRAS, 470, 427  
Román, J., & Trujillo, I. 2017, MNRAS, 468, 703  
Román, J., & Trujillo, I. 2017, MNRAS, 468, 4039  
Trujillo, I., & Fliri, J. 2016, ApJ, 823, 123  
Trujillo, I., Roman, J., Filho, M., & Sánchez Almeida, J. 2017, ApJ, 836, 191

Este documento incorpora firma electrónica, y es copia auténtica de un documento electrónico archivado por la ULL según la Ley 39/2015.  
Su autenticidad puede ser contrastada en la siguiente dirección <https://sede.ull.es/validacion/>

Identificador del documento: 2260218 Código de verificación: Sm21pjYh

Firmado por: JAVIER ROMAN GARCIA  
UNIVERSIDAD DE LA LAGUNA

Fecha: 02/11/2019 16:23:59

IGNACIO TRUJILLO CABRERA  
UNIVERSIDAD DE LA LAGUNA

02/11/2019 17:39:19

3.2 Paper II: *Spatial distribution of ultra-diffuse galaxies within large-scale structures*

XLIX

### 3.2 Paper II: *Spatial distribution of ultra-diffuse galaxies within large-scale structures*

After the work by van Dokkum et al. (2015) identifying a subset of low surface brightness ( $\mu_g(0) > 24 \text{ mag arcsec}^{-2}$ ), large effective radius ( $r_{eff} > 1.5 \text{ kpc}$ ) galaxies in the Coma cluster, the extragalactic community embarked on a frantic race in the study of these objects. At the time of publication of this article, ultra-diffuse galaxies had been studied only in galaxy clusters<sup>1</sup>: Coma cluster (Koda et al. 2015), Fornax cluster (Muñoz et al. 2015) and different nearby clusters (van der Burg et al. 2016).

One of the hypotheses (proposed by van Dokkum et al. 2015) for the existence of these galaxies was considering them Milky Way analogues (with similar halo mass and effective radius, "MW-like") that failed the formation of a similar amount of stars to that of the MW in the environment of galaxy clusters in which they were detected systematically. This would make ultra-diffuse galaxies objects intrinsically localized in galaxy clusters. Conversely, if ultra-diffuse galaxies are inherently low-luminosity objects (dwarf galaxies with very large effective radius), it is expected that they will be found in any kind of environment. In this sense, the above-mentioned works would be biased only exploring the presence of ultra-diffuse galaxies in clusters, obviating their possible presence in lower-density environments.

In order to explore the presence of ultra-diffuse galaxies in any type of environment, an 8x8 Mpc area centered around the Abell 168 galaxy cluster was selected. This area contains different structures such as a cluster of galaxies, different subgroups of lower mass and very low-density areas. Due to the huge number of sources in such a large area ( $2.5^\circ \times 2.5^\circ$ ), specific pipelines were designed for big data analysis. It should be noted that for the selection of objects with specific structural parameters, such as the central surface brightness or the effective radius, there is a need to perform modeling fitting, for example a Sersic model, to obtain these parameters. These fittings are very expensive from the point of view of computational time and difficult to manage due to the need of processes such as precise masking and accurate photometric measurements in extremely faint sources, in an unsupervised and automatic way. Given the huge number of sources in this large area, of the order of hundreds of thousands, each with different circumstances of deblending, crowding, morphology, etc, specific codes in which to be able to filter sources hierarchically according to different criteria, and applying different processes to each type of source, are necessary.

The most noteworthy result in this work is the first evidence of ultra-diffuse galaxies outside clusters, specifically in groups of galaxies, as can be seen in Figure 6 of this article. The spatial distribution and colors of ultra-diffuse galaxies were also compared with those of dwarf galaxies and MW-like galaxies, finding comparable spatial distribution and colors to those of dwarf galaxies being different from MW-like objects. These findings provided arguments in favor of the "dwarf nature" of ultra-diffuse galaxies.

<sup>1</sup>It is worth commenting that objects with similar characteristics to the so-called "ultra-diffuse galaxies" were reported decades ago (e.g. Sandage & Binggeli 1984; Ferguson & Sandage 1988; Impey et al. 1988; Bothun et al. 1991; Dalcanton et al. 1997; Conselice et al. 2003) as we show in the introduction of this and any article in this thesis about ultra-diffuse galaxies.

Este documento incorpora firma electrónica, y es copia auténtica de un documento electrónico archivado por la ULL según la Ley 39/2015.  
Su autenticidad puede ser contrastada en la siguiente dirección <https://sede.ull.es/validacion/>

Identificador del documento: 2260218 Código de verificación: Sm21pjYh

Firmado por: JAVIER ROMAN GARCIA  
UNIVERSIDAD DE LA LAGUNA

Fecha: 02/11/2019 16:23:59

IGNACIO TRUJILLO CABRERA  
UNIVERSIDAD DE LA LAGUNA

02/11/2019 17:39:19

## Spatial distribution of ultra-diffuse galaxies within large-scale structures

Javier Román<sup>1,2\*</sup> and Ignacio Trujillo<sup>1,2</sup>

<sup>1</sup>Instituto de Astrofísica de Canarias, c/ Vía Láctea s/n, E-38205, La Laguna, Tenerife, Spain  
<sup>2</sup>Departamento de Astrofísica, Universidad de La Laguna, E-38206, La Laguna, Tenerife, Spain

Accepted 2017 February 16. Received 2017 February 7; in original form 2016 March 10

### ABSTRACT

Taking advantage of the Sloan Digital Sky Survey Stripe82 data, we have explored the spatial distribution of ultra-diffuse galaxies (UDGs) within an area of  $8 \times 8$  Mpc<sup>2</sup> centred around the galaxy cluster Abell 168 ( $z = 0.045$ ). This intermediate massive cluster ( $\sigma = 550$  km s<sup>-1</sup>) is surrounded by a complex large-scale structure. Our work confirms the presence of UDGs in the cluster and in the large-scale structure that surrounds it, and it is the first detection of UDGs outside clusters. Approximately 50 per cent of the UDGs analysed in the selected area inhabit the cluster region ( $\sim 11 \pm 5$  per cent in the core and  $\sim 39 \pm 9$  per cent in the outskirts), whereas the remaining UDGs are found outside the main cluster structure ( $\sim 50 \pm 11$  per cent). The colours and the spatial distribution of the UDGs within this large-scale structure are more similar to dwarf galaxies than to  $L_*$  galaxies, suggesting that most UDGs could be bona fide dwarf galaxies.

**Key words:** galaxies: dwarf – galaxies: evolution – galaxies: formation – galaxies: photometry – galaxies: structure.

### 1 INTRODUCTION

Following pioneering work by Impey, Bothun & Malin (1988), Bothun, Impey & Malin (1991) and Dalcanton et al. (1997), a number of recent works (e.g. Koda et al. 2015; Mihos et al. 2015; van Dokkum et al. 2015a; van der Burg, Muzzin & Hoekstra 2016), using deep imaging of nearby clusters, have focused their attention on a type of galaxy that has low mass ( $10^7$ – $10^8$  M<sub>⊙</sub>), low surface brightness ( $24 < \mu_g(0) < 26$  mag arcsec<sup>-2</sup>) and extended size ( $1.5 < r_e < 4.5$  kpc). van Dokkum et al. (2015a) have called these objects ultra-diffuse galaxies (UDGs). To date, UDGs have been found mostly in galaxy clusters. However, it is unclear whether this is just a bias produced by the strategy used to detect these objects. Because of their extreme low surface brightness, it is very time-consuming to obtain a spectroscopic redshift of these galaxies, and their redshifts have been estimated by their proximity to a high-density region. In fact, of the two UDGs confirmed spectroscopically (van Dokkum et al. 2015b; Martínez-Delgado et al. 2016), one is in Coma and the other is in a much lower density environment. Moreover, there are also a small number of large, low surface brightness galaxies known in the field (Dalcanton et al. 1997; Burkholder, Impey & Sprayberry 2001). None the less, despite the observational bias towards galaxy clusters, the fact that the number of UDGs increases with cluster richness (van der Burg et al. 2016), with almost a doubling of the population of known galaxies in Coma (Koda et al. 2015) to barely adding a few candidates in Fornax (Muñoz

et al. 2015), suggests that the environmental density could play a role in the origin of UDGs.

From the theoretical point of view, Yozin & Bekki (2015) have shown that a scenario in which UDGs are satellites of a cluster, having infallen early at  $z \sim 2$  and quenching their further growth, is able to reproduce the structural properties of these objects. Interestingly, one of the predictions of this scenario is that UDGs should not survive close to the centre of clusters, as tides exerted by the cluster mass within that region will disrupt the infalling UDGs. This seems to be in agreement with the findings of van der Burg et al. (2016). For all the above reasons, it is clear that understanding in which environments UDGs are originally formed – i.e. whether they have been formed *in situ* in the clusters or whether they have been accreted through infalling substructures (group, filaments) – is fundamental to disentangle the origin of these mysterious galaxies. Another key feature to better understand the nature of UDGs is to compare their spatial distribution with two different families of galaxies: dwarf versus  $L_*$ . Among other scenarios, van Dokkum et al. (2015a) discuss the intriguing possibility that UDGs are failed  $L_*$  galaxies. Other works have explored the possibility that UDGs are regular dwarf galaxies embedded in very massive dark matter haloes (e.g. Beasley et al. 2016), dwarf galaxies inhabiting high-spin haloes (Amorisco & Loeb 2016), failed Large Magellanic Cloud (LMC)-like galaxies (Beasley & Trujillo 2016) or pure stellar halo galaxies (Peng & Lim 2016). We can shed extra light on the origin of these galaxies by addressing which spatial distribution UDGs resemble most.

In this paper, we explore the distribution and properties of the population of UDGs inside and around the Abell 168 galaxy cluster

\*E-mail: jroman@iac.es

Este documento incorpora firma electrónica, y es copia auténtica de un documento electrónico archivado por la ULL según la Ley 39/2015.  
Su autenticidad puede ser contrastada en la siguiente dirección <https://sede.ull.es/validacion/>

Identificador del documento: 2260218

Código de verificación: Sm21pjYh

Firmado por: JAVIER ROMAN GARCIA  
UNIVERSIDAD DE LA LAGUNA

Fecha: 02/11/2019 16:23:59

IGNACIO TRUJILLO CABRERA  
UNIVERSIDAD DE LA LAGUNA

02/11/2019 17:39:19

3.2 Paper II: *Spatial distribution of ultra-diffuse galaxies within large-scale structures*

LI

704 *J. Román and I. Trujillo*

( $z = 0.045$ ). Abell 168 is a cluster with a richness II–III (BM classification) located at RA(2000) =  $01^{\text{h}} 15^{\text{m}} 12.0^{\text{s}}$  and Dec. (2000) =  $+00^{\circ} 19' 48''$ . This cluster has a velocity dispersion of  $\sigma = 550 \text{ km s}^{-1}$  and a dynamical mass of  $M_{\text{dyn}} = 5.2 \times 10^{14} M_{\odot}$  (Yang et al. 2004). The large-scale structure surrounding this cluster is particularly relevant in order to probe where UDGs inhabit. In fact, there are many filaments and galaxy groups around Abell 168, as well as low-density regions. Our large-scale structure is fully embedded within the Sloan Digital Sky Survey (SDSS) Stripe 82. This means that we have deep photometry in three SDSS bands ( $g = 25.2 \text{ mag}$ ,  $r = 24.7 \text{ mag}$  and  $i = 24.3 \text{ mag}$ ;  $3\sigma$  point sources), which implies having an extra filter compared to previous UDG works in other clusters. We will show that this extra filter is key to cleaning our galaxy sample from background contaminants. This will allow us to select UDGs candidates at the redshift of the cluster, but significantly further away from its centre. To characterize in great detail the large-scale structure around Abell 168, we use the deep spectroscopic coverage of this field produced by the SDSS in this area of the Stripe 82. In this paper, we explore a field of view of  $2.5 \times 2.5$ , equivalent to  $8 \times 8 \text{ Mpc}$  around this cluster.

The structure of the paper is as follows. In Section 2, we describe the data. In Section 3, we explain how UDGs were identified. The structural properties of the UDG sample are detailed in Section 4 and their spatial distribution is explored in Section 5. In Section 6, we address a potential link between UDGs and regular dwarf galaxies. In Section 7, we present a discussion of the results, and finally, in Section 8, we summarize our main findings. Throughout this paper, we adopt the following cosmology:  $\Omega_{\text{m}} = 0.3$ ,  $\Omega_{\Lambda} = 0.7$  and  $H_0 = 70 \text{ km s}^{-1} \text{ Mpc}^{-1}$ . The spatial scale is  $0.885 \text{ kpc}^{-1}$  at the Abell 168 redshift ( $z = 0.045$ ). We use the AB magnitude system in this work.

2 DATA

The images used in this paper were obtained from the Instituto de Astrofísica de Canarias (IAC) Stripe 82 Legacy Survey<sup>1</sup> (Fliri & Trujillo 2016). The IAC Stripe 82 Legacy Survey consists of new deep co-adds of the Stripe 82 data from the SDSS, especially stacked to reach the faintest surface brightness limits of this data set. The average surface brightness limit is  $r \sim 28.5 \text{ mag arcsec}^{-2}$  ( $3\sigma$  obtained in  $10 \times 10 \text{ arcsec}^2$  boxes). The Stripe 82 covers a  $2.5$  wide region along the celestial equator ( $-50^{\circ} < \text{RA} < 60^{\circ}$ ,  $-1:25 < \text{Dec.} < 1:25$ ) with a total of  $275 \text{ deg}^2$ . The pixel scale of the imaging is  $0.396 \text{ arcsec}$ . This region of the sky has been imaged repeatedly approximately 80 times in all five SDSS filters ( $u$ ,  $g$ ,  $r$ ,  $i$  and  $z$ ). The IAC project provides the imaging data set in  $0.5 \times 0.5$  blocks. We created a final mosaic of  $2.5 \times 2.5$  using SWARP<sup>2</sup> (Bertin et al. 2002) centred approximately at the coordinates of the Abell 168 cluster (RA =  $18^{\text{h}} 8$ , Dec. =  $0^{\circ} 33$ ). The limiting surface brightness of the entire region was measured in each  $0.5 \times 0.5$  block. We have found that the surface brightness depth across the whole area is reasonably homogeneous, with a mean depth at the  $3\sigma$  level (in  $10 \times 10 \text{ arcsec}^2$  boxes) of  $29.2$ ,  $28.7$  and  $28.2 \text{ mag arcsec}^{-2}$  in the  $g$ ,  $r$  and  $i$  filters, respectively.

<sup>1</sup> <http://www.iac.es/proyecto/stripe82/>

<sup>2</sup> <http://www.astromatic.net/software/swarp>

MNRAS **468**, 703–716 (2017)

3 IDENTIFICATION

The goal of this paper is to find UDGs inside and around Abell 168. With this aim, we ran `SEXTRACTOR` (Bertin & Arnouts 1996) on the entire mosaic in the above three filters, plus another filter provided by the IAC project,  $r$ -deep, which is the combination of  $g$ ,  $r$  and  $i$ . As we are interested in the detection of extended sources with very low surface brightness, we use a detection threshold in all the bands of  $1\sigma$  and a minimum area of  $25 \text{ pixels}$  (i.e.  $4 \text{ arcsec}^2$  or  $3 \text{ kpc}^2$  at the cluster redshift). With these settings, `SEXTRACTOR` found a total of  $331\,891$  sources in the  $r$ -deep filter. We further reduced our list of galaxies by requesting that the sources were identified in all the above bands. In addition, all the sources are selected to have simultaneously a stellarity (`CLASS_STAR`) below  $0.15$  in each filter (to avoid selecting point-like objects).

The next selection criterion is based on the photometric colour (`MAG_AUTO`) of the sources. We conservatively select the following ranges:  $0 < g - r < 1.2$ ,  $0 < g - i < 1.7$  and  $-0.2 < r - i < 0.7$ . These colour intervals are broader than the expected colour values for the galaxy population (red and blue) at the cluster redshift (as we will show later). After all these selection criteria, we are left with  $75\,666$  galaxies.

The identification of UDGs requires a measurement of the size and surface brightness of the galaxies. For this reason, on all the pre-selected galaxies we ran the `IMFIT` code (Erwin 2015). We used a Sérsic model (Sérsic 1968) to extract the structural parameters of our pre-selected galaxies. We provided as input parameters for `IMFIT` the coordinates of the source, position angle and effective radius retrieved from the `SEXTRACTOR` run. `IMFIT` ran over the  $g$ ,  $r$  and  $i$  filters. For each individual fitting, we masked all the pixels of nearby sources detected by `SEXTRACTOR`. The Sérsic models were convolved with the point spread function (PSF) of the images. These PSFs are provided by the IAC Stripe 82 Legacy Survey for each individual block.

The structural parameters obtained from the Sérsic fit are position angle, ellipticity, Sérsic index  $n$ , effective radius  $r_e$  and total magnitude in each filter. Up to three slightly different input parameters in each individual fitting have been tried to ensure robustness of the output structural parameters of `IMFIT`. In most cases, the difference between the `IMFIT` results is negligible, but to be consistent we use the mean values of these three outputs. We compare the magnitude and effective radius values from `IMFIT` and `SEXTRACTOR` as a quality check of the fitting process, and we obtain a very good correlation between both magnitudes and a reasonably good correlation for the effective radii (see Fig. B1). The `SEXTRACTOR` effective radius value does not account for the PSF effect, so it is expected that these values will be slightly larger than those obtained by the `IMFIT` code, particularly for the most compact objects. Sources showing large magnitude differences ( $> 1 \text{ mag}$ ) between `IMFIT` and `SEXTRACTOR` were flagged and visually inspected. These objects represent a tiny fraction of the total number of fitted sources ( $\sim 0.5$  per cent in the  $g$  band). They are usually artefacts of the image, interacting galaxies, very bright galaxies with multiple pieces detected by `SEXTRACTOR`, bad fits of the `IMFIT` code, etc. We do not consider further these objects in the analysis.

3.1 Selection of ultra-diffuse galaxies

Following previous works in the literature, the selection of UDGs in our field is based on the size and surface brightness of the galaxies. We use the structural parameters (magnitude, effective radius,  $n$  and ellipticity) provided by `IMFIT` to perform our final cut. The

Downloaded from <https://academic.oup.com/mnras/article-abstract/468/1/703/3009801> by Instituto de Astrofísica de Canarias user on 30 August 2019

Este documento incorpora firma electrónica, y es copia auténtica de un documento electrónico archivado por la ULL según la Ley 39/2015.  
 Su autenticidad puede ser contrastada en la siguiente dirección <https://sede.ull.es/validacion/>

Identificador del documento: 2260218

Código de verificación: Sm21pjYh

Firmado por: JAVIER ROMAN GARCIA  
 UNIVERSIDAD DE LA LAGUNA

Fecha: 02/11/2019 16:23:59

IGNACIO TRUJILLO CABRERA  
 UNIVERSIDAD DE LA LAGUNA

02/11/2019 17:39:19

Spatial distribution of UDGs within large-scale structures 705

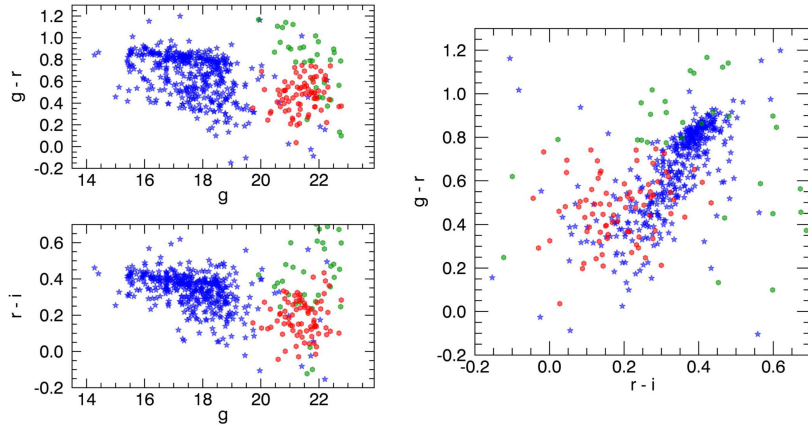


**Figure 1.** Colour–magnitude and colour–colour maps of the galaxies in the field of view of Abell 168. The blue stars correspond to galaxies in the area of Abell 168 with spectroscopic redshifts  $0.037 < z < 0.052$ . The red circles are the UDG candidates that have been selected as compatible with being at the cluster redshift using the colour distribution of the galaxies with spectroscopic redshifts. The green circles are those UDG candidates considered as potential contaminants because of their colours.

magnitudes of the galaxies were corrected by the dust extinction of our Galaxy. Across our field of view, the dust extinction is relatively homogeneous and we select the following corrections: 0.098, 0.068 and 0.051 mag for the  $g$ ,  $r$  and  $i$  filters, respectively (Schlafly & Finkbeiner 2011). Because of the low redshift of our galaxies,  $z \sim 0.045$ , the  $K$ -corrections are very small,  $K_g \sim 0.05$  (Chilingarian, Melchior & Zolotukhin 2010)<sup>3</sup> and therefore we have not corrected our galaxies for this effect.

Assuming that UDGs are well described by an exponential light distribution, van Dokkum et al. (2015a) use the following criteria to select them:  $\mu_g(0) > 24$  mag arcsec<sup>-2</sup> and semimajor effective radius  $r_e > 1.5$  kpc. By analysing a large number of UDG candidates, Koda et al. (2015) show that their Sérsic index  $n$  distribution peaks towards slightly lower values than  $n = 1$  (see their fig. 4). They also find that their axial ratio distribution has a broad shape with a maximum around 0.75. Based on this, we use the following criteria.

(i) We use  $\mu_g(0) > 24.0$  mag arcsec<sup>-2</sup> after correction by dust extinction, where  $\mu_g(0)$  is obtained using a Sérsic model with  $n$  free.

(ii) We use circularized  $R_e > 1.25$  kpc. Taking into account the typical axial ratio measured for these objects, this is equivalent to selecting galaxies with semimajor effective radius  $r_e \gtrsim 1.5$  kpc.

After applying these criteria, we obtain 124 UDG candidates. All these candidates were visually inspected in order to eliminate artefacts misclassified as real UDGs. Examples of incorrectly detected UDGs are either groups of sources detected as a single object by `SETRACTOR` or mergers of galaxies. To visually discard some of these contaminants, we took advantage of colour stamps created by

the combination of  $g$ ,  $r$  and  $i$  filters. After this visual inspection, we are left with 113 galaxies.

The next step is to select the UDGs that are at the distance of the Abell 168 structure and its surroundings. Lacking spectroscopic redshifts for our faint sources, the approach we have followed is to study the colour distribution of the galaxies with spectroscopic redshifts in the field compatible with being at the cluster redshift (i.e.  $z = 0.045$ ). In particular, we have selected all the galaxies with spectroscopic redshifts  $0.037 < z < 0.052$  (i.e. those compatible with being within  $3\sigma$  of the velocity distribution of the Abell 168 cluster and the observed redshift distribution around this peak in the redshift histogram). The colour–magnitude and colour–colour maps for these spectroscopic sources are presented in Fig. 1. The limiting apparent magnitude in this field for having spectroscopic redshift is  $g \sim 19$  mag. Fig. 1 shows that galaxies with spectroscopic redshifts have a broad distribution in colour, ranging from red galaxies defining a clear red sequence to objects following a blue cloud. The individual error in magnitude for each of the sources is key to characterize the broadening of the colour distribution,<sup>4</sup> particularly in the colour–colour maps. We have used the regular SDSS photometric data for our spectroscopic sources (these data are  $\sim 2$  mag shallower than Stripe 82). By doing this, we obtain (for the faintest galaxy with spectroscopic redshift) an uncertainty in the colour–colour map that is close to the one we obtain for the  $\sim 2$  mag fainter UDGs using Stripe 82 data.

The final step is to separate galaxies compatible with having the same colour distribution as the spectroscopic sample. For this

<sup>4</sup>The magnitude uncertainty for each of our UDG candidates is  $\sigma_g = 0.07$  mag,  $\sigma_r = 0.07$  mag and  $\sigma_i = 0.11$  mag. These values are obtained by comparing the magnitudes obtained in `DMFIT` versus `SETRACTOR` for galaxies in the range  $20.5 < g < 22.5$ .

<sup>3</sup> See, for example, <http://kcor.sai.msu.ru/>.

Este documento incorpora firma electrónica, y es copia auténtica de un documento electrónico archivado por la ULL según la Ley 39/2015.  
 Su autenticidad puede ser contrastada en la siguiente dirección <https://sede.ull.es/validacion/>

Identificador del documento: 2260218 Código de verificación: Sm21pjYh

Firmado por: JAVIER ROMAN GARCIA  
 UNIVERSIDAD DE LA LAGUNA

Fecha: 02/11/2019 16:23:59

IGNACIO TRUJILLO CABRERA  
 UNIVERSIDAD DE LA LAGUNA

02/11/2019 17:39:19

706 *J. Román and I. Trujillo*

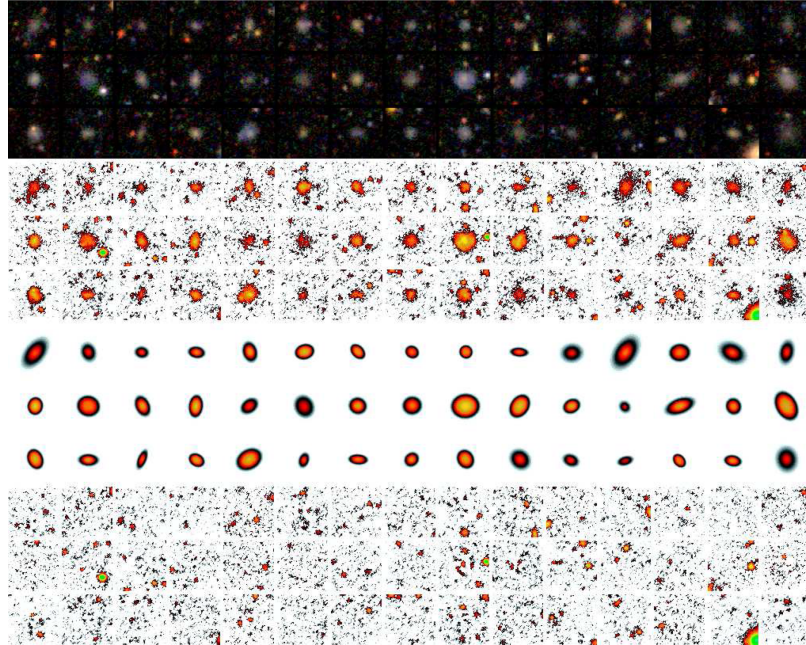


**Figure 2.** Mosaic showing a representative example of the UDGs explored in this paper. The colour stamps have been created using the filters  $g$ ,  $r$  and  $i$ . The second row of images are the same galaxies in the  $g$ -band filter. The third row corresponds to the  $mrrr$  model used to parametrize the galaxies. The last set of images shows the residuals after subtracting the  $mrrr$  models from the images.

reason, our final UDG candidates must share the same colour distribution as the spectroscopic sample in the colour-colour map shown in Fig. 1. To do this, we estimate the distance of each of our UDG candidates in the two-dimensional colour space ( $g - r$ ,  $r - i$ ) to the third nearest galaxy with spectroscopy. We select the third nearest object to have a more robust estimation than just using the first. We require that the third object is no further away than 0.2 mag in this colour-colour plane. Additionally, we restrict the colour of our UDGs to  $g - r < 0.75$  and  $r - i < 0.45$ , trying to avoid background contaminants from distant red galaxies. Those UDGs satisfying this criterion are shown with red symbols, and those with colours not compatible with the spectroscopic sample are shown with green dots. Our final sample of UDGs compatible with being at the redshift of Abell 168 consists of 80 objects. A representative sample of these UDGs is shown in Fig. 2. There are 33 galaxies incompatible with being at the cluster distance. This implies a typical contamination level for surveys such as ours that do not have this extra colour of  $\sim 30$  per cent. The average colours of the contaminant galaxies are  $\langle g - r \rangle = 0.75$  (rms = 0.29) and  $\langle r - i \rangle = 0.40$  (rms = 0.21).

MNRAS **468**, 703–716 (2017)

Despite the fact that we use a third filter to clean our sample of contaminants, it is clear that we still should have a level of contamination as a result of foreground and background objects. Not having spectroscopic redshifts, it is difficult to estimate accurately the level of this remaining contamination. Our colour-colour, size and surface brightness selection criteria eliminate most of the background interlopers (at least those with  $z > 0.1$ ). We have explored in Section 5.1 how much of this contamination could still be in place using the vicinity of the UDG candidates to spectroscopic galaxies in the large-scale structure of Abell 168 and the proximity to spectroscopic galaxies as a proxy.

#### 4 PROPERTIES OF THE ULTRA-DIFFUSE GALAXY SAMPLE

Once we have selected the sample of UDGs compatible with being at the redshift of cluster Abell 168, we explore the distribution of their structural properties (see Table B1). This is shown in Fig. 3. We show in the figure, for each filter, the distribution of the Sérsic index  $n$ , the axial ratio, the circularized effective radius  $R_e$  and the

Downloaded from https://academic.oup.com/mnras/article-abstract/468/1/703/5099801 by Instituto de Astrofísica de Canarias user on 30 August 2019

Este documento incorpora firma electrónica, y es copia auténtica de un documento electrónico archivado por la ULL según la Ley 39/2015.  
 Su autenticidad puede ser contrastada en la siguiente dirección <https://sede.ull.es/validacion/>

Identificador del documento: 2260218 Código de verificación: Sm21pjYh

Firmado por: JAVIER ROMAN GARCIA  
 UNIVERSIDAD DE LA LAGUNA

Fecha: 02/11/2019 16:23:59

IGNACIO TRUJILLO CABRERA  
 UNIVERSIDAD DE LA LAGUNA

02/11/2019 17:39:19

Spatial distribution of UDGs within large-scale structures 707

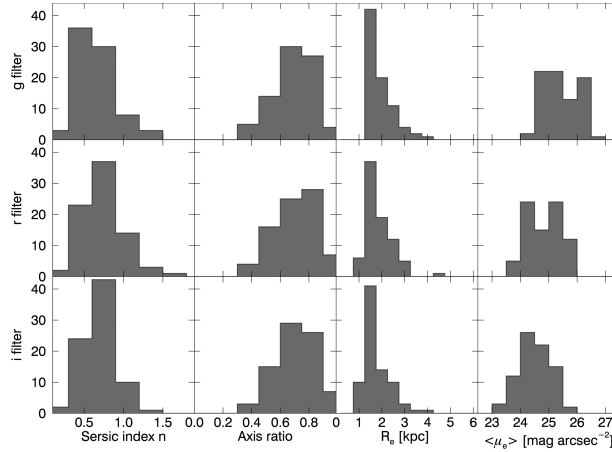


Figure 3. Distribution of structural parameters obtained using a Sérsic fit to the whole sample of UDGs in the  $g$ ,  $r$  and  $i$  filters.

average surface brightness within the effective radius ( $\mu_e$ ). The distribution of all the structural properties is similar in all the bands (see Fig. B2), except  $\langle \mu_e \rangle$  as expected, which changes because of the colours of the UDGs. As has been found in previous works (e.g. Koda et al. 2015; van der Burg et al. 2016) the Sérsic indices  $n$  of the UDGs are slightly below 1, with a peak around 0.7 ( $\langle n_g \rangle = 0.65$ ,  $\langle n_r \rangle = 0.74$  and  $\langle n_i \rangle = 0.69$ ). Interestingly, almost none of the UDGs has  $n > 1.5$ . Also, the axial ratio of these objects is around 0.7, suggesting a spheroidal shape. Moreover, the number of objects with circularized effective radius larger than 1.5 kpc declines very fast.

The apparent  $g$ -band magnitude of the UDGs within the explored area is  $20.5 < g < 22.5$  mag. This implies absolute magnitudes of  $-16 \lesssim M_g \lesssim -14$  mag. To put our UDGs in context with the rest of the galaxies in the Abell 168 area, we show in Fig. 4 the size versus absolute  $g$ -band magnitude plot for all the galaxies in the field of view at the redshift of the cluster. Galaxies with spectroscopic redshifts are shown with blue stars. We also include galaxies with photometric redshifts (purple dots) using the catalogue from Reis et al. (2012). A galaxy with photometric redshift is plotted if its redshift is compatible with being at the redshift of the cluster. We select those that are less than  $3\sigma$  (where  $\sigma$  is the photometric redshift error) away from  $z = 0.045$  and with a photometric redshift value of  $z < 0.15$ . For the UDGs in our sample, it is not reasonable to use the photometric redshift from Reis et al. (2012). The reason for this is that the UDGs are significantly fainter (in terms of surface brightness) than the more compact galaxies at the same absolute magnitude. This produces an unacceptable uncertainty of their photometric redshifts.

As has been found previously (e.g. Koda et al. 2015; Muñoz et al. 2015), Fig. 4 shows that there is a region where galaxies considered as normal dwarf galaxies and UDGs overlap. This is related to the criterion used for selecting UDGs, which uses the central surface brightness (a quantity that it is not directly measured but

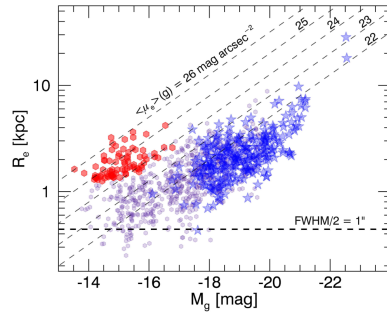


Figure 4. Circularized effective radius versus absolute  $g$ -band magnitude for all the galaxies in the Abell 168 area compatible with being at the cluster redshift. The structural parameters were derived using `imfit` (Erwin 2015). Galaxies with spectroscopic redshifts are shown with blue stars, whereas galaxies with photometric redshifts are shown with purple dots. The UDGs are plotted with red hexagons. The approximate value for the seeing FWHM of the images is 1 arcsec. In the figure, we plot with a horizontal dashed line the value of  $\text{FWHM}/2$ , which is equivalent to 0.45 kpc at the redshift of the cluster. The inclined dashed lines indicate equal average surface brightness.

extrapolated from the Sérsic fit to the surface brightness distribution of the galaxies). The apparent relation between the size of the UDGs and their absolute magnitude (found here and in previous works) is an artefact produced by the limiting surface brightness of the surveys.

MNRAS 468, 703–716 (2017)

Downloaded from https://academic.oup.com/mnras/article-abstract/468/1/703/3009801 by Instituto de Astrofísica de Canarias user on 30 August 2019

Este documento incorpora firma electrónica, y es copia auténtica de un documento electrónico archivado por la ULL según la Ley 39/2015.  
 Su autenticidad puede ser contrastada en la siguiente dirección <https://sede.ull.es/validacion/>

Identificador del documento: 2260218 Código de verificación: Sm21pjYh

Firmado por: JAVIER ROMAN GARCIA  
 UNIVERSIDAD DE LA LAGUNA

Fecha: 02/11/2019 16:23:59

IGNACIO TRUJILLO CABRERA  
 UNIVERSIDAD DE LA LAGUNA

02/11/2019 17:39:19

3.2 Paper II: *Spatial distribution of ultra-diffuse galaxies within large-scale structures*

LV

708 *J. Román and I. Trujillo*

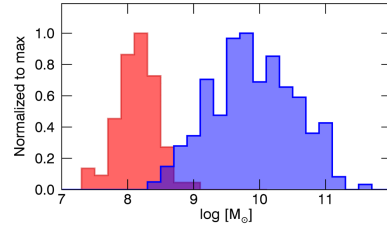


**Figure 5.** Stellar mass distribution of the galaxies in our sample. The red histogram shows the mass distribution of the UDGs whereas the blue histogram shows the distribution of galaxies with spectroscopic redshift  $0.037 < z < 0.052$ . The histograms have been normalized to peak at 1.

In relation to the colour characterization of our sample, we have a considerable advantage, having three filters compared to the two filters in previous work. van Dokkum et al. (2015a) find an average colour of  $(g - i) = 0.8 \pm 0.1$ , while here we find  $0.66 \pm 0.02$  (rms = 0.20). According to van Dokkum et al. (2015a), this colour can be either reproduced by a stellar population with 7 Gyr and  $[\text{Fe}/\text{H}] = -1.4$  or a population with 4 Gyr and  $[\text{Fe}/\text{H}] = -0.8$ . In both cases, this corresponds to galaxies significantly younger than the most massive galaxies of the cluster. Similarly, van der Burg et al. (2016) find a typical colour of  $g - r = 0.6$  (we find  $(g - r) = 0.47 \pm 0.02$  with rms = 0.15), which implies an age of 2 Gyr assuming solar metallicity or 6 Gyr with  $[\text{Fe}/\text{H}] = -0.7$ . Our average colour values are compatible also with relatively modest ages: 3 Gyr ( $[\text{Fe}/\text{H}] = -1.3$ ) or 2 Gyr ( $[\text{Fe}/\text{H}] = -1.7$ ) (Vazdekis et al. 2015). It is worth noting that if we had not corrected the contaminants by their position in the colour-colour map, the average UDG colours would be slightly redder:  $(g - r) = 0.55 \pm 0.02$  and  $(r - i) = 0.25 \pm 0.02$ .

Finally, we quantify the stellar mass distribution of our UDG galaxies. To do this, we take advantage of our colour measurements. In particular, we use  $g - r$  to determine the mass-to-light ratio in the  $r$  band ( $M/L$ ). We follow the method of Bell et al. (2003). We have used a Kroupa (2001) initial mass function (IMF). The stellar mass distribution of our galaxies is shown in Fig. 5, with a peak around  $10^8 M_{\odot}$ , similar to previous works using surveys with similar depths (e.g. van der Burg et al. 2016). As a comparison, we show the stellar mass distribution of the galaxies with spectroscopic redshifts  $0.037 < z < 0.052$ .

**5 SPATIAL DISTRIBUTION OF ULTRA-DIFFUSE GALAXIES IN LARGE-SCALE STRUCTURES**

The goal of this paper is to explore how UDGs are spatially distributed in a large variety of environments. Once the final sample of UDGs is selected, we can probe whether they preferentially inhabit a particular region of the complex structure surrounding the Abell Cluster 168. In Fig. 6, we show the spatial distribution of the UDGs and the galaxies with spectroscopic redshifts compatible with being at the cluster distance. The size of the area shown is limited by the declination width of the Stripe 82 survey (2:5). We have expanded in the RA direction the area shown by 0:25 on each side in order to illustrate how the large-scale structure in that direction continues. This is indicated with a darker blue colour. The blue stars are the

galaxies with spectroscopic redshifts at  $0.037 < z < 0.052$ . Large blue stars correspond to the dominant galaxies in each prominent substructure: UGC 00797 (RA = 18:73996, Dec. = 0:43081,  $z = 0.04482$ ), UGC 00842 (RA = 19:72338, Dec. = -1:00199,  $z = 0.04526$ ) and UGC 00753 (RA = 18:01924, Dec. = -0:24512,  $z = 0.04420$ ). Red dots are the UDGs. To enhance the visibility of the large-scale structure in Fig. 6, we have estimated the density distribution of the galaxies with spectroscopic redshifts at  $0.037 < z < 0.052$  using a bin size of  $0.1 \times 0.1$ . Then, we have smoothed the histogram for ease of visualization.

The most prominent structure, located a little above the central part of the plot, is the Abell Cluster 168. This cluster is not fully relaxed, with an overdensity of galaxies slightly offset from the position of the main galaxy UGC 00797 (Yang et al. 2004). The whole central structure has a radius of  $\sim 1.5$  Mpc. The two other most conspicuous structures are the fossil group centred around the galaxy UGC 00842 (Lopes de Oliveira et al. 2010) (bottom-left corner of the figure) and the group around UGC 00753. There are other filamentary-like structures, and also a big empty region in the bottom-right part of the image. The most remarkable result is that UDGs trace the large-scale structure of spectroscopic galaxies.

**5.1 Effect of interlopers in the spatial distribution of ultra-diffuse galaxies**

Our selection criteria (colours, size and surface brightness) are constructed to attempt to select all the UDGs at the redshift of the Abell 168 cluster. We try to avoid, as much as possible, contaminating sources projected in the line of sight. For instance, modelling different stellar population tracks (Vazdekis et al. 2015) in our colour-colour map, we find that at  $z > 0.2$ , the vast majority of these models do not follow our colour-colour selection criteria. Additionally, our selection criterion ( $r_e > 1.5$  kpc at  $z = 0.045$ ) is equivalent to selecting objects with  $r_e > 1.7$  arcsec. This value corresponds to the following physical sizes at different redshifts: 3.1 kpc ( $z = 0.1$ ), 5.6 kpc ( $z = 0.2$ ) and 7.6 kpc ( $z = 0.3$ ). Considering that our typical UDG has  $g = 21.5$  mag, the absolute  $g$ -band rest frame ( $K$ -corrected) at different redshifts will be  $-16.7$  mag ( $z = 0.1$ ),  $-18.3$  mag ( $z = 0.2$ ) and  $-19.2$  mag ( $z = 0.3$ ). Following Fig. 4, it can be easily seen that galaxies with the above absolute magnitudes and sizes are not expected to exist. In other words, if they exist, they are not common and, consequently, their importance as a source of contamination is expected to be very small. These numbers illustrate that the probability of having, in our catalogue of UDGs, interlopers with  $z > 0.1$  is very low. For this reason, in what follows, we concentrate on potential interlopers located in our line of sight up to  $z = 0.1$ .

To evaluate the number of potential interlopers within our catalogue of UDGs, we explore the following idea: we quantify whether a given UDG is more likely to belong to our large-scale structure (at  $z = 0.045$ ), or whether is more likely to be located in another large-scale structure found in the same field up to  $z = 0.1$ . To conduct this task, we assume that the likelihood of a given UDG candidate belonging to a given structure is proportional to the number of galaxies with a given spectroscopic redshift in its neighbourhood compatible with being part of that structure. On doing this, we are making the following assumption: UDGs are more abundant in the densest environments. This hypothesis is based on the findings by van der Burg et al. (2016) and Román & Trujillo (2016). These authors find a tight correlation between the number of UDGs and the mass of the host structure where they are embedded. This correlation has the following form:  $N_{\text{UDGs}} \propto M_{\text{host}}^{\alpha}$  with  $\alpha \sim 1$ . Based on this, we

Downloaded from https://academic.oup.com/mnras/article-abstract/doi/10.1093/mnras/stz1468/5481703/5089801 by Instituto de Astrofísica de Canarias user on 30 August 2019

MNRAS **468**, 703–716 (2017)

Este documento incorpora firma electrónica, y es copia auténtica de un documento electrónico archivado por la ULL según la Ley 39/2015.  
 Su autenticidad puede ser contrastada en la siguiente dirección <https://sede.ull.es/validacion/>

Identificador del documento: 2260218 Código de verificación: Sm21pjYh

Firmado por: JAVIER ROMAN GARCIA  
 UNIVERSIDAD DE LA LAGUNA

Fecha: 02/11/2019 16:23:59

IGNACIO TRUJILLO CABRERA  
 UNIVERSIDAD DE LA LAGUNA

02/11/2019 17:39:19

Spatial distribution of UDGs within large-scale structures 709

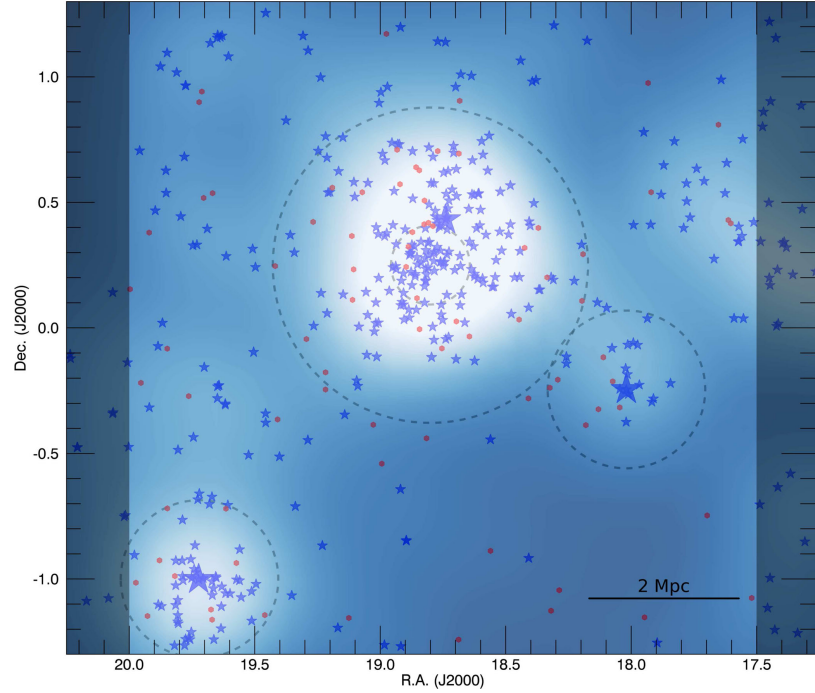


**Figure 6.** Spatial distribution of UDGs in the Abell cluster 168 and its surrounding large-scale structure. The blue stars are the galaxies with spectroscopic redshifts at  $0.037 < z < 0.052$ . Large blue stars correspond to the dominant galaxies in each substructure: UGC 00797 (RA = 18:73996, Dec. = 0:43081,  $z = 0.04482$ ), UGC 00842 (RA = 19:72338, Dec. = -1:00199,  $z = 0.04526$ ) and UGC 00753 (RA = 18:01924, Dec. = -0:24512,  $z = 0.04420$ ). Red dots are the UDGs. The white areas correspond to the density distribution of the galaxies with spectroscopic redshifts. The grey dashed circles enclose the different zones explored in this paper: the cluster core ( $R < 0.5$  Mpc) and its outskirts ( $0.5 < R < 2$  Mpc), the groups ( $R < 1$  Mpc) around UGC 00753 and UGC 00842, and filaments (remaining area). The horizontal bar indicates the equivalent size of 2 Mpc at the cluster distance.

estimate the probability of a given UDG in our list to pertain to a given structure as follows:

$$P[UDG(z)] \propto \sum_{i=1}^N M_i(z, M_i > 2 \times 10^{10} M_{\odot}, R < 0.5 \text{ Mpc}). \quad (1)$$

In other words, we sum the stellar mass of all the galaxies at a given (spectroscopic) redshift around our UDG candidate with  $M_i > 2 \times 10^{10} M_{\odot}$  and within a projected radial distance  $R < 0.5$  Mpc. The reason why we select only spectroscopic galaxies with  $M_i > 2 \times 10^{10} M_{\odot}$  is because this is the completeness stellar mass limit for galaxies up to  $z = 0.1$  in our SDSS spectroscopic sample (see fig. 4 in Cebrián & Trujillo 2014). We are also assuming that the total stellar mass contained in the most massive

galaxies is a proxy of the total mass of the structure where the UDG candidate is located.

To measure the above probability for each UDG candidate, we select different redshift slices following the distribution of the galaxies with spectroscopic redshift in our sample (see Fig. 7). Once we have estimated the probability for each of our UDG candidates, we sum the probability of the whole sample and we create the probability distribution of the UDGs to belong to different redshift slices within our field of view up to  $z = 0.1$ . The result of this analysis is shown in the second row of Fig. 7. This figure shows that 73 per cent of our UDG candidates are more likely to be located at the large-scale structure at the redshift of the cluster (i.e.  $z = 0.045$ ). Naturally, the probability is not the same depending on where the UDG candidate is located. For this reason, we have repeated this exercise for different subsamples of our UDG galaxies accounting

Downloaded from https://academic.oup.com/mnras/article-abstract/468/1/703/5098901 by Instituto de Astrofísica de Canarias user on 30 August 2019

Este documento incorpora firma electrónica, y es copia auténtica de un documento electrónico archivado por la ULL según la Ley 39/2015.  
 Su autenticidad puede ser contrastada en la siguiente dirección <https://sede.ull.es/validacion/>

Identificador del documento: 2260218 Código de verificación: Sm21pjYh

Firmado por: JAVIER ROMAN GARCIA  
 UNIVERSIDAD DE LA LAGUNA

Fecha: 02/11/2019 16:23:59

IGNACIO TRUJILLO CABRERA  
 UNIVERSIDAD DE LA LAGUNA

02/11/2019 17:39:19

3.2 Paper II: *Spatial distribution of ultra-diffuse galaxies within large-scale structures*

LVII

710 *J. Román and I. Trujillo*

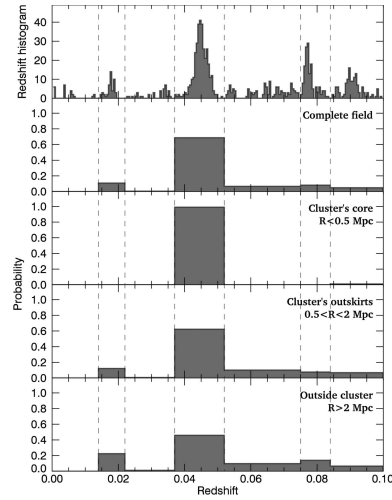


**Figure 7.** Redshift distribution and probability of UDGs belonging to different large-scale structures within our field of view up to  $z = 0.1$ . The redshift distribution is shown in the upper panel. The other panels show the probability of UDGs being located at a given redshift depending on their position within the field of view. The probabilities of membership of UDGs in the range of redshift  $0.037 < z < 0.052$  are: complete field, 77 per cent; cluster's core, 99 per cent; cluster's outskirts, 62 per cent; outside the cluster, 46 per cent.

for their position within our field of view. For the UDGs located in the cluster's core (i.e. in the inner  $R < 0.5$  Mpc), the probability of pertaining to the cluster itself is 99 per cent (in other words, the contamination in this region is negligible). For the region located in the outskirts of the cluster ( $0.5 < R < 2$  Mpc), the probability of UDGs being placed there is 62 per cent. Finally, for galaxies well outside the cluster, the probability of being located there is 46 per cent. It is worth noting that our method is biased against potential UDGs located in the lowest density environments. So, particularly in the regions beyond the cluster's core, our results are likely to be lower limits of the correct value.

Based on the above analysis, we can estimate the final number of UDGs in the different structures at  $z = 0.045$ . For the cluster's core, we will have (after removing the contamination) 5 UDGs, for the cluster's outskirts 17 UDGs and for the large-scale structure surrounding the cluster 22 UDGs. This translates into the following percentages of UDG galaxies, depending on the structure where they are located:  $11 \pm 5$  per cent (cluster's core),  $39 \pm 9$  per cent (cluster's outskirts) and  $50 \pm 11$  per cent (outside the cluster).

**5.2 Environment of ultra-diffuse galaxies**

We characterize the environment around each UDG in our sample by determining the average distance to its first five neighbours with stellar masses  $> 10^{9.5} M_{\odot}$  ( $r_5$ ). The choice of mass limit is

MNRAS **468**, 703–716 (2017)

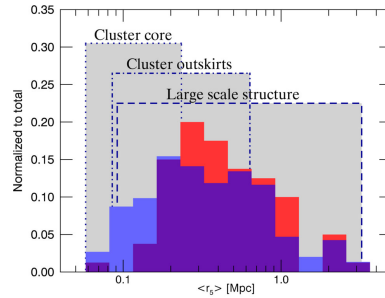


**Figure 8.** Average distance of the galaxies to their first five neighbours ( $r_5$ ), a proxy for local density (see text for details). The histogram showing the average local density of UDGs is plotted in red. The blue histogram shows the same information for galaxies with spectroscopic redshifts  $0.037 < z < 0.052$  in the cluster field.

motivated by the stellar mass distribution shape of the galaxies with spectroscopy in Fig. 5, which suggests that the spectroscopic sample is complete at  $z = 0.045$  for stellar masses above this value. In addition, we take the average distance to the closest five neighbours to have a robust estimation (i.e. not strongly affected by shot noise) of the typical distance to the surrounding galaxies. We assume that both UDGs and galaxies with spectroscopic redshifts are all at the same comoving radial distance (i.e.  $z = 0.045$ ). The result of our analysis is shown in Fig. 8. For comparison, we also show the local density distribution of all the galaxies with spectroscopic redshifts in the cluster (i.e. also including those with  $< 10^{9.5} M_{\odot}$ ) and its surrounding large-scale structure. To contextualize the meaning of our local densities, we also show with vertical lines the range in density found for spectroscopic galaxies placed in the core of the Abell Cluster 168, in the cluster outskirts and in the large-scale structure that surrounds it.

The result of this analysis is shown in Fig. 8. We caution the reader to avoid overinterpreting this figure, as the effect of the interlopers has not been corrected. Nevertheless, there is a lack of UDGs in the densest regions of our field, compared with the spectroscopic sample, which cannot be explained as an effect of the false projections. This absence of UDGs in the innermost part of the cluster is in agreement with theoretical and observational work by Yozin & Bekki (2015) and van der Burg et al. (2016), respectively. Additionally, we have checked the variation of the properties of the UDGs as a function of the density ( $r_5$ ) in Appendix A. That analysis, which should be considered as tentative because of the presence of interlopers, can give us some clues about the relationship of UDGs with their environment and it can provide a basis for future work.

The number densities of UDGs in each of the structures (after removing contamination):  $6 \pm 3 \text{ Mpc}^{-2}$  in the cluster core,  $1.4 \pm 0.4 \text{ Mpc}^{-2}$  in the cluster outskirts and  $0.4 \pm 0.1 \text{ Mpc}^{-2}$  in the large-scale structure. The contributions in stellar mass of the UDGs to the total stellar mass above  $3 \times 10^9 M_{\odot}$  in each substructure are:  $\sim 0.06$  per cent in the cluster core,  $\sim 0.08$  per cent in the outskirts of the cluster and  $\sim 0.10$  per cent in the external large-scale structure. The contribution of UDGs to the total stellar mass in the cluster is

Downloaded from https://academic.oup.com/mnras/article-abstract/468/1/703/5089801 by Instituto de Astrofísica de Canarias user on 30 August 2019

Este documento incorpora firma electrónica, y es copia auténtica de un documento electrónico archivado por la ULL según la Ley 39/2015.  
 Su autenticidad puede ser contrastada en la siguiente dirección <https://sede.ull.es/validacion/>

Identificador del documento: 2260218 Código de verificación: Sm21pjYh

Firmado por: JAVIER ROMAN GARCIA  
 UNIVERSIDAD DE LA LAGUNA

Fecha: 02/11/2019 16:23:59

IGNACIO TRUJILLO CABRERA  
 UNIVERSIDAD DE LA LAGUNA

02/11/2019 17:39:19

*Spatial distribution of UDGs within large-scale structures* 711

~0.10 per cent, a number similar (within a factor of 2) to the one (i.e. 0.2 per cent) reported by van der Burg et al. (2016).

**6 ULTRA-DIFFUSE AND DWARF GALAXIES**

The global distribution of UDGs in the large-scale structure, shown in Fig. 6, as well as the relationship between their colour and local density suggest a scenario where UDGs are not significantly different, as a population, from dwarf galaxies with stellar masses around  $10^9 M_{\odot}$  (i.e. similar to the LMC). In fact, we have explored whether the colours and spatial distribution of UDGs are similar to dwarf galaxies ( $1 < M_{*} < 3 \times 10^9 M_{\odot}$ ) with spectroscopic redshift in our area.<sup>5</sup> For these galaxies, we find the following colours:  $(g-r) = 0.48 \pm 0.02$  and  $(r-i) = 0.25 \pm 0.01$ , very similar to the colours we obtain for the UDGs. Their spatial distribution is also compatible to the UDGs. We find  $9 \pm 5$  per cent in the cluster core region,  $34 \pm 9$  per cent in the outskirts of the cluster and  $57 \pm 8$  per cent in the large-scale structure. Carrying out exactly the same analysis but for galaxies with  $\sim 5 \times 10^{10} M_{\odot}$  (i.e. Milky Way-like objects), we find  $(g-r) = 0.79 \pm 0.02$  and  $(r-i) = 0.38 \pm 0.01$  and the following number densities:  $25 \pm 6$  per cent in the cluster core region,  $37 \pm 7$  per cent in the outskirts of the cluster and  $38 \pm 6$  per cent in the large-scale structure. In other words,  $L_{*}$  galaxies are much redder than UDGs and are also spatially distributed differently than dwarf galaxies and UDGs. It is especially noteworthy that in the inner part of the cluster the fraction of  $L_{*}$  galaxies is much larger compared to UDGs or dwarf galaxies, which seems to favour a scenario where UDGs are more likely to be bona fide dwarf galaxies than failed  $L_{*}$  galaxies. We expand on this idea in the following section.

**7 DISCUSSION**

Within the standard galaxy formation scheme, very diffuse galaxies are expected to form in initial fluctuations with low density (Fall & Efstathiou 1980; Mo, Mao & White 1998) with blue colours, a large amount of gas and disc-like shapes (McGaugh & Bothun 1994). Moreover, these objects are not supposed to exist in high-density environments as the effect of tides will easily disrupt them (Dekel & Silk 1986; Rosenbaum et al. 2009; Galaz et al. 2011). However, UDGs are numerous in clusters, and the more massive the cluster, the more abundantly they can be found (e.g. Román & Trujillo 2016; van der Burg et al. 2016). There are two possible scenarios to explain these findings, as follows.

- (i) In the first scenario, UDGs are a population connected to the cluster environment and they are born and survive in these dense regions because they are embedded in very massive (Milky Way-like) dark matter haloes. They will be disrupted only in the very inner regions of the clusters, because of tidal effects. However, they should be common in the outer regions of clusters.
- (ii) In the second scenario, UDGs are regular dwarf galaxies that have been formed in the lowest-density regions of the large-scale structure. They have dark matter haloes typical of dwarf galaxies. This means that, if they are accreted to cluster and/or

<sup>5</sup> Ideally, we would like to perform this analysis with dwarf galaxies with lower masses (i.e. closer to UDGs masses); however, the very small number of spectroscopic objects with such low mass prevents us from doing this. For this reason, we have compromised, and we explore the spatial distribution of  $10^9 M_{\odot}$  dwarf galaxies.

group central regions, they can survive within them, but farther away from the densest regions compared to the first scenario. Once they reach the peripheral regions of the densest structures, unless they have a radial orbit towards the central regions, they can survive for a long time in the outer parts, as they are weakly influenced by dynamical friction (Smith, Davies & Nelson 2010; Smith et al. 2015).

Let us explore whether the current observational evidence supports either of the above scenarios. The strongest observational evidence disfavouring that UDGs are failed  $L_{*}$  galaxies is the evidence by Beasley et al. (2016), who find that VCC 1287, an UDG in the Virgo Cluster, has a dark matter halo of  $\sim 8 \times 10^{10} M_{\odot}$ . This is more than a factor of 10 smaller than expected for  $L_{*}$  galaxies ( $\geq 10^{12} M_{\odot}$ ). However, this result is just based on one single galaxy and VCC 1287 is a particularly low-mass ( $\sim 3 \times 10^7 M_{\odot}$ ) UDG (i.e. a factor of  $\sim 3$  less massive than most of the UDG population explored so far,  $\sim 10^8 M_{\odot}$ ). Assuming that in this range of masses,  $M_{\text{halo}}$  will scale proportionality to  $M_{*}$ , the result of Beasley et al. (2016) will still disfavour the idea that UDGs with  $M_{*} \sim 10^8 M_{\odot}$  are failed  $L_{*}$  galaxies. This is because the mass of its dark matter halo would still be too low by a factor of 3. It is clear then that we urgently need to estimate the dark matter masses of more UDGs.<sup>6</sup> In the meantime, we can evaluate the outcomes of the other observational results.

A good test to support or disfavour either of the above scenarios is to explore the spatial distribution of UDGs. This test is based on the following two assumptions: (i) the sizes of galaxies are a direct manifestation of the spin parameter of its halo (Mo et al. 1998); (ii) the spin distribution is not strongly dependent on environment (Amorisco & Loeb 2016). Based on the first assumption, it follows that UDGs can be either regular dwarf galaxies with high-spin haloes or  $L_{*}$  galaxies with average spin haloes. According to the second assumption, the spatial distribution of UDGs will resemble those of the dark matter haloes where they are embedded. Consequently, we have explored in this paper which spatial distribution UDGs resemble most:  $L_{*}$  galaxies or those of regular dwarf galaxies. In previous sections, we have shown that UDGs share the same spatial distributions and colours as regular dwarf galaxies with stellar mass  $10^9 M_{\odot}$ , while they do not have the same distributions as more massive ( $L_{*}$ -like) objects. Consequently, this could suggest that we can make the observation that UDGs are more likely to be dwarf galaxies than failed  $L_{*}$  objects.

Following a similar argument, Amorisco & Loeb (2016) make the following prediction. ‘Under the assumption that the spin distribution is not strongly dependent on environment and that these extended discs are capable of forming stars in a similar way when in isolation, our model suggests that an abundant tail of extended galaxies should be ubiquitous in both clusters and in the field.’ This is, in fact, what we see in this paper – UDGs are not a phenomenon exclusively linked to clusters of galaxies. Note that previously reported UDGs (with the exception of DGSAT 1 by Martínez-Delgado et al. 2016) have been found in dense (i.e. cluster) environments. However, we find that UDGs are common outside clusters, being

<sup>6</sup> Recently, using the number of globular clusters as a proxy for the dark matter halo mass of the galaxy, Peng & Lim (2016) and Beasley & Trujillo (2016) have also found that the UDG DF17 inhabits a dark matter halo with  $\sim 10^{11} M_{\odot}$ . Also, van Dokkum et al. (2016) have found  $\sim 10^{12} M_{\odot}$  for the DF44 UDG and Amorisco, Monachesi & White (2016), analyzing *Hubble Space Telescope* imaging of 54 UDGs in the Coma Cluster, have found low-mass haloes for this set of UDGs.

Este documento incorpora firma electrónica, y es copia auténtica de un documento electrónico archivado por la ULL según la Ley 39/2015.  
 Su autenticidad puede ser contrastada en la siguiente dirección <https://sede.ull.es/validacion/>

Identificador del documento: 2260218 Código de verificación: Sm21pjYh

Firmado por: JAVIER ROMAN GARCIA  
 UNIVERSIDAD DE LA LAGUNA

Fecha: 02/11/2019 16:23:59

IGNACIO TRUJILLO CABRERA  
 UNIVERSIDAD DE LA LAGUNA

02/11/2019 17:39:19

3.2 Paper II: *Spatial distribution of ultra-diffuse galaxies within large-scale structures*

LIX

712 *J. Román and I. Trujillo*

clearly located around groups and with hints of existence in the less dense structure in our field.<sup>7</sup>

Both UDGs and  $L_*$  galaxies are found in the same proportions ( $\sim 38$  per cent) in the outskirts of the Abell Cluster 168. However, they strongly differ in the inner core region of the cluster (25 per cent  $L_*$  galaxies versus 11 per cent UDGs) as well as outside clusters (38 per cent  $L_*$  galaxies versus 50 per cent UDGs). This supports the idea that UDGs are not failed  $L_*$  galaxies as they are scarce in the regions where the tides are strong on these objects. If they were sharing the same type of dark matter haloes, then they should better withstand the harsh conditions of the cluster's core.<sup>8</sup>

A final question we want to address is the following. Do we have any evidence favouring UDGs being formed outside clusters and later being accreted to the cluster periphery? If this were the case, then this would be another hint that the second proposed scenario is more likely than the first. Clusters of galaxies are very active locations within the large-scale structure of the Universe, with significant continuous accretion of other galaxies by infall of minor substructures occurring with high frequency (e.g. Fakhouri, Ma & Boylan-Kolchin 2010). For this reason, UDGs formed outside Abell 168 have to infall to the cluster at some point. This being the case, both the structural and colour properties of UDGs should reflect a gradual change in their values as we approach the densest regions. Yozin & Bekki (2015) suggest that UDGs undergoing tidal fields should show a decrease on their stellar mass, a flattening of their structure (i.e. a decrease of their axial ratio) and a decline in their surface brightness. In this work, we have looked for any hint of such structural transformation of UDGs (see Appendix A). Given the possible presence of interlopers, especially in the lower-density areas, our work does not allow us to obtain a robust analysis. However, assuming these limitations, we have found a decrease in radius, surface brightness and stellar mass with increasing density. Very interestingly, in their recent work Román & Trujillo (2016) found a similar trend using a different environment, of three isolated compact groups. Although these trends cannot be considered robust at this time, and must be confirmed by later and more extensive works, these would point to the progressive transformation of the UDGs by their infall to the cluster. Similarly, Amorisco & Loeb (2016) predict: '[i]t can be expected that the isolated counterparts of cluster UDGs should have more clearly discy morphologies, and not appear as red and quenched.' In this work, we do not find any clear hint, either in colour or in axial ratio, to support this conclusion.<sup>9</sup>

8 SUMMARY

In this paper, we have explored the properties of UDGs inhabiting the Abell Cluster 168 ( $z = 0.045$ ) and its rich surrounding large-

scale structure. This work represents an important step forward in understanding in which environments UDGs are born, and it allows us to address in more detail the ultimate nature of UDGs. For instance, among other scenarios, we ask whether most UDGs are regular dwarf galaxies or failed  $L_*$  galaxies. The main conclusions of this observational work can be summarized as follows.

(i) UDGs are found over the whole scale structure defined by the Abell cluster 168 and its surroundings. Our data allow us to confirm the existence of UDGs in the Abell cluster 168 and groups present in our field, showing hints of the presence of UDGs in the filamentary structure, which is the first detection of UDGs outside a cluster of galaxies.

(ii) UDGs are distributed (after removal of potential interlopers) as follows:  $11 \pm 5$  per cent in the cluster's core,  $39 \pm 9$  per cent in the outskirts of the cluster and  $50 \pm 11$  per cent in the large-scale structure around the cluster. The number densities of UDGs in each of the substructures are:  $6 \pm 3 \text{ Mpc}^{-2}$  in the cluster core,  $1.4 \pm 0.4 \text{ Mpc}^{-2}$  in the cluster outskirts and  $0.4 \pm 0.1 \text{ Mpc}^{-2}$  in the large-scale structure.

(iii) The spatial distribution of the UDGs is similar to that found for regular ( $\sim 10^9 M_\odot$ ) dwarf galaxies but significantly different from that of  $L_*$  objects. Under the assumption that the spin distribution is not strongly dependent on the environment, this can be understood as favouring the idea that UDGs are dwarf galaxies inhabiting high-spin haloes (Amorisco & Loeb 2016).

(iv) The colours of UDGs ( $(g-r) = 0.48 \pm 0.02$ ,  $(r-i) = 0.21 \pm 0.02$ ) are compatible with the dwarf galaxies ( $(g-r) = 0.48 \pm 0.02$ ,  $(r-i) = 0.25 \pm 0.01$ ) in the analysed large-scale structure. The colours of  $L_*$  galaxies ( $(g-r) = 0.79 \pm 0.02$  and  $(r-i) = 0.38 \pm 0.01$ ), much redder, are indicative of the dwarf nature of the UDGs.

ACKNOWLEDGEMENTS

We are grateful to the referees for their constructive comments. We want to specially thank Mike Beasley for his helpful comments during the development of this work. We thank Juergen Fliri for his careful work on the IAC Stripe 82 Legacy Project. Lee Kelvin is also acknowledged for his help. This research was supported by the Instituto de Astrofísica de Canarias. The authors of this paper acknowledge support from grant AYA2013-48226-C3-1-P from the Spanish Ministry of Economy and Competitiveness (MINECO). JR thanks MINECO for financing his PhD through an FPI grant.

REFERENCES

Amorisco N. C., Loeb A., 2016, MNRAS, 459, L51  
 Amorisco N. C., Monachesi A., White S. D. M., 2016, preprint (arXiv:1610.01595)  
 Beasley M. A., Trujillo I., 2016, ApJ, 830, 23  
 Beasley M. A., Romanowsky A. J., Pota V., Navarro I. M., Martinez Delgado D., Neyer F., Deich A. L., 2016, ApJ, 819, L20  
 Bell E. F., McIntosh D. H., Katz N., Weinberg M. D., 2003, ApJ, 149, 289  
 Bellazzini M., Belokurov V., Magrini L., Fraternali F., Testa V., Beccari G., Marchetti A., Carini R., 2017, MNRAS, 467, 3751  
 Bertin E., Arnouts S., 1996, A&AS, 117, 393  
 Bertin E., Mellier Y., Radovich M., Missonnier G., Didelon P., Morin B., 2002, in Bohlender D. A., Durand D., Handley T. H., eds, ASP Conf. Proc. Vol. 281, Astronomical Data Analysis Software and Systems XI. Astron. Soc. Pac., San Francisco, p. 228  
 Bothun G. D., Impey C. D., Malin D. F., 1991, ApJ, 376, 404  
 Burkholder V., Impey C., Sprayberry D., 2001, AJ, 122, 2318  
 Cebrián M., Trujillo I., 2014, MNRAS, 444, 682

MNRAS 468, 703–716 (2017)

Downloaded from https://academic.oup.com/mnras/article-abstract/468/1/703/5009801 by Instituto de Astrofísica de Canarias user on 30 August 2019

Este documento incorpora firma electrónica, y es copia auténtica de un documento electrónico archivado por la ULL según la Ley 39/2015.  
 Su autenticidad puede ser contrastada en la siguiente dirección <https://sede.ull.es/validacion/>

Identificador del documento: 2260218 Código de verificación: Sm21pjYh

Firmado por: JAVIER ROMAN GARCIA  
 UNIVERSIDAD DE LA LAGUNA

Fecha: 02/11/2019 16:23:59

IGNACIO TRUJILLO CABRERA  
 UNIVERSIDAD DE LA LAGUNA

02/11/2019 17:39:19

Spatial distribution of UDGs within large-scale structures 713

Chilingarian I. V., Melchior A.-L., Zolotukhin I. Yu., 2010, MNRAS, 405, 1409  
 Dalcanton J. J., Spergel D. N., Gunn J. E., Schmidt M., Schneider D. P., 1997, AJ, 114, 635  
 Dekel A., Silk J., 1986, ApJ, 303, 39  
 Di Cintio A., Brook C. B., Dutton A. A., Macciò A. V., Obreja A., Dekel A., 2017, MNRAS, 466, L1  
 Erwin P., 2015, ApJ, 799, 226  
 Fakhouri O., Ma C.-P., Boylan-Kolchin M., 2010, MNRAS, 406, 2267  
 Fall S. M., Efstathiou G., 1980, MNRAS, 193, 189  
 Fliri J., Trujillo I., 2016, MNRAS, 456, 1359  
 Galaz G., Herrera-Camus R., Garcia-Lambas D., Padilla N., 2011, ApJ, 728, 74  
 Impey C., Bothun G., Malin D., 1988, ApJ, 330, 634  
 Koda J., Yagi M., Yamanoi H., Komiyama Y., 2015, ApJ, 807, L2  
 Kroupa P., 2001, MNRAS, 322, 231  
 Lopes de Oliveira R., Carrasco E. R., Mendes de Oliveira C., Bortoletto D. R., Cypriano E., Sodré L. Jr, Lima Neto G. B., 2010, AJ, 139, L216  
 Martínez-Delgado D. et al., 2016, AJ, 151, 96  
 McLaugh S. S., Bothun G. D., 1994, AJ, 107, 530  
 Merritt A., van Dokkum P., Danieli S., Abraham R., Zhang J., Karachentsev I. D., Makarova L. N., 2016, ApJ, 833, 168  
 Mihos J. C. et al., 2015, ApJ, 809, L21  
 Mo H. J., Mao S., White S. D. M., 1998, MNRAS, 295, 319  
 Muñoz R. P. et al., 2015, ApJ, 813, L15  
 Peng E. W., Lim S., 2016, ApJ, 822, L31  
 Reis R. R. et al., 2012, ApJ, 747, 59  
 Román J., Trujillo I., 2016, preprint (arXiv:1610.08980)  
 Rosenbaum S. D., Krusch E., Bomans D. J., Dettmar R.-J., 2009, A&A, 504, 807  
 Schlafly E. F., Finkbeiner D. P., 2011, ApJ, 737, 103  
 Sérsic J. L., 1968, Atlas de Galaxias Australes. Observatorio Astronomico, Cordoba, Argentina  
 Smith Castelli A. V., Faifer F. R., Escudero C. G., 2016, A&A, 596, A23  
 Smith R., Davies J. L., Nelson A. H., 2010, MNRAS, 405, 1723  
 Smith R. et al., 2015, MNRAS, 454, 2502  
 Trujillo I., Román J., Filho M., Sánchez Almeida J., 2017, ApJ, 836, 191  
 van der Burg R. F. J., Muzzin A., Hoekstra H., 2016, A&A, 590, A20  
 van Dokkum P. G., Abraham R., Merritt A., Zhang J., Geha M., Conroy C., 2015a, ApJ, 798, L45  
 van Dokkum P. G. et al., 2015b, ApJ, 804, L26  
 van Dokkum P. et al., 2016, ApJ, 828, L6  
 Vazdekis A. et al., 2015, MNRAS, 449, 1177  
 Yang Y., Zhou X., Yuan Q., Jiang Z., Ma J., Wu H., Chen J., 2004, ApJ, 600, 141  
 Yozin C., Bekki K., 2015, MNRAS, 452, 937  
 Zaritsky D., 2017, MNRAS, 464, L110

APPENDIX A: PROPERTIES OF ULTRA-DIFFUSE GALAXIES AS A FUNCTION OF THEIR ENVIRONMENT

If UDGs were progressively infalling to the cluster centre, then it would be expected that during such a process their structural properties would be modified until they become disrupted (Yozin & Bekki 2015). To explore any trend between the structural parameters and local density (see Fig. A1), we separate our sample of UDGs into two groups with similar numbers of galaxies: those with  $\langle r_s \rangle < 0.45$  Mpc and those with  $\langle r_s \rangle > 0.45$  Mpc. In Table A1, we show the results of this exercise. We find a dependence on the structural properties of our UDGs sample as a function of the environment. We find a decrease of the stellar mass (by a factor of  $\sim 1.5$ ), a decrease of the radius (by a mean of 0.23 kpc), fainter average surface brightness ( $\sim 0.4$  mag arcsec $^{-2}$ ), a larger Sérsic index  $n$  (a factor of  $\sim 1.1$ ) and a marginal lower axial ratio. These numbers are not corrected by the effect of contaminants as we

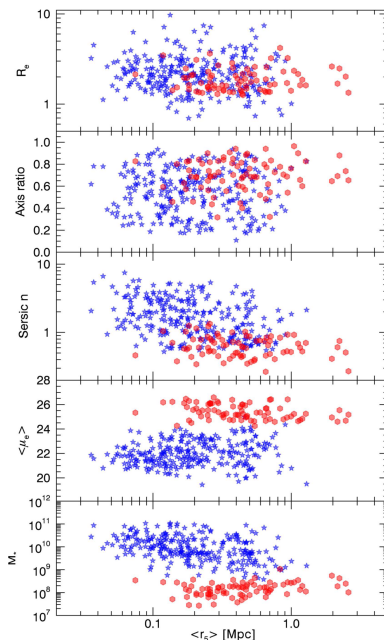


Figure A1. Structural properties of the galaxies in our sample (in the  $g$  band) versus the average distance of the galaxies to their closest five neighbours with spectroscopic redshift ( $r_s$ ) (a proxy for the local density): the distribution of the UDGs is in red and the galaxies with spectroscopic redshifts  $0.037 < z < 0.052$  are in blue.

Table A1. Average properties of the UDGs as a function of their local density ( $r_s$ ).

	$\langle r_s \rangle < 0.45$ Mpc	$\langle r_s \rangle > 0.45$ Mpc
$\langle g-r \rangle$	$0.47 \pm 0.02$	$0.47 \pm 0.02$
$\langle r-i \rangle$	$0.19 \pm 0.02$	$0.18 \pm 0.02$
$\langle n \rangle$	$0.67 \pm 0.04$	$0.62 \pm 0.04$
$\langle r_e \rangle$ (kpc)	$1.71 \pm 0.06$	$1.94 \pm 0.09$
$\langle \mu_e \rangle$ (mag arcsec $^{-2}$ )	$25.6 \pm 0.1$	$25.2 \pm 0.1$
$\langle b/a \rangle$	$0.69 \pm 0.02$	$0.71 \pm 0.02$
$\langle M_* \rangle$ ( $\times 10^8 M_\odot$ )	$1.3 \pm 0.1$	$1.9 \pm 0.2$

assume that the interlopers will not modify the average properties of our subsamples.

Additionally, we explore whether the colour distribution of the UDGs depends on the environment where they reside. In Fig. A2, we show the colour distribution of the UDGs as a function of their local density, as characterized by the average distance to their five

Este documento incorpora firma electrónica, y es copia auténtica de un documento electrónico archivado por la ULL según la Ley 39/2015.  
Su autenticidad puede ser contrastada en la siguiente dirección <https://sede.ull.es/validacion/>

Identificador del documento: 2260218 Código de verificación: Sm21pJYh

Firmado por: JAVIER ROMAN GARCIA  
UNIVERSIDAD DE LA LAGUNA

Fecha: 02/11/2019 16:23:59

IGNACIO TRUJILLO CABRERA  
UNIVERSIDAD DE LA LAGUNA

02/11/2019 17:39:19

714 *J. Román and I. Trujillo*

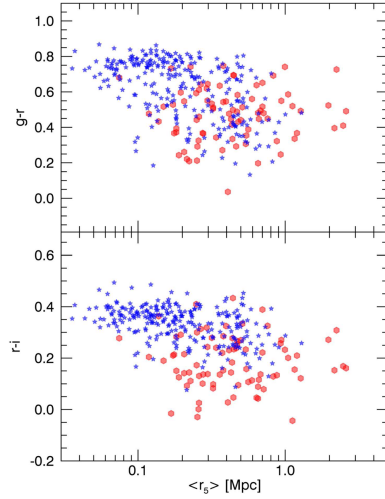


**Figure A2.** Colour versus the average distance of our galaxies to their closest five neighbours with spectroscopic redshift ( $r_5$ ) (a proxy for the local density): the distribution of the UDGs is shown in red and the galaxies with spectroscopic redshifts  $0.037 < z < 0.052$  are shown in blue.

closest neighbours ( $r_5$ ). According to that figure, the colours of UDGs are independent of their local density.

#### APPENDIX B: ROBUSTNESS OF THE STRUCTURAL PARAMETERS

In this appendix, we compare the structural properties, apparent magnitude and effective radius provided by IMFT and SExtractor for the whole set of galaxies in our field. This comparison is done for those objects that satisfy the SExtractor detection criteria and the primordial colour cut explained in Section 3. Our results are

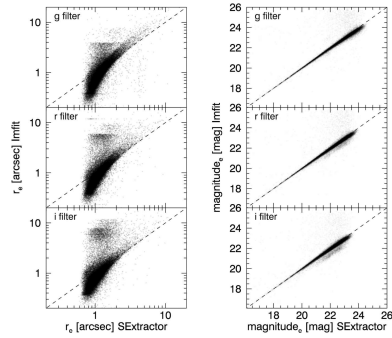


**Figure B1.** Size and apparent magnitude comparison between SExtractor and IMFT for all the galaxies detected in the cluster field.

shown in Fig. B1. In Table B1, we list the positions and structural properties of the selected UDG candidates in the area surrounding Abell Cluster 168.

There is very good agreement in all the filters related to the global apparent magnitude of the objects. At the magnitude limit where most of the UDGs are located ( $20.5 < g < 22.5$  mag), the rms between SExtractor and IMFT is around 0.1 mag. In relation to the effective radius along the semimajor axis,  $r_e$ , we find that there is a good 1:1 relation for those galaxies larger than the typical seeing of the Stripe 82 data ( $\sim 1$  arcsec). This is as expected, as SExtractor does not take into account the seeing of the data when estimating  $r_e$ . For this reason, their  $r_e$  is overestimated. The typical  $r_e$  of the UDGs in our image is  $\sim 2$  arcsec. At these values, the rms in the size estimation between both codes is 10 per cent.

In addition, we have checked the robustness of the structural parameters for our UDGs comparing the sizes and Sérsic indices among the different filters used. The result of this comparison is shown in Fig. B2. We do find good agreement between these structural parameters independent of the filter used. As expected, the effective radius along the semimajor axis  $r_e$  is estimated more precisely than the Sérsic index.

**Table B1.** Position and structural properties of the selected UDG candidates in the area surrounding Abell Cluster 168. The structural parameters were derived using IMFT (Erwin 2015). In the table, the effective radius is a parameter  $r_e$  is the value along the semimajor axis.

ID	RA (°) (J2000)	Dec. (°) (J2000)	$\mu_g(0)$ mag arcsec <sup>-2</sup>	$r_e$ (kpc)	$M_g$ (mag)	$b/a$	$n$
IAC01	19.9966	0.1540	$25.4^{+0.5}_{-0.5}$	$4.4 \pm 0.4$	$-15.6 \pm 0.1$	$0.54 \pm 0.08$	$0.93 \pm 0.23$
IAC02	19.9733	-1.0147	$25.3^{+0.5}_{-0.4}$	$2.5 \pm 0.2$	$-14.6 \pm 0.1$	$0.76 \pm 0.11$	$0.87 \pm 0.22$
IAC03	19.9533	-0.2186	$24.8^{+0.4}_{-0.3}$	$1.7 \pm 0.2$	$-14.6 \pm 0.1$	$0.62 \pm 0.09$	$0.65 \pm 0.16$
IAC04	19.9272	-1.1476	$24.4^{+0.4}_{-0.4}$	$2.0 \pm 0.2$	$-15.2 \pm 0.1$	$0.65 \pm 0.10$	$0.78 \pm 0.19$
IAC05	19.9205	0.3794	$24.4^{+0.3}_{-0.2}$	$1.9 \pm 0.2$	$-15.6 \pm 0.1$	$0.73 \pm 0.11$	$0.41 \pm 0.10$
IAC06	19.8794	-0.9259	$25.0^{+0.2}_{-0.2}$	$1.5 \pm 0.2$	$-14.5 \pm 0.1$	$0.86 \pm 0.13$	$0.35 \pm 0.09$
IAC07	19.8484	-0.0829	$24.6^{+0.2}_{-0.2}$	$1.4 \pm 0.1$	$-14.8 \pm 0.1$	$0.94 \pm 0.14$	$0.27 \pm 0.07$
IAC08	19.8480	-0.7186	$25.5^{+0.4}_{-0.3}$	$2.1 \pm 0.2$	$-14.3 \pm 0.1$	$0.40 \pm 0.06$	$0.63 \pm 0.16$
IAC09	19.8180	-0.9883	$24.1^{+0.2}_{-0.2}$	$1.7 \pm 0.2$	$-15.7 \pm 0.1$	$0.80 \pm 0.12$	$0.38 \pm 0.09$
IAC10	19.7629	-0.2714	$24.8^{+0.3}_{-0.3}$	$2.2 \pm 0.2$	$-15.3 \pm 0.1$	$0.78 \pm 0.12$	$0.51 \pm 0.13$

MNRAS **468**, 703–716 (2017)

Downloaded from https://academic.oup.com/mnras/article-abstract/doi/10.1093/mnras/stz1468/5481703/5481703 by Instituto de Astrofísica de Canarias user on 30 August 2019

Este documento incorpora firma electrónica, y es copia auténtica de un documento electrónico archivado por la ULL según la Ley 39/2015.  
 Su autenticidad puede ser contrastada en la siguiente dirección <https://sede.ull.es/validacion/>

Identificador del documento: 2260218 Código de verificación: Sm21pjYh

Firmado por: JAVIER ROMAN GARCIA  
 UNIVERSIDAD DE LA LAGUNA

Fecha: 02/11/2019 16:23:59

IGNACIO TRUJILLO CABRERA  
 UNIVERSIDAD DE LA LAGUNA

02/11/2019 17:39:19

*Spatial distribution of UDGs within large-scale structures* 715

Table B1 – continued

ID	RA (°) (J2000)	Dec. (°) (J2000)	$\mu_r(0)$ mag arcsec <sup>-2</sup>	$r_e$ (kpc)	$M_g$ (mag)	$b/a$	$n$
IAC11	19.7214	0.8993	24.9 <sup>+0.2</sup> <sub>-0.2</sub>	2.6 ± 0.3	-15.8 ± 0.1	0.90 ± 0.13	0.35 ± 0.09
IAC12	19.7106	0.9414	24.5 <sup>+0.4</sup> <sub>-0.4</sub>	2.1 ± 0.2	-15.3 ± 0.1	0.60 ± 0.09	0.70 ± 0.18
IAC13	19.7034	0.5177	24.4 <sup>+0.4</sup> <sub>-0.4</sub>	1.6 ± 0.2	-14.7 ± 0.1	0.80 ± 0.12	0.75 ± 0.19
IAC14	19.6741	-1.1219	25.2 <sup>+0.3</sup> <sub>-0.2</sub>	1.5 ± 0.1	-14.1 ± 0.1	0.80 ± 0.12	0.48 ± 0.12
IAC15	19.6678	0.5367	24.5 <sup>+0.3</sup> <sub>-0.2</sub>	2.2 ± 0.2	-15.7 ± 0.1	0.55 ± 0.08	0.48 ± 0.12
IAC16	19.6697	-1.1622	25.7 <sup>+0.3</sup> <sub>-0.3</sub>	2.4 ± 0.2	-14.6 ± 0.1	0.68 ± 0.10	0.54 ± 0.14
IAC17	19.6144	-0.7196	24.3 <sup>+0.3</sup> <sub>-0.3</sub>	1.7 ± 0.2	-15.2 ± 0.1	0.74 ± 0.11	0.53 ± 0.13
IAC18	19.5731	-0.9363	25.8 <sup>+0.3</sup> <sub>-0.2</sub>	3.0 ± 0.3	-15.0 ± 0.1	0.83 ± 0.12	0.45 ± 0.11
IAC19	19.4598	-1.1439	25.5 <sup>+0.4</sup> <sub>-0.3</sub>	2.8 ± 0.3	-15.0 ± 0.1	0.59 ± 0.09	0.61 ± 0.15
IAC20	19.4180	0.2460	24.8 <sup>+0.3</sup> <sub>-0.3</sub>	2.1 ± 0.2	-15.2 ± 0.1	0.94 ± 0.14	0.50 ± 0.13
IAC21	19.4088	-0.3643	24.0 <sup>+0.3</sup> <sub>-0.2</sub>	2.8 ± 0.3	-16.8 ± 0.1	0.84 ± 0.13	0.40 ± 0.10
IAC22	19.2940	-0.0448	24.4 <sup>+0.2</sup> <sub>-0.2</sub>	2.6 ± 0.3	-16.2 ± 0.1	0.69 ± 0.10	0.39 ± 0.10
IAC23	19.2672	0.4220	24.5 <sup>+0.2</sup> <sub>-0.2</sub>	2.1 ± 0.2	-15.7 ± 0.1	0.68 ± 0.10	0.37 ± 0.09
IAC24	19.2176	-0.1766	24.6 <sup>+0.4</sup> <sub>-0.4</sub>	2.0 ± 0.2	-14.9 ± 0.1	0.52 ± 0.08	0.77 ± 0.19
IAC25	19.2178	-0.2451	25.7 <sup>+0.4</sup> <sub>-0.4</sub>	2.4 ± 0.2	-14.3 ± 0.1	0.32 ± 0.05	0.75 ± 0.19
IAC26	19.1906	0.5585	24.4 <sup>+0.3</sup> <sub>-0.2</sub>	1.6 ± 0.2	-15.1 ± 0.1	0.70 ± 0.11	0.46 ± 0.11
IAC27	19.1249	-1.1553	24.4 <sup>+0.3</sup> <sub>-0.3</sub>	2.7 ± 0.3	-16.1 ± 0.1	0.71 ± 0.11	0.51 ± 0.13
IAC28	19.1129	0.3658	25.5 <sup>+0.3</sup> <sub>-0.2</sub>	2.2 ± 0.2	-14.6 ± 0.1	0.45 ± 0.07	0.46 ± 0.12
IAC29	19.1103	0.1114	24.4 <sup>+0.4</sup> <sub>-0.3</sub>	1.5 ± 0.2	-14.7 ± 0.1	0.84 ± 0.13	0.64 ± 0.16
IAC30	19.1059	0.2328	24.4 <sup>+0.3</sup> <sub>-0.2</sub>	2.0 ± 0.2	-15.5 ± 0.1	0.81 ± 0.12	0.44 ± 0.11
IAC31	19.0715	0.5402	25.2 <sup>+0.4</sup> <sub>-0.4</sub>	2.7 ± 0.3	-15.1 ± 0.1	0.85 ± 0.13	0.73 ± 0.18
IAC32	19.0276	-0.3854	24.5 <sup>+0.3</sup> <sub>-0.3</sub>	2.1 ± 0.2	-15.4 ± 0.1	0.69 ± 0.10	0.53 ± 0.13
IAC33	18.9934	-0.5405	24.6 <sup>+0.4</sup> <sub>-0.4</sub>	1.8 ± 0.2	-14.8 ± 0.1	0.83 ± 0.12	0.70 ± 0.18
IAC34	18.9753	1.1713	25.4 <sup>+0.3</sup> <sub>-0.2</sub>	2.7 ± 0.3	-15.2 ± 0.1	0.48 ± 0.07	0.46 ± 0.11
IAC35	18.9325	0.7096	24.2 <sup>+0.3</sup> <sub>-0.2</sub>	2.5 ± 0.3	-16.3 ± 0.1	0.69 ± 0.10	0.44 ± 0.11
IAC36	18.9211	0.5722	25.3 <sup>+0.6</sup> <sub>-0.5</sub>	3.2 ± 0.3	-14.9 ± 0.1	0.81 ± 0.12	1.00 ± 0.25
IAC37	18.8968	0.2427	25.0 <sup>+0.6</sup> <sub>-0.5</sub>	4.5 ± 0.5	-15.8 ± 0.1	0.59 ± 0.09	1.04 ± 0.26
IAC38	18.8872	0.3236	25.0 <sup>+0.3</sup> <sub>-0.2</sub>	2.3 ± 0.2	-15.3 ± 0.1	0.83 ± 0.12	0.46 ± 0.12
IAC39	18.8716	0.3812	24.8 <sup>+0.6</sup> <sub>-0.6</sub>	3.7 ± 0.4	-15.4 ± 0.1	0.69 ± 0.10	1.14 ± 0.29
IAC40	18.8571	0.6398	24.5 <sup>+0.5</sup> <sub>-0.4</sub>	1.7 ± 0.2	-14.6 ± 0.1	0.73 ± 0.11	0.88 ± 0.22
IAC41	18.8534	0.1183	25.3 <sup>+0.6</sup> <sub>-0.5</sub>	3.3 ± 0.3	-14.9 ± 0.1	0.57 ± 0.09	1.02 ± 0.26
IAC42	18.8441	0.6275	25.4 <sup>+0.4</sup> <sub>-0.4</sub>	3.1 ± 0.3	-15.2 ± 0.1	0.44 ± 0.07	0.76 ± 0.19
IAC43	18.8432	-0.0056	24.9 <sup>+0.4</sup> <sub>-0.3</sub>	1.5 ± 0.1	-14.2 ± 0.1	0.84 ± 0.13	0.60 ± 0.15
IAC44	18.8248	0.4125	25.5 <sup>+0.2</sup> <sub>-0.2</sub>	1.7 ± 0.2	-14.2 ± 0.1	0.68 ± 0.10	0.34 ± 0.09
IAC45	18.8234	0.5071	24.3 <sup>+0.4</sup> <sub>-0.4</sub>	2.2 ± 0.2	-15.5 ± 0.1	0.59 ± 0.09	0.79 ± 0.20
IAC46	18.8153	-0.4392	24.2 <sup>+0.3</sup> <sub>-0.3</sub>	2.0 ± 0.2	-15.5 ± 0.1	0.66 ± 0.10	0.60 ± 0.15
IAC47	18.8077	0.4186	25.3 <sup>+0.3</sup> <sub>-0.3</sub>	2.1 ± 0.2	-14.6 ± 0.1	0.82 ± 0.12	0.57 ± 0.14
IAC48	18.7897	0.4053	25.6 <sup>+0.4</sup> <sub>-0.4</sub>	2.1 ± 0.2	-14.1 ± 0.1	0.46 ± 0.07	0.71 ± 0.18
IAC49	18.7707	0.7043	24.2 <sup>+0.3</sup> <sub>-0.3</sub>	1.7 ± 0.2	-15.2 ± 0.1	0.74 ± 0.11	0.60 ± 0.15
IAC50	18.7542	-0.0821	24.7 <sup>+0.7</sup> <sub>-0.6</sub>	1.8 ± 0.2	-13.7 ± 0.1	0.83 ± 0.12	1.25 ± 0.31
IAC51	18.6968	0.0255	24.8 <sup>+0.5</sup> <sub>-0.4</sub>	3.1 ± 0.3	-15.7 ± 0.1	0.46 ± 0.07	0.79 ± 0.20
IAC52	18.6864	0.6942	25.6 <sup>+0.3</sup> <sub>-0.3</sub>	2.5 ± 0.2	-14.6 ± 0.1	0.63 ± 0.09	0.58 ± 0.15
IAC53	18.6833	0.9045	24.5 <sup>+0.3</sup> <sub>-0.3</sub>	1.7 ± 0.2	-15.0 ± 0.1	0.88 ± 0.13	0.59 ± 0.15
IAC54	18.6877	-1.2416	24.7 <sup>+0.3</sup> <sub>-0.2</sub>	3.2 ± 0.3	-16.4 ± 0.1	0.65 ± 0.10	0.41 ± 0.10
IAC55	18.6447	-0.0344	25.2 <sup>+0.5</sup> <sub>-0.5</sub>	2.3 ± 0.2	-14.3 ± 0.1	0.32 ± 0.05	0.96 ± 0.24
IAC56	18.5604	-0.8880	24.8 <sup>+0.4</sup> <sub>-0.4</sub>	2.6 ± 0.3	-15.3 ± 0.1	0.88 ± 0.13	0.75 ± 0.19
IAC57	18.4465	0.0327	25.5 <sup>+0.1</sup> <sub>-0.1</sub>	1.7 ± 0.2	-14.4 ± 0.1	0.67 ± 0.10	0.12 ± 0.03
IAC58	18.4244	0.3189	24.5 <sup>+0.7</sup> <sub>-0.6</sub>	3.0 ± 0.3	-15.2 ± 0.1	0.56 ± 0.08	1.23 ± 0.31
IAC59	18.4093	-0.2806	24.6 <sup>+0.3</sup> <sub>-0.3</sub>	1.6 ± 0.2	-14.8 ± 0.1	0.76 ± 0.11	0.52 ± 0.13
IAC60	18.3700	0.3980	25.3 <sup>+0.5</sup> <sub>-0.4</sub>	2.1 ± 0.2	-14.3 ± 0.1	0.69 ± 0.10	0.81 ± 0.20

Downloaded from https://academic.oup.com/mnras/article-abstract/468/1/703/5089801 by Instituto de Astrofísica de Canarias user on 30 August 2019

MNRAS 468, 703–716 (2017)

Este documento incorpora firma electrónica, y es copia auténtica de un documento electrónico archivado por la ULL según la Ley 39/2015.  
 Su autenticidad puede ser contrastada en la siguiente dirección <https://sede.ull.es/validacion/>

Identificador del documento: 2260218 Código de verificación: Sm21pJYh

Firmado por: JAVIER ROMAN GARCIA  
 UNIVERSIDAD DE LA LAGUNA

Fecha: 02/11/2019 16:23:59

IGNACIO TRUJILLO CABRERA  
 UNIVERSIDAD DE LA LAGUNA

02/11/2019 17:39:19

3.2 Paper II: *Spatial distribution of ultra-diffuse galaxies within large-scale structures*

LXIII

716 *J. Román and I. Trujillo*

Table B1 – continued

ID	RA (°) (J2000)	Dec. (°) (J2000)	$\mu_g(0)$ mag arcsec <sup>-2</sup>	$r_c$ (kpc)	$M_g$ (mag)	$b/a$	$n$
IAC61	18.3349	0.2009	26.2 <sup>+0.3</sup> <sub>-0.3</sub>	2.1 ± 0.2	-13.8 ± 0.1	0.50 ± 0.07	0.53 ± 0.13
IAC62	18.3193	-1.1266	25.1 <sup>+0.2</sup> <sub>-0.2</sub>	1.7 ± 0.2	-14.7 ± 0.1	0.65 ± 0.10	0.27 ± 0.07
IAC63	18.3238	-0.2380	24.8 <sup>+0.5</sup> <sub>-0.4</sub>	4.8 ± 0.5	-16.5 ± 0.1	0.78 ± 0.12	0.84 ± 0.21
IAC64	18.2922	-0.2059	25.5 <sup>+0.5</sup> <sub>-0.4</sub>	3.5 ± 0.4	-15.1 ± 0.1	0.83 ± 0.13	0.88 ± 0.22
IAC65	18.2867	-1.0447	24.3 <sup>+0.3</sup> <sub>-0.3</sub>	2.3 ± 0.2	-15.9 ± 0.1	0.74 ± 0.11	0.51 ± 0.13
IAC66	18.1960	0.1074	24.5 <sup>+0.3</sup> <sub>-0.2</sub>	1.4 ± 0.1	-14.8 ± 0.1	0.91 ± 0.14	0.41 ± 0.10
IAC67	18.1917	0.2934	24.8 <sup>+0.6</sup> <sub>-0.5</sub>	2.5 ± 0.3	-14.8 ± 0.1	0.57 ± 0.09	1.02 ± 0.26
IAC68	18.1807	-0.3870	24.8 <sup>+0.5</sup> <sub>-0.4</sub>	2.9 ± 0.3	-15.4 ± 0.1	0.77 ± 0.12	0.84 ± 0.21
IAC69	18.1305	-0.3235	24.9 <sup>+0.3</sup> <sub>-0.2</sub>	1.5 ± 0.2	-14.4 ± 0.1	0.68 ± 0.10	0.45 ± 0.11
IAC70	18.1110	-0.1171	24.7 <sup>+0.4</sup> <sub>-0.3</sub>	2.1 ± 0.2	-15.1 ± 0.1	0.56 ± 0.08	0.66 ± 0.17
IAC71	18.0735	-0.2127	24.2 <sup>+0.5</sup> <sub>-0.4</sub>	1.6 ± 0.2	-14.7 ± 0.1	0.90 ± 0.13	0.86 ± 0.22
IAC72	18.0456	-0.3164	24.4 <sup>+0.7</sup> <sub>-0.7</sub>	4.0 ± 0.4	-15.7 ± 0.1	0.82 ± 0.12	1.34 ± 0.33
IAC73	17.9467	-1.1528	24.1 <sup>+0.4</sup> <sub>-0.4</sub>	2.0 ± 0.2	-15.7 ± 0.1	0.69 ± 0.10	0.61 ± 0.15
IAC74	17.9327	0.9754	24.4 <sup>+0.3</sup> <sub>-0.3</sub>	2.4 ± 0.2	-15.8 ± 0.1	0.60 ± 0.09	0.53 ± 0.13
IAC75	17.9204	0.5405	24.1 <sup>+0.5</sup> <sub>-0.5</sub>	1.8 ± 0.2	-15.0 ± 0.1	0.71 ± 0.11	0.89 ± 0.22
IAC76	17.6973	-0.7469	24.2 <sup>+0.5</sup> <sub>-0.4</sub>	2.4 ± 0.2	-15.4 ± 0.1	0.96 ± 0.14	0.92 ± 0.23
IAC77	17.6523	0.8092	24.6 <sup>+0.4</sup> <sub>-0.4</sub>	2.2 ± 0.2	-15.1 ± 0.1	0.68 ± 0.10	0.75 ± 0.19
IAC78	17.6129	0.4294	24.9 <sup>+0.4</sup> <sub>-0.4</sub>	1.9 ± 0.2	-14.6 ± 0.1	0.70 ± 0.10	0.70 ± 0.18
IAC79	17.6030	0.4164	25.0 <sup>+0.3</sup> <sub>-0.3</sub>	1.9 ± 0.2	-14.7 ± 0.1	0.65 ± 0.10	0.60 ± 0.15
IAC80	17.5198	-1.0757	24.0 <sup>+0.4</sup> <sub>-0.3</sub>	2.3 ± 0.2	-15.9 ± 0.1	0.90 ± 0.13	0.69 ± 0.17

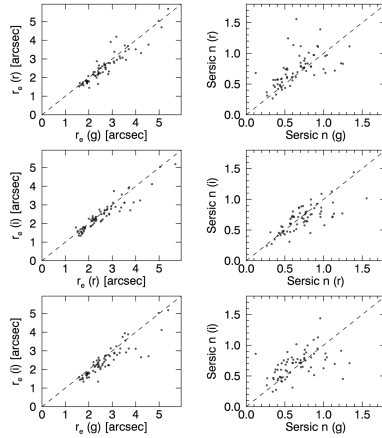


Figure B2. Robustness of the structural parameters  $r_c$  and  $n$  obtained with IMFIT for the set of UDGs explored in this work. The size and shape of the UDGs are compared between the different filters:  $g$ ,  $r$  and  $i$ .

This paper has been typeset from a  $\text{\LaTeX}$  file prepared by the author.

MNRAS **468**, 703–716 (2017)

Downloaded from https://academic.oup.com/mnras/article-abstract/468/1/703/3009801 by Instituto de Astrofísica de Canarias user on 30 August 2019

Este documento incorpora firma electrónica, y es copia auténtica de un documento electrónico archivado por la ULL según la Ley 39/2015.  
 Su autenticidad puede ser contrastada en la siguiente dirección <https://sede.ull.es/validacion/>

Identificador del documento: 2260218 Código de verificación: Sm21pjYh

Firmado por: JAVIER ROMAN GARCIA  
 UNIVERSIDAD DE LA LAGUNA

Fecha: 02/11/2019 16:23:59

IGNACIO TRUJILLO CABRERA  
 UNIVERSIDAD DE LA LAGUNA

02/11/2019 17:39:19

### 3.3 Paper III: *Ultra-diffuse galaxies outside clusters: clues to their formation and evolution*

In the previous article by Román & Trujillo (2017a) severe uncertainties over the absence of distance estimates to ultra-diffuse galaxies were highlighted. This makes the presence of interlopers (false projections in the line of sight) systematic, preventing obtaining clear correlations as color gradients based on density environment. With the aim of minimizing the number of false projections, three Hickson compact groups were selected to minimize the presence of interlopers in the line of sight, as by definition Hickson compact groups are isolated. The presence of ultra-diffuse galaxies was explored, with a total of 11 objects being found. Interestingly, all detected UDGs are located in the vicinity of the selected host groups, while exploring very wide areas, suggesting that these objects are most likely physically associated to the explored host groups, showing the reliability of the approach reducing the number of interlopers.

By analyzing the properties of these UDGs, it was found that objects in the outermost regions of the groups have bluer colors, therefore they are younger, with more irregular morphology and signs of current star formation. These "blue UDGs" were the first evidence of progenitor objects of the typically "red UDGs" with more spheroidal morphology found abundantly in galaxy clusters. Two of these blue UDGs were confirmed to be at the distance of the groups through spectroscopy by SDSS in blue knots of strong star formation of the galaxies, adding robustness to our statement. The presence of these younger UDGs in the outermost regions of the groups and the presence of older UDGs in the inner regions suggested a formation mechanism or evolutionary path in which the typically red UDGs found in galaxy clusters have been firstly accreted as young starforming galaxies, being later quenched by environmental processing. The extrapolation in time, after quenching, of the properties of the blue UDGs are consistent with the observed properties of the red UDGs, making this evolutionary path very likely (see Figure 5 in the article).

The presence of these blue UDGs in low-density environments or field was reported later by many works (Bellazzini et al. 2017; Leisman et al. 2017; Greco et al. 2018a,b; Alabi et al. 2018; Zaritsky et al. 2019; Prole et al. 2019) including the work by Spekkens & Karunakaran (2018) in which the distance of the six blue UDGs found in this article was confirmed by HI detection, matching with the distances of the host groups. Additionally, different works using cosmological simulations (Chan et al. 2018; Liao et al. 2019; Carleton et al. 2019; Jiang et al. 2019) showed that the environmental factor is undoubtedly fundamental in the formation and evolution of ultra diffuse galaxies, supporting the results presented in this article. This hypothesis of formation of UDGs through environmental processing is widely accepted in the community nowadays.

Another interesting result in this article was to extend the relationship, first proposed by van der Burg et al. (2016), between the halo mass of the host and the number of ultra-diffuse galaxies contained in it. Here a slightly lower value than the unit for the slope of this relation was found, again suggesting an ultra-diffuse galaxy formation located in the field and subsequent accretion to the groups and clusters. This result has been confirmed by subsequent works (see e.g. Mancera Piña et al. 2018, for the most recent compilation).

Este documento incorpora firma electrónica, y es copia auténtica de un documento electrónico archivado por la ULL según la Ley 39/2015.  
 Su autenticidad puede ser contrastada en la siguiente dirección <https://sede.ull.es/validacion/>

Identificador del documento: 2260218 Código de verificación: Sm21pjYh

Firmado por: JAVIER ROMAN GARCIA  
 UNIVERSIDAD DE LA LAGUNA

Fecha: 02/11/2019 16:23:59

IGNACIO TRUJILLO CABRERA  
 UNIVERSIDAD DE LA LAGUNA

02/11/2019 17:39:19

3.3 Paper III: *Ultra-diffuse galaxies outside clusters: clues to their formation and evolution*

LXV

Monthly Notices  
of the  
ROYAL ASTRONOMICAL SOCIETY  
MNRAS **468**, 4039–4047 (2017)



## Ultra-diffuse galaxies outside clusters: clues to their formation and evolution

Javier Román<sup>1,2\*</sup> and Ignacio Trujillo<sup>1,2\*</sup>

<sup>1</sup>Instituto de Astrofísica de Canarias, c/ Vía Láctea s/n, E-38205, La Laguna, Tenerife, Spain  
<sup>2</sup>Departamento de Astrofísica, Universidad de La Laguna, E-38206, La Laguna, Tenerife, Spain

Accepted 2017 March 17. Received 2017 March 15; in original form 2016 October 27

### ABSTRACT

We identify six ultra-diffuse galaxies (UDGs) outside clusters in three nearby isolated groups ( $0.014 < z < 0.026$ ) using very deep imaging in three different Sloan Digital Sky Survey filters ( $g$ ,  $r$  and  $i$  bands) from the IAC Stripe 82 Legacy Project. By comparing with the abundance of UDGs in rich galaxy clusters, we find that the density of UDGs (i.e. the number per unit mass of the host structure where they are located) decreases towards the most massive systems. This is compatible with a scenario where UDGs are formed preferentially outside clusters. In the periphery ( $D > 250$  kpc) of our three groups, we identify a population of potential UDG progenitors (two of them confirmed spectroscopically). These progenitors have similar masses, shapes and sizes but are bluer,  $g - i \sim 0.45$  [and for this reason brighter,  $\mu_g(0) < 24$  mag arcsec<sup>-2</sup>] than traditional UDGs ( $g - i \sim 0.76$ ). Passive evolution of these progenitors will transform them into regular [i.e.  $\mu_g(0) > 24$  mag arcsec<sup>-2</sup>] UDGs after  $\sim 6$  Gyr. If confirmed, our observations support a scenario where UDGs are old, extended, low surface brightness dwarf galaxies ( $M_* \sim 10^8 M_\odot$ ) born in the field, are later processed in groups and, ultimately, infall into galaxy clusters by group accretion.

**Key words:** galaxies: dwarf – galaxies: evolution – galaxies: formation – galaxies: photometry – galaxies: structure.

### 1 INTRODUCTION

In the last few years, there has been renewed interest in the study of extended and low surface brightness galaxies (Impey, Bothun & Malin 1988; Bothun, Impey & Malin 1991; Dalcanton et al. 1997). Galaxies with  $\mu_g(0) > 24$  mag arcsec<sup>-2</sup> and  $R_e > 1.5$  kpc<sup>1</sup> have been coined ultra-diffuse galaxies (UDGs) by van Dokkum et al. (2015). These objects have typical stellar masses around  $10^8 M_\odot$  and relatively red colours ( $g - i \sim 0.8$ ). There has been an intense debate about the ultimate nature of these galaxies. For instance, van Dokkum et al. (2015, 2016) suggest the intriguing hypothesis that these galaxies could be failed Milky Way-like objects ( $L_*$ ). On the other hand, using their population of globular clusters, Beasley & Trujillo (2016) support the idea that these are failed Large Magellanic Cloud-like galaxies (see also, Peng & Lim 2016). Both theoretically and observationally, there is increasing agreement towards

the idea that the vast majority of UDGs are dwarf galaxies (Yozin & Bekki 2015a; Beasley et al. 2016; Beasley & Trujillo 2016; Amorisco & Loeb 2016; Amorisco, Monachesi & White 2016; Di Cintio et al. 2017).

The extremely low surface brightness of these galaxies makes it almost impossible to measure their distance using spectroscopic redshifts (exceptions being DF44 and VCC1287). For this reason, these galaxies have been explored in galaxy clusters, where the distance to the UDGs is inferred by their proximity to the massive structure (e.g. Koda et al. 2015; Mihos et al. 2015; Muñoz et al. 2015; van der Burg, Muzzin & Hoekstra 2016). This selection effect towards galaxy clusters could affect our understanding of the nature of these galaxies. In fact, not all the known UDGs are in galaxy clusters, as some have been found outside these structures. At least two UDGs have been confirmed spectroscopically (Martínez-Delgado et al. 2016; Trujillo et al. 2017), and a large number of candidates are shown in Román & Trujillo (2017). These last authors, exploring a wide area of  $8 \times 8$  Mpc around the galaxy cluster Abell 168, find UDGs both in the cluster and in the large-scale structure surrounding this massive object. Having established the existence of UDGs both inside and outside clusters, the question that arises is whether these objects are formed outside the clusters and are later aggregated to them through the infall of galaxy groups.

\* E-mail: jroman@iac.es (JR); itc@iac.es (IT)

<sup>1</sup> It is worth stressing that there is no particular physical motivation behind this observational definition. An effective radius of 1.5 kpc corresponds to  $\sim 3.2$  arcsec at the distance of the Coma galaxy cluster. This angular size is roughly the pixel size (2.8 arcsec) of the Dragonfly lens array (the telescope used to define this galaxy population; van Dokkum et al. 2015).

Este documento incorpora firma electrónica, y es copia auténtica de un documento electrónico archivado por la ULL según la Ley 39/2015.  
Su autenticidad puede ser contrastada en la siguiente dirección <https://sede.ull.es/validacion/>

Identificador del documento: 2260218

Código de verificación: Sm21pjYh

Firmado por: JAVIER ROMAN GARCIA  
UNIVERSIDAD DE LA LAGUNA

Fecha: 02/11/2019 16:23:59

IGNACIO TRUJILLO CABRERA  
UNIVERSIDAD DE LA LAGUNA

02/11/2019 17:39:19

4040 *J. Román and I. Trujillo*

Answering this question could give us important hints on the formation mechanisms of UDGs. In this paper, we explore this scenario.

To achieve our goal, we probed the presence of UDGs in a number of well-known galaxy groups in the deep Stripe 82 survey (Jiang et al. 2008; Abazajian et al. 2009). We benefit from the careful reduction of this data set (the IAC Stripe 82 Legacy Survey) performed by Fliri & Trujillo (2016). Among the different groups available in the IAC Stripe 82 Legacy Survey, we selected Hickson compact groups (HCGs) (Hickson 1982). These are especially useful for our analysis as they are isolated groups by definition. Consequently, the spatial association of UDGs presented in the field of view with these objects is more straightforward.

This paper is structured as follows. In Section 2, we present the data set and in Section 3, we explain the criteria for selecting UDGs. Section 4 describes how UDGs can be grouped into two differentiated samples according to their colour characteristics and stellar population properties. In Section 5, we present an evolutionary scenario linking the properties of the blue and red populations of UDGs. Section 6 shows how the abundance of UDGs is tightly correlated with the halo mass of the structure where they are embedded. Finally, we discuss our results in Section 7. We adopt the following cosmology:  $\Omega_m = 0.3$ ,  $\Omega_\Lambda = 0.7$  and  $H_0 = 70 \text{ km s}^{-1} \text{ Mpc}^{-1}$ . We use the AB-magnitude system in this work.

## 2 DATA

The images used in this work are based on the IAC Stripe 82 Legacy Survey (Fliri & Trujillo 2016).<sup>2</sup> This survey consists of new deep coadds of the Sloan Digital Sky Survey (SDSS) Stripe 82 data, carefully stacked to preserve the faintest surface brightness structures. The pixel scale of these images is the same as regular SDSS data, i.e. 0.396 arcsec. The average seeing of our data set is around 1 arcsec. In this work, we used the rectified images of the survey. In these images, the residuals of the stacking process have been removed and the sky level has been measured with high precision. This produces high-quality and homogenized deep images. The mean limiting surface brightnesses of our data set ( $3\sigma$ ;  $10 \times 10$  arcsec boxes) are 29.1, 28.6 and 28.1 mag arcsec<sup>-2</sup> for the *g*, *r* and *i* bands, respectively. This is  $\sim 1.2$  mag deeper than the Dragonfly images used to explore UDGs (van Dokkum et al. 2015) and a similar depth like in Koda et al. (2015).

Galaxy groups are gravitationally bound structures with typical values of  $M_{200} \sim 10^{13} M_\odot$  and  $R_{200} \sim 500$  kpc. The groups we explore here are HCG07 (RA = 9.816, Dec = +0.888,  $z = 0.0141$ ), HCG25 (RA = 50.182, Dec = -1.052,  $z = 0.0212$ ) and HCG98 (RA = 358.55, Dec = +0.37,  $z = 0.0266$ ). HCGs are defined based on the number of bright galaxy members ( $\geq 4$ ) within some specific magnitude range. Together with the number of bright galaxies, HCGs are also defined based on criteria of isolation and compactness, which make them dense galactic associations. These structures can be as dense as the centre of rich clusters, but with modest velocity dispersions. They are expected to be dynamically dominated by dark matter (Hickson et al. 1992; Pompei & Iovino 2012). X-ray emission (Ponman et al. 1996) and intra-group diffuse light (e.g. Nishiura et al. 2000; White et al. 2003; Da Rocha & Mendes de Oliveira 2005; Da Rocha, Ziegler & Mendes de Oliveira 2008; Hess et al. 2017) have been detected in these objects, confirming their spatial association and intense dynamic activity. We assume a

<sup>2</sup> <http://www.iac.es/proyecto/stripe82/>

MNRAS **468**, 4039–4047 (2017)

spatial scale of 0.288 kpc arcsec<sup>-1</sup> for HCG07, 0.429 kpc arcsec<sup>-1</sup> for HCG25 and 0.535 kpc arcsec<sup>-1</sup> for HCG98.

To explore our groups, we have created wide-field imaging mosaics using the software SWARP (Bertin et al. 2002). This allows us to combine different images from the IAC Stripe 82 project and increase the search area. For the HCG07 group, we explored the area:  $9.5^\circ < \text{RA} < 10.5^\circ$  and  $0.25^\circ < \text{Dec} < 1.25^\circ$  equivalent to  $1.04 \times 1.04$  Mpc at the group distance. For HCG25, the area probed was  $49.5^\circ < \text{RA} < 50.5^\circ$  and  $-1.25^\circ < \text{Dec} < -0.75^\circ$ , i.e.  $1.54 \times 0.77$  Mpc (in this case, the area is limited in declination by the spatial coverage of the Stripe 82 survey). Finally, for HCG98, the area used is  $358^\circ < \text{RA} < 359^\circ$  and  $-0.25^\circ < \text{Dec} < 0.75^\circ$  equivalent to  $1.93 \times 1.93$  Mpc.

## 3 IDENTIFICATION OF ULTRA-DIFFUSE GALAXIES

A first list of galaxy candidates in our mosaics was done using SExtractor (Bertin & Arnouts 1996). We require all our sources to be detected simultaneously in the *g*, *r* and *i* bands. To remove as much as possible of the contamination from point sources, all our targets have a stellarity factor below 0.2 and a minimum area of 15 pixels ( $\sim 2.35$  arcsec<sup>2</sup>). In addition, we require that the selected sources satisfy the following colour cuts:  $g - r < 1.4$  and  $g - i < 1.8$ . These colour criteria remove a large number of targets that have colours not representative of nearby populations (i.e. background contamination). After applying these restrictions, we reduce our initial sample to  $\sim 15\,000$  galaxies deg<sup>-2</sup>.

All the sources in the previous sample were fitted using a single Sérsic model (Sérsic 1968). The fitting code used was IMFIT (Erwin 2015). The Sérsic models were convolved with the point spread function (PSF) of the image. The IAC Stripe 82 Legacy Survey provides a PSF representative of the local conditions of the image. Each piece of the Stripe 82 survey ( $0.5^\circ \times 0.5^\circ$ ) has its own PSF. As input parameters for IMFIT, we use the spatial coordinates of the source, the position angle and the effective radius retrieved from the previous SExtractor run. In addition, we mask the closest sources to the target under study.

To avoid missing potential UDGs sources, we conduct the following sanity checks on the outputs of our model fitting. Any time that IMFIT produces structural parameters representative of a bad fit (like Sérsic index close to 0 or very large  $R_e$ ) or where the magnitude of the model is different from the magnitude obtained from SExtractor by more than 1 mag, then we restart the IMFIT modelling with a different random input seed and slightly different masking configurations. This process is repeated until a robust solution is reached. The structural parameters obtained from the IMFIT Sérsic fit are position angle, ellipticity, Sérsic index  $n$ , effective radius (along the semi-major axis)  $R_e$  and the global magnitude in each band.

Once the structural parameters of all galaxies in our data are determined, we select those with  $R_e > 1.3$  kpc (in the *g* band) and observed  $\mu_g(0) > 23.5$  mag arcsec<sup>-2</sup>. This provides around 40 UDG candidates. However, an important fraction of these sources are artefacts produced by misidentification of objects in the neighbourhood of bright stars or galaxies. Therefore, we visually explore all the UDG candidates and we reject all the false positives. After this visual inspection, we end up with a final sample of 11 UDGs (see Fig. 1). Additionally, for this clean sample, we double-check their structural parameters by masking, if necessary, any close or overlapping source to the target that were not masked in the automatic masking process. As a last step, we obtain the extinction

Este documento incorpora firma electrónica, y es copia auténtica de un documento electrónico archivado por la ULL según la Ley 39/2015.

Su autenticidad puede ser contrastada en la siguiente dirección <https://sede.ull.es/validacion/>

Identificador del documento: 2260218

Código de verificación: Sm21pjYh

Firmado por: JAVIER ROMAN GARCIA  
 UNIVERSIDAD DE LA LAGUNA

Fecha: 02/11/2019 16:23:59

IGNACIO TRUJILLO CABRERA  
 UNIVERSIDAD DE LA LAGUNA

02/11/2019 17:39:19

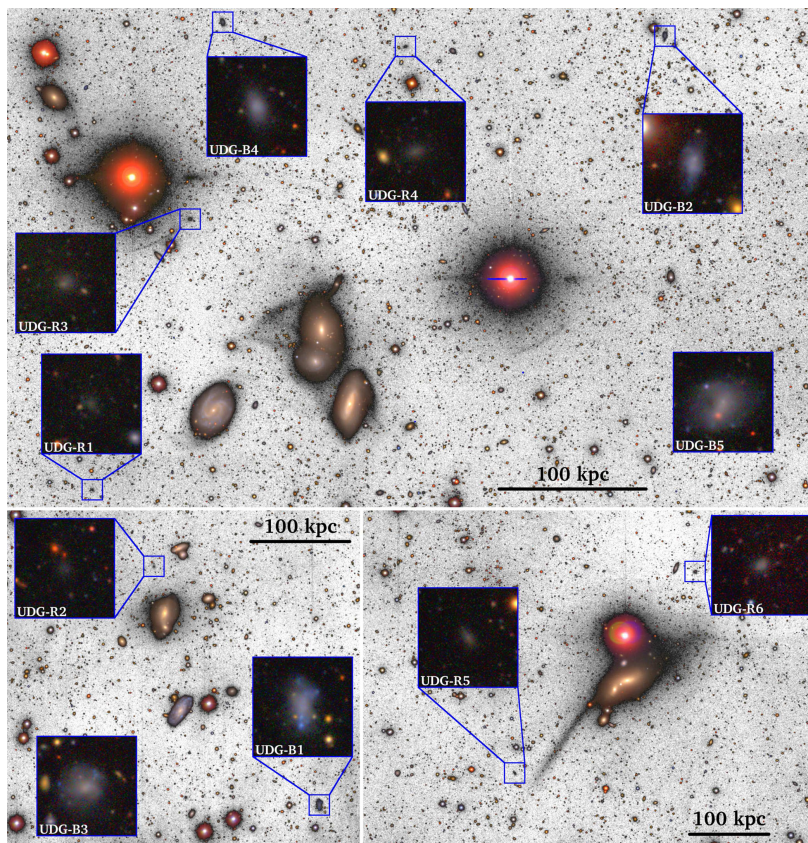


**Figure 1.** UDGs discovered around the Hickson compact groups HCG07 (upper panel), HCG25 (lower left-hand panel) and HCG98 (lower right-hand panel). The sizes of these images (which are a portion of our original mosaics) are: HCG07 ( $31.65 \times 19.64$  arcmin), HCG25 ( $13.91 \times 13.20$  arcmin) and HCG98 ( $17.66 \times 13.20$  arcmin). The inset boxes ( $50 \times 50$  arcsec) are a zoom-in to the individual UDGs. UDG-B5 and UDG-B3 are outside the field of view shown in this figure.

values for each galaxy from Schlafly & Finkbeiner (2011) using their spatial coordinates and we correct their magnitudes.

Note that the final sample of UDGs is located at near the projected distances from the host groups, and we are exploring wider areas. These HCGs are isolated structures both in redshift and spatially, consequently, the proximity of the UDGs to these groups shows that any possible contamination by interlopers, if present, must be very low.

#### 4 TWO TYPES OF ULTRA-DIFFUSE GALAXIES: BLUE AND RED POPULATIONS

The analysis of the population of extended low surface brightness galaxies in the neighbourhood of our groups shows two types of objects. On the one hand, we find a subset of six galaxies (three in HCG07, one in HCG25 and two in HCG98) with structural and colour properties like those UDGs reported previously in the

MNRAS 468, 4039–4047 (2017)

Downloaded from https://academic.oup.com/mnras/article-abstract/468/4/4039/3770503 by Instituto de Astrofísica de Canarias user on 30 August 2019

Este documento incorpora firma electrónica, y es copia auténtica de un documento electrónico archivado por la ULL según la Ley 39/2015.  
 Su autenticidad puede ser contrastada en la siguiente dirección <https://sede.ull.es/validacion/>

Identificador del documento: 2260218 Código de verificación: Sm21pjYh

Firmado por: JAVIER ROMAN GARCIA  
 UNIVERSIDAD DE LA LAGUNA

Fecha: 02/11/2019 16:23:59

IGNACIO TRUJILLO CABRERA  
 UNIVERSIDAD DE LA LAGUNA

02/11/2019 17:39:19

4042 *J. Román and I. Trujillo*

**Table 1.** UDGs sorted by increasing  $g - i$  colour. All magnitudes and derived parameters are corrected for Galactic extinction.

ID	RA (°) (J2000)	Dec (°) (J2000)	$R_e$ [kpc]	$\mu_g(0)$ [mag arcsec <sup>-2</sup> ]	$n$	$b/a$	$g - i$ [mag]	$M_g$ [mag]	$M_{*,g-i}$ [10 <sup>8</sup> M <sub>⊙</sub> ]	$D$ [kpc]
UDG-B1	50.088	-1.170	3.7 ± 0.4	24.0 <sup>+0.4</sup> <sub>-0.5</sub>	0.61 ± 0.15	0.46 ± 0.06	0.27 ± 0.05	-17.01	2.2 <sup>+0.3</sup> <sub>-0.3</sub>	234
UDG-B2	9.599	+1.106	2.0 ± 0.2	24.0 <sup>+0.5</sup> <sub>-0.6</sub>	0.87 ± 0.22	0.50 ± 0.07	0.41 ± 0.05	-15.23	0.6 <sup>+0.1</sup> <sub>-0.1</sub>	319
UDG-B3	49.960	-0.855	3.2 ± 0.3	23.3 <sup>+0.6</sup> <sub>-0.7</sub>	1.02 ± 0.25	0.86 ± 0.12	0.50 ± 0.05	-16.70	3.4 <sup>+0.5</sup> <sub>-0.4</sub>	458
UDG-B4	9.889	+1.115	1.7 ± 0.2	23.8 <sup>+0.6</sup> <sub>-0.7</sub>	1.00 ± 0.25	0.60 ± 0.09	0.53 ± 0.05	-14.95	0.7 <sup>+0.1</sup> <sub>-0.1</sub>	247
UDG-B5	9.969	+0.383	3.1 ± 0.3	23.9 <sup>+0.6</sup> <sub>-0.6</sub>	0.96 ± 0.24	0.75 ± 0.11	0.55 ± 0.05	-16.10	2.2 <sup>+0.3</sup> <sub>-0.3</sub>	547
UDG-R1	9.974	+0.808	1.4 ± 0.1	26.1 <sup>+0.5</sup> <sub>-0.6</sub>	0.79 ± 0.20	0.64 ± 0.09	0.63 ± 0.15	-12.46	0.1 <sup>+0.1</sup> <sub>-0.1</sub>	183
UDG-R2	50.196	-1.014	1.8 ± 0.2	25.9 <sup>+0.5</sup> <sub>-0.5</sub>	0.77 ± 0.19	0.73 ± 0.10	0.66 ± 0.15	-13.31	0.2 <sup>+0.1</sup> <sub>-0.1</sub>	62
UDG-R3	9.910	+0.985	1.5 ± 0.1	25.0 <sup>+0.6</sup> <sub>-0.6</sub>	0.92 ± 0.23	0.90 ± 0.13	0.74 ± 0.15	-13.41	0.4 <sup>+0.2</sup> <sub>-0.1</sub>	140
UDG-R4	9.769	+1.099	1.8 ± 0.2	25.4 <sup>+0.6</sup> <sub>-0.7</sub>	0.98 ± 0.24	0.63 ± 0.09	0.78 ± 0.15	-13.36	0.4 <sup>+0.2</sup> <sub>-0.1</sub>	224
UDG-R5	358.616	+0.322	2.1 ± 0.2	25.3 <sup>+0.5</sup> <sub>-0.6</sub>	0.81 ± 0.20	0.59 ± 0.08	0.85 ± 0.15	-14.21	1.1 <sup>+0.5</sup> <sub>-0.3</sub>	157
UDG-R6	358.497	+0.454	1.8 ± 0.2	24.1 <sup>+0.6</sup> <sub>-0.6</sub>	0.93 ± 0.23	0.73 ± 0.10	0.87 ± 0.15	-14.92	2.0 <sup>+1.0</sup> <sub>-0.6</sub>	192

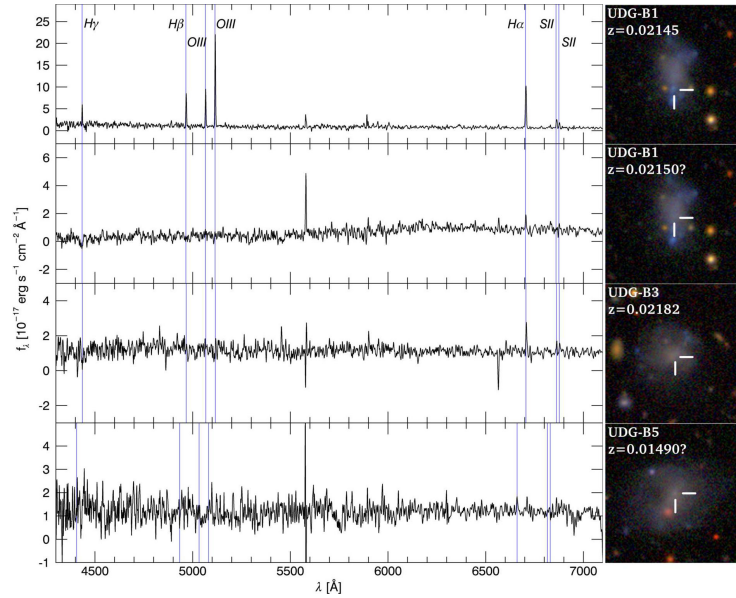


**Figure 2.** Available spectroscopic data from the SDSS survey of the UDGs in this work. The redshifts with a question mark have insufficient signal-to-noise ratio for a robust match, and indicate the most likely redshift. The UDG-B5 redshift remains doubtful.

literature, i.e.  $R_e \geq 1.4$  kpc,  $\mu_g(0) \geq 24.1$  mag arcsec<sup>-2</sup>, mean Sérsic index  $n = 0.86 \pm 0.04$  and mean colour  $g - i = 0.75 \pm 0.04$ . These galaxies are at a mean projected distance of  $D \approx 160$  kpc, i.e. quite close to the group centres. On the other hand, there is a number (three in HCG07 and two in HCG25) of extended low surface brightness galaxies in our field of view that are significantly bluer than the

previous population. They have  $0.27 < g - i < 0.55$  and structural parameters  $R_e \gtrsim 1.7$  kpc and  $23.3 < \mu_g(0) < 24.0$  mag arcsec<sup>-2</sup>. These objects are located at projected radial distances significantly further away than the redder sample with  $D \approx 360$  kpc. Importantly, three of the five blue UDGs (UDG-B1, UDG-B3 and UDG-B5) have spectroscopic data from SDSS (see Fig. 2), two of which

MNRAS **468**, 4039–4047 (2017)

Downloaded from https://academic.oup.com/mnras/advance-article-abstract/doi/10.1093/mnras/stz177/55059 by Instituto de Astrofísica de Canarias user on 30 August 2019

Este documento incorpora firma electrónica, y es copia auténtica de un documento electrónico archivado por la ULL según la Ley 39/2015.  
 Su autenticidad puede ser contrastada en la siguiente dirección <https://sede.ull.es/validacion/>

Identificador del documento: 2260218

Código de verificación: Sm21pjYh

Firmado por: JAVIER ROMAN GARCIA  
 UNIVERSIDAD DE LA LAGUNA

Fecha: 02/11/2019 16:23:59

IGNACIO TRUJILLO CABRERA  
 UNIVERSIDAD DE LA LAGUNA

02/11/2019 17:39:19

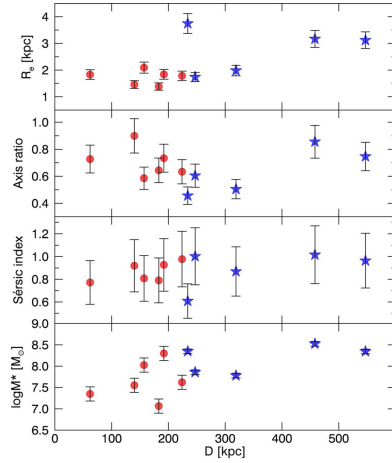


**Figure 3.** Structural and stellar mass properties of the UDGs presented in this work. The blue stars represent the population of blue UDGs ( $g-i < 0.6$ ) and the red dots the red UDGs ( $g-i > 0.6$ ). Red UDGs are predominantly located at a projected distance less than 200 kpc from the group central regions.

have robust redshifts confirming their association with the group structure. The properties of these 11 galaxies are shown in Table 1 and their morphological appearance can be observed in Fig. 1. We name these galaxies according to their  $g-i$  colour as UDG-R (red ones;  $g-i > 0.6$ ) and UDG-B (blue ones;  $g-i < 0.6$ ). The relation between the structural properties of the UDGs and the projected distance to the group centre is shown in Fig. 3. These results are like those found in Román & Trujillo (2017), with a decrease in stellar mass, the Sérsic index and the effective radius of the UDGs towards the centre of the group. The morphologies of the blue UDGs are quite irregular, with some of them showing blue clumps of apparently intense star formation. Despite their irregular morphologies, the average Sérsic index of the blue UDGs is quite like that of the red population, i.e.  $n \sim 0.9$ .

#### 4.1 Stellar population properties of the ultra-diffuse galaxies

The very low surface brightness of the UDGs makes studying their stellar population properties using spectroscopy with present-day instrumentation extremely challenging. Some of our brightest galaxies have spectra provided by the SDSS. However, their signal-to-noise ratio is insufficient to get reliable information about their stellar population properties. There is one exception, for the UDG-B1 galaxy, in which the SDSS pipeline took a spectrum of one of its bright blue clumps located at the spatial position (RA = 50.088, Dec = -1.172). According to that spectrum, this region of the galaxy has low metallicity and an extremely young age ( $< 0.1$  Gyr). Due to the colour characteristics of this clump (significantly much bluer than the rest of the object), we consider that these stellar population

properties are not representative of the whole galaxy. For the above reasons, we need to address the problem of the stellar population properties of the UDGs using integrated deep photometry. In this paper, we use the  $g$ ,  $r$  and  $i$  bands for this. Some of our galaxies, especially the bluer ones, are detected in the  $u$  band as well. However, we restrict ourselves to only those SDSS filters where all the galaxies in the sample have been detected.

To get a rough estimation of the stellar masses of our galaxies, we use the method provided by Roediger & Courteau (2015) [assuming a Chabrier initial mass function (IMF)]. In particular, we use the  $g-i$  colour and the absolute magnitude in the  $r$  band. The stellar masses are provided in Table 1. The mean stellar mass of the blue UDGs is  $\sim 1.8 \times 10^8 M_{\odot}$ , whereas the red ones are a factor of  $\sim 2$  less massive:  $\sim 0.9 \times 10^8 M_{\odot}$ . As a further test, we re-estimated the stellar masses of our UDGs using the stellar population predictions provided by Vazdekis et al. (2015) using a universal Kroupa IMF (Kroupa 2001). We use the  $g-r$  and  $r-i$  colour map as a proxy for estimating the best age and metallicities describing the observed colours. We follow a similar approach as the one used in Montes & Trujillo (2014). The outcome of this exercise is given in Fig. 4. Using this new method, the mean stellar mass of the blue UDGs is  $\sim 1.2 \times 10^8 M_{\odot}$ , whereas the red UDGs have a mean stellar mass of  $\sim 0.6 \times 10^8 M_{\odot}$ . Both approaches provide similar stellar masses for the two populations. The clumpy appearance of the blue UDGs suggests that the colours (and consequently, the stellar population properties) of these galaxies are heavily affected by these knots of intense star formation. In this sense, it is worth exploring whether the stellar masses of the blue UDGs would change on using the colours of the central part ( $R < 4$  arcsec)<sup>3</sup> of these objects, where star formation is less prominent. Using these colours, we estimate ( $M/L$ ), and together with the absolute magnitude of the galaxies in the  $i$  band (to minimize the contribution of the star-forming regions), we derive again the stellar masses of the blue population. We obtain a mean stellar mass for the blue UDGs of  $\sim 1.4 \times 10^8 M_{\odot}$ , in good agreement with all the previous different methods.

Once the stellar masses of our UDGs were estimated, we focussed our attention on the ages and metallicities of the two populations of UDGs. Having only two colours, the expected degeneracy between the age and the metallicity is very high. This is, in fact, what we see in Fig. 4. The red UDGs show mean colours of  $g-r = 0.55 \pm 0.04$  and  $g-i = 0.75 \pm 0.04$  ( $r-i = 0.20 \pm 0.04$ ), compatible with a metallicity in the range  $-2 < [\text{Fe}/\text{H}] < -1$  and  $t > 2$  Gyr, although the possibility that red UDGs have a younger population 1 Gyr  $< t < 2$  Gyr with a solar metallicity is, however, not rejected. These metallicities and age ranges are in agreement with previous works. For instance, van Dokkum et al. (2015) found  $g-i = 0.8$ , suggesting a stellar population of 7 Gyr with  $[\text{Fe}/\text{H}] = -1.4$  or 4 Gyr and  $[\text{Fe}/\text{H}] = -0.8$ . Other authors, like van der Burg et al. (2016), found  $g-r = 0.6$  populations with an age of 2 Gyr assuming solar metallicity or 6 Gyr with  $[\text{Fe}/\text{H}] = -0.7$ . Note that the gap present around 1.2 Gyr in the age-metallicity map corresponds to the transition from the light contribution of asymptotic giant branch stars to red giant branch stars (see e.g. Bertelli et al. 1994).

Finally, the sample of blue UDGs have these mean colours:  $g-r = 0.30 \pm 0.03$  and  $r-i = 0.15 \pm 0.03$ . These bluer colours imply that  $t < 1$  Gyr (see Fig. 4). However, we can say little about their metallicities. If we focus our attention on the core of the blue

<sup>3</sup> Using a  $R < 4$  arcsec aperture, we get to select the core regions for all galaxies avoiding blue knots.

Este documento incorpora firma electrónica, y es copia auténtica de un documento electrónico archivado por la ULL según la Ley 39/2015.  
 Su autenticidad puede ser contrastada en la siguiente dirección <https://sede.ull.es/validacion/>

Identificador del documento: 2260218

Código de verificación: Sm21pjYh

Firmado por: JAVIER ROMAN GARCIA  
 UNIVERSIDAD DE LA LAGUNA

Fecha: 02/11/2019 16:23:59

IGNACIO TRUJILLO CABRERA  
 UNIVERSIDAD DE LA LAGUNA

02/11/2019 17:39:19

4044 *J. Román and I. Trujillo*

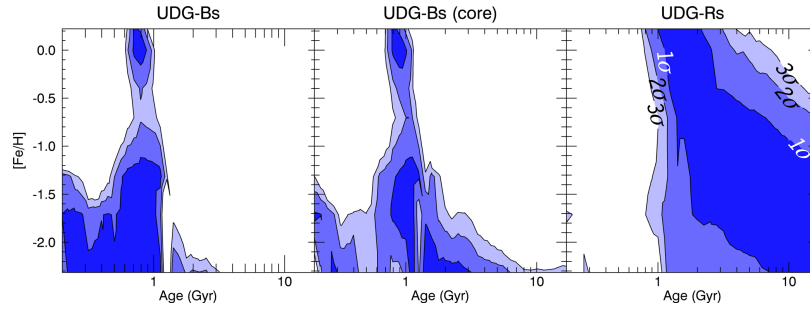


Figure 4. Age and metallicity distribution of our sample of UDGs. The different colour regions correspond to the  $1\sigma$ ,  $2\sigma$  and  $3\sigma$  confidence intervals.

UDGs, their redder colours  $g - r = 0.34 \pm 0.04$  and  $r - i = 0.17 \pm 0.02$  are suggestive of a slightly older population with  $1 \text{ Gyr} \lesssim t \lesssim 2 \text{ Gyr}$ .

#### 5 AN EVOLUTIONARY SCENARIO

In this section, we explore the following evolutionary scenario: red UDGs are the result of the group environmental processing of the blue UDGs located in the outskirts. In other words, blue UDGs eventually infall into the group centre where their gas is removed by ram pressure or tidal stripping and they become red UDGs with time. In this process, their stellar population gets redder and older but their metallicity should not change. During this process, it is likely that the UDGs lose part of their stellar mass (decreasing their effective radius) and become more rounded. Is this evolutionary scenario compatible with our observations? To start with, blue UDGs are, in fact, systematically located in the outskirts of the groups (see Fig. 3). In that sense, the star-formation activity of the UDGs seems to be strongly related with the location of these galaxies within the dark matter halo of the group. Moreover, the sizes and stellar masses of the red UDGs are smaller than the blue UDGs. The red UDGs are also roundish.

We can try to quantify the above evolutionary scenario more by comparing the stellar population properties of blue and red UDGs with the expected theoretical transformation for dwarf galaxies within group environments. Yozin & Bekki (2015b) studied the environmental processing of dwarf galaxies infalling into groups ( $10^{13} M_{\odot}$ ). According to these authors, the dwarf galaxies become gas poor after 6 Gyr of the first infall. Note, however, that these simulations are for dwarf galaxies that are more massive ( $10^9 M_{\odot}$ ) than our blue UDGs ( $10^8 M_{\odot}$ ). Having said that, it is reasonable to explore whether a passive evolution of our blue UDGs will lead to properties that resemble those of our red UDGs.

We conduct such an exercise in Fig. 5. In this figure (upper left-hand panel), we show the location of our UDGs (red and blue) in the colour-colour map  $g - r$  versus  $r - i$ . Overplotted on the galaxies are the tracks (for different metallicities) of the time evolution of passively evolving stellar populations from the models of Vazdekis et al. (2015). To simplify our exercise, we calculate the passive evolution of the colours of the blue UDGs for a fixed metallicity. We

select  $[\text{Fe}/\text{H}] = -1.31$ .<sup>4</sup> Once we have selected a metallicity, it is straightforward to add a colour increase to the observed colours of the blue UDGs after a given amount of time. In our case, we decided to use 6 Gyr (although our main results are basically unchanged if the time evolution is selected to be within 6 to 10 Gyr).<sup>5</sup> We use 6 Gyr motivated by the simulation of Yozin & Bekki (2015b). The results of the time evolution of the blue UDGs in the colour-colour map are shown in the lower left-hand panel of Fig. 5. The location on this map of the average UDG in the Abell 168 cluster and its surroundings is also shown (Román & Trujillo 2017). In addition, we include also the location of the galaxy VCC1287 (Beasley et al. 2016). We add these extra points as these are the only studies (besides this one) with a characterization of UDGs in three optical bands. The scatter of the red UDGs in this colour-colour map is larger due to the higher photometric uncertainties at measuring the colours of these fainter objects. Note how, after 6 Gyr of passive evolution, the locations of the blue UDGs are in nice agreement with the location of the red UDGs. It is important to stress that some of our galaxies (like UDG-B4) have some properties in between the red and the blue population, reinforcing the idea that both populations are connected.

Once the evolution in the colour-colour map of the blue UDGs has been explored, it is worth looking at the change of the surface brightness profiles of these objects assuming a passive evolution. This is, of course, an oversimplification of the real scenario. In fact, it is expected that these infalling dwarf galaxies will have some stellar mass loss during the infall process to the group. An eventual stellar mass loss will produce a decrease in their effective radius (as most of the mass loss will likely be produced in the outskirts of these objects). The right column (upper panel) in Fig. 5 shows the observed surface brightness profiles of both blue and red UDGs. The passive evolution of the blue UDGs is modelled in the lower panel of the same figure. As can be seen, after 6 Gyr of passive

<sup>4</sup> A solar metallicity will also represent the colour position of the blue UDGs but considering the low mass of our UDGs, we prefer to do this by assuming they have a low metallicity. Low-mass galaxies are not expected to have solar metallicity because of the inefficiency of their star formation (e.g. Vazdekis et al. 1996).

<sup>5</sup> Every gigayear increase produces a reddening in our colours of  $\sim 0.01$  in this time interval.

MNRAS **468**, 4039–4047 (2017)

Downloaded from https://academic.oup.com/mnras/article-abstract/468/4/4039/3770508 by Instituto de Astrofísica de Canarias user on 30 August 2019

Este documento incorpora firma electrónica, y es copia auténtica de un documento electrónico archivado por la ULL según la Ley 39/2015.  
 Su autenticidad puede ser contrastada en la siguiente dirección <https://sede.ull.es/validacion/>

Identificador del documento: 2260218 Código de verificación: Sm21pjYh

Firmado por: JAVIER ROMAN GARCIA  
 UNIVERSIDAD DE LA LAGUNA

Fecha: 02/11/2019 16:23:59

IGNACIO TRUJILLO CABRERA  
 UNIVERSIDAD DE LA LAGUNA

02/11/2019 17:39:19

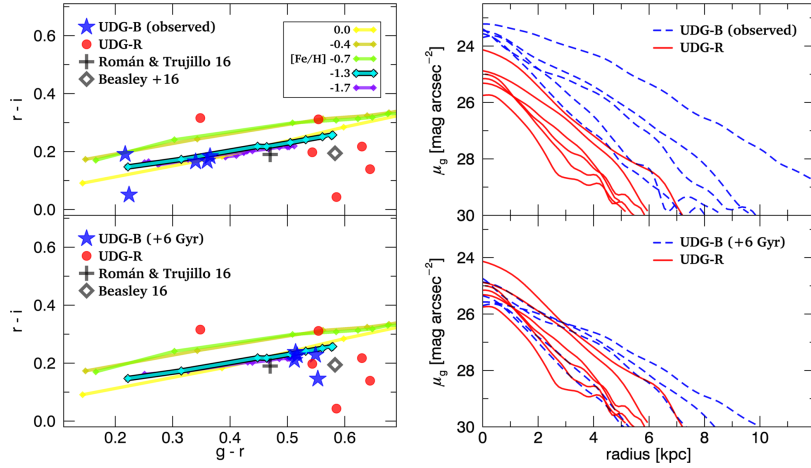


**Figure 5.** An evolutionary scenario between blue and red UDGs. Left column: Colour-colour map for the UDGs in this work. The upper panel shows the location of the blue UDGs (blue stars) and red UDGs (red dots). Overplotted are the stellar population tracks from the Vazdekis et al. (2015) models. We also show the location of the UDGs from the work by Román & Trujillo (2017) and Beasley et al. (2016). The ticks on the stellar population tracks represent the ages (from left to right): 0.5, 1.0, 2.0, 3.2, 5.0, 10.0, 12.5 and 15 Gyr. The lower panel shows the location of the blue UDGs after 6 Gyr of passive evolution. Right column: The upper panel shows the observed surface brightness profiles in the  $g$  band of the blue and red UDGs. The bottom panel shows the expected location of the surface brightness profiles of the blue galaxies after 6 Gyr of passive evolution (there has been no attempt to model any mass or size evolution).

evolution all the current blue UDGs will be classified as regular UDGs [i.e. large objects with  $\mu_g(0) > 24$  mag arcsec $^{-2}$ ]. As the Sérsic indices of both blue and red UDGs are very similar ( $n > 0.8$ ), a passive transformation of the blue population will resemble the red population. However, despite the similar appearance of the evolved blue UDGs in relation to the red UDGs, some of the evolved blue UDGs show an excess of light in their outer regions compared to the red population. This is as expected considering that (i) we have not modelled any mass loss in the profiles of the blue UDGs and (ii) the profiles of the blue UDGs are affected by the presence of intense star-forming regions in the outer parts. Considering that these star-forming regions are relevant in light but not as much in mass, the time evolution of the surface brightness profiles of the blue galaxies in the outer regions will approximate the shape of the red population. Summarizing, under the hypothesis that the blue UDGs will passively evolve as the result of their infall into the group's gravitational potential, the global colour and shape properties will be close to those of the red UDG population, making a scenario linking the two types of galaxies plausible.

#### 6 THE ABUNDANCE OF UDGs AS A FUNCTION OF THE HALO MASS

Van der Burg et al. (2016) showed that there is a tight correlation between the number of UDGs in a given cluster and the mass of the cluster as parametrized by  $M_{200}$ . According to that work, the abundance of UDGs increases almost proportionally to the mass of the cluster in which they are embedded. Van der Burg et al. (2016)

studied this relation for clusters with  $M_{200} \gtrsim 10^{14} M_{\odot}$ . In this work, we want to probe where that relation also holds for less massive gravitationally bound systems. To do this, we have compiled in Fig. 6 the number of UDGs observed in different works as a function of their host velocity dispersion and  $M_{200}$ . For the clusters provided by van der Burg et al. (2016), we use their  $M_{200}$  and the velocity dispersion from Sifón et al. (2015). For the Abell 168 cluster and the UGC 842 group presented in Román & Trujillo (2017), we use as sources for their velocity dispersions Yang et al. (2004) (for the cluster) and Lopes de Oliveira et al. (2010) (for the group). For the Coma cluster (Koda et al. 2015), the velocity dispersion was taken from Girardi et al. (1993), whereas for the Fornax cluster (Muñoz et al. 2015), the velocity dispersion is obtained from Drinkwater, Gregg & Colless (2001). Finally, for the groups presented in this paper, we have used the velocity dispersions given by Tovmassian, Plionis & Torres-Papaqui (2006). Once we have the velocity dispersions, we follow Munari et al. (2013) to get  $M_{200}$  for these structures.

Fig. 6 shows that the tight correlation between the abundance of UDGs and the halo mass of the structures in which they are located extends also towards lower masses than those originally explored by van der Burg et al. (2016). We have fitted our relations assuming a power law, as was done by van der Burg et al. (2016):  $N \propto \sigma^{\alpha}$  and  $N \propto M_{200}^{\beta}$ . We find the following values:  $\alpha = 2.43 \pm 0.14$  and  $\beta = 0.85 \pm 0.05$ . In our plot of  $M_{200}$ , the estimation of this quantity comes from two different sources (Munari et al. 2013; Sifón et al. 2015); however, our results remain basically the same ( $\beta = 0.87 \pm 0.05$ ) if we use the methodology of Munari et al. (2013) for estimating  $M_{200}$  for all the structures. Interestingly, van der Burg

Este documento incorpora firma electrónica, y es copia auténtica de un documento electrónico archivado por la ULL según la Ley 39/2015.  
 Su autenticidad puede ser contrastada en la siguiente dirección <https://sede.ull.es/validacion/>

Identificador del documento: 2260218 Código de verificación: Sm21pjYh

Firmado por: JAVIER ROMAN GARCIA  
 UNIVERSIDAD DE LA LAGUNA

Fecha: 02/11/2019 16:23:59

IGNACIO TRUJILLO CABRERA  
 UNIVERSIDAD DE LA LAGUNA

02/11/2019 17:39:19

4046 *J. Román and I. Trujillo*

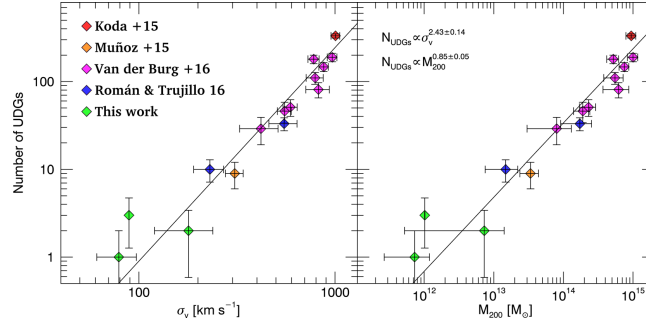


**Figure 6.** The abundance of UDGs as a function of the velocity dispersion and halo mass of the structure in which they are located. The data shown are a compilation from the literature and our own work here. See text for further details.

et al. (2016) found a value for  $\beta = 0.93 \pm 0.16$  in agreement (within the error bars) with the expanded mass sample we have explored here. Determining the exponent  $\beta$  is key for understanding in which structures the UDGs are formed with higher efficiency. We discuss the implication of our finding in the next section.

## 7 DISCUSSION AND SUMMARY

In this paper, we have suggested an evolutionary scenario where present-day UDGs are the result of the environmental transformation (mainly by gas stripping) of infalling low surface brightness dwarf galaxies (of similar stellar mass and structural parameters) into the gravitational potential of the groups and clusters. We want to expand this discussion further and explore which kind of structures (groups or clusters) are more favourable for the formation of UDGs. Initially, clusters were considered the natural place for finding UDGs; however, there is increasing evidence (first noted by Román & Trujillo 2017 and recently by Merritt et al. 2016; see also: Ordenes-Briceno et al. 2016; Smith Castelli, Faifer & Escudero 2016) that UDGs are also found outside clusters. The existence of UDGs in the field has also been motivated theoretically by Di Cintio et al. (2017). As there is a tight correlation between the abundance of UDGs and the mass of the host structures in which they are located (van der Burg et al. 2016), it is worth exploring what can be learned from this relation.

The relation between the abundance of UDGs and  $M_{200}$  is characterized by a power law with an exponent slightly lower than 1, i.e.  $\beta = 0.85 \pm 0.05$ . If  $\beta$  were larger than 1, the UDGs would be formed preferentially in clusters. Let us expand on this. Under the assumption (see e.g. Buote 2002; Girardi & Biviano 2002) that clusters were purely the result of the merging of smaller sub-units (i.e. groups of galaxies), the abundance of UDGs will never be larger (i.e.  $\beta > 1$ ) than the contribution of UDGs accreted through the infalling of groups to the cluster. Consequently, observations showing that  $\beta > 1$  would be a strong argument favouring the preferential (in situ) formation of UDGs in clusters of galaxies. If  $\beta < 1$ , however, the observational result is not straightforward to interpret. Naively, one could understand that if  $\beta < 1$  then UDGs form preferentially in groups. As groups infall into clusters, one would expect that some UDGs could be disrupted during the accretion process and

thus,  $\beta \leq 1$ .  $\beta < 1$  could be also expected if UDGs are more easily destroyed in clusters than in groups over time.<sup>6</sup> For this reason, if  $\beta < 1$ , we cannot firmly conclude that UDGs form preferentially in groups than in clusters. Nonetheless, the observational result does not contradict this hypothesis.

Another interesting issue to explore is why the relation between the abundance of UDGs and  $\sigma$  is so tight (Pearson correlation coefficient  $r = 0.964$ ). This is not at all expected as the number of UDGs in a given structure is a function of the depth of the survey used to detect these objects and the background and foreground contamination. The limiting surface brightnesses of the different surveys presented in Fig. 6 are  $29.2 \text{ mag arcsec}^{-2}$  ( $3\sigma$ ,  $10 \times 10 \text{ arcsec}$  in the  $g$  band; Román & Trujillo 2017),  $28.8\text{--}29.2 \text{ mag arcsec}^{-2}$  ( $3\sigma$ ,  $10 \times 10 \text{ arcsec}$  in the  $R$  band; Koda et al. 2015),  $28.9 \text{ mag arcsec}^{-2}$  ( $3\sigma$ ,  $10 \times 10 \text{ arcsec}$  in the  $i$  band; Muñoz et al. 2015) and  $28.9 \text{ mag arcsec}^{-2}$  ( $3\sigma$ ,  $10 \times 10 \text{ arcsec}$  in the  $r$  band; van der Burg et al. 2016). As can be seen, all the surveys have a relatively similar surface brightness limit. This is as expected due to the technical limits of present-day telescopes (see a discussion in Trujillo & Fliri 2016). This could explain why the number of UDGs detected is similar among clusters of similar masses for different groups. Another crucial issue is related to the expected contamination by foreground and background interlopers. All the previous authors applied some particular recipe for cleaning their number counts. The tightness of the correlation indicates that the abundance of UDGs is somehow robust to the different methodologies.

To conclude, our observations support a scenario where present-day UDGs are old ( $> 2 \text{ Gyr}$ ), extended, low surface brightness [ $\mu(g, 0) > 24 \text{ mag arcsec}^{-2}$ ] dwarf ( $M_* \sim 10^8 M_\odot$ ) galaxies. These galaxies would have been formed preferentially in the field, where they would be brighter [i.e.  $\mu(g, 0) < 24 \text{ mag arcsec}^{-2}$ ] and eluding the current criteria for selecting UDGs) and younger. Later they would be processed in groups (on scales of around  $6 \text{ Gyr}$ ) and, ultimately, infall into galaxy clusters by group accretion.

<sup>6</sup>Note, however, that from the theoretical point of view, the situation is the opposite: groups are more effective at destroying dwarf galaxies than clusters (see e.g. Mihos 2003).

MNRAS **468**, 4039–4047 (2017)

Downloaded from https://academic.oup.com/mnras/advance-article-abstract/doi/10.1093/mnras/stz1050 by Instituto de Astrofísica de Canarias user on 30 August 2019

Este documento incorpora firma electrónica, y es copia auténtica de un documento electrónico archivado por la ULL según la Ley 39/2015.  
 Su autenticidad puede ser contrastada en la siguiente dirección <https://sede.ull.es/validacion/>

Identificador del documento: 2260218

Código de verificación: Sm21pjYh

Firmado por: JAVIER ROMAN GARCIA  
 UNIVERSIDAD DE LA LAGUNA

Fecha: 02/11/2019 16:23:59

IGNACIO TRUJILLO CABRERA  
 UNIVERSIDAD DE LA LAGUNA

02/11/2019 17:39:19

3.3 Paper III: *Ultra-diffuse galaxies outside clusters: clues to their formation and evolution*

LXXIII

Formation and evolution of ultra-diffuse galaxies 4047

ACKNOWLEDGEMENTS

We thank the referee for a careful review and useful comments. We want to thank Alejandro Borlaff for his help in producing some of the plots used in this paper. We thank also Alejandro Vazdekis, Mike Beasley and Jorge Sánchez Almeida for helpful discussions. This research was supported by the Instituto de Astrofísica de Canarias. The authors of this paper acknowledge support from grant AYA2016-77237-C3-1-P from the Spanish Ministry of Economy and Competitiveness (MINECO). JR thanks MINECO for financing his PhD through an FPI grant.

REFERENCES

Abazajian K. N. et al., 2009, *ApJS*, 182, 543  
Amorisco N. C., Loeb A., 2016, *MNRAS*, 459, L51  
Amorisco N. C., Monachesi A., White S. D. M., 2016, *MNRAS*, preprint (arXiv:1610.01595)  
Beasley M. A., Trujillo I., 2016, *ApJ*, 830, 23  
Beasley M. A., Romanowsky A. J., Pota V., Navarro I. M., Martínez Delgado D., Neyer F., Deich Aaron L., 2016, *ApJ*, 819, L20  
Bertelli G., Bressan A., Chiosi C., Fagotto F., Nasi E., 1994, *A&AS*, 106, 393  
Bertin E., Arnouts S., 1996, *A&AS*, 117, 393  
Bertin E., Mellier Y., Radovich M., Missonnier G., Didelon P., Morin B., 2002, in Bohlender D. A., Durand D., Handley T. H., eds, *ASP Conf. Ser. Vol. 281, Astronomical Data Analysis Software and Systems XI*. Astron. Soc. Pac., San Francisco, p. 228  
Bothun G. D., Impey C. D., Malin D. F., 1991, *ApJ*, 376, 404  
Butte D. A., 2002, in Feretti L., Gioia I. M., Giovannini G., eds, *Merging Processes in Galaxy Clusters*, Optical Analysis of Cluster Mergers. Astrophysics and Space Science Library, Vol. 272. Kluwer Academic Publisher, the Netherlands  
Da Rocha C., Mendes de Oliveira C., 2005, *MNRAS*, 364, 1069  
Da Rocha C., Ziegler B. L., Mendes de Oliveira C., 2008, *MNRAS*, 388, 1433  
Dalcanton J. J., Spergel D. N., Gunn J. E., Schmidt M., Schneider D. P., 1997, *AJ*, 114, 635  
Di Cintio A., Brook C. B., Dutton A. A., Macciò A. V., Ojreja A., Dekel A., 2017, *MNRAS*, 466, L1  
Drinkwater M. J., Gregg M. D., Colless M., 2001, *ApJ*, 548, L139  
Erwin P., 2015, *ApJ*, 799, 226  
Fliri J., Trujillo I., 2016, *MNRAS*, 456, 1359  
Girardi M., Biviano A., 2002, *Merging Processes in Galaxy Clusters*, vol. 272, p. 39  
Girardi M., Biviano A., Giuricin G., Mardrossian F., Mezzetti M., 1993, *ApJ*, 404, 38  
Hess K. M., Cluver M. E., Yahya S., Leisman L., Serra P., Lucero D. M., Passmoor S. S., Carignan C., 2017, *MNRAS*, 464, 957  
Hickson P., 1982, *ApJ*, 255, 382

Hickson P., Mendes de Oliveira C., Huchra J. P., Palumbo G. G., 1992, *ApJ*, 399, 353  
Impey C., Bothun G., Malin D., 1988, *ApJ*, 330, 634  
Jiang L. et al., 2008, *AJ*, 135, 1057  
Koda J., Yagi M., Yamanoi H., Komiyama Y., 2015, *ApJ*, 807, L2  
Kroupa P., 2001, *MNRAS*, 322, 231  
Lopes de Oliveira R., Carrasco E. R., Mendes de Oliveira C., Bortoletto D. R., Cypriano E., Sodré L., Jr, Lima Neto G. B., 2010, *AJ*, 139, 216  
Martínez-Delgado D. et al., 2016, *AJ*, 151, 96  
Merritt A., van Dokkum P., Danielli S., Abraham R., Zhang J., Karachentsev I. D., Makarova L. N., 2016, *ApJ*, 833, 168  
Mihos C., 2003, preprint (astro-ph/030512)  
Mihos J. C. et al., 2015, *ApJ*, 809, L21  
Montes M., Trujillo I., 2014, *ApJ*, 794, 137  
Munari E., Biviano A., Borgani S., Murante G., Fabjan D., 2013, *MNRAS*, 430, 2638  
Muñoz R. P. et al., 2015, *ApJ*, 813, L15  
Nishiura S., Murayama T., Shimada M., Sato Y., Nagao T., Molikawa K., Taniguchi Y., Sanders D. B., 2000, *AJ*, 120, 2355  
Ordenes-Briccio Y. et al., 2016, *MNRAS*, 463, 1284  
Peng E. W., Lim S., 2016, *ApJ*, 822, L31  
Pompei E., Iovino A., 2012, *A&A*, 539, A106  
Ponman T. J., Bourner P. D. J., Ebeling H., Böhringer H., 1996, *MNRAS*, 283, 690  
Roediger J. C., Courteau S., 2015, *MNRAS*, 452, 3209  
Román J., Trujillo I., 2017, *MNRAS*, 468, 703  
Schlafly E. F., Finkbeiner D. P., 2011, *ApJ*, 737, 103  
Sérsic J. L., 1968, *Cordoba, Argentina: Observatorio Astronomico, Atlas de Galaxias Australes*  
Sifón C., Hoekstra H., Cacciato M., Viola M., Köhlinger F., van der Burg R. F. J., Sand D. J., Graham M. L., 2015, *A&A*, 575, A48  
Smith Castelli A. V., Faifer F. R., Escudero C. G., 2016, *A&A*, 596, A23  
Tovmassian H., Plionis M., Torres-Papaqui J. P., 2006, *A&A*, 456, 839  
Trujillo I., Fliri J., 2016, *ApJ*, 823, 123  
Trujillo I., Roman J., Filho M., Sánchez Almeida J., 2017, *ApJ*, 836, 191  
van der Burg R. F. J., Muzzin A., Hoekstra H., 2016, *A&A*, 590, A20  
van Dokkum P. G., Abraham R., Merritt A., Zhang J., Geha M., Conroy C., 2015, *ApJ*, 798, L45  
van Dokkum P. et al., 2016, *ApJ*, 828, L6  
Vazdekis A., Casuso E., Peletier R. F., Beckman J. E., 1996, *ApJS*, 106, 307  
Vazdekis A. et al., 2015, *MNRAS*, 449, 1177  
White P. M., Bothun G., Guerrero M. A., West M. J., Barkhouse W. A., 2003, *ApJ*, 585, 739  
Yang Y., Zhou X., Yuan Q., Jiang Z., Ma J., Wu H., Chen J., 2004, *ApJ*, 600, 141  
Yozin C., Bekki K., 2015a, *MNRAS*, 452, 937  
Yozin C., Bekki K., 2015b, *MNRAS*, 453, 14

This paper has been typeset from a  $\TeX$  file prepared by the author.

Downloaded from https://academic.oup.com/mnras/article-abstract/468/4/4039/3770508 by Instituto de Astrofísica de Canarias user on 30 August 2019

MNRAS 468, 4039–4047 (2017)

Este documento incorpora firma electrónica, y es copia auténtica de un documento electrónico archivado por la ULL según la Ley 39/2015.  
Su autenticidad puede ser contrastada en la siguiente dirección <https://sede.ull.es/validacion/>

Identificador del documento: 2260218 Código de verificación: Sm21pjYh

Firmado por: JAVIER ROMAN GARCIA  
UNIVERSIDAD DE LA LAGUNA

Fecha: 02/11/2019 16:23:59

IGNACIO TRUJILLO CABRERA  
UNIVERSIDAD DE LA LAGUNA

02/11/2019 17:39:19

#### 3.4 Paper IV: *The Nearest Ultra Diffuse Galaxy: UGC 2162*

This letter explores the properties of the nearby UGC 2162 galaxy. Serendipitously, it was found that this galaxy meets the UDG criterion, this is, large effective radius and very low surface brightness, being additionally a galaxy with very blue colors, with properties similar to those described by Román & Trujillo (2017b).

The most important characteristic of this galaxy was the detection of large amounts of HI in it, approximately 10 times more HI in mass than its stellar content. This was, in fact, the first published HI detection in an ultra-diffuse galaxy, prior to the work by Leisman et al. (2017) in the identification of the so-called "HI-bearing ultra diffuse galaxies". Using the HI line, the total mass was estimated at  $8 \times 10^{10} M_{\odot}$ , which favors the dwarf nature of this ultra-diffuse galaxy. Another striking characteristic of this galaxy was its high-metallicity, being outlier of the mass-metallicity relation and the magnitude-metallicity relation. This fact was confirmed through deep spectroscopy with the GTC telescope in a later work by Sánchez Almeida et al. (2018), and other galaxies of similar properties were also found with this characteristic (Greco et al. 2018b).

One issue highlighted in this letter is the crucial surface brightness fading as the age of objects increases. A simulation was carried out in which the surface brightness of the galaxy was artificially evolved assuming a quenching and temporal evolution of 6 Gyr in the future. The properties of this simulated galaxy correspond to extremely low surface brightness, undetectable for most of the current surveys. This shows the expected presence of many hidden objects which are the "aged" versions of the blue/young low surface brightness galaxies present in deep images. These extremely low surface brightness "faded" galaxies could be found in future ultra-deep surveys such as LSST.

Este documento incorpora firma electrónica, y es copia auténtica de un documento electrónico archivado por la ULL según la Ley 39/2015.  
Su autenticidad puede ser contrastada en la siguiente dirección <https://sede.ull.es/validacion/>

Identificador del documento: 2260218 Código de verificación: Sm21pjYh

Firmado por: JAVIER ROMAN GARCIA  
UNIVERSIDAD DE LA LAGUNA

Fecha: 02/11/2019 16:23:59

IGNACIO TRUJILLO CABRERA  
UNIVERSIDAD DE LA LAGUNA

02/11/2019 17:39:19



## The Nearest Ultra Diffuse Galaxy: UGC 2162

Ignacio Trujillo<sup>1,2</sup>, Javier Roman<sup>1,2</sup>, Mercedes Filho<sup>1,2</sup>, and Jorge Sánchez Almeida<sup>1,2</sup>

<sup>1</sup>Instituto de Astrofísica de Canarias, Calle Vía Lactea, La Laguna, Tenerife, Spain; [trujillo@iac.es](mailto:trujillo@iac.es)  
<sup>2</sup>University of La Laguna, Avda. Astrofísico Fco. Sánchez, La Laguna, Tenerife, Spain  
Received 2017 January 12; revised 2017 January 24; accepted 2017 January 25; published 2017 February 21

### Abstract

We describe the structural, stellar population and gas properties of the nearest ultra diffuse galaxy discovered so far: UGC 2162 ( $z = 0.00392$ ;  $R_{e,g} = 1.7(\pm 0.2)$  kpc;  $\mu_g(0) = 24.4 \pm 0.1$  mag arcsec<sup>-2</sup>;  $g - i = 0.33 \pm 0.02$ ). This galaxy, located at a distance of 12.3( $\pm 1.7$ ) Mpc, is a member of the M77 group. UGC 2162 has a stellar mass of  $\sim 2^{(+2)} \times 10^7 M_\odot$  and is embedded within a cloud of HI gas  $\sim 10$  times more massive:  $\sim 1.9(\pm 0.6) \times 10^8 M_\odot$ . Using the width of its HI line as a dynamical proxy, the enclosed mass within the inner  $R \sim 5$  kpc is  $\sim 4.6(\pm 0.8) \times 10^7 M_\odot$  (i.e.,  $M/L \sim 200$ ). The estimated virial mass from the cumulative mass curve is  $\sim 8(\pm 2) \times 10^{10} M_\odot$ . Ultra-deep imaging from the IAC Stripe82 Legacy Project show that the galaxy is irregular and has many star-forming knots, with a gas-phase metallicity around one-third of the solar value. Its estimated star-formation rate is  $\sim 0.01 M_\odot \text{ yr}^{-1}$ . This SFR would double the stellar mass of the object in  $\sim 2$  Gyr. If the object were to stop forming stars at this moment, after a passive evolution, its surface brightness would become extremely faint:  $\mu_g(0) \sim 27$  mag arcsec<sup>-2</sup> and its size would remain large  $R_{e,g} \sim 1.8$  kpc. Such faintness would make it almost undetectable to most present-day surveys. This suggests that there could be an important population of  $M_* \sim 10^7 M_\odot$  “dark galaxies” in rich environments (depleted of HI gas) waiting to be discovered by current and future ultra-deep surveys.

**Key words:** galaxies: dwarf – galaxies: evolution – galaxies: structure

### 1. Introduction

In the last few years, there has been a renewed interest in the study of extended low-surface brightness galaxies (Impey et al. 1988; Bothun et al. 1991; Dalcanton et al. 1997; Caldwell 2006). The discovery of dozens of these objects in the Coma Cluster (coined Ultra Diffuse Galaxies (UDGs) by van Dokkum et al. 2015) has been followed by a large number of detections in other clusters (Koda et al. 2015; Mihos et al. 2015; Muñoz et al. 2015; Román & Trujillo 2016a; van der Burg et al. 2016), groups (Merritt et al. 2016; Román & Trujillo 2016b; Smith Castelli et al. 2016), and in the field (Martínez-Delgado et al. 2016). The low stellar mass ( $10^7$ – $10^8 M_\odot$ ) of these objects together with their large size ( $R_e > 1.5$  kpc) have opened a number of questions about the ultimate nature of these galaxies: are UDGs “failed” galaxies (i.e., do they inhabit dark matter halos larger than those expected according to their stellar mass content; van Dokkum et al. 2015; Beasley & Trujillo 2016)? What is the role of environment? Are the properties of UDGs produced by their interaction with dense environments (Yozin & Bekki 2015a)? Are they simply the high-spin tail of normal dwarf galaxies (Amorisco & Loeb 2016)? Are UDGs produced by feedback-driven gas outflows and subsequent dark matter and stellar expansion (Di Cintio et al. 2017)?

Observations indicate that UDGs are a heterogeneous population of dwarf galaxies. Some of them are relatively red ( $g - i \sim 0.8$ ), have spheroidal shapes, and inhabit rich galaxy clusters (e.g., van Dokkum et al. 2015), whereas other UDGs are blue ( $g - i \sim 0.4$ ), have irregular shapes, and are found in groups (e.g., Román & Trujillo 2016b). Are all these UDGs connected evolutionally? Recently, Román & Trujillo (2016b) have suggested a scenario where all this diversity could be understood if UDG progenitors were born in the field, processed by groups, and ended their lives inhabiting clusters.

To answer all the above questions and shed more light on the nature of UDGs, it would be extremely useful to have the opportunity to probe, in full detail, the properties of a close ( $D < 15$  Mpc) UDG. This would give us the opportunity to explore its individual stars. In particular, it would be extremely useful to have some information about the gas content of one of these galaxies. In this work, we present the serendipitous discovery of a very nearby UDG: the galaxy UGC 2162. This galaxy is located in the M77 group (at only 12.3 Mpc distance from us) and has HI observations. This proximity allows us to have a superb spatial resolution of 60 pc arcsec<sup>-1</sup>. In this work, we conduct a detailed analysis of the characteristics of this galaxy and confront the observational data with the theoretical expectations. As we will show, this galaxy is quite rich in HI gas and is currently forming stars at a rate of 0.01  $M_\odot \text{ yr}^{-1}$ . If this galaxy were suddenly depleted of its gas, it would evolve into a red ( $g - i \sim 0.8$ ) object with  $R_e \sim 1.8$  kpc and  $\mu_g(0) \sim 27$  mag arcsec<sup>-2</sup>. All of these are characteristics of the population of the faintest UDGs currently found in rich clusters (Mihos et al. 2015; Beasley et al. 2016).

### 2. Data

UGC 2162 (R.A. =  $02^{\text{h}}40^{\text{m}}23^{\text{s}}.1$  and decl. =  $+01^{\circ}13^{\text{m}}45^{\text{s}}$ ) is located within the IAC Stripe82 Legacy Survey (Fliri & Trujillo 2016). The galaxy has a spectroscopic redshift of  $z = 0.00392$ . The IAC Stripe82 data set is a careful new co-addition of the SDSS Stripe82 data with the aim of preserving the faintest surface brightness structures. The pixel scale of these images is 0.396 arcsec and the average seeing is 1 arcsec. The following work is based on the rectified images of this data set (<http://www.iac.es/proyecto/stripe82/>). The mean limiting surface brightness of this data co-addition is 29.1, 28.6, and 28.1 mag arcsec<sup>-2</sup> in the  $g$ ,  $r$ , and  $i$  bands respectively ( $3\sigma$  in boxes of  $10 \times 10$  arcsec). To put this data

1

Este documento incorpora firma electrónica, y es copia auténtica de un documento electrónico archivado por la ULL según la Ley 39/2015.  
Su autenticidad puede ser contrastada en la siguiente dirección <https://sede.ull.es/validacion/>

Identificador del documento: 2260218

Código de verificación: Sm21pjYh

Firmado por: JAVIER ROMAN GARCIA  
UNIVERSIDAD DE LA LAGUNA

Fecha: 02/11/2019 16:23:59

IGNACIO TRUJILLO CABRERA  
UNIVERSIDAD DE LA LAGUNA

02/11/2019 17:39:19

THE ASTROPHYSICAL JOURNAL, 836:191 (6pp), 2017 February 20

Trujillo et al.

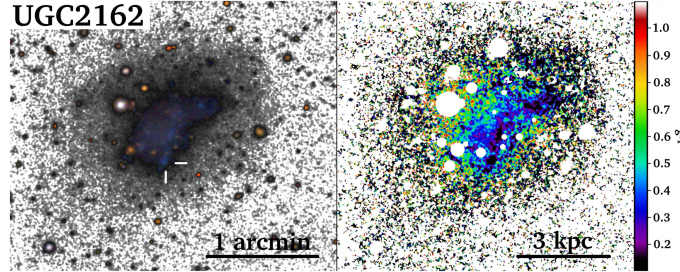


**Figure 1.** Left panel:  $g, r, i$  IAC Stripe82 composite image centered on UGC 2162. The spatial location of the SDSS spectrum of this galaxy is indicated with white ticks. Right panel:  $g - i$  color map of UGC 2162. The central irregular region is located on top of a more rounded extended disk-like structure. The white circles are the masked regions used in this work.

into context, they are  $\sim 1.2$  mag deeper than the Dragonfly images used to explore UDGs in Coma (van Dokkum et al. 2015) and similar to Koda et al. (2015).

UGC 2162 is located in the vicinity of M77 (R.A. =  $02^{\text{h}}42^{\text{m}}40^{\text{s}}.7$ , decl. =  $00^{\circ}00'48''$ ;  $z = 0.00379$ ). Its projected radial separation to this galaxy is  $1^{\circ}3684$ . A redshift independent measurement of the distance to M77 (Tully et al. 2009) locates this galaxy at a distance of  $D = 12.3(\pm 1.7)$  Mpc. Because this is the most massive galaxy of the group, we use its distance as a reliable measurement for the distance of UGC 2162.<sup>3</sup> At that distance, the projected radial separation from UGC 2162 to M77 is  $293.8(\pm 40.6)$  kpc and 1 arcsec corresponds to  $60(\pm 8)$  pc. M77 is the central member of the M77 Group. This is a small group of galaxies that also harbors NGC 1055, NGC 1073, UGC 2275, UGC 2302, UGCA 44, and Markarian 600.

Figure 1 shows a color image of UGC 2162 as seen in the IAC Stripe82 images. UGC 2162 appears to be an irregular galaxy, in fact, it has been morphologically classified as Im (de Vaucouleurs et al. 1991). The depth of the Stripe82 image allows us to see that the inner star-forming region of the galaxy is surrounded by an extended disk-like structure.

UGC 2162 has been observed by HIPASS (HI Parkes All Sky Survey; Meyer et al. 2004) with a spectral resolution of  $18 \text{ km s}^{-1}$ . The HIPASS survey detects at the position of the galaxy a HI line with a radial velocity peak of  $1171.9 \text{ km s}^{-1}$  (in agreement with the velocity recession of its optical counterpart:  $1175 \pm 3 \text{ km s}^{-1}$ ). The HI line flux peaks at  $0.089 \text{ Jy}$  and has an integrated HI flux density ( $S_{\text{HI}}$ ) of  $5.4 \text{ Jy km s}^{-1}$ . The integrated HI flux density corresponds to a HI mass  $M_{\text{HI}} = 2.36 \times 10^8 \times D^2 \times S_{\text{HI}} = 1.9(\pm 0.6) \times 10^8 M_{\odot}$  (see, e.g., Filho et al. 2013). One can also use the HI line width  $W_{20} = 89.7 \text{ km s}^{-1}$  to infer a dynamical mass  $M_{\text{dyn}} = 2.326 \times 10^8 \times (W/2)^2 \times r_{\text{HI}}$  within the HI radius ( $r_{\text{HI}}$ ). To have an estimation of the dynamical mass, it is necessary to correct the line width  $W_{20}$  for the inclination  $i$  of the galaxy, i.e.,  $W = W_{20}/\sin i$ . We estimate the inclination using the axis ratio of the  $27 \text{ mag arcsec}^{-2}$  isophote ( $g$  band).

<sup>3</sup> In what follows, we will consider the uncertainty in the distance to M77 as the main source of error at estimating all the remaining quantities, which depend on that distance. These errors will be enclosed within parenthesis to indicate their origin.

This isophote is still bright enough, but sufficiently far away from the central part of the galaxy, to produce a reliable estimation of the shape of its outer disk. We obtain an axis ratio  $b/a = 0.7$ . This translates into an inclination (under the assumption of a thin disk) of  $i \sim 45^{\circ}$ , and consequently,  $W = 128 \text{ km s}^{-1}$ . We assume  $r_{\text{HI}}$  to be three times the optical  $R_{25}$  radius (see, e.g., Filho et al. 2013). For our galaxy,  $R_{25} = 26 \text{ arcsec} = 1.6(\pm 0.3) \text{ kpc}$  (measured in  $g$  band). With these values, we estimate  $M_{\text{dyn}} = 4.6(\pm 0.8) \times 10^9 M_{\odot}$  within the inner  $R \sim 5 \text{ kpc}$ .

Once a dynamical mass in the inner region of the galaxy has been estimated, it is possible, using the expected cumulative mass curve, to have an estimation of the total virial mass of the dark matter halo. We follow the same approach as in Beasley et al. (2016). In that work, the authors compare the cumulative mass distribution from the EAGLE simulation (Schaller et al. 2015) with the observed dynamical mass of their galaxy within a given radius (see their Figure 4, right panel). From that comparison they infer a virial mass for the dark matter halo. Using our measurement of the enclosed mass  $\sim 4.6(\pm 0.8) \times 10^9 M_{\odot}$  within the inner  $R \sim 5 \text{ kpc}$ , we estimate a virial  $M_{200}$  mass similar to that found by Beasley et al. (2016) for their galaxy (i.e.,  $\sim 8(\pm 2) \times 10^{10} M_{\odot}$ ).

### 3. Structural and Stellar Population Properties of UGC 2162

To obtain the structural properties of UGC 2162 we have used the code IMFIT (Erwin 2015). The surface brightness distribution of the galaxy in each band was modeled using a single Sérsic component. The Sérsic model was convolved with the PSF of the image. The IAC Stripe82 Legacy Survey provides, for each band, a PSF representative of the local ( $0.5 \times 0.5$ ) conditions of the image. To have a first estimate of the spatial coordinates of the source, the position angle and the effective radius, we use SExtractor. These values are used later as input parameters for IMFIT. In addition, we mask the closest sources surrounding our galaxy (see Figure 1).

We derived the structural parameters of the galaxy in the  $g, r,$  and  $i$  bands. In all of these bands, the structural parameters of the galaxy were very similar. We obtained  $R_e = 28 \text{ arcsec}$  (which is equivalent to  $1.7(\pm 0.2) \text{ kpc}$ ). The central surface brightnesses were  $\mu_g(0) = 24.4 \pm 0.1 \text{ mag arcsec}^{-2}$ ,

Este documento incorpora firma electrónica, y es copia auténtica de un documento electrónico archivado por la ULL según la Ley 39/2015.  
 Su autenticidad puede ser contrastada en la siguiente dirección <https://sede.ull.es/validacion/>

Identificador del documento: 2260218

Código de verificación: Sm21pjYh

Firmado por: JAVIER ROMAN GARCIA  
 UNIVERSIDAD DE LA LAGUNA

Fecha: 02/11/2019 16:23:59

IGNACIO TRUJILLO CABRERA  
 UNIVERSIDAD DE LA LAGUNA

02/11/2019 17:39:19

THE ASTROPHYSICAL JOURNAL, 836:191 (6pp), 2017 February 20

Trujillo et al.

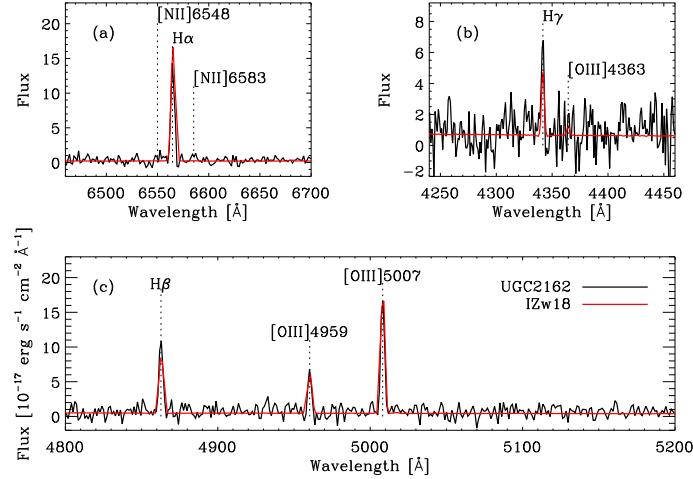


**Figure 2.** Piecewise SDSS-DR12 spectrum of UGC 2162 (the black solid line) and of the extremely metal-poor galaxy IZw18 (the red solid line), the later included for reference. The main lines are labeled. (a) Region around H $\alpha$ . The ratio between [N II]6583 and H $\alpha$  is used to estimate the gas-phase metallicity. [N II] is very small in metal-poor systems (see the red solid line). The flux in H $\alpha$  is used as a proxy for the present SFR. (b) Region around [O III]4363. This line shows up in metal-poor systems, but is always very small (see the red solid line). (c) Region around [O III]5007, which includes H $\beta$ . The spectrum of IZw18 has been scaled so that it has the same flux in [O III]5007 as UGC 2162. The units of the flux are shared by the three panels and are given in panel (c). Wavelengths are in Å.

$\mu_r(0) = 24.2 \pm 0.1$  mag arcsec $^{-2}$ , and  $\mu_i(0) = 24.1 \pm 0.1$  mag arcsec $^{-2}$ . These values have been corrected for Galactic reddening (0.117, 0.081, and 0.060 in the  $g$ ,  $r$ , and  $i$  bands respectively; Schlafly & Finkbeiner 2011). The Sérsic index in all the bands was around  $n = 0.9$ . The total apparent magnitudes were  $g = 16.1$  mag,  $r = 15.9$  mag, and  $i = 15.8$  mag.

Using the global color of the galaxy and its absolute magnitude, we can have a rough estimate of its stellar mass. We follow the recipe by Roediger & Courteau (2015); assuming a Chabrier IMF, using the  $g - i$  color and the absolute magnitude in the  $r$  band ( $M_r = -14.6(\pm 0.3)$  mag). We obtain a stellar mass of  $\sim 2(\pm 1) \times 10^7 M_\odot$ .

UGC 2162 has an SDSS spectrum (Plate = 1070; Fiber = 450; MJD = 52591) located at the coordinates: R.A. = 40°09751 and decl. = 1°22476 (see Figure 2). The spatial location of the SDSS spectrum is indicated in Figure 1. This region corresponds to the brightest knot of star formation of the galaxy. This knot has a radius of 1.2 arcsec (Petrosian mag at 90%) and a magnitude in the  $r$  band of only 21.9 mag. Using the ratio  $N2 \equiv [\text{N II}]\lambda 6583 / \text{H}\alpha$  from the SDSS spectrum and the calibration by Pettini & Pagel (2004), we have estimated an oxygen abundance for the star-forming ionized gas  $12 + \log(\text{O}/\text{H}) = 8.22 \pm 0.07$ , which corresponds to one-third of the solar abundance. The gas of UGC 2162 is fairly metallic for its mass and magnitude, since the galaxy is a high-metallicity outlier of the mass–metallicity relation and the magnitude–metallicity relation worked out by Berg et al. (2012). We also checked the spectrum for the presence of

[O III] $\lambda 4363$ , which appears in low metallicity objects (e.g., Sánchez Almeida et al. 2017). The line is not in the spectrum, which is consistent with the moderate metallicity inferred from N2. Since the SDSS spectrum is quite noisy, the estimated O abundance should be regarded as an upper limit.

Using the H $\alpha$  flux (uncorrected for extinction since H $\beta$  does not seem to be reddened), the distance to the source, and the recipe of Kennicutt (1998), we have estimated the SFR and the surface SFR of the bright knot, which turn out to be  $\text{SFR} = 8.7 (\pm 1.2) \times 10^{-3} M_\odot \text{ yr}^{-1}$  and  $\Sigma_{\text{SFR}} = 3.4 (\pm 0.5) \times 10^{-3} M_\odot \text{ yr}^{-1} \text{ kpc}^{-2}$ . Assuming that the galaxy has 100 such star-forming knots (reasonable in view of the shape and size of the galaxy) the total SFR of the galaxy would be  $\text{SFR} = 8.7 (\pm 1.2) \times 10^{-3} M_\odot \text{ yr}^{-1}$ . This value is consistent with the value around  $10^{-2} M_\odot \text{ yr}^{-1}$  worked out by Hunter & Elmegreen (2004) for this object using H $\alpha$  imaging. Using the above value, we can derive a specific SFR for UGC 2162:  $\text{sSFR} \sim 5 (\pm 0.7) \times 10^{-10} \text{ yr}^{-1}$ . If the SFR of UGC 2162 were constant, the galaxy would double its stellar mass in  $\sim 2$  Gyr.

#### 4. The Future of UGC 2162

UGC 2162 is currently located at (a projected separation of)  $\sim 300$  kpc from M77. Due to its large amount of HI gas ( $\sim 10$  times larger than its stellar mass), we can speculate that UGC 2162 is undergoing its first infall to the M77 galaxy group. When a galaxy like UGC 2162 falls into a group environment, it suffers a number of physical mechanisms that eventually will quench its star formation. These mechanisms can be either slow (of the order of a few gigayears) due to gas strangulation (see,

Este documento incorpora firma electrónica, y es copia auténtica de un documento electrónico archivado por la ULL según la Ley 39/2015.  
 Su autenticidad puede ser contrastada en la siguiente dirección <https://sede.ull.es/validacion/>

Identificador del documento: 2260218 Código de verificación: Sm21pjYh

Firmado por: JAVIER ROMAN GARCIA  
 UNIVERSIDAD DE LA LAGUNA

Fecha: 02/11/2019 16:23:59

IGNACIO TRUJILLO CABRERA  
 UNIVERSIDAD DE LA LAGUNA

02/11/2019 17:39:19

THE ASTROPHYSICAL JOURNAL, 836:191 (6pp), 2017 February 20

Trujillo et al.

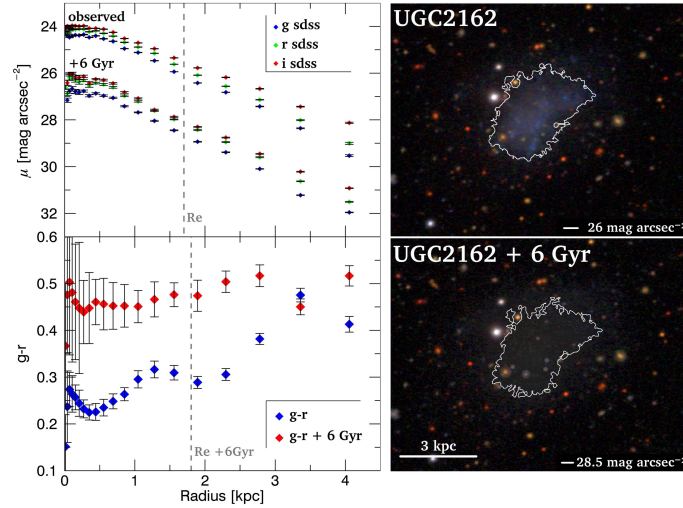


**Figure 3.** Left column: the  $g$ ,  $r$ , and  $i$  present-day surface brightness profiles of UGC 2162 and their passive evolution after 6 Gyr. The lower panel displays the  $g - r$  color radial profiles. After 6 Gyr of passive evolution, the galaxy would get significantly dimmer, redder, and maintain a similar size. The vertical dashed lines show the position of the effective radius for the present-day UGC 2162 and its potential future evolution. Right column: a color composite of how UGC 2162 looks today and how the galaxy would eventually look in the future (after 6 Gyr of passive evolution). The contours indicate the position of the ( $g$  band)  $26 \text{ mag arcsec}^{-2}$  (top panel) and  $28.5 \text{ mag arcsec}^{-2}$  isophotes (bottom panel).

e.g., McCarthy et al. 2008) or they can be relatively rapid if they are produced by ram pressure stripping (e.g., Wang et al. 2007). Following recent simulations (Yozin & Bekki 2015b), one can assume that gas rich dwarf galaxies will be depleted of gas 6 Gyr after their first infall into typical groups of galaxies ( $10^{13-13.5} M_\odot$ ). Motivated by this number, we simulate how our galaxy would look in 6 Gyr time if the object were to stop forming stars and followed a passive evolution. Naturally, this is an oversimplification of the actual evolution of the galaxy, but it can be an interesting exercise to understand how our object would look in the future.

To model the color and structural evolution of UGC 2162, we have used its present-day  $g - r$  color map and its current  $g$ ,  $r$ , and  $i$  surface brightness distributions. Then, we have estimated how every pixel of the images would look if we make their colors evolve passively for 6 Gyr. To quantify the color change and the dimming in surface brightness of every pixel, we have used the Vazdekis et al. (2015) models assuming a Kroupa IMF. Due to this passive evolution, the galaxy would not only change its global color (becoming  $g - i = 0.77$ ) but would also get dimmer (by  $\sim 2.6 \text{ mag arcsec}^{-2}$ ). The result of this evolution is illustrated in Figure 3. After 6 Gyr of passive evolution, the galaxy would have  $\mu_g(0) = 27 \pm 0.1 \text{ mag arcsec}^{-2}$  and  $R_e = 1.8(\pm 0.2) \text{ kpc}$ . Its profile shape would not change dramatically, and its passively evolved Sérsic index  $n \sim 0.8$  would be similar to its original value. With these characteristics, the galaxy would

resemble closely the faintest UDG galaxies discovered so far in the Virgo cluster (Mihos et al. 2015). In fact, considering the virial mass of UGC 2162, in an eventual future, this galaxy could look very similar to VCC 1287, a very low-surface brightness UDG galaxy ( $\mu_g(0) = 26.7 \text{ mag arcsec}^{-2}$ ,  $R_e = 2.4 \text{ kpc}$ ,  $g - i = 0.83$ ,  $M_* \sim 3 \times 10^7 M_\odot$ ) inhabiting the Virgo cluster (Beasley et al. 2016).

### 5. Discussion and Conclusions

The structural and stellar population properties of UGC 2162 seem to fit very well within a scheme where the UDGs found both outside and inside clusters are just different evolutionary stages of the same type of objects (Román & Trujillo 2016b). In this view, UDGs outside clusters would be simply the progenitors of the redder UDGs found in rich clusters. The link between both types of UDGs would be an evolution due to the removal of their gas produced by the infall of these galaxies in rich environments. If this picture is correct UDGs outside dense environments should be dwarf galaxies with a large HI content. In fact, low-surface brightness dwarf galaxies with a large amount of HI seem to be fairly common in the field (e.g., Skillman et al. 2013; James et al. 2015; Hirschauer et al. 2016; Sanchez Almeida et al. 2017). On the contrary, those UDGs found in the richest environments should be depleted of HI gas due to the removal of this component.

UGC 2162 also teaches us an important lesson about UDGs and how these objects are observationally selected. This galaxy

Este documento incorpora firma electrónica, y es copia auténtica de un documento electrónico archivado por la ULL según la Ley 39/2015.  
 Su autenticidad puede ser contrastada en la siguiente dirección <https://sede.ull.es/validacion/>

Identificador del documento: 2260218 Código de verificación: Sm21pjYh

Firmado por: JAVIER ROMAN GARCIA  
 UNIVERSIDAD DE LA LAGUNA

Fecha: 02/11/2019 16:23:59

IGNACIO TRUJILLO CABRERA  
 UNIVERSIDAD DE LA LAGUNA

02/11/2019 17:39:19

THE ASTROPHYSICAL JOURNAL, 836:191 (6pp), 2017 February 20

Trujillo et al.

has a relatively low stellar mass ( $\sim 10^7 M_\odot$ ) compared to the general population of UDGs, which peaks at  $\sim 10^8 M_\odot$  (e.g., Román & Trujillo 2016a). This issue is connected to the way UDGs are defined. UDGs are observationally selected using their surface brightness ( $\mu(0) > 24 \text{ mag arcsec}^{-2}$ ) and size ( $R_e > 1.5 \text{ kpc}$ ). This observational definition immediately biases the selection of the galaxies depending on their stellar populations. The redder UDGs will be more massive and older, whereas the bluer UDGs will be younger and with lower stellar mass. This implies that if one wants to connect the observed UDGs with their progenitors or with their descendants, it is important to take this into account. For instance, most of the progenitors of massive and red UDGs found in rich clusters would not satisfy the observational criteria to be classified as UDGs. These progenitors would have central surface brightnesses brighter than  $\mu(0) = 24 \text{ mag arcsec}^{-2}$  and would have been classified as regular (blue) dwarf galaxies. On the other hand, those blue UDGs that have been discovered outside clusters (as is the case of UGC 2162) would evolve into the less massive (and red) UDGs found in rich clusters (as is the case of VCC 1287). Accounting for this selection effect in selecting UDGs is key to have a comprehensive picture about the nature of these objects and how to connect their different evolutionary stages.

UGC 2162 has many of the structural and stellar population properties expected if the large size of this galaxy is the result of feedback-driven gas outflows (Di Cintio et al. 2017). For instance, UGC 2162 has a large amount of HI gas and it is currently forming stars as the cosmological simulations predicted. In addition, Di Cintio et al. (2017) simulations are able to predict the dwarf-like halo mass of this galaxy, as well as its stellar mass, gas mass, Sérsic index, effective radius, absolute magnitude, SFR, irregular appearance, and off-center-star-formation episodes. According to these simulations, these galaxies would not be at all rare and they will be found in abundance outside clusters. In fact, many of these have already been detected (Román & Trujillo 2016a) in low density environments. If the picture sketched by the cosmological simulations is correct, a large number of the descendants of UDGs found in low density environments would be found in rich clusters having the following characteristics:  $M_* \gtrsim 10^7 M_\odot$ ,  $\mu_g(0) \gtrsim 27 \text{ mag arcsec}^{-2}$ ,  $R_e > 1.5 \text{ kpc}$ ,  $n \lesssim 1$ ,  $g - i \sim 0.8$  and low HI gas content. These objects would be hard to find even for current deep surveys. In fact, UDGs with  $\mu_g(0) \gtrsim 27 \text{ mag arcsec}^{-2}$  have only been reported by Mihos et al. (2015), while the remaining UDGs found in rich clusters have all been found with  $\mu_g(0) < 27 \text{ mag arcsec}^{-2}$  (e.g., Koda et al. 2015; Muñoz et al. 2015; van Dokkum et al. 2015; Román & Trujillo 2016a; van der Burg et al. 2016). The existence of a large number of “dark”  $M_* \sim 10^7 M_\odot$  extended galaxies in rich clusters is a natural prediction of cosmological simulations if the above evolutionary picture for the UDGs is correct.

Finally, it is worth noting that there are a number of extremely low-surface brightness galaxies at a distance closer than UGC 2162 that technically satisfy the criteria to be considered UDGs (i.e.,  $R_e > 1.5 \text{ kpc}$  and  $\mu(0) > 24 \text{ mag arcsec}^{-2}$ ). These objects are: (a) a satellite of M31, Andromeda XIX ( $R_e > 1.7 \text{ kpc}$  and  $\mu(0) = 29.3 \text{ mag arcsec}^{-2}$ ; McConnachie et al. 2008; Martin et al. 2016); (b) a satellite of our own galaxy, the Sagittarius dwarf ( $R_e = 1.6 \text{ kpc}$  and  $\mu(0) = 25.2 \text{ mag arcsec}^{-2}$ ; Ibata et al. 1994; Majewski et al. 2003); (c) and a satellite of the galaxy NGC 4449 located at

3.8 Mpc, NGC 4449B ( $R_e = 2.7 \text{ kpc}$  and  $\mu(0) = 25.5 \text{ mag arcsec}^{-2}$ ; Martínez-Delgado et al. 2012; Rich et al. 2012). Andromeda XIX has a very low mass ( $M_V = -9.3$  and  $\sigma = 4.7 \text{ km s}^{-1}$ ; Collins et al. 2013) and it is significantly less massive than the population of UDGs that has been discussed in the literature (which are a factor of  $\sim 100$  times more massive). For this reason, And XIX cannot be considered to be representative of the population of UDGs originally discovered in the Coma Cluster. In fact, at that distance, the object would appear invisible in present-day surveys. Martin et al. (2016) discuss the possibility that the And XIX large extension could be produced by the gravitational tides of M31. The other two galaxies (though with stellar masses around  $10^7 M_\odot$  or larger) are being tidally disrupted. In this sense, their large effective radii are a consequence of the ongoing disruption process. Compared to the previous objects, the fact that UGC 2162 has a gas reservoir is strong evidence that it is not diffuse and extended because it is being tidally disrupted. For this reason, UGC 2162 is currently the nearest not tidally disrupted UDG known, whose large size is probably due to an internal origin alone.

We thank the referee for a report. We would also like to thank Michelle Collins for interesting insights into the population of extremely diffuse Local Group galaxies. We thank Michael Beasley and Chris Brook for their useful comments during the development of this work. The authors of this paper acknowledge support from grant AYA2013-48226-C3-1-P from the Spanish Ministry of Economy and Competitiveness (MINECO). J.R. thanks the Spanish Ministry of Economy and Competitiveness (MINECO) for financing his PhD through an FPI grant.

#### References

- Amorisco, N. C., & Loeb, A. 2016, *MNRAS*, 459, L51  
 Beasley, M. A., Romanowsky, A. J., Pota, V., et al. 2016, *ApJL*, 819, L20  
 Beasley, M. A., & Trujillo, I. 2016, *ApJ*, 830, 23  
 Berg, D. A., Skillman, E. D., Marble, A. R., et al. 2012, *ApJ*, 754, 98  
 Bothun, G. D., Impey, C. D., & Malin, D. F. 1991, *ApJ*, 376, 404  
 Caldwell, N. 2006, *ApJ*, 651, 822  
 Collins, M. L. M., Chapman, S. C., Rich, R. M., et al. 2013, *ApJ*, 768, 172  
 Dalcanton, J. J., Spergel, D. N., Gunn, J. E., Schmidt, M., & Schneider, D. P. 1997, *AJ*, 114, 635  
 de Vaucouleurs, G., de Vaucouleurs, A., Corwin, H. G., Jr., et al. 1991, Third Reference Catalogue of Bright Galaxies, Vol. I, II, III (New York: Springer), 2091  
 Di Cintio, A., Brook, C. B., Dutton, A. A., et al. 2017, *MNRAS*, 466, L1  
 Erwin, P. 2015, *ApJ*, 799, 226  
 Filho, M. E., Winkel, B., Sánchez Almeida, J., et al. 2013, *A&A*, 558, A18  
 Fliri, J., & Trujillo, I. 2016, *MNRAS*, 456, 1359  
 Hirschauer, A. S., Salzer, J. J., Skillman, E. D., et al. 2016, *ApJ*, 822, 108  
 Hunter, D. A., & Elmegreen, B. G. 2004, *AJ*, 128, 2170  
 Ibata, R. A., Gilmore, G., & Irwin, M. J. 1994, *Nature*, 370, 194  
 Impey, C., Bothun, G., & Malin, D. 1988, *ApJ*, 330, 634  
 James, B. L., Kpossov, S., Stark, D. P., et al. 2015, *MNRAS*, 448, 2687  
 Kennicutt, R. C., Jr. 1998, *ARA&A*, 36, 189  
 Koda, J., Yagi, M., Yamanoi, H., & Komiyama, Y. 2015, *ApJL*, 807, L2  
 Majewski, S. R., Skrutskie, M. F., Weinberg, M. D., & Ostheimer, J. C. 2003, *ApJ*, 599, 1082  
 Martin, N. F., Ibata, R. A., Lewis, G. F., et al. 2016, *ApJ*, 833, 167  
 Martínez-Delgado, D., Lisker, R., Sharina, M., et al. 2016, *AJ*, 151, 96  
 Martínez-Delgado, D., Romanowsky, A. J., Gabany, R. J., et al. 2012, *ApJL*, 748, L24  
 McCarthy, I. G., Frenk, C. S., Font, A. S., et al. 2008, *MNRAS*, 383, 593  
 McConnachie, A. W., Huxor, A., Martin, N. F., et al. 2008, *ApJ*, 688, 1009  
 Merritt, A., van Dokkum, P., Danieli, S., et al. 2016, *ApJ*, 833, 168  
 Meyer, M. J., Zwaan, M. A., Webster, R. L., et al. 2004, *MNRAS*, 350, 1195

Este documento incorpora firma electrónica, y es copia auténtica de un documento electrónico archivado por la ULL según la Ley 39/2015.

Su autenticidad puede ser contrastada en la siguiente dirección <https://sede.ull.es/validacion/>

Identificador del documento: 2260218

Código de verificación: Sm21pjYh

Firmado por: JAVIER ROMAN GARCIA  
 UNIVERSIDAD DE LA LAGUNA

Fecha: 02/11/2019 16:23:59

IGNACIO TRUJILLO CABRERA  
 UNIVERSIDAD DE LA LAGUNA

02/11/2019 17:39:19

THE ASTROPHYSICAL JOURNAL, 836:191 (6pp), 2017 February 20

Mihos, J. C., Durrell, P. R., Ferrarese, L., et al. 2015, *ApJL*, 809, L21  
Muñoz, R. P., Eigenthaler, P., Puzia, T. H., et al. 2015, *ApJL*, 813, L15  
Pettini, M., & Pagel, B. E. J. 2004, *MNRAS*, 348, L59  
Rich, R. M., Collins, M. L. M., Black, C. M., et al. 2012, *Natur*, 482, 192  
Roediger, J. C., & Courteau, S. 2015, *MNRAS*, 452, 3209  
Román, J., & Trujillo, I. 2016a, arXiv:1603.03494  
Román, J., & Trujillo, I. 2016b, arXiv:1610.08980  
Sanchez Almeida, J., Filho, M. E., Dalla Vecchia, C., & Skillman, E. D. 2017, *ApJ*, 835, 159  
Sánchez Almeida, J., Pérez-Montero, E., Morales-Luis, A. B., et al. 2016, *ApJ*, 819, 110

Trujillo et al.

Schaller, M., Frenk, C. S., Bower, R. G., et al. 2015, *MNRAS*, 451, 1247  
Schlafly, E. F., & Finkbeiner, D. P. 2011, *ApJ*, 737, 103  
Skillman, E. D., Salzer, J. J., Berg, D. A., et al. 2013, *AJ*, 146, 3  
Smith Castelli, A. V., Faifer, F. R., & Escudero, C. G. 2016, *A&A*, 596, A23  
Tully, R. B., Rizzi, L., Shaya, E. J., et al. 2009, *AJ*, 138, 323  
van der Burg, R. F. J., Muzzin, A., & Hoekstra, H. 2016, *A&A*, 590, A20  
van Dokkum, P. G., Abraham, R., Merritt, A., et al. 2015, *ApJ*, 798, L45  
Vazdekis, A., Coelho, P., Cassisi, S., et al. 2015, *MNRAS*, 449, 1177  
Wang, L., Li, C., Kauffmann, G., & De Lucia, G. 2007, *MNRAS*, 377, 1419  
Yozin, C., & Bekki, K. 2015a, *MNRAS*, 452, 937  
Yozin, C., & Bekki, K. 2015b, *MNRAS*, 453, 14

Este documento incorpora firma electrónica, y es copia auténtica de un documento electrónico archivado por la ULL según la Ley 39/2015.  
Su autenticidad puede ser contrastada en la siguiente dirección <https://sede.ull.es/validacion/>

Identificador del documento: 2260218 Código de verificación: Sm21pjYh

Firmado por: JAVIER ROMAN GARCIA  
UNIVERSIDAD DE LA LAGUNA

Fecha: 02/11/2019 16:23:59

IGNACIO TRUJILLO CABRERA  
UNIVERSIDAD DE LA LAGUNA

02/11/2019 17:39:19

3.5 Paper V: *Discovery of a red ultra-diffuse galaxy in a nearby void based on its globular cluster luminosity function* LXXXI

**3.5 Paper V: *Discovery of a red ultra-diffuse galaxy in a nearby void based on its globular cluster luminosity function***

One of the biggest problems in astronomy is the calculation of distances. This problem even increases in the case of low surface brightness sources due to the extremely expensive time required by spectroscopic observations in obtaining a redshift, being in some cases unfeasible on objects with  $\mu > 26$  mag arcsec<sup>-2</sup>.

It is important to emphasize that the method used for detecting low surface brightness objects is to assume that they are associated to a host structure with known distance. By detecting objects with given characteristics, making statistical corrections for the presence of interlopers gives an effective density number of objects in that structure. Although adequate corrections for the presence of interlopers provides reasonable numbers on average densities, the distances to individual objects remain uncertain. Additionally, this selection based on spatial associations introduces a systematic bias towards high density environments. Particularly problematic is the case for the red objects in low density environments, in which the absence of gas and their extreme low surface brightness, in contrast with the high HI abundance and higher surface brightness of the blue objects, leads to the only option of confirming their distances through deep spectroscopic observations of their stellar content. It makes obtaining distances for isolated objects, out of range of spectroscopy due to its low surface brightness, virtually unfeasible. The problem of the distances may be considered an additional limitation, apart from those discussed in Section 1.3, of the low surface brightness objects.

In this article, we explore the possibility of obtaining distances to extreme low surface brightness objects through photometry of their globular clusters luminosity function (GCLF). The use of GCLF has been used to calculate distances to massive galaxies for nearly 50 years. However, its application to low surface brightness galaxies has an even greater potential due to the high cost of its spectroscopic measurements. Considering that, due to the low number of globular clusters in these low-mass galaxies and the use of ground-based data, the application of this technique is much more challenging than usual GCLF characterizations.

In this work, we calculate the distance of an ultra-diffuse galaxy (S82-DG-I) using its GCLF, taking into account all the uncertainties arising from its challenging low number of GCs, modest resolution, presence of interlopers in the GCs detection, etc. For this distance estimate, a spectroscopic follow-up was performed with the GTC telescope, which confirmed the reliability of the distance obtained by the GCLF. As a main result, once the distance for S82-DG-I was known, the object appeared to be located in an extremely low density environment along with NGC 1211, a massive galaxy with a similar distance and redshift and in close angular projection, being one of the most isolated galaxies known.

Beyond calculating the distance of this particular galaxy, this article demonstrates the reliability of using the GCLF to obtain distances to very low surface brightness galaxies. With the imminent arrival of ultra-deep, high-quality seeing surveys, the potential of this technique could be great. It could establish an excellent distance estimation for the huge number of extremely faint objects, inaccessible to spectroscopy, that are expected to be detected with the imminent arrival of the LSST.

Este documento incorpora firma electrónica, y es copia auténtica de un documento electrónico archivado por la ULL según la Ley 39/2015.  
Su autenticidad puede ser contrastada en la siguiente dirección <https://sede.ull.es/validacion/>

Identificador del documento: 2260218 Código de verificación: Sm21pjYh

Firmado por: JAVIER ROMAN GARCIA  
UNIVERSIDAD DE LA LAGUNA

Fecha: 02/11/2019 16:23:59

IGNACIO TRUJILLO CABRERA  
UNIVERSIDAD DE LA LAGUNA

02/11/2019 17:39:19

## Discovery of a red ultra-diffuse galaxy in a nearby void based on its globular cluster luminosity function

Javier Román,<sup>1,2\*</sup> Michael A. Beasley,<sup>1,2</sup> Tomás Ruiz-Lara<sup>1,2</sup> and David Valls-Gabaud<sup>3</sup>

<sup>1</sup>Instituto de Astrofísica de Canarias, Calle Vía Láctea s/n, E-38205 La Laguna, Tenerife, Spain

<sup>2</sup>Departamento de Astrofísica, Universidad de La Laguna, E-38200 La Laguna, Tenerife, Spain

<sup>3</sup>LERMA, CNRS, PSL, Observatoire de Paris, 61 Avenue de l'Observatoire, F-75014 Paris, France

Accepted 2019 March 15. Received 2019 March 7; in original form 2019 February 15

### ABSTRACT

Distance determinations of extremely low-surface-brightness galaxies are expensive in terms of spectroscopic time. Because of this, their distances are often inferred by associating such galaxies with larger structures such as groups or clusters, leading to a systematic bias by selecting objects in high-density environments. Here we report the discovery of a red ultra-diffuse galaxy (S82-DG-1:  $r_{\text{eff}} = 1.6$  kpc;  $\langle \mu_g \rangle = 25.7$  mag arcsec<sup>-2</sup>;  $g - i = 0.78$  mag) located in a nearby cosmic void. We used multiband luminosity functions of its globular clusters to obtain the distance to S82-DG-1, at  $28.7^{+4.2}_{-3.6}$  Mpc. Follow-up deep spectroscopy with the GTC telescope yields a redshift of  $3353 \pm 29$  km s<sup>-1</sup>, making its association with the NGC 1211 galaxy (one of the most isolated galaxies known) highly likely. Both galaxies have compatible distances and redshifts, share a high peculiar velocity ( $\sim 1000$  km s<sup>-1</sup>) and lie within a void of radius 7 Mpc. The local surface density is  $\Sigma_5 \sim 0.06$  Mpc<sup>-2</sup>, an order of magnitude smaller than the field population and similar to the voids found in the GAMA survey. Our work shows: (i) The high potential of using optical ground-based photometry of associated globular clusters to explore distances to ultra-diffuse galaxies and (ii) the presence of red ultra-diffuse galaxies even in the most sparse environments, suggesting a wide range of formation mechanisms.

**Key words:** methods: observational – galaxies: distances and redshifts – galaxies: dwarf.

### 1 INTRODUCTION

The faint galaxy population offers an extraordinary potential to unravel critical issues in the formation and hierarchical evolution of galaxies. For instance, the comparison of the number densities of observed satellite galaxies (e.g. Drlica-Wagner et al. 2015, and references therein) with those in simulations (e.g. Madau, Diemand & Kuhlen 2008; Springel et al. 2008) has been a major test of the current Lambda cold dark matter cosmological paradigm (e.g. Klypin et al. 1999; Moore et al. 1999; Kim, Peter & Hargis 2018). This and many other motivations have triggered significant observational efforts to try to detect galaxies of increasingly low surface brightness. While the approach of counting stars is able to detect galaxies with surface brightnesses of up to  $\mu \approx 30$  mag arcsec<sup>-2</sup> (McConnachie 2012; Mu noz et al. 2018), potentially offering a distance estimate through, e.g. the tip of the red giant branch (Lee, Freedman & Madore 1993), this technique is limited by image resolution (few Mpc for ground observations and  $\sim 16$  Mpc for the *Hubble Space Telescope*, see Zackrisson, de Jong &

Micheva 2012) and stochasticity (Willman 2010; Martin et al. 2014). This makes integrated photometry the only alternative for detecting sources beyond the resolution limit of individual stars, and leads to greater uncertainties any distance measurements.

Current deep photometric observations are able to detect unresolved and extremely low surface brightness galaxies (ultra-faint galaxies) in nearby galaxy associations: e.g. M81 Group (Chiboucas, Karachentsev & Tully 2009; Chiboucas et al. 2013), Sculptor Group (Sand et al. 2014), Centaurus Group (Crnojević et al. 2014; Müller, Jerjen & Binggeli 2017), M101 Group (Benett et al. 2017), and other nearby systems (e.g. Javanmardi et al. 2016). However, the presence of false projections in the line-of-sight limits this approach to very nearby structures where the size contrast against background sources is high.

The existence of a subset of galaxies with very low surface brightness and large effective radius (e.g. Sandage & Binggeli 1984; Ferguson & Sandage 1988; Impey, Bothun & Malin 1988; Bothun, Impey & Malin 1991; Dalcanton et al. 1997; Conselice et al. 2003; Koda et al. 2015; Mihos et al. 2015; Mu noz et al. 2015; Venhola et al. 2017; Mancera Pi na et al. 2019), recently coined as ultra-diffuse galaxies (UDGs) by van Dokkum et al. (2015), has permitted the tracing of the abundance of the faint

\* E-mail:

© 2019 The Author(s)  
Published by Oxford University Press on behalf of the Royal Astronomical Society

Downloaded from https://academic.oup.com/mnras/article-abstract/486/1/823/5398551 by guest on 01 June 2019

Este documento incorpora firma electrónica, y es copia auténtica de un documento electrónico archivado por la ULL según la Ley 39/2015.  
Su autenticidad puede ser contrastada en la siguiente dirección <https://sede.ull.es/validacion/>

Identificador del documento: 2260218

Código de verificación: Sm21pjYh

Firmado por: JAVIER ROMAN GARCIA  
UNIVERSIDAD DE LA LAGUNA

Fecha: 02/11/2019 16:23:59

IGNACIO TRUJILLO CABRERA  
UNIVERSIDAD DE LA LAGUNA

02/11/2019 17:39:19

3.5 Paper V: *Discovery of a red ultra-diffuse galaxy in a nearby void based on its globular cluster luminosity function* LXXXIII

824 J. Román et al.

galaxy population at considerably greater distances using spatial correlations with massive clusters of galaxies (e.g. van der Burg, Muzzin & Hoekstra 2016; Lee et al. 2017; Román & Trujillo 2017a). Although adequate corrections for the presence of interlopers provide reasonable numbers on average densities (Mancera Pi et al. 2018), the distances of individual objects remain uncertain. Additionally, this selection based on spatial associations introduces a systematic bias towards high-density environments. This could have an important impact on our understanding of these galaxies as the UDG population suffers from strong environmental variations in their average properties: they appear bluer and irregularly shaped in low-density environments (blue UDGs; Bellazzini et al. 2017; Leisman et al. 2017; Román & Trujillo 2017b; Trujillo et al. 2017; Greco et al. 2018a, b; Jones et al. 2018) in contrast to the red colours and roundish morphologies found in galaxy clusters (red UDGs). This suggests an evolutionary path similar to that followed by the general dwarf population: blue irregular to red spheroidal through environmental processing (e.g. Weinmann et al. 2006; Kazantzidis et al. 2011; Yozin & Bekki 2015).

Therefore, the number densities of extended and low surface brightness galaxies in different environments offers very valuable information. However, even though these objects are readily detected in photometric campaigns, spectroscopic observations are expensive in terms of telescope time, and in some cases not feasible for galaxies with  $\mu > 26$  mag arcsec<sup>-2</sup>. Particularly problematic is the case for the red objects in low-density environments, in which the absence of gas and their extreme low surface brightness, in contrast with the high H I abundance and higher surface brightness of the blue objects<sup>1</sup> (Papastergis, Adams & Romanowsky 2017; Spekkens & Karunakaran 2018), leads to the only option of confirming their distances through deep spectroscopic observations of their stellar content (Martínez-Delgado et al. 2016). Another uncertainty to be taken into account, even if spectroscopy is carried out, is the possible deviation of radial velocities from the Hubble Flow (Trujillo et al. 2019). This makes obtaining distances for large samples of diffuse objects problematic with the current methodologies and instrumentation. It is therefore mandatory for the community to explore new ways to obtain distances to extremely low surface brightness galaxies (Carlsten et al. 2019a, b).

Interestingly, faint dwarf galaxies do have a number of globular clusters (e.g. Georgiev et al. 2009). This has been exploited extensively for the particular case of UDGs (Beasley et al. 2016; Beasley & Trujillo 2016; Peng & Lim 2016; van Dokkum et al. 2016, 2017; Amorisco et al. 2018; Lim et al. 2018; Toloba et al. 2018; Prole et al. 2019) offering an interesting tool to obtain their virial masses indirectly (Beasley et al. 2016; Burkert & Forbes 2019). In this work we explore a different approach to obtain the distance of a diffuse galaxy detected in the IAC Stripe82 Legacy Survey. We use as a priori the fact that the luminosity function of GCs (the GCLF, a standard candle) appears to be nearly universal (Rejkuba 2012, and references therein), making it an important distance indicator for these systems. This technique has been widely used for massive galaxies, offering very competitive distance measurements, similar to other redshift-independent distance methods (e.g. Racine 1968; Jacoby et al. 1992; Whitmore 1997; Tammann & Sandage 1999; Richtler 2003; Villegas et al. 2010), allowing for complementary calibration of the Hubble Constant (e.g. Sandage 1968; Ferrarese

et al. 2000). This technique could be very useful in the specific case of extremely low surface brightness galaxies, presenting an alternative to the requirement of (sometimes not feasible) spectroscopy, as it exclusively requires deep photometric data with an appropriate spatial resolution.

This work is structured as follows: we describe the object and its detected globular cluster system in Section 2. In Section 3 we perform the fitting of the GCLF, obtaining the distance to the object. In Section 4 we suggest the spatial association of the object with the NGC 1211 galaxy. In Section 5 we present a general discussion and comments about this technique. We adopt the following cosmology ( $\Omega_m = 0.3$ ,  $\Omega_\Lambda = 0.7$ , and  $H_0 = 73$  km s<sup>-1</sup> Mpc<sup>-1</sup>). We use the AB-magnitude photometric system. All photometric and derived values have been corrected from extinction as  $A^*(u) = 0.281$  mag,  $A^*(g) = 0.219$  mag,  $A^*(r) = 0.152$  mag,  $A^*(i) = 0.113$  mag, and  $A^*(z) = 0.084$  mag (Schlafly & Finkbeiner 2011).

2 A DIFFUSE GALAXY AND ITS GLOBULAR CLUSTER SYSTEM

Using data from the IAC Stripe82 Legacy Survey (Fliri & Trujillo 2016; Román & Trujillo 2018) we serendipitously discovered a galaxy with very low surface brightness and quite extended size at coordinates R.A. = +03<sup>h</sup> 07<sup>m</sup> 18.0<sup>s</sup>, Dec. = -00° 47' 34.7". There is no previous detection of this galaxy according to NASA/IPAC Extragalactic Data base (NED). We name the object as S82-DG-1. We performed a photometric fit to the galaxy using the IMFIT (Erwin 2015) package with a single Sérsic model (Sérsic 1963). The fittings were performed for all the  $u, g, r, i,$  and  $z$  individual bands, masking for external sources, using point spread function (PSF) deconvolution with the PSFs provided by the IAC Stripe82 Legacy Survey. We performed a previous fitting to the  $g, r,$  and  $i$  bands and we calculated the average ellipticity and position angle, producing  $PA = 121.9$  and  $\epsilon = 0.15$ . Afterwards, we fix these values for all the bands, leaving the rest of parameters free. The results of the Sérsic fitting are shown in Fig. 1; upper panels. As can be seen, the Sérsic model well approximates the morphology of the galaxy. We found good compatibility of the structural parameters between different bands, but a lower effective radius in the  $u$  band, likely related to the extreme low surface brightness of S82-DG-1 in this spectral range together with the shallower  $u$  band (see a discussion of the effects of low signal to noise on the structural parameters of diffuse galaxies by Prole et al. 2018). After analysing the residual images, we found small deviations from the model evidenced by areas of very slight oversubtraction and asymmetries. We also created photometric profiles, which is shown in Fig. 1; lower panels. The profiles are compatible with a low-index Sérsic profile, although slight deviations are found in the inner region within one effective radius, as in the case of residual images. Additionally, the colour profiles show some trend to redder colours at larger apertures. It is worth mentioning about the great depth limit of the profiles, which reach up to three effective radii in the case of individual bands ( $g, r,$  and  $i$ ) and two effective radii for the colour profiles ( $g-r$  and  $r-i$ ). Both the morphological and photometric parameters indicate that the galaxy is a low surface brightness quenched spheroid:  $r_{\text{eff},g} = 11.7$  arcsec,  $n_g = 0.66$ ,  $\mu_g(0) = 25.1$  mag arcsec<sup>-2</sup>,  $<\mu_g > = 25.7$  mag arcsec<sup>-2</sup>, and  $g-i = 0.78$  mag.

We searched for possible host structures with which to associate S82-DG-1 spatially. We did not find any Abell cluster of galaxies according to Struble & Rood (1991), however, using the SDSS spectroscopy in this area of the sky (a cone of 30 arcmin radius centred in the object; see Fig. 2), different galactic associations

<sup>1</sup>The fact that blue UDGs are brighter means that often they do not meet the criterion of  $\mu_g(0) > 24$  mag arcsec<sup>-2</sup>, which has contributed to their exclusion in UDG catalogues.

MNRAS 486, 823–835 (2019)

Downloaded from https://academic.oup.com/mnras/article-abstract/486/1/823/5398551 by guest on 01 June 2019

Este documento incorpora firma electrónica, y es copia auténtica de un documento electrónico archivado por la ULL según la Ley 39/2015.  
 Su autenticidad puede ser contrastada en la siguiente dirección <https://sede.ull.es/validacion/>

Identificador del documento: 2260218 Código de verificación: Sm21pjYh

Firmado por: JAVIER ROMAN GARCIA  
 UNIVERSIDAD DE LA LAGUNA

Fecha: 02/11/2019 16:23:59

IGNACIO TRUJILLO CABRERA  
 UNIVERSIDAD DE LA LAGUNA

02/11/2019 17:39:19

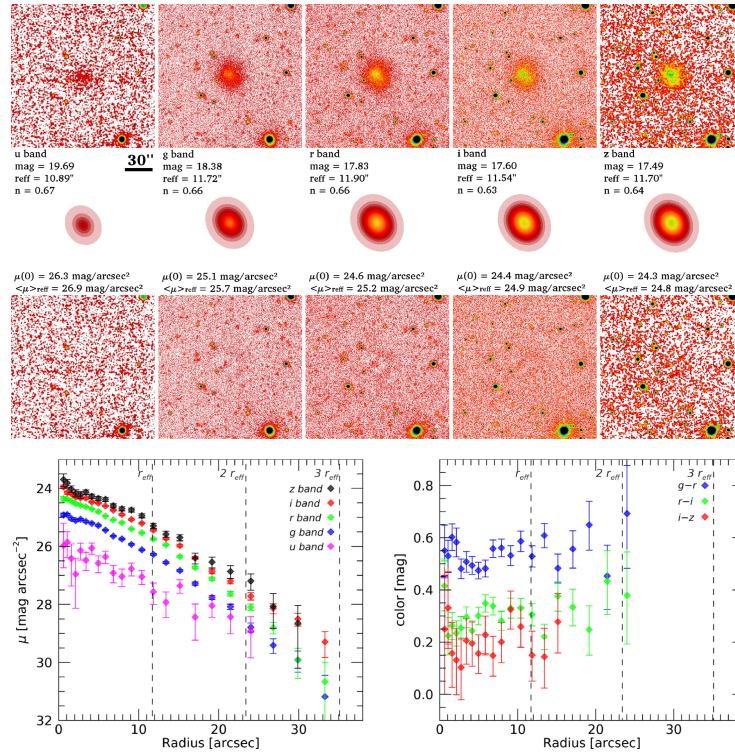


**Figure 1.** Structural and photometric properties of S82-DG-1. The top panels show the fitting of S82-DG-1 through a Sérsic function. We show the original images of the galaxy (top row), models (middle row), and residuals (bottom row) in the five SDSS bands (columns). The text adjacent to the model shows the S82-DG-1 Sérsic parameters and derived values. Original and residual images in  $u$  and  $z$  bands have been enhanced with a Gaussian kernel smooth of 3 pixels. The stamps have a size of  $2.6 \text{ arcmin} \times 2.6 \text{ arcmin}$ . In the lower panels the photometric profiles of S82-DG-1 are shown. In the lower left-hand panel, the photometric profiles are shown in individual bands. In the plot at the bottom right, the colour profiles are shown. Only points with enough statistical significance are included. The vertical dotted lines mark multiples of the effective radius ( $r_{\text{eff},g} = 11.7 \text{ arcsec}$ ).

are found. A structure located at  $z = 0.038$  with 47 spectroscopic objects is the dominant structure in the line of sight. Other galactic associations with  $\sim 15$  spectroscopic objects are also found at  $z = 0.025, 0.027,$  and  $0.045$  that can be considered groups of galaxies. Interestingly, if S82-DG-1 were located in any of these galactic associations, its effective radius would be considerable. However, since there are various structures along line of sight, it is not possible to confirm which might contain S82-DG-1, leaving its distance, and therefore its physical size and luminosity, uncertain.

Encouraged by the presence of numerous point sources clumped around the object after visual inspection, and the possibility to

characterize its globular cluster system, we carried out a detection of GCs candidates in a wide area around the galaxy. Sources were detected and aperture photometry was performed on the original images of S82-DG-1 using Source Extractor (SExtractor; Bertin & Arnouts 1996). The detection was performed on the individual, unsharp masked  $g, r,$  and  $i$  images. We ruled out the use of the  $u$  and  $z$  bands due to their shallowness after previous testing. Colours and magnitudes were determined using a 4-pixel diameter fixed aperture, and aperture corrections were applied by constructing a curve-of-growth with apertures ranging from 4 to 50 pixels. Point sources were identified as objects with a  $g$ -band SExtractor

Downloaded from https://academic.oup.com/mnras/article-abstract/486/1/823/5398551 by guest on 01 June 2019

Este documento incorpora firma electrónica, y es copia auténtica de un documento electrónico archivado por la ULL según la Ley 39/2015.  
Su autenticidad puede ser contrastada en la siguiente dirección <https://sede.ull.es/validacion/>

Identificador del documento: 2260218

Código de verificación: Sm21pjYh

Firmado por: JAVIER ROMAN GARCIA  
UNIVERSIDAD DE LA LAGUNA

Fecha: 02/11/2019 16:23:59

IGNACIO TRUJILLO CABRERA  
UNIVERSIDAD DE LA LAGUNA

02/11/2019 17:39:19

3.5 Paper V: *Discovery of a red ultra-diffuse galaxy in a nearby void based on its globular cluster luminosity function* LXXXV

826 *J. Román et al.*

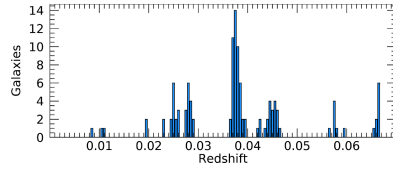


**Figure 2.** Redshift distribution of galaxies within a cone of 30 arcmin around S82-DG-1. The data were obtained from the SDSS DR14 Skyserver query.

parameters  $FLUX\_RADIUS < 5.0$  and  $ELLIP < 0.5$ . The final magnitudes were extinction corrected and we selected the GCs candidates as objects with  $0.0 < g - r < 1.3$ ,  $0.5 < g - i < 1.5$ ,  $0.0 < r - i < 0.7$ . These criteria aim for a conservative selection of possible GCs taking into account the relatively large expected photometric uncertainties, rejecting likely background galaxies. The selected sample shows a significant overdensity of GCs candidates, centred on the location of the galaxy, within a radius approximately twice of its physical size (Fig. 3, upper left-hand panel). This suggests the presence of a well-detected globular cluster system associated with the galaxy. However, this selection also shows the presence of interlopers as a background distribution of GC-like candidates in addition to the overdensity clumped around S82-DG-1. Fortunately, the area in which the galaxy is located contains a relatively low number of background galaxies, favouring a cleaner analysis.

We obtained radial density profiles in circular annuli of the GCs candidates centred over the location of S82-DG-1, which is shown in Fig. 3, upper right-hand panel. We obtain a strong peak within a radius of 30 arcsec ( $\times 2.5$  the effective radius of S82-DG-1:  $r_{eff} = 11.7$  arcsec) with a maximum value of 57 GCs candidates per arcmin<sup>2</sup>. This fact is in general agreement within uncertainties with the galactic effective radius versus globular cluster system effective radius relation for UDGs by Forbes (2017), which is a further indication of the existence of a detected globular clusters system around S82-DG-1. Therefore, we selected globular clusters candidates within a 30 arcsec radius ( $2.5 \times r_{eff}$ ) for the GCLF analysis, resulting in 11 selected sources. We list their coordinates and photometry in Table 1.

### 3 OBTAINING THE DISTANCE THROUGH THE GCLF

The most common way to obtain a distance value from the GCLF is to fit a Gaussian function, whose peak or turn-off is considered a universal value, as introduced by Hanes (1977). Hence, the comparison of this peak with reference GCs distributions in local well-known galaxies allows the determination of the distance modulus. While this peak is considered nearly universal, the width of the distribution is a free parameter even though well correlated with the luminosity of the galaxy (see e.g. Jordán et al. 2007). For the specific case of metal-poor GCs in early-type galaxies, the peak of this distribution shows a low intrinsic dispersion between different galaxies (Rejkuba 2012). Thus, the analysis of the GCLF allows obtaining quite accurate redshift-independent distances, frequently applied to local massive galaxies, obtaining complementary constraints on Hubble's law (see very first examples

using the M87 galaxy by Racine 1968; Sandage 1968; van den Bergh, Pritchet & Grillmair 1985).

In this work, we aim to explore the possibility of obtaining distances to diffuse objects through the GCLF. However, the fact that we are using ground-based observations (in contrast to the usual space-based observations), the low mass of the diffuse objects (therefore, low number of GCs expected to be found) and the few studies about the globular cluster systems in such low-mass galaxies with which to support this work, makes this task more challenging than usual GCLF characterizations. These circumstances create methodological difficulties that are summarized as follows:

- (i) The seeing-limited resolution together with the colour degeneracy between GCs and background point-like sources causes a relatively high fraction of interlopers. This uncertainty has to be taken into account for the GCLF fitting.
- (ii) There is no complete detection of the GCLF. In Fig. 3 we show the magnitude cumulative histogram of the selected GCs candidates. As can be seen, the depth of the data limits the detection. Clearly, the fitting of the GCLF is blind beyond the region of completeness. This creates the need to fix the Gaussian width of the GCLF ( $\sigma_{GCLF}$ ) for a correct fitting. Additionally, this creates an important Malmquist bias in which the peak of the observed luminosity function may differ significantly from the real peak (see Appendix A).
- (iii) The  $\sigma_{GCLF}$  is a function of the luminosity of the galaxy, and as the distance of our object is unknown, this causes a degeneracy of not being able to know a priori the luminosity of the galaxy. However, this variation of  $\sigma_{GCLF}$  is relatively small, reaching  $\sigma_{GCLF} = 0.5$  mag for the less massive galaxies ( $M_B = -15$ ) (see e.g. Jordán et al. 2007), being also approximately constant between different bands at a given luminosity.
- (iv) There are few studies on the detailed properties of the GCLF for diffuse galaxies. Work by Peng & Lim (2016) on the DF17 galaxy ( $8.4 \times 10^7 M_\odot$ ) and Trujillo et al. (2019) on the KKS04 galaxy ( $6.0 \times 10^7 M_\odot$ ) show  $\sigma_{GCLF} \sim 0.7$  mag, a value in agreement with the  $\sigma_{GCLF}$  versus luminosity relation followed by the general dwarf population of similar luminosity (e.g. Villegas et al. 2010).

Taking into account everything discussed above, we proceed to obtain the peak of the GCLF in each band. Due to the low number of GCs candidates we use an approach based on cumulative histograms. In Fig. 3 we plotted the cumulative curve of the 11 GCs candidates associated with S82-DG-1 (green histogram). This cumulative curve, which approximates the S82-DG-1 GCLF, has two main uncertainties. On the one hand a certain number of sources are expected to be interlopers. Taking the average value of the density profiles between 30 and 100 arcsec (considered interlopers) we obtain 4.1 expected interlopers inside the  $2.5 \times r_{eff}$  of S82-DG-1. On the other hand, the GCLF suffers from photometric incompleteness. We calculate the incompleteness curve by injecting/recovering PSFs in each band, and this is shown as a dotted curve in each band in Fig. 3. This incompleteness generates a strong bias in which the observed GCLF tends to be brighter than the real GCLF. We show a visualization of this effect in Appendix A. To take these uncertainties into account, we obtain the peak of the luminosity function through a  $\chi^2$  minimization:

$$\chi^2(\mu) = \sum_m \left[ \frac{GCLF'_m - LF_m(\mu)}{\epsilon_m} \right]^2$$

where  $GCLF'_m$  is the cumulative histogram of the 11 GCs to which we randomly extract a number of 4.1 sources (four or five sources in each iteration with a probability of 4.1 sources).

Downloaded from https://academic.oup.com/mnras/article-abstract/486/1/823/5398551 by guest on 01 June 2019

MNRAS **486**, 823–835 (2019)

Este documento incorpora firma electrónica, y es copia auténtica de un documento electrónico archivado por la ULL según la Ley 39/2015.  
 Su autenticidad puede ser contrastada en la siguiente dirección <https://sede.ull.es/validacion/>

Identificador del documento: 2260218 Código de verificación: Sm21pjYh

Firmado por: JAVIER ROMAN GARCIA  
 UNIVERSIDAD DE LA LAGUNA

Fecha: 02/11/2019 16:23:59

IGNACIO TRUJILLO CABRERA  
 UNIVERSIDAD DE LA LAGUNA

02/11/2019 17:39:19

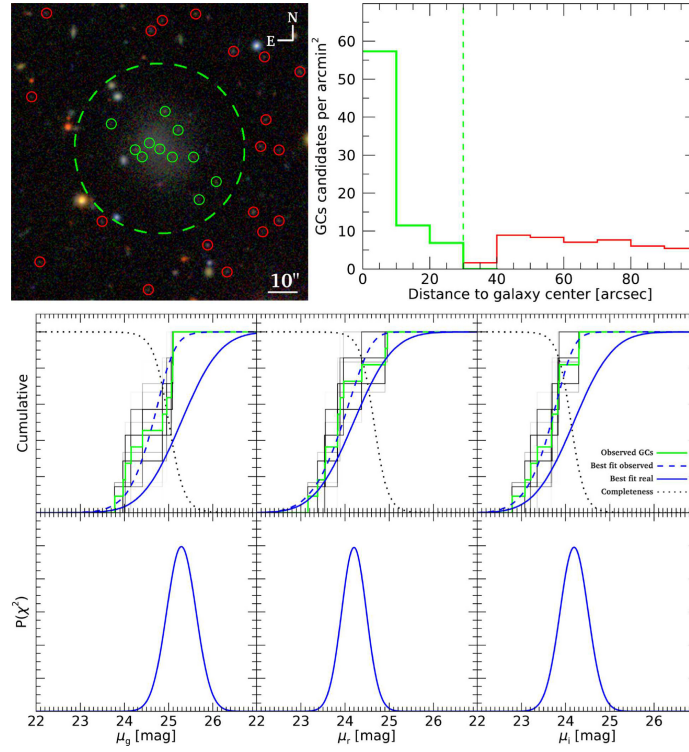


**Figure 3.** Analysis of the globular cluster system of S82-DG-1. Upper left-hand panel: The sources for the GCLF analysis are selected within a radius of  $2.5 \times r_{\text{eff}}$  or 30 arcsec (green dashed line), marked in green circles. The image shows a zoom-in of the whole explored area, focusing on the GCs candidates around S82-DG-1. Upper right-hand panel: Radial density profiles of the GCs (green) and interlopers (red). Bottom panel: The upper row shows the cumulative histograms of the GCs candidates (green). The black histograms correspond to different iterations in which 4.1 sources were extracted on average, and plotted with a certain transparency. The blue line shows the best model and the dashed blue line shows the best model convolved with the completeness curve. Photometric completeness curves for point sources were calculated by injecting artificial PSFs into the original images and determining the recovered fraction with `SEXTRACTOR`, and are shown by the dotted lines. The photometry is 100 per cent complete to  $g = 24.1$ ,  $r = 23.8$ ,  $i = 23.2$  and 50 per cent complete to  $g = 25.0$ ,  $r = 24.7$ ,  $i = 24.1$ . The bottom row shows the probability distributions of the GCLF peak resulting from the  $\chi^2$  minimization.

$LF_m(\mu)$  is the cumulative histogram of the comparison model centred on  $\mu_c$ , convolved with the completeness curve, or in other words, the cumulative curve of observable GCs of a Gaussian function with peak at  $\mu$ .  $\epsilon_m$  are the uncertainties in the cumulative curves in each magnitude bin  $m$ , and were calculated by injecting luminosity functions with a number of sources similar to this case and taking into account the photometric uncertainties of the GCs in the magnitude bin  $m$ . Since both the  $\sigma_{\text{GCLF}}$  and the number of

GCs of S82-DG-1 are unknown, we set a range of these parameters in the model. We set an arbitrary  $\sigma_{\text{GCLF}}$  in each iteration within a range  $\sigma_{\text{GCLF}} = [0.5, 1.1]$  mag, motivated by the dispersion of this parameter observed in galaxies of similar luminosity (Jordán et al. 2007; Villegas et al. 2010). Additionally we limited the number of GCs of the model. After preliminary tests we observed a high degeneracy between the number of GCs,  $\sigma_{\text{GCLF}}$ , and  $\mu$ . This causes that the peak of the distribution  $\mu$  can take arbitrarily faint values

Este documento incorpora firma electrónica, y es copia auténtica de un documento electrónico archivado por la ULL según la Ley 39/2015.  
 Su autenticidad puede ser contrastada en la siguiente dirección <https://sede.ull.es/validacion/>

Identificador del documento: 2260218 Código de verificación: Sm21pjYh

Firmado por: JAVIER ROMAN GARCIA  
 UNIVERSIDAD DE LA LAGUNA

Fecha: 02/11/2019 16:23:59

IGNACIO TRUJILLO CABRERA  
 UNIVERSIDAD DE LA LAGUNA

02/11/2019 17:39:19

3.5 Paper V: *Discovery of a red ultra-diffuse galaxy in a nearby void based on its globular cluster luminosity function* LXXXVII

828 *J. Román et al.*

**Table 1.** Globular cluster candidates selected for the GCLF analysis.

ID	R.A. (J2000) (deg)	Dec. (J2000) (deg)	g (mag)	r (mag)	i (mag)
GC1	46.82492	-0.78917	24.15 ± 0.19	23.39 ± 0.08	23.22 ± 0.06
GC2	46.83103	-0.79061	25.09 ± 0.39	24.97 ± 0.28	24.31 ± 0.14
GC3	46.82339	-0.79130	24.42 ± 0.23	23.84 ± 0.11	23.69 ± 0.08
GC4	46.82688	-0.79246	23.97 ± 0.17	23.54 ± 0.09	23.36 ± 0.07
GC5	46.82553	-0.79315	23.79 ± 0.15	23.16 ± 0.07	22.79 ± 0.04
GC6	46.82814	-0.79361	24.02 ± 0.18	23.56 ± 0.09	23.08 ± 0.05
GC7	46.82163	-0.79442	25.07 ± 0.39	24.39 ± 0.17	23.85 ± 0.10
GC8	46.82393	-0.79444	24.96 ± 0.35	23.98 ± 0.13	23.70 ± 0.08
GC9	46.82755	-0.79442	24.87 ± 0.33	23.89 ± 0.12	23.86 ± 0.10
GC10	46.81908	-0.79724	25.11 ± 0.40	23.85 ± 0.12	23.82 ± 0.09
GC11	46.82107	-0.79936	25.11 ± 0.40	24.91 ± 0.27	24.30 ± 0.14

whenever  $\sigma_{GCLF}$  and the number of GCs is sufficiently high. This would make that luminosity functions with a very high  $\sigma_{GCLF}$ , an arbitrarily high number of GCs (thousands of sources) and a very faint peak ( $\mu$ ) could reproduce the observed properties of the GCLF of S82-DG-1 (only the few brightest GCs of the thousands of the GCLF would be observed). However, we consider this scenario as highly unlikely and incompatible with observations. For this we set the maximum number of GCs of the model to 50 GCs, motivated observationally for galaxies of this luminosity range (see Fig. 5 by Prole et al. 2019). Only two UDGs in the Coma cluster are thought to have more than 50 GCs (DFX1 63 ± 17 GCs and DF44 76 ± 18 GCs; van Dokkum et al. 2017). The optimal case would be to use an arbitrarily high number of GCs in the model to avoid the shot noise, having a continuous cumulative histogram for the model. Hence, assuming 50 GCs instead of an arbitrarily high number will increase the  $\chi^2$  dispersion in each iteration. Nevertheless, with a sufficiently high number of iterations this effect is minimized. Additionally, we tested possible biases by assuming a smaller number of GCs. We did not find any difference in the most likely recovered peak, being the only bias the one discussed above for an arbitrarily high number of GCs. This leads us to rely on 50 GCs for the model as the best compromise between reducing the  $\chi^2$  shot noise and avoiding a bias towards scenarios not compatible with the observations. Note that the errors ( $\epsilon_m$ ) are based on this assumption. Summarizing: we perform iterations in which in each step we extract a number of sources to the observed S82-DG-1 GCLF, obtaining a vector  $\chi^2(\mu)$  by comparison to a luminosity function model located in different peaks ( $\mu$ ) with the properties described above. The result after 20000 iterations is plotted in Fig. 3. We show the different S82-DG-1 GCLF cumulative curves in which 4.1 sources were extracted on average as the black curves with a certain transparency. It allows to visualize the different steps of each iteration (darker areas are more frequent/likely histograms). We plot the average probability density distribution  $P(\chi^2)$  for all the iterations performed (Fig. 3, bottom rows). As can be seen, it has a well-defined Gaussian shape. Therefore we fit the probability distribution with a Gaussian function, considering the centre of the fitted distribution as the most likely peak and the width its error ( $1\sigma$ ). Additionally, we plot the cumulative curve of the most likely luminosity function, both for the real case (without completeness effects, continuous blue curve) and for what would be observed under the incompleteness regime of the data set (dashed blue curve). As can be seen, the best fit under incompleteness conditions is located in the average of the different  $GCLF_m$  iterations (interlopers subtractions). Finally, the values obtained through this method in the different bands

are:  $\mu_g = 25.27 \pm 0.33$  mag,  $\mu_r = 24.20 \pm 0.28$  mag, and  $\mu_i = 24.19 \pm 0.32$  mag.

As reference for the GCLF peak we use the value reported by Rejkuba (2012) of  $\mu_{V,ref} = -7.66$  mag. We transformed this value into SDSS bands using stellar population models by Vazdekis et al. (2015) with a single stellar population model of 6 Gyr and [Fe/H] = -1 (see the next section). The transformed values are  $\mu_{g,ref} = -7.27$  mag,  $\mu_{r,ref} = -7.86$  mag, and  $\mu_{i,ref} = -8.13$  mag, in agreement to those values reported by Jordán et al. (2007) and Villegas et al. (2010) ( $\mu_g \approx -7.20$  mag) for galaxies of similar luminosity. We also assume an error from the intrinsic dispersion among galaxies for the GCLF peak of  $\Delta\mu_{j,ref} = \pm 0.2$  mag, which is a more conservative value than the one provided by Rejkuba (2012) of  $\Delta\mu_j = \pm 0.09$  mag, trying to take into account the uncertainty due to the few studies of GCLFs in low-mass galaxies and the uncertainty in the globular cluster system metallicity (Ashman, Conti & Zepf 1995). Therefore, the value of the distance modulus for each  $j$ -th band using the globular cluster system and its error are

$$(m - M)_j = \mu_j - \mu_{j,ref}$$

$$\Delta(m - M)_j = \Delta\mu_j + \Delta\mu_{j,ref}$$

The peak values are transformed into the following distance modulus:  $(m - M)_g = 32.54 \pm 0.53$  mag,  $(m - M)_r = 32.06 \pm 0.48$  mag, and  $(m - M)_i = 32.32 \pm 0.52$  mag, values compatible between bands within the error intervals. As the final value for the distance modulus we calculate the weighted mean using the three available bands, resulting in  $(m - M) = 32.29 \pm 0.29$  mag, equivalent to  $D = 28.7^{+4.2}_{-3.6}$  Mpc, which we consider the distance for S82-DG-1 through the GCLF analysis.

As an additional test, we performed the same procedure but without taking into account the incompleteness effects, i.e. a direct fitting of the observed S82-DG-1 GCLF. We obtained:  $\mu_g = 24.62 \pm 0.18$  mag,  $\mu_r = 23.88 \pm 0.18$  mag, and  $\mu_i = 23.57 \pm 0.17$  mag. The results of this test are significantly brighter peaks, which would be equivalent to a distance of  $D = 22.6^{+2.4}_{-2.3}$  Mpc, significantly closer. This shows the great importance in taking into account the effects of incompleteness in the fit of the GCLF.

Finally, assuming a fixed distance of  $D = 28.7$  Mpc,  $\sigma_{GCLF} = 0.7$  mag and taking into account the presence of interlopers, the most likely number of GCs for S82-DG-1 is  $14.6 \pm 4.8$  GCs, assuming as error the standard deviation between bands.

MNRAS 486, 823–835 (2019)

Downloaded from https://academic.oup.com/mnras/article-abstract/486/1/823/5398551 by guest on 01 June 2019

Este documento incorpora firma electrónica, y es copia auténtica de un documento electrónico archivado por la ULL según la Ley 39/2015.  
 Su autenticidad puede ser contrastada en la siguiente dirección <https://sede.ull.es/validacion/>

Identificador del documento: 2260218 Código de verificación: Sm21pjYh

Firmado por: JAVIER ROMAN GARCIA  
 UNIVERSIDAD DE LA LAGUNA

Fecha: 02/11/2019 16:23:59

IGNACIO TRUJILLO CABRERA  
 UNIVERSIDAD DE LA LAGUNA

02/11/2019 17:39:19

#### 4 SPATIAL ASSOCIATION WITH THE NGC 1211 GALAXY AND SPECTROSCOPIC CONFIRMATION

The analysis of the GCs system associated with S82-DG-1 provides a redshift-independent distance of  $D = 28.7^{+4.2}_{-3.6}$  Mpc. We explored, using the NED Database, nearby galaxies or galactic associations with which to associate our object spatially. The result is the likely association with the NGC 1211 galaxy, located at only 6.4 arcmin of angular separation to the west of S82-DG-1. The NGC 1211 galaxy has three redshift-independent distances. Lagattuta et al. (2013), using the Tully–Fisher relation, obtained  $m - M = 32.27 \pm 0.69$  mag equivalent to  $D = 28.4^{+0.6}_{-0.7}$  Mpc. Springob et al. (2014), using the Fundamental Plane method, obtained  $m - M = 32.38 \pm 0.51$  mag equivalent to  $D = 29.9^{+7.9}_{-4.2}$  Mpc and *Cosmicflows-3* (Tully, Courtois & Sorice 2016) gives a value of  $m - M = 32.29 \pm 0.50$  mag equivalent to  $D = 28.7^{+7.4}_{-3.9}$  Mpc. These values overlap with the distance obtained through the GCLF analysis, suggesting the association between S82-DG-1 and the NGC 1211 galaxy. Further, the NGC 1211 galaxy exhibits very distinctive and interesting properties. According to the work by Fuse, Marcum & Fanelli (2012), NGC 1211 is considered an ‘extremely isolated galaxy’. The authors define such a galaxy as ‘isolated from nearest neighbours more luminous than  $M_V = -16.5$  mag by a minimum distance corresponding to 2.5 Mpc and  $350 \text{ km s}^{-1}$  in redshift space’. Another interesting characteristic of NGC 1211 is its high peculiar velocity, which is perhaps related to its relative isolation. While the redshift-independent values for its distance indicate  $D = 29.1^{+4.6}_{-4.0}$  Mpc (value obtained averaging the available distances for NGC 1211), its radial velocity obtained from SDSS spectroscopy is  $V_{\text{helio}} = 3211 \pm 3 \text{ km s}^{-1}$  ( $z = 0.01071$ ; see Fig. 2). Once corrected to the Cosmic Microwave Background reference ( $V_{\text{CMB}} = 3015 \pm 3 \text{ km s}^{-1}$ ), NGC 1211 has a peculiar velocity of  $V_{\text{pec, CMB}} = 891^{+292}_{-336} \text{ km s}^{-1}$ , a rather high value. Note that the naive distance obtained directly from the redshift would be equivalent to 41.6 Mpc, and hence incompatible with the available redshift-independent distances. This high peculiar velocity gives us a very interesting opportunity to test if S82-DG-1 is associated with the NGC 1211 galaxy, and in the process, corroborate the effectiveness of our distance method through the GCLF analysis, as if in fact they are associated, the radial velocity of S82-DG-1 should have a similar high peculiar velocity.

In order to confirm the spatial association with the NGC 1211 galaxy and the reliability of our distance estimation based on the GCs, we obtained deep spectroscopy of S82-DG-1 with the 10.4m Gran Telescopio Canarias (GTC) telescope in the Roque de los Muchachos Observatory, La Palma, Spain. The observations were carried out through Director Discretionary Time (GTC06-17BDDT program: ‘Detection of a UDG in a low-density environment using as prior distance its globular cluster system. Spectroscopic confirmation’) on the 18th and 19th of 2018 January. We used the OSIRIS spectrograph with the R2000B grism, covering the spectral range 3950–5700 Å. This configuration provides a spectral resolution of  $\sim 9.5$  Å, equivalent to  $\sim 300 \text{ km s}^{-1}$ . The slit width was of 2.5 arcsec to maximize the light gathered by the instrument due to the extremely low surface brightness of the target. The sky conditions were good, dark time and  $\sim 2$  arcsec seeing. The total exposure time was 16 800 s (4.66 h), divided in 12 individual exposures of 1400 s. The reduction process was carried out with an automatic pipeline that includes the standard steps of bias subtraction and flat-fielding,  $\lambda$  calibration, sky subtraction using Kelson algorithm (Kelson 2003) and coadding of the individual

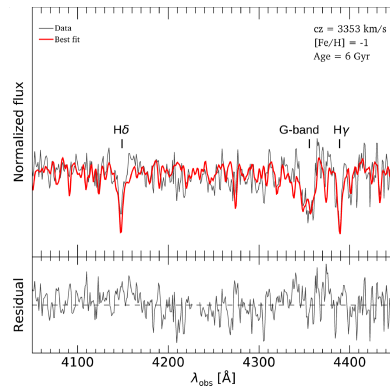


**Figure 4.** Final stacked spectrum (4.6 h) using the 10.4m GTC telescope of S82-DG-1. The spectrum and residual are shown with the grey line. The indicated values of radial velocity, metallicity, and age correspond to the best fit and its model spectrum is showed with the red line.

exposures. The two-dimensional spectrum was collapsed in a range of 60 pixels (15 arcsec) that covers the region of the 65th percentile in flux along the slit. The final stacked one-dimensional spectrum presented some residual wiggles due to sky variations increased due to the extremely low surface brightness of the object ( $< \mu_g > = 25.7 \text{ mag arcsec}^{-2}$ ). This was corrected by fitting a low-order polynomial in a similar way to that performed by Ruiz-Lara et al. (2018) observing a target of similar surface brightness with a similar instrumental configuration of the OSIRIS spectrograph. In spite of this correction, the regions of the spectrum outside the range 4050–4450 Å still contains some residual fluctuations, and a lower signal to noise in the redder part of the spectra, likely associated to the higher sky emission in this spectral range and exacerbated by defects in the OSIRIS CCD. Therefore, we restrict our subsequent analysis to the more reliable region between 4050 and 4450 Å. We consider it worth commenting on the difficulties of spectroscopic observations for objects of such low surface brightness, whose brightness is up to two orders of magnitude lower than the sky brightness by itself.

The final spectrum is plotted in Fig. 4. The spectrum has signal to noise of around 10 per pixel (1 pix = 0.9 Å) in the H $\delta$  region. To obtain its radial velocity and a possible stellar population analysis, we first tried a full spectrum fitting using the PPIX software (Cappellari 2017). However, given the low spectral resolution of  $\sim 300 \text{ km s}^{-1}$  and the narrow spectral range of 4050–4450 Å, the obtained model is not reliable enough. These circumstances also do not allow us to constrain any stellar population properties through STARLIGHT (Cid Fernandes et al. 2005) or STECKMAP (Ocvirk et al. 2006). Therefore, we compared visually the spectrum with synthetic single stellar population galactic models from the MILES library (Vazdekis et al. 2010; Falcón-Barroso et al. 2011). This visual comparison leads us to limit the age and metallicity of our object in a region around  $[\text{Fe}/\text{H}] = -1$  and Age = 6 Gyr. We

Este documento incorpora firma electrónica, y es copia auténtica de un documento electrónico archivado por la ULL según la Ley 39/2015.  
 Su autenticidad puede ser contrastada en la siguiente dirección <https://sede.ull.es/validacion/>

Identificador del documento: 2260218 Código de verificación: Sm21pjYh

Firmado por: JAVIER ROMAN GARCIA  
 UNIVERSIDAD DE LA LAGUNA

Fecha: 02/11/2019 16:23:59

IGNACIO TRUJILLO CABRERA  
 UNIVERSIDAD DE LA LAGUNA

02/11/2019 17:39:19

3.5 Paper V: *Discovery of a red ultra-diffuse galaxy in a nearby void based on its globular cluster luminosity function* LXXXIX

830 *J. Román et al.*

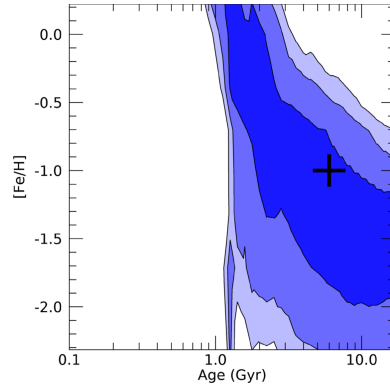


**Figure 5.** Age versus metallicity probability contours for S82-DG-1 derived from the available photometric data. The blue areas show the 1, 2, and 3 $\sigma$  probability contours. The black cross indicates the value of age and metallicity obtained from the spectrum.

obtained radial velocities through cross-correlation (Tonry & Davis 1979) between a set of synthetic spectra and our object spectrum using the *fixcor* IRAF routine. We tested the cross-correlation with ages and metallicities far from the mentioned most likely value and we obtained the lowest error with these values in particular.

As a further test, we compared the probability map of age versus metallicity derived from the photometric data using the available *u*, *g*, *r*, *i*, and *z* bands through comparison with photometric predictions by Vazdekis et al. (2015). As can be seen in Fig. 5, the values from the spectra are located within the 1 $\sigma$  contour, i.e. compatible with the photometric data, giving some robustness to this value. Therefore, we consider [Fe/H] = -1 and Age = 6 Gyr as the best-fitting model, being in general agreement with galaxies of similar characteristics (e.g. Kadowaki, Zaritsky & Donnerstein 2017; Fensch et al. 2018; Ferré-Mateu et al. 2018; Gu et al. 2018; Pandya et al. 2018; Ruiz-Lara et al. 2018), but see work by Martín-Navarro et al. (2019) in the DGSAT-1 galaxy. We find a final radial velocity for S82-DG-1, once corrected to the heliocentric frame of  $V_{\text{helio}} = 3353 \pm 29 \text{ km s}^{-1}$  ( $z = 0.01118 \pm 0.00010$ ).

Trying to address in a more precise way the association of S82-DG-1 with NGC 1211 once known its redshift, we used the NED data base to select galaxies brighter than 16 mag in the *r* band in a  $2 \times 2$  deg area around S82-DG-1 (approximately 1 Mpc in projection assuming a distance of 28.7 Mpc for S82-DG-1) and with radial velocity of  $\pm 1000 \text{ km s}^{-1}$  from that obtained for S82-DG-1. Galaxies with this criterion are shown in Table 2. Of all the galaxies capable of hosting S82-DG-1, based exclusively on the redshift, only NGC 1211 has a radial velocity compatible with S82-DG-1, having also a compatible redshift-independent distance. It makes the association between NGC 1211 and S82-DG-1 highly likely and gives reliability to the GCLF analysis method. We show in Fig. 6 a colour composite image of the field surrounding the NGC 1211 and S82-DG-1 galaxies. In Table 3 we summarize the distance values available for both objects.

MNRAS **486**, 823–835 (2019)

**Table 2.** Galaxies candidates to be associated with S82-DG-1 (see the text). Distances (if available) refer to redshift-independent methods.

Galaxy	$V - V_{\text{S82-DG-1}}$ ( $\text{km s}^{-1}$ )	Distance (Mpc)	<i>r</i> mag (mag)
UGC 02482	-712	-	15.5
UGC 02479	-511	$49.4^{+4.8}_{-3.2}$ Mpc	15.1
NGC 1211	-142	$29.1^{+4.6}_{-4.0}$ Mpc	12.2
UGC 02517	502	-	14.1
UGC 02505	717	-	15.7
NGC 1194	700	-	12.5

## 5 DISCUSSION

In this paper we have explored the possibility of obtaining distances to diffuse galaxies through ground-based photometry of their globular cluster systems. For this we have carried out a thorough analysis of the GCLF of a diffuse galaxy detected in the IAC Stripe82 Legacy Survey, named S82-DG-1 in this work. As follow-up, we have also carried out deep spectroscopic observations of S82-DG-1 to confirm its distance and prove the reliability of the method. The analysis of the S82-DG-1 GCLF has allowed us to obtain a distance modulus of  $32.29 \pm 0.29$  mag, equivalent to  $D = 28.7^{+4.2}_{-3.6}$  Mpc. There are numerous lines of evidence suggesting the spatial association of S82-DG-1 with the NGC 1211 galaxy. Up to three different redshift-independent methods, the Fundamental Plane, the Tully–Fisher relation, and *cosmicflows-3* for NGC 1211<sup>2</sup> and the GCLF analysis for S82-DG-1 are in agreement. The fact that both galaxies have similar radial velocities, with the addition of the high peculiar velocities that both galaxies share, makes their spatial association highly likely.

The calculated distance for S82-DG-1 gives an effective radius of 1.6 kpc, which together with its low surface brightness of  $\mu_{\text{e}}(0) = 25.1$  makes this galaxy fall into the category of the so-called UDGs. The comprehensive analysis of S82-DG-1 carried out in this work has allowed us to obtain a detailed characterization of this UDG. We summarize its properties in Table 4. The environment of S82-DG-1, characterized indirectly with the work by Fuse et al. (2012), shows that NGC 1211 and S82-DG-1 are located in an extremely low-density environment. We have used the NED data base to search for galaxies with redshifts within 10 deg of this pair of galaxies, and compute the redshift-space distances as:

$$s = \frac{1}{H_0} \sqrt{V^2 + V_{\text{NGC 1211}}^2 - 2 V V_{\text{NGC 1211}} \cos \theta},$$

where the velocities are in the heliocentric frame, and  $\theta$  is their angular separation. The resulting distribution of separations is given in Fig. 7 where the absolute magnitudes are also indicated. The distribution of neighbouring galaxies confirms the isolation of this pair, and adopting the criterion of the GAMA survey for voids (no galaxy brighter than  $M_r = -20.09$ ), the nearest galaxy would be at some 7 Mpc away. This is the typical size of voids found in the GAMA survey (Penny et al. 2015) and similar to the ones found in other void surveys such as SDSS (Pan et al. 2012). Using the fifth nearest neighbour as a proxy for the surface density, we get

<sup>2</sup>We do not perform a similar analysis for the NGC 1211 GCLF. The reason is the difficulty in extracting a precise photometry for GCs due to the morphology of NGC 1211, which has a remarkable central bar with three different rings one of which is clearly young with many knots of current star formation. This creates problems in the identification and photometry of GC candidates given our limited spatial resolution.

Este documento incorpora firma electrónica, y es copia auténtica de un documento electrónico archivado por la ULL según la Ley 39/2015.  
 Su autenticidad puede ser contrastada en la siguiente dirección <https://sede.ull.es/validacion/>

Identificador del documento: 2260218 Código de verificación: Sm21pjYh

Firmado por: JAVIER ROMAN GARCIA  
 UNIVERSIDAD DE LA LAGUNA

Fecha: 02/11/2019 16:23:59

IGNACIO TRUJILLO CABRERA  
 UNIVERSIDAD DE LA LAGUNA

02/11/2019 17:39:19

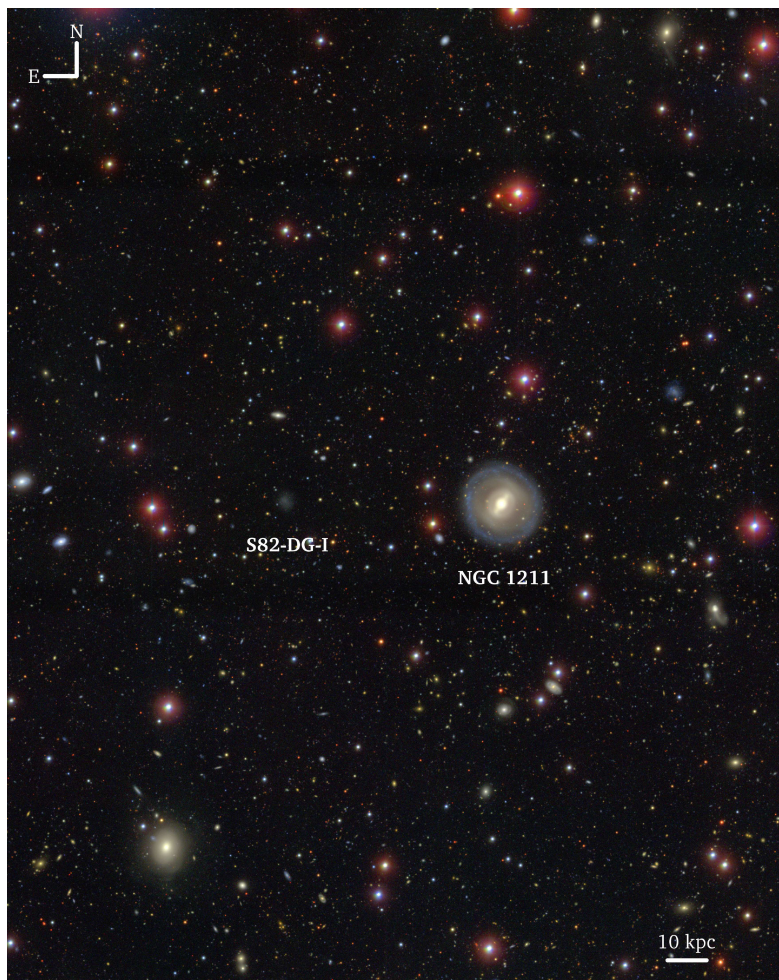


**Figure 6.** Composite colour image in *g*, *r*, and *i* SDSS bands from the IAC Stripe82 Legacy Survey showing the environment (23 arcmin  $\times$  29 arcmin) of the S82-DG-1 and NGC 1211 galaxies. The scale marking 10 kpc ( $\sim$ 70 arcsec) corresponds to the distance of 29 Mpc, and it is only valid for the S82-DG-1 and NGC 1211 galaxies. This work has demonstrated that both galaxies are spatially associated through a method in which globular clusters are used as distance estimators.

MNRAS 486, 823–835 (2019)

Este documento incorpora firma electrónica, y es copia auténtica de un documento electrónico archivado por la ULL según la Ley 39/2015.  
Su autenticidad puede ser contrastada en la siguiente dirección <https://sede.ull.es/validacion/>

Identificador del documento: 2260218

Código de verificación: Sm21pjYh

Firmado por: JAVIER ROMAN GARCIA  
UNIVERSIDAD DE LA LAGUNA

Fecha: 02/11/2019 16:23:59

IGNACIO TRUJILLO CABRERA  
UNIVERSIDAD DE LA LAGUNA

02/11/2019 17:39:19

3.5 Paper V: *Discovery of a red ultra-diffuse galaxy in a nearby void based on its globular cluster luminosity function* XCI

832 J. Román et al.

**Table 3.** Summary of distances and radial velocities for S82-DG-1 and NGC 1211. The peculiar velocity is calculated by averaging the available distances (Tully–Fisher, Fundamental Plane, and cosmicflows-3 methods) for NGC 1211 ( $D = 29.1^{+4.6}_{-4.0}$  Mpc) and the GCLF distance for S82-DG-1 ( $D = 28.7^{+4.2}_{-3.6}$  Mpc).

Method	S82-DG-1	NGC 1211
FP	–	$29.9^{+7.9}_{-4.2}$ Mpc
TF	–	$28.4^{+10.6}_{-7.7}$ Mpc
Cosmicflows-3	–	$28.7^{+7.4}_{-5.9}$ Mpc
GCLF	$28.7^{+4.2}_{-3.6}$ Mpc	–
$V_{\text{helio}}$	$3353 \pm 29$ km s $^{-1}$	$3211 \pm 3$ km s $^{-1}$
$V_{\text{pec, CMB}}$	$1067^{+263}_{-307}$ km s $^{-1}$	$891^{+292}_{-336}$ km s $^{-1}$

**Table 4.** Summary of properties for the S82-DG-1 galaxy.

Parameter	Value
R.A.	$+03^{\text{h}} 07^{\text{m}} 18.0^{\text{s}}$
Dec.	$-00^{\circ} 47' 34.7''$
$u$ band	$19.69 \pm 0.40$ mag
$g$ band	$18.38 \pm 0.03$ mag
$r$ band	$17.83 \pm 0.03$ mag
$i$ band	$17.60 \pm 0.07$ mag
$z$ band	$17.49 \pm 0.15$ mag
$g - i$	$0.78 \pm 0.10$ mag
$\langle \mu_g \rangle$	$25.7 \pm 0.1$ mag arcsec $^{-2}$
$\mu_g(0)$	$25.1 \pm 0.1$ mag arcsec $^{-2}$
Sérsic index	$0.65 \pm 0.01$
Axis ratio	$0.85 \pm 0.01$
Position angle	$122 \pm 2$ deg
[Fe/H] <sup>a</sup>	–1
Age <sup>a</sup>	6 Gyr
$M/L_r - \text{band}^a$	$1.3 \Upsilon_{\odot}$
Distance	$28.7^{+4.2}_{-3.6}$ Mpc
Redshift	$0.0118 \pm 0.00010$
Effective radius ( $g$ band)	$1.6 \pm 0.2$ kpc
$M_g$	$-13.9 \pm 0.3$ mag
$M_r^b$	$6.2^{+2.0}_{-1.4} \times 10^7 M_{\odot}$

Notes:

<sup>a</sup>Most likely values through cross-correlation with synthetic spectra. No error interval is available.  
<sup>b</sup>Value obtained using the mass to light ratio in the  $r$  band.

$\Sigma_s = 0.06$  Mpc $^{-2}$ , an order of magnitude smaller than the field population and confirms that this void has properties similar to the ones found in GAMA ( $\Sigma_s = 0.09$  Mpc $^{-2}$ ). It makes S82-DG-1 the most isolated red-UDG so far.

While many examples of star-forming, irregularly shaped, and large-sized low surface brightness galaxies (blue UDGs) are found mostly in the field (Román & Trujillo 2017b; Trujillo et al. 2017; Bellazzini et al. 2017; Leisman et al. 2017; Jones et al. 2018; Greco et al. 2018a,b), S82-DG-1 and DGSAT-1 (Martínez-Delgado et al. 2016) are striking examples of red-UDGs whose formation does not require high-density environments such as galaxy clusters. The fact of finding red or quenched UDGs in such low-density environments promote the idea that these galaxies undergo a formation process not exclusively related to high-density environments, where they are found in large numbers. In addition, the coexistence of red and blue UDGs in groups of galaxies are evidence of quenching and subsequent passive evolution prior to their infall to a galaxy cluster

via aggregation of minor mergers (Román & Trujillo 2017b; Alabi et al. 2018).

The peculiar properties of S82-DG-1 make it an excellent laboratory for testing formation mechanisms of UDGs. The extremely low-density environment of S82-DG-1 raises the question of what could be the cause of its quenching. It could indicate the result of internal processes, as the consequence of supernova feedback (Di Cintio et al. 2017), which would support this formation mechanism for UDGs. Additionally, the exceptional depth of the photometric profiles made in Fig. 1 allows us to observe a tendency to redness of the  $g - r$  and  $r - i$  colour profiles as the radius increases. This could indicate an older component to the main luminosity-weighted average colour, suggesting an extended star formation history, which is one of the predictions of this scenario and in agreement with observational results (Ferré-Mateu et al. 2018; Ruiz-Lara et al. 2018). However, the low signal to noise of the profiles makes this result uncertain and deeper observations are needed. It is also interesting to analyse the possible influence of NGC 1211 on the properties of S82-DG-1. In this aspect it is key to verify if S82-DG-1 is really a satellite of NGC 1211 or if it is only in projection proximity. A fact that would indicate that it is a true satellite is the presence of another object associated with the system: J030627.79-005247.9, located at only 66 kpc in projection from the NGC 1211 galaxy (assuming 29.1 Mpc as distance for the system). This galaxy is a star-forming dwarf ( $M_r = -10.9$  mag) with a radial velocity of  $-107$  km s $^{-1}$  relative to that of NGC 1211 galaxy ( $38$  km s $^{-1}$  from that of S82-DG-1). This would indicate that NGC 1211, despite its large-scale isolation, has a satellite system that S82-DG-1 would form part of. The relatively high velocity of S82-DG-1 with respect to NGC 1211 ( $142$  km s $^{-1}$ ) makes their expected interaction low. The redshift-space ( $s$ ) between both galaxies is  $\approx 1.9$  Mpc. The naive calculation of the crossing time of S82-DG-1 at this distance gives approximately 13 Gyr, so if the galaxies have interacted, only a fly-by is expected. Additionally, quenching mechanisms as tidal stirring (D’Onghia et al. 2009; Kazantzidis et al. 2011) are not expected. The tidal radius (more properly the Jacobi radius  $r_j$ ) can be estimated as:

$$(r_j/r)^3 = M_{\text{S82-DG-1}}/3M_{\text{NGC1211}}(<r),$$

where  $r$  is the separation between the two galaxies,  $M_{\text{S82-DG-1}}$  is the total mass of S82-DG-1, and  $M_{\text{NGC1211}}(<r)$  is the total mass enclosed within  $r \sim 2$  Mpc. Adopting  $M_{\text{NGC1211}}(<2\text{Mpc}) = 2 \times 10^{12} M_{\odot}$ , and  $M_{\text{S82-DG-1}} \sim 10^{10} M_{\odot}$ , the Jacobi radius would be  $r_j \sim 240$  kpc, over two orders of magnitude larger than the effective radius. Tidal effects produced by NGC 1211 on this UDG are therefore negligible. Additionally, if a fly-by interaction has occurred, some byproduct is expected, such as the presence of tidal features. We do not find evidences of such features. Nevertheless, such structures are expected to have extremely low surface brightnesses and could be not detectable under the depth limits of our data set. All these arguments do not allow us to address about the interaction between S82-DG-1 and NGC 1211, so it remains uncertain. Future deeper observations, both in the optical or H I, could shed some light about the issue.

The use of globular cluster systems to obtain distances to extremely low surface brightness galaxies can be extremely useful in the discovery of new objects in low-density environments. However, it is necessary to investigate in greater depth what are the properties of the globular cluster systems of these galaxies. Depending on the universality of the GCLFs found, this could support this method as effective. In this sense, it is important to identify diffuse objects in low-density environments where their GCLF can be studied with

Downloaded from https://academic.oup.com/mnras/article-abstract/486/1/823/5398551 by guest on 01 June 2019

MNRAS 486, 823–835 (2019)

Este documento incorpora firma electrónica, y es copia auténtica de un documento electrónico archivado por la ULL según la Ley 39/2015.  
 Su autenticidad puede ser contrastada en la siguiente dirección <https://sede.ull.es/validacion/>

Identificador del documento: 2260218 Código de verificación: Sm21pjYh

Firmado por: JAVIER ROMAN GARCIA  
 UNIVERSIDAD DE LA LAGUNA

Fecha: 02/11/2019 16:23:59

IGNACIO TRUJILLO CABRERA  
 UNIVERSIDAD DE LA LAGUNA

02/11/2019 17:39:19

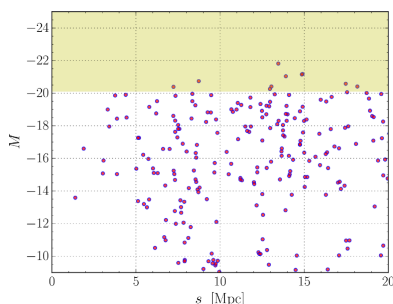


**Figure 7.** Distribution of galaxies within 10 deg of S82-DG-1 and NGC 1211. Following the criteria adopted by the GAMA survey (Penny et al. 2015), galaxies brighter than  $-20.09$  in the  $r$  band define the properties of the void. The nearest galaxy lies at over 7 Mpc and shows that S82-DG-1 and NGC 1211 lie in a well-defined void.

accuracy without the presence of interloping GCs in projection that may be associated to the cluster environment or other nearby massive galaxies. A perfect sample would be those detected by Greco et al. (2018a), in which 781 low surface brightness galaxies are found in a wide area ( $\sim 200 \text{ deg}^2$ ) using the Hyper Suprime-Cam Subaru Strategic Program (HSC-SSP). Given the great depth of the survey for point sources, and the large angular sizes of the detected objects (effective radius between 2.5 and 14 arcsec), it is expected the detection of the GCLF for a large fraction of nearby objects. In fact, in a spectroscopic follow-up carried out by Greco et al. (2018b), distances of 25 and 41 Mpc are obtained for two blue objects which are therefore amenable to the detection of GCs. The systematic study of the GCLF for the galaxies of this sample would be an excellent starting point for the accurate characterization of the GC systems properties of diffuse galaxies. It could establish an excellent statistical catalogue for the huge number of extremely faint objects, inaccessible to spectroscopy, that are expected to be detected with the imminent arrival of the LSST.

It is also worth briefly discussing the exploitation of this technique for different surveys. In this work, we have used data from the IAC Stripe82 Legacy Survey (Fliri & Trujillo 2016). However, this data set is not particularly competitive in the detection of point sources. This imposes a limitation of the method to distances of up to approximately 30 Mpc, as it is the case of this work. Nevertheless, the potential of this method is expected to be greater when applied to deeper and higher resolution data sets. For instance, surveys such as the Hyper Suprime-Cam Subaru Strategic Program (HSC-SSP; Aihara et al. 2018) or the under development Large Synoptic Survey Telescope (LSST; LSST Science Collaboration et al. 2009) are designed to reach a  $5\sigma$  point source detection of  $\sim 27.5$  mag in the  $r$  band,  $\sim 3$  mag deeper in the detection of point sources than the data presented in this work. This would imply the detection of GCs up to a distance modulus of  $(m - M) \approx 35$  mag, equivalent to 100 Mpc. However, the seeing-limited resolution at such distances could be a serious drawback. Assuming a median seeing of 0.6 arcsec, the resolution at 100 Mpc would be half of that presented in this work. It is therefore unknown what are the achievable limits for the detection of GCs for the particular conditions of each data set.

Such a study is beyond the scope of our work. Nevertheless, for objects with similar distances to that presented here, considerably higher signal to noise, better resolution, and multiband detection including  $u$  and/or infrared bands, would result in a much higher accuracy in the obtained distances. This would both reduce the number of interlopers and improve the photometric uncertainties, greatly increasing the potential of this technique.

#### ACKNOWLEDGEMENTS

This work has been possible using observations from the GTC telescope, in the Spanish Observatorio del Roque de los Muchachos of the Instituto de Astrofísica de Canarias, under Director's Discretionary Time. We thank the anonymous referee for a careful review and useful comments. We thank Ignacio Trujillo for crucial discussions that helped the development of this work. We thank Antonio Cabrera for his help and support with the observations and Alexandre Vazdekis for a visual identification of the main features of the spectrum. We thank Mireia Montes, Lourdes Verdes-Montenegro, and Michael Jones for helpful discussions. We also thank the participants of the Workshop 'The Bewildering Nature of ultra-diffuse galaxies' hosted in the Lorentz Center, Leiden, for fruitful and enjoyable conversations. The authors of this paper acknowledge support from grants AYA2014-56795-P and AYA2016-77237-C3-1-P from the Spanish Ministry of Economy and Competitiveness (MINECO). JR thanks MINECO for financing his PhD through FPI grant. MAB acknowledges financial support from the Severo Ochoa Excellence programme (SEV-2015-0548). This work has used PYTHON (<http://www.python.org>) and IRAF (<http://iraf.noao.edu>) software.

#### REFERENCES

- Aihara H. et al., 2018, *PASJ*, 70, S4  
 Alabi A. et al., 2018, *MNRAS*, 479, 3308  
 Amorisco N. C., Monachesi A., Agnello A., White S. D. M., 2018, *MNRAS*, 475, 4235  
 Ashman K. M., Conti A., Zepf S. E., 1995, *AJ*, 110, 1164  
 Beasley M. A., Trujillo I., 2016, *Apl*, 830, 23  
 Beasley M. A., Romanowsky A. J., Pota V., Navarro I. M., Martinez D. D., Neyer F., Deich A. L., 2016, *Apl*, 819, L20  
 Bellazzini M., Belokurov V., Magrini L., Fraternali F., Testa V., Beccari G., Marchetti A., Carini R., 2017, *MNRAS*, 467, 3751  
 Bennet P., Sand D. J., Crojjević D., Spekkens K., Zaritsky D., Karunakaran A., 2017, *Apl*, 850, 109  
 Bertin E., Arnouts S., 1996, *A&AS*, 117, 393  
 Bothun G. D., Impey C. D., Malin D. F., 1991, *Apl*, 376, 404  
 Burkert A., Forbes D., 2019, preprint ([arXiv:1901.00900](https://arxiv.org/abs/1901.00900))  
 Cappellari M., 2017, *MNRAS*, 466, 798  
 Carlsten S., Beaton R., Greco J., Greene J., 2019a, preprint ([arXiv:1901.07575](https://arxiv.org/abs/1901.07575))  
 Carlsten S., Beaton R., Greco J., Greene J., 2019b, preprint ([arXiv:1901.07578](https://arxiv.org/abs/1901.07578))  
 Chiboucas K., Karachentsev I. D., Tully R. B., 2009, *AJ*, 137, 3009  
 Chiboucas K., Jacobs B. A., Tully R. B., Karachentsev I. D., 2013, *AJ*, 146, 126  
 Cid Fernandes R., Mateus A., Sodré L., Stasińska G., Gomes J. M., 2005, *MNRAS*, 358, 363  
 Conselice C. J., Gallagher J. S., III, Wyse R. F. G., 2003, *AJ*, 125, 66  
 Crojjević D. et al., 2014, *Apl*, 795, L35  
 D'Onghia E., Besla G., Cox T. J., Hernquist L., 2009, *Nature*, 460, 605  
 Dalcanton J. J., Spergel D. N., Gunn J. E., Schmidt M., Schneider D. P., 1997, *AJ*, 114, 635  
 Di Cintio A., Brook C. B., Dutton A. A., Macciò A. V., Obreja A., Dekel A., 2017, *MNRAS*, 466, L1

MNRAS 486, 823–835 (2019)

Downloaded from <https://academic.oup.com/mnras/article-abstract/486/1/823/5398551> by guest on 01 June 2019

Este documento incorpora firma electrónica, y es copia auténtica de un documento electrónico archivado por la ULL según la Ley 39/2015.  
 Su autenticidad puede ser contrastada en la siguiente dirección <https://sede.ull.es/validacion/>

Identificador del documento: 2260218 Código de verificación: Sm21pjYh

Firmado por: JAVIER ROMAN GARCIA  
 UNIVERSIDAD DE LA LAGUNA

Fecha: 02/11/2019 16:23:59

IGNACIO TRUJILLO CABRERA  
 UNIVERSIDAD DE LA LAGUNA

02/11/2019 17:39:19

3.5 Paper V: *Discovery of a red ultra-diffuse galaxy in a nearby void based on its globular cluster luminosity function* XCIII

834 J. Román et al.

- Drica-Wagner A. et al., 2015, *Apl*, 813, 109  
Erwin P., 2015, *Apl*, 799, 226  
Falcón-Barroso J., Sánchez-Blázquez P., Vazdekis A., Ricciardelli E., Cardiel N., Cenarro A. J., Gorgas J., Peletier R. F., 2011, *A&A*, 532, A95  
Fensch J. et al., 2018, preprint (arXiv:1812.07346)  
Ferguson H. C., Sandage A., 1988, *AJ*, 96, 1520  
Ferrarese L. et al., 2000, *ApJS*, 128, 431  
Ferré-Mateu A. et al., 2018, *MNRAS*, 479, 4891  
Fliri J., Trujillo I., 2016, *MNRAS*, 456, 1359  
Forbes D. A., 2017, *MNRAS*, 472, L104  
Fuse C., Marcum P., Fanelli M., 2012, *AJ*, 144, 57  
Georgiev I. Y., Puzia T. H., Hilker M., Goudfrooij P., 2009, *MNRAS*, 392, 879  
Greco J. P. et al., 2018, *Apl*, 857, 104  
Greco J. P., Goulding A. D., Greene J. E., Strauss M. A., Huang S., Kim J. H., Komiya Y., 2018, *Apl*, 866, 112  
Gu M. et al., 2018, *Apl*, 859, 37  
Hanes D. A., 1977, *MNRAS*, 180, 309  
Impey C., Bothun G., Malin D., 1988, *Apl*, 330, 634  
Jacoby G. H. et al., 1992, *PASP*, 104, 599  
Javannardi B. et al., 2016, *A&A*, 588, A89  
Jones M. G., Papastergis E., Pandya V., Leisman L., Romanowsky A. J., Yung L. Y. A., Somerville R. S., Adams E. A. K., 2018, *A&A*, 614, A21.  
Jordán A. et al., 2007, *ApJS*, 171, 101  
Kadowaki J., Zaritsky D., Donnerstein R. L., 2017, *Apl*, 838, L21  
Kazantzidis S., Łokas E. L., Callegari S., Mayer L., Moustakas L. A., 2011, *Apl*, 726, 98  
Kelson D. D., 2003, *PASP*, 115, 688  
Kim S. Y., Peter A. H. G., Hargis J. R., 2018, *Phys. Rev. Lett.*, 121, 211302  
Klypin A., Kravtsov A. V., Valenzuela O., Prada F., 1999, *Apl*, 522, 82  
Koda J., Yagi M., Yamanoi H., Komiya Y., 2015, *Apl*, 807, L2  
Lagattuta D. J., Mould J. R., Staveley-Smith L., Hong T., Springob C. M., Masters K. L., Koribalski B. S., Jones D. H., 2013, *Apl*, 771, 88  
Lee M. G., Freedman W. L., Madore B. F., 1993, *Apl*, 417, 553  
Lee M. G., Kang J., Lee J. H., Jang I. S., 2017, *Apl*, 844, 157  
Leisman L. et al., 2017, *Apl*, 842, 133  
Lim S., Peng E. W., Côté P., Sales L. V., den Brok M., Blakeslee J. P., Guhathakurta P., 2018, *Apl*, 862, 82  
LSST Science Collaboration, 2009, preprint (arXiv:0912.0201)  
Madau P., Diemand J., Kuhlen M., 2008, *Apl*, 679, 1260  
Mancera Piña P. E., Peletier R. F., Aguerri J. A. L., Venhola A., Trager S., Choque C. N., 2018, *MNRAS*, 481, 4381  
Mancera Piña P. E., Aguerri J. A. L., Peletier R. F., Venhola T., Challap C., 2019, *MNRAS*, 485, 1036  
Martín-Navarro I. et al., 2019, *MNRAS*, 484, 3425.  
Martínez-Delgado D. et al., 2016, *AJ*, 151, 96  
Martin N. F. et al., 2014, *Apl*, 787, 19  
McConnachie A. W., 2012, *AJ*, 144, 4  
Mihos J. C. et al., 2015, *Apl*, 809, L21  
Moore B., Ghigna S., Governato F., Lake G., Quinn T., Stadel J., Tozzi P., 1999, *Apl*, 524, L19  
Müller O., Jerjen H., Binggeli B., 2017, *A&A*, 597, A7  
Muñoz R. P. et al., 2015, *Apl*, 813, L15  
Muñoz R. R., Côté P., Santana F. A., Geha M., Simon J. D., Oyarzún G. A., Stetson P. B., Djorgovski S. G., 2018, *Apl*, 860, 66  
Oevirk P., Pichon C., Lançon A., Thiébaud E., 2006, *MNRAS*, 365, 74  
Pandya V. et al., 2018, *Apl*, 858, 29  
Pan D. C., Vogeley M. S., Hoyle F., Choi Y.-Y., Park C., 2012, *MNRAS*, 421, 926  
Papastergis E., Adams E. A. K., Romanowsky A. J., 2017, *A&A*, 601, L10  
Peng E. W., Lim S., 2016, *Apl*, 822, L31  
Penny S. J. et al., 2015, *MNRAS*, 453, 3519  
Prole D. J. et al., 2019, *MNRAS*, 484, 4865  
Prole D. J., Davies J. I., Keenan O. C., Davies L. J. M., 2018, *MNRAS*, 478, 667  
Racine R., 1968, *J. R. Astron. Soc. Can.*, 62, 367  
Rejkuba M., 2012, *Ap&SS*, 341, 195  
Richtler T., 2003, in Alloin D. M., Gieren W., eds, *Stellar Candles for the Extragalactic Distance Scale*. Springer-Verlag, Berlin, p. 281  
Román J., Trujillo I., 2017, *MNRAS*, 468, 703  
Román J., Trujillo I., 2017, *MNRAS*, 468, 4039  
Román J., Trujillo I., 2018, *Res. Notes Am. Astron. Soc.*, 2, 144  
Ruiz-Lara T. et al., 2018, *A&A*, 617, A18  
Ruiz-Lara T. et al., 2018, *MNRAS*, 478, 2034  
Sandage A., 1968, *Apl*, 152, L149  
Sandage A., Binggeli B., 1984, *AJ*, 89, 919  
Sand D. J. et al., 2014, *Apl*, 793, L7  
Schlafly E. F., Finkbeiner D. P., 2011, *Apl*, 737, 103  
Sérsic J. L., 1963, *Bol. Asociacion Argentina Astron. La Plata Argentina*, 6, 41  
Spekkens K., Karunakaran A., 2018, *Apl*, 855, 28  
Springel V. et al., 2008, *MNRAS*, 391, 1685  
Springob C. M. et al., 2014, *MNRAS*, 445, 2677  
Struble M. F., Rood H. J., 1991, *ApJS*, 77, 363  
Tanmann G. A., Sandage A., 1999, in Egret D., Heck A., eds, *ASP Conf. Ser. Vol. 167, Harmonizing Cosmic Distance Scales in a Post-Hipparcos Era*. Astron. Soc. Pac., San Francisco, p. 204  
Toloba E. et al., 2018, *Apl*, 856, L31  
Tonry J., Davis M., 1979, *AJ*, 84, 1511  
Trujillo I., Roman J., Filho M., Sánchez Almeida J., 2017, *Apl*, 836, 191  
Trujillo I. et al., 2019, *MNRAS*, 733, in press  
Tully R. B., Courtois H. M., Sorce J. G., 2016, *AJ*, 152, 50  
van den Bergh S., Pritchett C., Grillmair C., 1985, *AJ*, 90, 595  
van der Burg R. F. J., Muzzin A., Hoekstra H., 2016, *A&A*, 590, A20  
van Dokkum P. et al., 2016, *Apl*, 828, L6  
van Dokkum P. et al., 2017, *Apl*, 844, L11  
van Dokkum P. G., Abraham R., Merritt A., Zhang J., Geha M., Conroy C., 2015, *Apl*, 798, L45  
Vazdekis A., Sánchez-Blázquez P., Falcón-Barroso J., Cenarro A. J., Beasley M. A., Cardiel N., Gorgas J., Peletier R. F., 2010, *MNRAS*, 404, 1639  
Vazdekis A. et al., 2015, *MNRAS*, 449, 1177  
Venhola A. et al., 2017, *A&A*, 608, A142  
Villegas D. et al., 2010, *Apl*, 717, 603  
Weinmann S. M., van den Bosch F. C., Yang X., Mo H. J., 2006, *MNRAS*, 366, 2  
Whitmore B. C., 1997, in Livio M., Donahue M., Panagia N., eds, *The Extragalactic Distance Scale*. Cambridge University Press, Cambridge, p. 254  
Willman B., 2010, *Adv. Astron.*, 2010, 285454  
Yozin C., Bekki K., 2015, *MNRAS*, 453, 14  
Zackrisson E., de Jong R. S., Micheva G., 2012, *MNRAS*, 421, 190

APPENDIX A: EFFECTS OF INCOMPLETENESS IN THE LUMINOSITY FUNCTION

In this appendix we recreate a simulation to visualize the effects of incompleteness in a globular clusters luminosity function and the recovered observational parameters under different incompleteness regimes. For this we create a Gaussian distribution with a width of 0.7 mag and an arbitrarily high number of GCs to avoid shot noise effects. Next, we apply the effects of incompleteness to this distribution. For this we assign a probability to each GC of not being observed, which will depend on its magnitude and the parameters of completeness. We recreate this effect for the *g* band. In Fig. A1 we plot the real distribution (light blue) and the observed distribution (dark blue) for different peaks of the luminosity function in a range between 23 (totally observed luminosity function) and 27 mag (almost non-observed luminosity function). We also plot the cumulative histograms, with an arbitrarily small cumulative bin, for the case of the real luminosity function (solid line) and the observed luminosity function (dashed line). The completeness curve is also

MNRAS 486, 823–835 (2019)

Downloaded from https://academic.oup.com/mnras/article-abstract/486/1/823/5398551 by guest on 01 June 2019

Este documento incorpora firma electrónica, y es copia auténtica de un documento electrónico archivado por la ULL según la Ley 39/2015.  
Su autenticidad puede ser contrastada en la siguiente dirección <https://sede.ull.es/validacion/>

Identificador del documento: 2260218

Código de verificación: Sm21pjYh

Firmado por: JAVIER ROMAN GARCIA  
UNIVERSIDAD DE LA LAGUNA

Fecha: 02/11/2019 16:23:59

IGNACIO TRUJILLO CABRERA  
UNIVERSIDAD DE LA LAGUNA

02/11/2019 17:39:19

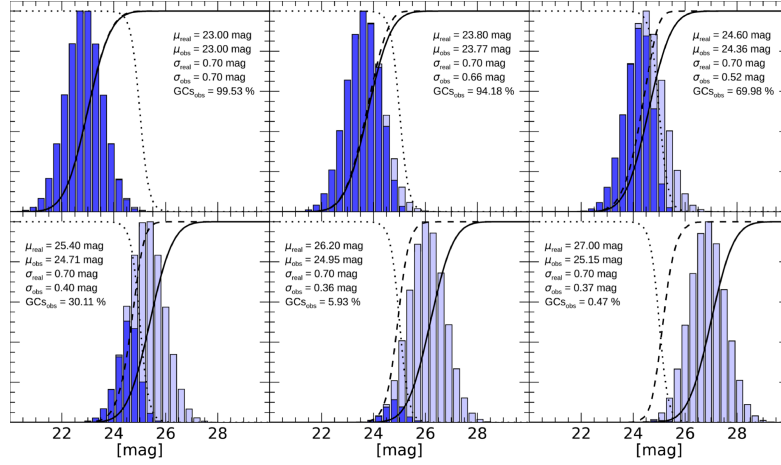


**Figure A1.** Illustrative scheme of the effect of completeness on the luminosity function of globular clusters. The real luminosity function is plotted in a light blue histogram while the observed one is plotted in dark blue. The line of completeness is shown with a dotted line and corresponds with the values obtained for the S82-DG-1 field in the *g* band. The dashed line curve represents the cumulative histogram of the observed distribution while the continuous line represents the cumulative histogram of the real distribution. The text shows the properties of the real and observed luminosity functions.

plotted with a dotted line. We perform a Gaussian function fitting to the observed luminosity function for the different cases. In each panel, the fitted peak, width, and number of globular clusters of the observed distribution are written. As expected, there is a bias in which the peak of the observed luminosity function is systematically

brighter than the real one. Additionally the width of the observed distribution is systematically narrower than the real distribution.

This paper has been typeset from a  $\text{\LaTeX}$  file prepared by the author.

Downloaded from https://academic.oup.com/mnras/article-abstract/486/1/823/5398551 by guest on 01 June 2019

Este documento incorpora firma electrónica, y es copia auténtica de un documento electrónico archivado por la ULL según la Ley 39/2015.  
 Su autenticidad puede ser contrastada en la siguiente dirección <https://sede.ull.es/validacion/>

Identificador del documento: 2260218 Código de verificación: Sm21pjYh

Firmado por: JAVIER ROMAN GARCIA  
 UNIVERSIDAD DE LA LAGUNA

Fecha: 02/11/2019 16:23:59

IGNACIO TRUJILLO CABRERA  
 UNIVERSIDAD DE LA LAGUNA

02/11/2019 17:39:19

### 3.6 Paper VI: *Galactic cirri in deep optical imaging*

The problem of Galactic cirri confusion is currently the most complex limitation to address in the study of low surface brightness sources. Although many works currently suffer from the presence of cirri, there is currently no solution for discerning them from extragalactic sources, being the only approach the use of far IR data to guess the presence of dust in the observations. This is useless for small-scale angular features due to the lousy resolution of IRAS or Planck data. The prospects for the future are even more pessimistic. With the advent of ultra-deep optical surveys such as LSST, the presence of faint dust will be revealed at any Galactic latitude. It is, therefore, a priority for the extragalactic community to address the problem of the cirri contamination in order to study the low surface brightness Universe.

In this article, we face the problem of cirri contamination by performing a characterization of their colors in optical bands, with the aim of finding cirri colors different from that of the extragalactic sources. It would provide a method for detecting the presence of Galactic dust. However, the photometry of these diffuse, extended and extremely low surface brightness structures, as the cirri are, is really challenging. First, the scattered light by the stars has surface brightness similar to that of the cirri. This required PSF modeling in all bands and the subsequent removal of the stars in the fields to be analyzed. Also, a perfect masking of the sources is necessary to isolate the flux contribution of the dust in order to perform photometry. Moreover, due to the low surface brightness of the cirri, the effect of Poissonian noise on color photometry has bias effects. To do this, a specific photometric technique was created to obtain the colors of the cirri. These techniques and analyses were applied to different regions with presence of dust in the footprint of the IAC Stripe82 Legacy Survey, with a total of 26.5 square degrees, about 10% of the total of the survey.

The results are that, in fact, the colors of the cirri in optical bands are different from those of extragalactic sources. It provides a very promising method for identifying the presence of dust in ultra deep imaging through the use of multiple photometric bands. Its use on the future LSST is of particular importance. Considering that LSST will have the  $u$ ,  $g$ ,  $r$ ,  $i$ ,  $z$  and  $y$  photometric bands, this method could be used to break the confusion regarding dust and extragalactic sources.

Another interesting result of this work is a correlation found between the amount of dust in the line of sight and the colors observed, in which the cirri become redder with the increasing dust column density. This correlation has not been found in previous works. In addition, as a complementary result, the first characterization of the colors of the scattered light by the stars was made, finding strong color variations at small scales because of the complex morphology of the PSFs in the SDSS data.

Este documento incorpora firma electrónica, y es copia auténtica de un documento electrónico archivado por la ULL según la Ley 39/2015.  
Su autenticidad puede ser contrastada en la siguiente dirección <https://sede.ull.es/validacion/>

Identificador del documento: 2260218 Código de verificación: Sm21pjYh

Firmado por: JAVIER ROMAN GARCIA  
UNIVERSIDAD DE LA LAGUNA

Fecha: 02/11/2019 16:23:59

IGNACIO TRUJILLO CABRERA  
UNIVERSIDAD DE LA LAGUNA

02/11/2019 17:39:19

## Galactic cirri in deep optical imaging

Javier Román<sup>1,2,3\*</sup>, Ignacio Trujillo<sup>1,2</sup>, and Mireia Montes<sup>4</sup>

<sup>1</sup> Instituto de Astrofísica de Canarias, c/ Vía Láctea s/n, E-38205, La Laguna, Tenerife, Spain

<sup>2</sup> Departamento de Astrofísica, Universidad de La Laguna, E-38206, La Laguna, Tenerife, Spain

<sup>3</sup> Instituto de Astrofísica de Andalucía, CSIC, Apdo. 3004, 18080 Granada, Spain

<sup>4</sup> School of Physics, University of New South Wales, Sydney, NSW 2052, Australia

May 1, 2019

### ABSTRACT

The presence of diffuse filaments associated with reflected starlight from dust particles of the Milky Way (the Galactic cirri) becomes a major challenge for the current generation of deep optical observations. The optical properties of the cirri are not yet well understood, resulting in a strong source of confusion in the analysis of low surface brightness extragalactic features. We have carried out an observational study exploring the optical properties of cirri using  $g$ ,  $r$ ,  $i$  and  $z$  SDSS bands along the Stripe82 region. Through comprehensive image processing techniques, including the modeling and removal of the scattered light produced by stars, we manage to isolate the optical diffuse emission by cirri, allowing a photometric characterization. We show that the optical colors of the cirri are driven by the dust column density: the cirri become redder as the  $100\ \mu\text{m}$  emission increases. This could explain the extended red emission previously found in cirri clouds. We show that, in general, the cirri optical colors are incompatible with those of extragalactic sources, suggesting if confirmed, the use of multi-band optical photometry for the detection of cirri with a higher spatial resolution than that provided by surveys in the infrared. Finally, we suggest the extraordinary potential of the future LSST in the study of the Galactic foreground dust. The combination of very deep data and multi-band photometry could make it possible to build dust and extinction maps of unprecedented quality.

**Key words.** ISM: clouds – ISM: dust, extinction – Techniques: image processing – Techniques: photometric

### 1. Introduction

The present generation of deep optical surveys allow us, for the first time, to unravel critical issues of the hierarchical evolution of galaxies that are intrinsically connected with the low surface brightness Universe. For instance, the detection of galaxies of decreasing surface brightness (e.g. Sandage & Binggeli 1984; Impey et al. 1988; Dalcanton et al. 1997; Blanton et al. 2005; Mihos et al. 2015; Javanmardi et al. 2016; Mihos et al. 2018), the stellar halos and tidal features surrounding nearby galaxies (e.g. Bullock & Johnston 2005; Abadi et al. 2006; Johnston et al. 2008; Martínez-Delgado et al. 2010; Duc et al. 2015; Trujillo & Fliri 2016) or the intracluster light (ICL) in galaxy clusters (e.g. Uson et al. 1991; Mihos et al. 2005; Rudick et al. 2010; Giallongo et al. 2014; Montes & Trujillo 2018) are all crucial observational pillars for testing the current  $\Lambda$ CDM cosmological paradigm (e.g. Moore et al. 1999; Klypin et al. 1999; Cooper et al. 2010, 2015).

The star counting method reaches a depth equivalent to 30 mag arcsec<sup>-2</sup> in the detection of galaxy satellites (McConnachie 2012, and references therein) and 32 mag arcsec<sup>-2</sup> in galactic substructures as tidal features and stellar streams (e.g. Ibata et al. 2009; Tanaka et al. 2011; Ibata et al. 2014; Martin et al. 2014; McConnachie et al. 2018). However, the resolved star count method is only able to study the Local Universe, limited by the spatial resolution of the images (e.g. 16 Mpc using the Hubble Space Telescope; Zackrisson et al. 2012), and stochasticity (Willman 2010). That makes the integrated photometry the only alternative to detect extragalactic sources beyond the resolution

limit of its individual stars. However, the use of integrated photometry is affected by systematic effects, severely restricting the detection limits in surface brightness, in particular: i) poor data reduction processes creating gradients and different artifacts in the images, what forces to ii) subtraction of the sky background by surface fitting, removing or over-subtracting the low surface brightness information around extended sources and iii) the presence of the scattered light from sources due to the point spread function (PSF). Different approaches have been made trying to minimize these effects, such as better astronomical data reduction pipelines (Akhlaghi & Ichikawa 2015; Borlaff et al. 2019), improvements in the observational techniques (e.g. Ferrarese et al. 2012; Duc et al. 2015; Trujillo & Fliri 2016), a better characterization of the PSF and internal reflections due to optical instrumentation (Slater et al. 2009; Sandin 2014; Infante-Sainz et al. 2019 in prep.) or the development of simple optic telescopes (Abraham & van Dokkum 2014; Muslimov et al. 2017; Valls-Gabaud & MESSIER Collaboration 2017).

Despite all the observational and technical advances to improve the quality of deep optical datasets, the presence of interstellar material from our own Galaxy reflecting the starlight (Elvey & Roach 1937; Henyey & Greenstein 1941; Sandage 1976; Mattila 1979) is unavoidable. These filamentary clouds of dust, called "Galactic cirri", have peak emission in the far infrared due to its low temperature component (Low et al. 1984; Veneziani et al. 2010). However, their reflected light is detectable in optical (de Vries & Le Poole 1985; Laureijs et al. 1987; Witt et al. 2008) and ultraviolet (Witt et al. 1997; Boissier et al. 2015) wavelengths. With the increasing depth of optical observations, the presence of cirri has become a major challenge even at high Galactic latitudes, mimicking the shape and brightness of faint

\* e-mail: jromanastro@gmail.com

Este documento incorpora firma electrónica, y es copia auténtica de un documento electrónico archivado por la ULL según la Ley 39/2015.

Su autenticidad puede ser contrastada en la siguiente dirección <https://sede.ull.es/validacion/>

Identificador del documento: 2260218

Código de verificación: Sm21pjYh

Firmado por: JAVIER ROMAN GARCIA  
UNIVERSIDAD DE LA LAGUNA

Fecha: 02/11/2019 16:23:59

IGNACIO TRUJILLO CABRERA  
UNIVERSIDAD DE LA LAGUNA

02/11/2019 17:39:19

extragalactic features (e.g. Chiboucas et al. 2009; Cortese et al. 2010; Sollima et al. 2010; Rudick et al. 2010; Davies et al. 2010; Chiboucas et al. 2013; Hodges-Kluck & Bregman 2014; Besla et al. 2016; Duc et al. 2018; Barrera et al. 2018; Ramírez-Moreta et al. 2018). Far infrared or sub-millimetre full-sky maps, as the IR Astronomical Satellite (IRAS) mission or the Planck Space Observatory, are used as counterpart to the optical data seeking for the presence of cirri in the observations. However, the poor resolution of these instruments (FWHM  $\approx$  5 arcmins; Miville-Deschênes & Lagache 2005; Lamarre et al. 2003) make them inefficient for small angular scale features. Only with the availability of better spatial resolution far infrared data, as the ESA Herschel Space Observatory (FWHM of 18 arcseconds in the 250  $\mu$ m band; Pilbratt et al. 2010) it is possible to correctly identify, or even remove, the dust foreground contamination (see Mihos et al. 2017). However, the Herschel Space Observatory data only exists for a very limited number of available fields. Therefore, it would be desirable the use of the optical data itself to identify the presence of cirri without the need to resort to complementary data at other wavelengths. This means knowing what are the range in colors of the cirri.

Previous studies about the optical properties of cirri (e.g. Guhathakurta & Tyson 1989; Witt et al. 2008; Ienaka et al. 2013) have neglected important systematic effects, as the presence of scattered light by stars due to the PSF. This could have a significant impact on the photometry due to the extremely low surface brightness of the cirri clouds, especially in areas where the dust clouds have a low column density or surface brightness.

The imminent arrival of the Large Synoptic Survey Telescope (LSST; LSST Science Collaboration et al. 2009) and the new generation of extremely large telescopes will light up the presence of Galactic cirri at any Galactic latitude. It is, therefore, a priority for the extragalactic community to address the problem of cirri contamination, being also an important source of uncertainty in aspects such as the Cosmic Microwave Background and its polarization (e.g. Planck Collaboration et al. 2011; Das et al. 2014) or the Infrared Cosmic Background (e.g. Thacker et al. 2013). In this work we aim to carry out a comprehensive photometric analysis of the Galactic cirri, taking into account the possible systematic uncertainties due to the extremely low surface brightness regime, allowing us to provide the colors of the cirri in optical wavelengths.

This paper is structured as follows: In Section 2 we describe the data and data processing. The correlation between the IR and optical bands is explored in Section 3. In Section 4 we describe the colors of the Galactic cirri. We address our main conclusions in section 5. We use the AB photometric system in this work.

## 2. Data and data processing

A common problem affecting deep optical surveys is the over-subtraction of flux around the sources. This is due to aggressive sky subtraction (see a full discussion and an approach addressing this problem by Borlaff et al. 2019, in the Hubble Ultra-Deep Field). Current versions of the Hyper Suprime-Cam Subaru Strategic Program (HSC-SSP) (Aihara et al. 2018) or the Dark Energy Camera Legacy Survey (DECaLS) (Dark Energy Survey Collaboration et al. 2016) are examples of this circumstance. This over-subtraction prevent the study of extended diffuse emission, since it would be systematically removed. To overcome this problem, we use data from the IAC Stripe82 Legacy Survey (Fliri & Trujillo 2016). This dataset consists on a new reduction of the SDSS Stripe82 data (Abazajian et al. 2009) with the aim of preserving the lowest surface brightness fea-

tures, minimizing the over-subtraction around the sources. The Stripe82 region covers a 2.5 degree wide stripe along the Celestial Equator in the Southern Galactic Cap ( $-50^\circ < R.A. < 60^\circ$ ,  $-1.25^\circ < Dec. < 1.25^\circ$ ) reaching a total of 275 square degrees. The total exposure time per field is around 1 hour, using the 2.5m Telescope at Apache Point Observatory (SDSS) in all the five SDSS filters ( $u, g, r, i, z$ ). The pixel scale is 0.396 arcsec and the average seeing is around 1 arcsec. In this work we use the new set of rectified images of the survey described by Román & Trujillo (2018) in which the residuals of the coadding process have been removed. This produces high-quality and homogenized deep images, allowing a clean photometry of the faintest structures. The average surface brightness limits of the dataset are:  $\mu_{lim}(3\sigma; 10'' \times 10'') = 28.0, 29.1, 28.6, 28.2$  and  $26.6$  mag arcsec $^{-2}$  for the ( $u, g, r, i, z$ ) bands respectively. We describe in detail how these limits are calculated in Appendix A.

Although this dataset preserves the diffuse emission, the photometry of extended sources is not straight forward to obtain. For instance, the scattered light due to the PSF wings of the stars contaminate strongly the faint cirri emission. Additionally, an exquisite masking of sources is necessary to obtain a reliable photometry. In the following, we describe the data processing in order to isolate the Galactic cirri flux.

### 2.1. Modeling the scattered light produced by stars

The removal of the scattered light by stars is becoming a common technique to obtain a clean photometry of extremely low surface brightness sources. For instance, work by Slater et al. (2009) modeled the stars and their internal reflections in deep images of the Burrell Schmidt telescope (Rudick et al. 2010; Watkins et al. 2014, 2015, 2016, 2017; Mihos et al. 2017; Watkins et al. 2018), work by Trujillo & Fliri (2016) modeled the scattered light by stars in very deep observations of the UGC 00180 galaxy using a PSF characterization of the 10.4m GTC telescope and work by (Karabal et al. 2017) modeled the internal reflections and PSF using images of the Canada France Hawaii Telescope (CFHT) to provide reliable deep photometry of galaxies.

The specific characteristics of the internal reflections due to the optical instrumentation of the telescope is an important issue to take into account when modeling the stars. Depending on the optical instrumentation of the telescope, the sum of the reflections can contaminate a significant fraction of the total area of the image. This circumstance would require a modeling of the reflections. In the case of the IAC Stripe82 Legacy Survey or SDSS in general, the internal reflection is fixed at the same position for each star, with a small angular size (up to  $30''$ , see Infante-Sainz et al. 2019 in prep.), being relatively faint, only noticeable for bright stars. Therefore, we do not carry out a modeling of these reflections, being enough to perform the modeling of the stars using exclusively the PSF (image of a point source through the main optical path, without reflections on the CCD) in the final coadded data. The sum of the scattered light by all the stars in a given field due to the PSF is what we call the "scattered light field".

Obtaining the scattered light field by stars means characterizing accurately the PSF model. Once this PSF model is obtained, the scattered light field is fixed by the position and fluxes of the stars present in the image. Thus, the only information needed to produce the scattered light field is the PSF and the coordinates and fluxes of the stars to be modeled. In Appendix B we describe the process followed to obtain the PSF models for the IAC Stripe82 Legacy Survey in the five SDSS bands. To obtain

Román et al.: Galactic cirri in deep optical imaging

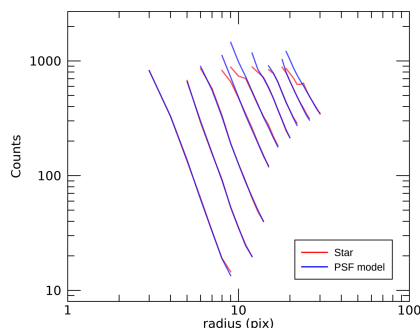


**Fig. 1.** Example of star fitting using the PSF model in a random field in the  $g$  band. The plot shows the profiles of the fitted stars (red) and the profile of the flux scaled PSF models (blue). Nine stars are fitted in this example, with magnitudes ranging approximately between 7.5 and 15.5 in the  $g$  band. The profiles extend to the radial region used to calculate the flux of the star. The radial region selected for the profile fitting is dynamic for each star and depends on the circumstances of saturation, crowding or magnitude of the star (see text). Note that the saturation region appears above approximately 800 counts, creating severe deviations from the PSF model in the inner region of the profiles of the brightest stars due to CCD bleeding.

the exact coordinates and fluxes of the stars there are a number of practical problems, as the inner saturated region of the bright stars or the presence of adjacent or overlapping sources, making direct photometry unreliable to obtain the flux of the stars. In this work, we have created a specific pipeline that obtains precise position and accurate photometry of the stars, even if the stars are saturated. The main tasks of this pipeline are summarized as follows:

For each field we produce a catalog of stars. We run SExtractor (Bertin & Arnouts 1996) obtaining position and stellarity for each source of the field. We select stars as sources with stellarity (CLASS\_STAR) higher than 0.75 in the  $r$ -deep band, which is a combination of the  $g$ ,  $r$  and  $i$  SDSS bands provided by the IAC Stripe82 survey. This criteria produces an excellent filtering by exclusively selecting PSF-like sources. However, very bright stars do not match this criterion, as they are detected with a lower stellarity due to the strong inner saturation and bleeding. Since these stars are very bright, and hence very few, we included their coordinates manually, completing the final catalog. The next step is to obtain accurate spatial coordinates of the selected stars, which is crucial for the PSF modeling (Lu et al. 2018). For each star we mask the saturation region (if present) by masking pixels with counts above the saturation threshold for each band. We also mask all the sources that are adjacent or overlapping the star using the segmentation maps provided by SExtractor. Because these detection maps do not cover well enough the sources, in particular the faint external regions, we enlarge the masks to cover most of the flux of the sources. To obtain accurate spatial coordinates of each star, we fit a Moffat function to the masked star using the IMFIT (Erwin 2015) package and we get the coordinates provided by this fitting. Once the star is masked and centered we perform the flux fitting. We use an approach based on the PSF model pro-

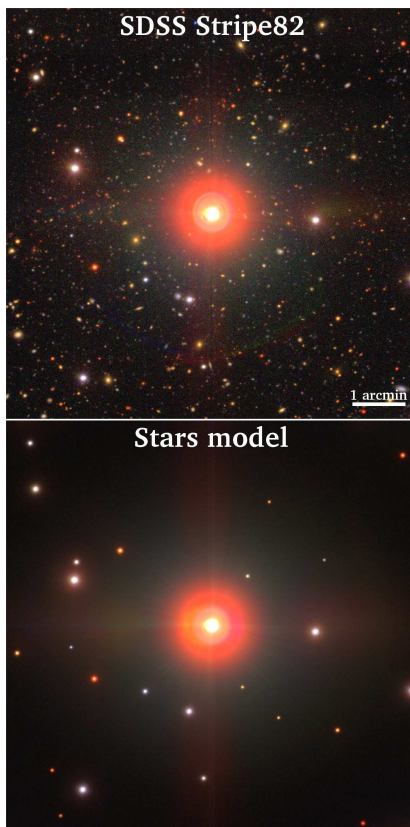


**Fig. 2.** Composite colour image using  $g$ ,  $r$  and  $i$  SDSS bands of real data of the IAC Stripe Legacy Survey (upper panel) and the stars model (bottom panel).

files. Other methods such as a  $\chi^2$  minimization using the two-dimensional PSF model are also valid, however we choose using profiles to be more resistant to any masking residual, crowding or artifact that could remain in the image. The circular aperture (or annulus if saturation is present) for the profiles is selected with an adaptive range in radius, whose criteria depend on the approximate magnitude of the star from SExtractor and the crowding of nearby sources. The selected region tries to cover the area with enough signal to noise for an accurate profile fitting avoiding spurious detection as masking residuals of adjacent sources. Once the star profile is obtained we scale it to match the normalized PSF profile, giving the flux of the star. For the

Article number, page 3 of 23

Este documento incorpora firma electrónica, y es copia auténtica de un documento electrónico archivado por la ULL según la Ley 39/2015.  
 Su autenticidad puede ser contrastada en la siguiente dirección <https://sede.ull.es/validacion/>

Identificador del documento: 2260218

Código de verificación: Sm21pjYh

Firmado por: JAVIER ROMAN GARCIA  
 UNIVERSIDAD DE LA LAGUNA

Fecha: 02/11/2019 16:23:59

IGNACIO TRUJILLO CABRERA  
 UNIVERSIDAD DE LA LAGUNA

02/11/2019 17:39:19

A&A proofs: manuscript no. output

most accurate measurement possible, we average the fractions between the star and the PSF profiles at each radius discarding outliers beyond  $2\sigma$ , creating a robust mean normalization value. We show an illustrative example in Fig. 1 of the high accuracy of the profile fitting of the stars using the PSF models. Repeating this process for the complete catalogue of stars, we obtain the positions and integrated fluxes of all the stars in the field. For the purposes of this work, we modeled all the stars up to magnitude 15 in the  $r$ -band for reasons of computational efficiency. This cut in magnitude is justified, since the flux of the PSF in the outer region for stars of magnitude 15 and fainter is negligible. Finally, using the software SWARP (Bertin et al. 2002) we place PSFs over a blank field with the calculated positions and fluxes of the fitted stars, creating the scattered light field. We show in the Fig. 2 an illustrative example of an arbitrary field modeled with our procedure. The average number of fitted stars is approximately 400 per square degree. Due to the strong presence of "ghosts" artifacts in the  $u$  band, added to the high sky background fluctuations in this band, we restrict ourselves to the reliable  $g$ ,  $r$ ,  $i$  and  $z$  bands for further analysis.

### 2.2. Properties of the scattered light field produced by stars

Obtaining the scattered light field model provides interesting information about its influence on the data. The availability of the  $g$ ,  $r$ ,  $i$  and  $z$  SDSS bands gives us the possibility to obtain a photometric description of the colors of the scattered light by the stars. In Fig. 3 we show that on a random field of  $1 \times 1$  degree of the IAC Stripe82 Legacy Survey. In the upper left panel, we show the surface brightness map of the scattered light field produced by the stars in the  $r$  band. We also show the surface brightness distributions for all the bands in that field in the lower plot of the panel. As can be seen, the mean surface brightness of the scattered light field vary between different bands. In the case of the  $r$  band, there is an average surface brightness of approximately  $29 \text{ mag arcsec}^{-2}$ , similar to the value reported by Trujillo & Fliri (2016) using the GTC telescope in that same band (see also work by Slater et al. 2009). The average surface brightness of the scattered light field increase as the band is redder, ranging from a typical surface brightness of  $30 \text{ mag arcsec}^{-2}$  in the  $g$  band to  $28 \text{ mag arcsec}^{-2}$  in the  $z$  band. It is of course, expected, as the average star is brighter in redder bands. This is, in fact, what is observed in the other panels of Fig. 3, in which color maps of the scattered light field are shown, together with the color distributions, on average red colors. However, the scattered light field colors are far from having an homogeneous distribution in the image, suffering from strong color variations at small spatial scales. Particularly striking is the effect of the bump of the  $i$  band PSF within 30 arcseconds radius (de Jong 2008; Infante-Sainz et al. 2019 in prep., see also Fig. B.2), creating complex color patches around stars, clearly noticeable also in Fig. 2 visually.

In spite of the low surface brightness of the scattered light field, it could have a significant impact on the photometry of extremely faint sources, as it is the case of the Galactic cirri. Although this contamination is especially important in the proximity of the bright stars, the maximum surface brightness of the Galactic cirri analyzed in this work is around  $26 \text{ mag arcsec}^{-2}$  in the  $r$  band. Therefore the average scattered light field surface brightness can also affect the global photometry. Finally, it is worth mentioning that the results shown in this section are only descriptive of the data used in this work, this is SDSS data from the IAC Stripe82 Legacy Survey. The use of another data set with different PSFs could create different scattered light fields and derived photometric properties.

Article number, page 4 of 23

**Table 1.** Summary of parameters applied for the different masking layers using SExtractor.

Mask	DETECT MINAREA	DETECT MAXAREA	DETECT THRESH	BACK SIZE	Enlarged mask size
1	5	150	3	10	0
2	150	500	3	10	5
3	450	1500	2	10	15
4	1900	7500	4	200	20
5	1000	2500	3	10	30
6	7000	inf.	4	100	30

### 2.3. Isolating the extended diffuse emission

The modeling and subtraction of the stars produces images almost free of contamination by scattered light. However, faint stars, galaxies, residuals of the scattered light subtraction and different artifacts still remain in the image (see Fig. 4). In order to isolate the diffuse emission, such as the Galactic cirri present in the images, it is necessary to accurately mask all the sources. However, the masking of low surface brightness structures is not an easy task. The use of SExtractor in its simple form is not able to detect the faintest outer regions of the sources, producing an incomplete masking and a potential source of contamination. After several testing, we ended up with a modified masking process based on SExtractor. The reason is that SExtractor performs a source detection targeting exclusively stars and galaxies. In this sense, the ineffectiveness of SExtractor in the detection of amorphous low surface brightness features is an advantage for our purpose, since only stars and galaxies are aimed to be masked. To mask completely the sources, we performed a specific algorithm to improve the masks provided by SExtractor. It consists in six different layers of masking, focused in the detection of different sources in sizes and deblending levels (sources over sources), each of one with a different enlargement of the mask. We show the SExtractor parameters for each masking layer in Table 1. This masking sequence manages to hide all the sources, exposing the diffuse emission by the cirri in the images, and it is constructed in a conservative way, that is, the masks are systematically larger than the actual size of the sources. However, due to the large area occupied by the cirri in relation to the sources to be masked, that loss of area is acceptable for the purposes of this work. Since our goal is precision photometric measurements of Galactic cirri, any possible systematic uncertainty should be treated conservatively.

The masking algorithm has as input the original  $r$ -deep band image of the field, that is, with all the stars present in the image. All the masks obtained in the sequence described above are combined in a unique mask, which is applied to all the bands corrected from the scattered light produced by the stars. Note that the presence of the stars in the input image facilitates the masking of the centers of the removed stars (only the centers, since SExtractor is not able to mask the PSF wings of the stars), hiding all the subtraction residuals. The application of this masking process produces an excellent isolation of the diffuse emission by cirri. However, "ghosts" and different artifacts still remain in the images. Nevertheless, these are well documented<sup>1</sup> and are easily identified both visually or through color maps, presenting extreme colors against real sources. Therefore, we apply an additional manual masking focused on those artifacts. We show an illustrative example of the final result of the masking process in Fig. 5. As a final step we increase the pixel size of the images.

<sup>1</sup> <http://skyserver.sdss.org/dr12/en/tools/places/page6.aspx>

Este documento incorpora firma electrónica, y es copia auténtica de un documento electrónico archivado por la ULL según la Ley 39/2015.  
 Su autenticidad puede ser contrastada en la siguiente dirección <https://sede.ull.es/validacion/>

Identificador del documento: 2260218 Código de verificación: Sm21pjYh

Firmado por: JAVIER ROMAN GARCIA  
 UNIVERSIDAD DE LA LAGUNA

Fecha: 02/11/2019 16:23:59

IGNACIO TRUJILLO CABRERA  
 UNIVERSIDAD DE LA LAGUNA

02/11/2019 17:39:19

Román et al.: Galactic cirri in deep optical imaging

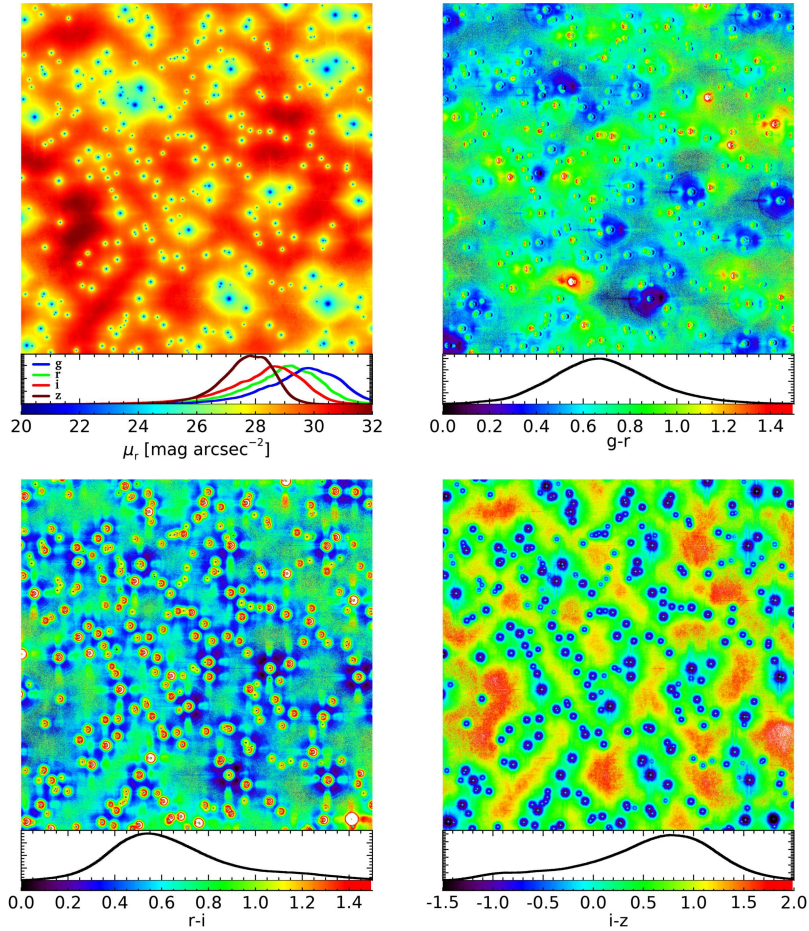


**Fig. 3.** Photometric properties of the scattered light field produced by the stars on a random field of  $1 \times 1$  degree of the IAC Stripe82 Legacy Survey. The upper left panel shows the surface brightness of the field in the  $r$  band. The upper right, bottom left and bottom right panels show the  $g-r$ ,  $r-i$  and  $i-z$  colors respectively. The bottom plots in each panel represent the distribution histograms.

Due to the large angular size of the Galactic cirri, there is a large margin to increase the pixel size without a reasonable loss of spatial resolution. This increases the signal to noise by reducing the Poisson noise averaging the pixels. We choose a 6 arcsec final pixel scale as a compromise between optimal spatial resolution and depth of the images. With this pixel size the average surface

brightness limit in pixel to pixel variations is  $\mu_{lim}(3\sigma; 6'' \times 6'') = 28.5, 28.0, 27.6$  and  $26.0$  mag arcsec $^{-2}$  for the  $g, r, i$  and  $z$  bands respectively (see Appendix A). After the rebinning process we found a small fraction of pixels (less than 1 percent) whose values are much higher than that of adjacent pixels. These pixels appear prominent in comparison with the soft background light

Article number, page 5 of 23

Este documento incorpora firma electrónica, y es copia auténtica de un documento electrónico archivado por la ULL según la Ley 39/2015.  
 Su autenticidad puede ser contrastada en la siguiente dirección <https://sede.ull.es/validacion/>

Identificador del documento: 2260218

Código de verificación: Sm21pjYh

Firmado por: JAVIER ROMAN GARCIA  
 UNIVERSIDAD DE LA LAGUNA

Fecha: 02/11/2019 16:23:59

IGNACIO TRUJILLO CABRERA  
 UNIVERSIDAD DE LA LAGUNA

02/11/2019 17:39:19

A&A proofs: manuscript no. output

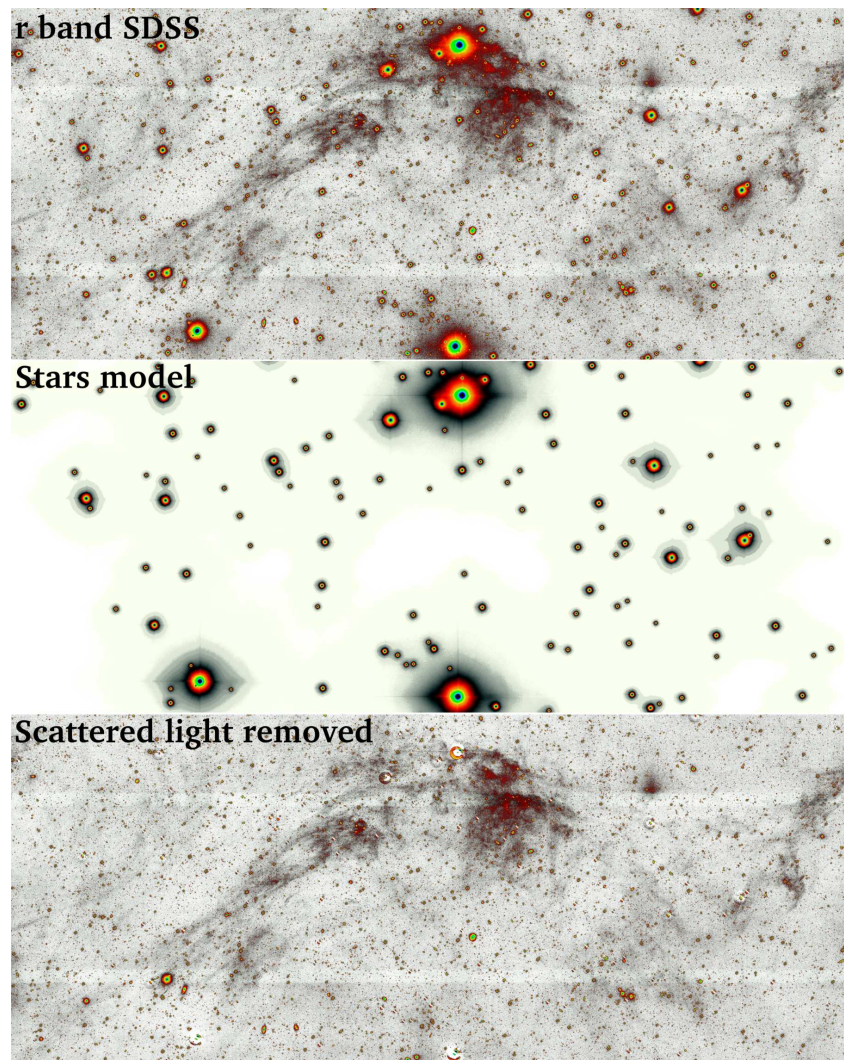


**Fig. 4.** Example field of the removal of the scattered light produced by the stars. Top panel: Original IAC Stripe82 field in the r-band. Middle panel: Model of the scattered field produced by the stars. Bottom panel: Same as the top panel but with the scattered field subtracted. The pixel scale in 0.396 arcseconds.

Article number, page 6 of 23

Este documento incorpora firma electrónica, y es copia auténtica de un documento electrónico archivado por la ULL según la Ley 39/2015.  
Su autenticidad puede ser contrastada en la siguiente dirección <https://sede.ull.es/validacion/>

Identificador del documento: 2260218 Código de verificación: Sm21pjYh

Firmado por: JAVIER ROMAN GARCIA  
UNIVERSIDAD DE LA LAGUNA

Fecha: 02/11/2019 16:23:59

IGNACIO TRUJILLO CABRERA  
UNIVERSIDAD DE LA LAGUNA

02/11/2019 17:39:19

Román et al.: Galactic cirri in deep optical imaging

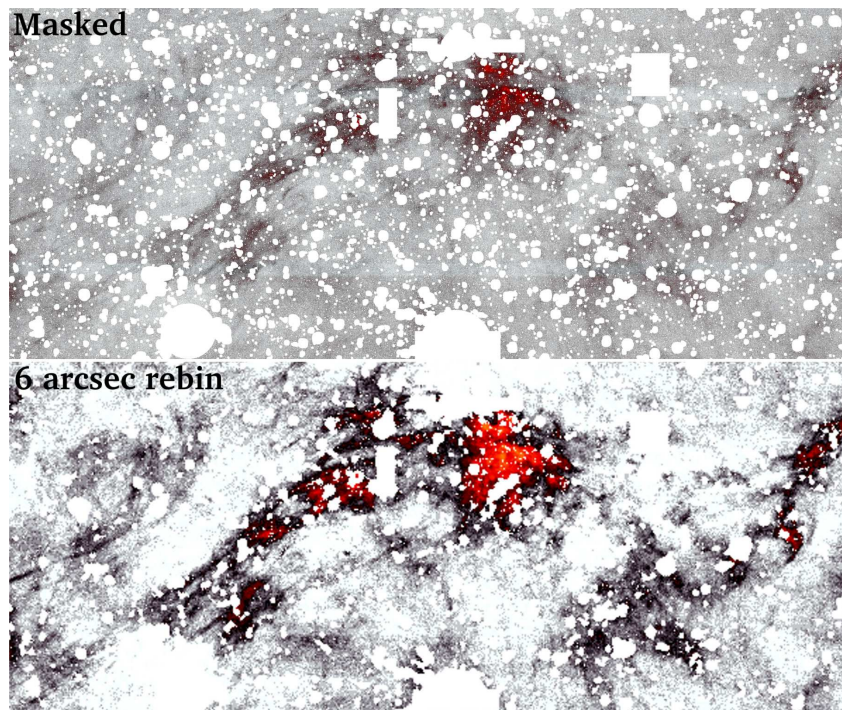


Fig. 5. Result of the masking process (upper panel) and rebinning (bottom panel) applied to the scattered light removed image in Fig. 4. Masked regions appear as white color.

of the diffuse emission. By inspecting the images, we detected that these hot pixels are the result of residuals in the masking process using the original pixel scale. These are typically faint tidal features or haloes of galaxies, not detectable in the processed image but enhanced in the rebinned images. To remove these residual pixels, we carry out a last masking step in the rebinned images. Due to the isolated nature of these "hot pixels" in comparison with the smooth background of the diffuse emission, we mask pixels with counts  $5\sigma$  above the noise with respect to the average value of their adjacent pixels. With this we guarantee that the masked pixels are not statistical fluctuations of the Poisson noise but true anomalous fluxes coming from residuals in the masking process.

Finally, we perform a calibration of the reference sky background level. To do this we perform a masking of the diffuse light present in the images. For that we performed a strong gaussian smoothing with a kernel width of 30 arcsec to the 6 arcsec pixel scaled masked images and we run SExtractor with a specific setup to detect most of the diffuse emission. This detection of the diffuse light in the image based on SExtractor

is not accurate, therefore it is not reliable to perform photometric measurements, but it is sufficient to hide most of the diffuse emission, leaving unmasked the regions that can be considered as a sky background. We used an algorithm of the type mean-median, specifically design to obtain a reliable sky background level even in very contaminated fields, to compute the reference flux sky level. We use the routine SKY from IDL to perform this task.

### 3. Galactic cirri: Optical vs. far IR counterparts

The data processing described in the previous section allows to isolate the extended diffuse emission present in optical data. However, it is necessary to clarify whether this diffuse emission is due entirely to Galactic dust, or on the contrary, there is another source of emission in the optical, including residuals of the data processing. Since Galactic cirri appear clearly at far IR wavelengths, any emission by cirri in the optical should have an infrared counterpart, and equivalently, any optical diffuse emission without IR counterpart could be considered not due to cirri.

Article number, page 7 of 23

Este documento incorpora firma electrónica, y es copia auténtica de un documento electrónico archivado por la ULL según la Ley 39/2015.  
 Su autenticidad puede ser contrastada en la siguiente dirección <https://sede.ull.es/validacion/>

Identificador del documento: 2260218 Código de verificación: Sm21pjYh

Firmado por: JAVIER ROMAN GARCIA  
 UNIVERSIDAD DE LA LAGUNA

Fecha: 02/11/2019 16:23:59

IGNACIO TRUJILLO CABRERA  
 UNIVERSIDAD DE LA LAGUNA

02/11/2019 17:39:19

A&A proofs: manuscript no. output

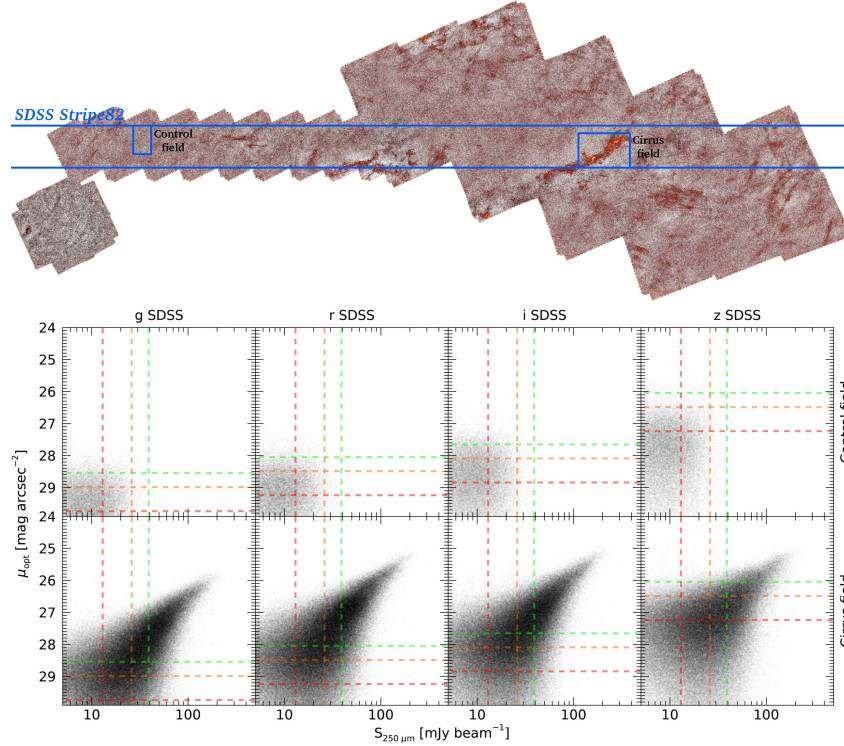


**Fig. 6.** Optical vs. far IR diffuse emission. In the upper panel it is shown the Hershel Stripe82 survey footprint overlapped with the SDSS Stripe82 footprint. The lower panels show the correlation between the diffuse emission in the far IR data and  $g$ ,  $r$ ,  $i$  and  $z$  optical bands for the Control field (upper row) and the Cirrus field (lower row).

We performed a direct photometric comparison of the diffuse emission present in the optical data of the IAC Stripe82 Legacy Survey with the diffuse emission found in the far IR in the Herschel Multi-tiered Extragalactic Survey (HerMES) (Levenson et al. 2010; Viero et al. 2013) and the Hershel Stripe82 survey (HerS) (Viero et al. 2014). These data cover a wide region matching the Stripe82 area within  $350^\circ < \text{R.A.} < 36^\circ$  using the Spectral and Photometric Imaging Receiver (SPIRE) of the *Herschel Space Observatory* at 250, 350, and 500  $\mu\text{m}$  bands. We use the HerS-HeLMS-XMM-LSS combined SPIRE maps (DR4) publicly available on the Herschel Database in Marseille<sup>2</sup>. The design of this survey is focused on the study of extragalactic sources as infrared-emitting dusty star-forming galaxies or active galactic nuclei. However, Galactic cirri are detectable in the area mapped by the survey. The relative high resolution of this

<sup>2</sup> <https://hedam.lam.fr/HerMES/>.

far IR data compared with the IRAS survey allows a direct photometric comparison of the extended diffuse emission. For the purposes of this work, we use only the 250  $\mu\text{m}$  band due to its higher angular resolution (6" pixel scale, 18.1" FWHM) and optimal wavelength for the detection of the Galactic dust emission.

In Fig. 6 we show the HerS-HeLMS-XMM-LSS map at 250  $\mu\text{m}$  and the footprint of the SDSS Stripe82 survey indicated by blue lines. While the mapped area has a relatively low presence of dust, some conspicuous filamentary clouds are clearly visible in the 250  $\mu\text{m}$  image. We selected an area of  $3 \times 2$  degrees with the highest presence of Galactic cirri, labelled in Fig. 6 as "Cirrus field". We did not conduct any analysis of additional regions due to the low emissivity of the clouds present in the footprint, both in the far IR and in optical bands, especially in the shallower  $z$  band. We also selected an area free of Galactic cirri, with a size of  $1.0 \times 1.5$  degrees, being considered as a control field, labelled in Fig. 6 as "Control field". For the two selected fields we cre-

Este documento incorpora firma electrónica, y es copia auténtica de un documento electrónico archivado por la ULL según la Ley 39/2015.  
 Su autenticidad puede ser contrastada en la siguiente dirección <https://sede.ull.es/validacion/>

Identificador del documento: 2260218 Código de verificación: Sm21pjYh

Firmado por: JAVIER ROMAN GARCIA  
 UNIVERSIDAD DE LA LAGUNA

Fecha: 02/11/2019 16:23:59

IGNACIO TRUJILLO CABRERA  
 UNIVERSIDAD DE LA LAGUNA

02/11/2019 17:39:19

Román et al.: Galactic cirri in deep optical imaging

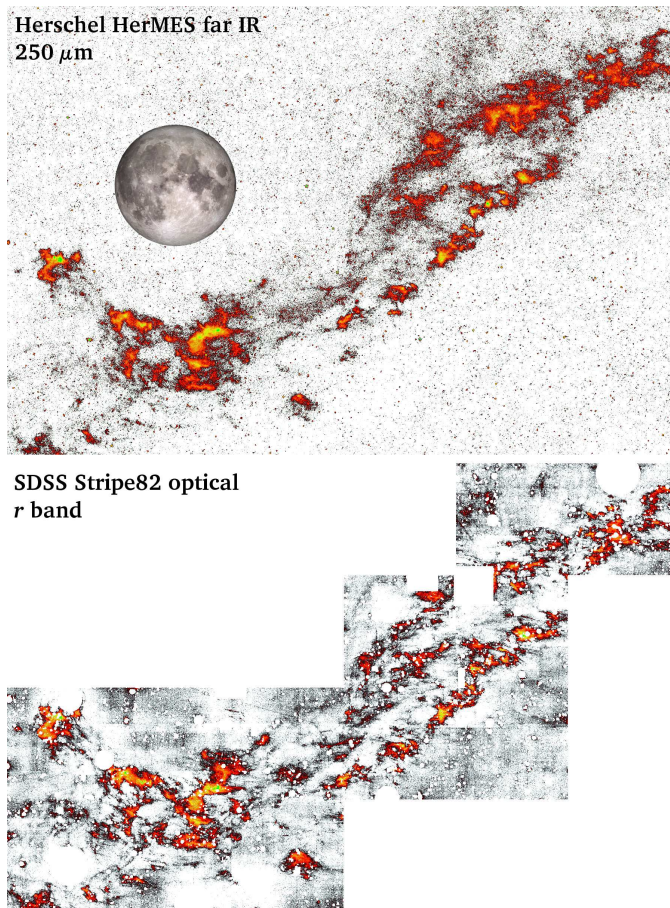


**Fig. 7.** Comparison between far IR and optical of the "Cirrus field" (see text). Top panel: 250  $\mu\text{m}$  band from the HerMES map. Lower panel:  $r$  band from the IAC Stripe82 Legacy Survey. The pixel scale for both images is 6 arcsec. An image of the moon (31 arcmin diameter) is placed as angular scale reference.

ated five mosaics, one for each of the 250  $\mu\text{m}$ ,  $g$ ,  $r$ ,  $i$  and  $z$  bands, with astrometric matching allowing pixel to pixel comparison. We perform the data processing described in the previous section for the optical bands. Additionally, we perform a masking of the 250  $\mu\text{m}$  image, focused on extragalactic sources leaving unmasked the emission by Galactic cirri. Finally, because the FWHM of the 250  $\mu\text{m}$  band is 18 arcseconds, we perform a 3-

pixel kernel smoothing to the optical images (pixel scale of 6 arcseconds), ensuring that the optical bands match the resolution of the 250  $\mu\text{m}$  data.

The correlation between the 250  $\mu\text{m}$  and optical bands is shown in the lower panel of Fig. 6 for the Control field (upper row) and for the Cirrus field (lower row). We represent each pixel of the image as a dot in the plot with a given transparency.

Article number, page 9 of 23

Este documento incorpora firma electrónica, y es copia auténtica de un documento electrónico archivado por la ULL según la Ley 39/2015.  
 Su autenticidad puede ser contrastada en la siguiente dirección <https://sede.ull.es/validacion/>

Identificador del documento: 2260218 Código de verificación: Sm21pjYh

Firmado por: JAVIER ROMAN GARCIA  
 UNIVERSIDAD DE LA LAGUNA

Fecha: 02/11/2019 16:23:59

IGNACIO TRUJILLO CABRERA  
 UNIVERSIDAD DE LA LAGUNA

02/11/2019 17:39:19

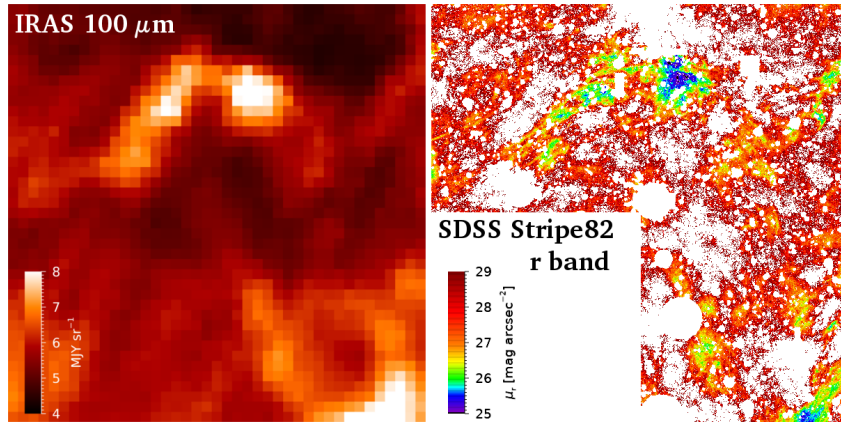


**Fig. 8.** IRAS 100  $\mu\text{m}$  band image (left panel) and  $r$  band image (right panel) of the Field 2 presented in Table 2. Masked areas appear white in the  $r$  band. The field has dimensions of  $1 \times 1$  degrees. The pixel scale is 6 arcseconds in the optical image. A region of this mosaic was used as an example of the image processing in Section 2, Fig. 4.

The detection limits are indicated as dashed lines in red, orange and green, corresponding to the  $1\sigma$ ,  $2\sigma$  and  $3\sigma$  depth limits respectively. We use the values of the 250  $\mu\text{m}$  depth detection limit provided by Viero et al. (2014) corresponding to  $1\sigma = 13 \text{ mJy beam}^{-1}$ . The analysis in the Control Field shows a distribution compatible with Poisson noise in both 250  $\mu\text{m}$  and optical bands, being the fluctuations of such noise consistent with the detection limits of each band. We find no evidence of optical diffuse emission in the Control field by visual inspection of the images, neither in the correlation plot, existing only random fluctuations in the sky background due to the drift scan mode of the observations, and below the detection limits. Conversely, we find a tight correlation between all the optical bands and the far IR emission in the Cirrus field. While for the  $g$ ,  $r$  and  $i$  bands there is a sufficient margin to observe this correlation in a wide range (around  $2.5 - 3 \text{ mag arcsec}^{-2}$ ) of surface brightness above the detection limits, in the  $z$  band the magnitude range of detection is significantly smaller due to the shallower depth of this band. Nevertheless, it is possible to obtain a detection in  $z$  above the  $3\sigma$  limit in areas with surface brightness above  $26 \text{ mag arcsec}^{-2}$ . It is worth noticing the higher signal to noise of the cirri in the optical compared to the far IR. This can be seen by observing that the cirrus emission is further away from the 3 sigma limit in the optical bands (except for the  $z$  band) than for the 250  $\mu\text{m}$  band. It is also remarkable the similar emission in surface brightness of the  $r$ ,  $i$  and  $z$  bands, at least in the brightest regions, being the emission in the  $g$  band  $\sim 0.5 \text{ mag arcsec}^{-2}$  fainter. This would correspond to  $r-i$  and  $i-z$  colors close to 0, while the  $g-r$  color would be considerably redder. We will explore this matter in detail in the next section.

We show in Fig. 7 a visual comparison of the Cirrus field in the far IR unmasked 250  $\mu\text{m}$  band with the processed optical  $r$  band. The morphology of the diffuse emission in both images is remarkably similar, existing a perfect optical counterpart to what is detected in the far IR. As can be noted, the presence of

sky background fluctuations and oversubtraction due to the observational drift scan mode are the main limitation in the recovery of the diffuse emission in the optical dataset. However, these fluctuations and oversubtracted patches are below the detection limits. This analysis is compatible with the idea that any far IR emission by Galactic cirri has a counterpart in the optical. It is worth also emphasizing the extremely low surface brightness of the features detected in this analysis.

The Herschel data allows to explore the optical counterparts of Galactic dust clouds with a relatively high resolution (FWHM = 18 arcseconds). However, the scarce presence of Galactic cirri in the footprint of the HerS-HeLMS-XMM-LSS maps makes the conclusions obtained so far limited to a relatively narrow region, both in Galactic latitude and in terms of IR emission. In order to obtain a more significant sample, we have expanded our analysis to other areas of the Stripe82 region with presence of Galactic cirri. However, the resolution of the available full-sky surveys as the IRAS 100  $\mu\text{m}$  band (FWHM = 5 arcmin) is significantly worse than that of the Herschel SPIRE data, but it can be still used to check the presence of Galactic cirri in the explored areas. We visually compare a set of selected fields (we will describe these fields and the criteria for selecting them in the next section), to which the diffuse emission isolation treatment has been carried out. We find a good match between the optical data and its far IR counterpart within the resolution limits of IRAS, and importantly, we did not detect any optical diffuse emission without a far IR counterpart. We show in Fig. 8 an example field of Galactic cirri emission and its counterpart in the 100  $\mu\text{m}$  IRAS band. This comparison shows something remarkable: the great advantage of deep optical imaging in revealing in a more effective way the morphology of the Galactic dust clouds than the IRAS maps. While the far IR has traditionally been used to detect the presence of interstellar dust, our analysis shows that it is possible to obtain a map of the Galactic dust with higher spatial

Román et al.: Galactic cirri in deep optical imaging

Table 2. Selected fields for the Galactic cirri photometric analysis.

Field #	R.A. (J2000) [deg]	Dec. (J2000) [deg]	l [deg]	b [deg]	Area [deg <sup>2</sup> ]	<g-r> [mag]	<r-i> [mag]	<i-z> [mag]	<S <sub>100μm</sub> > [MJy sr <sup>-1</sup> ]
1	324.0	0.0	54.7	-35.8	2	0.57±0.04	0.12±0.04	0.00±0.11	3.84±0.46
2	333.0	-0.75	60.8	-43.6	0.75	0.60±0.04	0.05±0.04	0.01±0.11	5.02±0.77
3	342.75	0.25	71.4	-50.2	1.75	0.63±0.04	0.13±0.04	0.10±0.11	5.59±0.58
4	344.0	-0.25	72.3	-51.4	2	0.53±0.04	0.12±0.04	0.08±0.11	4.54±0.72
5	2.5	-0.25	100.9	-61.3	3	0.57±0.04	0.06±0.04	0.04±0.11	3.97±0.77
6	326.0	0.25	56.4	-37.4	2.0	0.57±0.04	0.17±0.04	0.11±0.11	4.04±0.49
7	327.0	0.0	56.7	-38.3	2.25	0.63±0.04	0.20±0.04	0.02±0.11	5.82±1.37
8	328.0	0.0	57.5	-39.0	2.5	0.67±0.04	0.20±0.04	0.07±0.11	6.19±1.38
9	329.0	-0.25	58.1	-40.0	1.75	0.59±0.04	0.17±0.04	0.10±0.11	5.89±1.23
10	330.0	-0.75	59.1	-40.7	0.75	0.57±0.04	0.13±0.04	0.08±0.11	5.20±0.58
11	54.95	0.50	185.6	-41.0	1.35	0.61±0.04	0.14±0.04	0.09±0.11	5.41±0.66
12	55.85	0.50	186.3	-40.3	1.35	0.69±0.04	0.15±0.04	-0.10±0.11	5.98±1.30
13	56.75	0.50	187.1	-39.6	1.35	0.73±0.04	0.18±0.04	-0.05±0.11	8.28±1.34
14	57.65	0.50	187.8	-38.9	1.35	0.72±0.04	0.17±0.04	0.01±0.11	9.01±0.98
15	58.55	0.50	188.4	-38.2	1.35	0.83±0.04	0.25±0.04	0.05±0.11	14.02±3.37
16	59.5	-0.75	190.4	-38.1	1.0	0.92±0.04	0.30±0.04	0.01±0.11	15.73±2.30

resolution and higher depth using optical data. In summary, the analysis carried out in this section shows that:

1. The scattered light field removal process and subsequent masking of the optical images is effective in isolating the optical diffuse emission. The IAC Stripe82 Survey ultimate limitation is the sky background fluctuations. Nonetheless, these are below the surface brightness limits of the explored Galactic cirri regions.
2. We find no optical diffuse emission without a far IR counterpart, at least down to 29 mag arcsec<sup>-2</sup>. Consequently, all the diffuse emission present in the optical data can be considered due to the Galactic dust above the surface brightness limit.
3. Deep optical data can be used to detect Galactic cirri as well as far IR data, but having the advantage of a much better resolution.

#### 4. The optical colors of the Galactic cirri

The presence of Galactic cirri creates confusion with structures of extragalactic origin in deep optical observations. Such structures as tidal streams or any stellar diffuse feature appears with a similar morphology to that of the Galactic cirri. It is therefore imperative to explore what is the range in optical colors of the Galactic dust. The aim is to explore any difference between the optical colors of Galactic cirri and extragalactic sources. Assuming that the optical colors of the cirri are due to the light reflected by the surrounding stars, these colors may vary depending on the chemical composition of the dust grains, the dust column density or the average colors of the surrounding stars. In order to explore possible color trends, we selected a number of fields in the Stripe82 region.

Our selection of the fields was carried out using only the optical images through visual exploration. With such strategy, we wanted to avoid any potential bias towards selecting diffuse optical emission with obvious IR counterpart. We selected fields with optical diffuse emission including regions with little or no emission, allowing to measure accurately the 0 flux sky background level. The morphology of the cirri should be unambiguous, avoiding several clouds in the line of sight. In the case of large interesting areas (several square degrees) susceptible to analysis, we split the region into different fields. This is done to provide smaller fields with the aim to explore possible color

trends. The selected fields under these guidelines are listed in Table 2 as fields ranging from # = 1 to 5, and are located in the Stripe82 region between R.A. = [324°, 4°]. Additionally, we selected areas with strong optical diffuse emission in order to draw possible correlations with the dust column density. These fields are more problematic in terms of the photometric analysis due to the difficulty in referencing the sky background level. An additional problem comes from the drift scan observational mode of SDSS. The SDSS reduction pipeline fits a polynomial to the sky emission whose typical length is of the order of several arcmin. Under the presence of any diffuse emission of similar or higher spatial scale, this SDSS algorithm will tend to interpret the diffuse emission as the sky emission itself. This causes a systematic over-subtraction of the data. Nevertheless, the sky fitting algorithm from SDSS performs the same sky subtraction polynomial structure between different bands. Hence, for fields with a high contamination and large extension of diffuse emission, we only consider the colors as reliable but not the absolute value of surface brightness in individual bands. The higher presence of optical diffuse emission is found in two regions. Fields ranging from # = 6 to 10 are located within the R.A. = [326°, 330°] and fields from # = 11 to 16 are located within the R.A. = [54°, 60°]. All the selected fields were processed following the methodology described in Section 2, that includes the removal of the stars, masking, rebinning to 6 arcsec pixel scale and calibration of the sky background level. The final number of selected fields according with these criteria are 16 (including the "Cirrus Field" analyzed in the previous section as Field # = 5). We compared the optical emission of the selected fields with the emission in the 100 μm IRAS band, and we always found an equivalent counterpart within the spatial resolution limits of the IRAS data. As a tracer of the dust column density we use the average emission values of the 100 μm IRAS band, listed for each field in Table 2.

##### 4.1. Methodology for obtaining the optical colors of the cirri

Performing photometry of extended and extremely faint sources is not a straight forward task. First, the use of specialized software to produce segmentation maps in which to perform automatic photometry of astronomical sources is not optimal in this case. Based on the techniques developed previously, we consider that all the flux contained in the images is due to cirri, which will be considered as a single source. To obtain the colors, the inte-

Article number, page 11 of 23

Este documento incorpora firma electrónica, y es copia auténtica de un documento electrónico archivado por la ULL según la Ley 39/2015.  
 Su autenticidad puede ser contrastada en la siguiente dirección <https://sede.ull.es/validacion/>

Identificador del documento: 2260218 Código de verificación: Sm21pjYh

Firmado por: JAVIER ROMAN GARCIA  
 UNIVERSIDAD DE LA LAGUNA

Fecha: 02/11/2019 16:23:59

IGNACIO TRUJILLO CABRERA  
 UNIVERSIDAD DE LA LAGUNA

02/11/2019 17:39:19

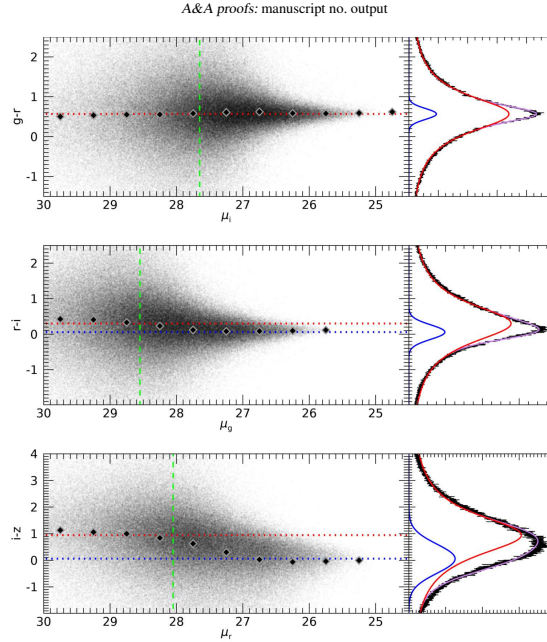


**Fig. 9.** Obtaining the colors of the Cirrus field. Left panels show the color map vs. surface brightness. Each point represents a pixel (6 arcsec). The black diamonds represent the average color in bins of  $0.5 \text{ mag arcsec}^{-2}$ . The green dashed line marks the  $3\sigma$  detection limit of the band in the  $x$ -axis. The blue and red dotted lines mark the center of the Gaussian and Lorentzian fitted functions respectively ( $x_g$  and  $x_L$ ). Right panels correspond to the color distribution histograms. The black line shows the observed color distribution. The purple line shows the Gaussian + Lorentzian fitted function, while the blue and red lines show the Gaussian and Lorentzian functions independently.

gration of the total flux in the images is not possible due to the presence of oversubtraction and sky background fluctuation regions, which would strongly alter the photometry. The effect of the Poisson noise in the images should also be taken into account due to the extremely low surface brightness of the cirri. Having in mind all the previous considerations, we decided to use an approach based on the color distribution of the images.

In the case of the total absence of sources, that is, purely Poisson noise, the color distribution of the pixels of an image is described by a Lorentzian distribution. This Lorentzian distribution is the result of the convolution of the two Gaussian distributions of the noise of each band for the given color (see Appendix A). The Lorentzian distribution is centered approximately on the color corresponding to the Gaussian width difference between both bands. The inclusion of any dust emission will create a distribution added to this Lorentzian distribution. The intrinsic color distribution of the cirri emission is, in principle, unknown. A good approximation is to assume an average constant color with random color variations, and therefore Gaussian. Following this approach, we fit the distribution of the colors of the pixels with a Lorentzian plus a Gaussian function:

$$f(x) \equiv I_L \frac{\frac{1}{2}\Gamma}{(x - x_L)^2 + (\frac{1}{2}\Gamma)^2} + I_g \exp\left(-\frac{(x - x_g)^2}{2\sigma^2}\right)$$

Where  $x$  is the given optical color and  $\{I_L, \Gamma, x_L\}$ ,  $\{I_g, \sigma, x_g\}$  are the intensity, width and center of the Lorentzian and Gaussian functions respectively. Thus, the resulting  $x_g$  parameter of the fit will give the average color value in the analyzed field. Additionally, the Gaussian width ( $\sigma$ ) will account for intrinsic variations of the color of the cirri. For this reason, the colors obtained by this technique must be considered as average colors in the analyzed area. We tested this approach through simulations carried out in the Control Field described in the previous section (with no dust). We injected structures with constant color and similar surface brightness to that of the typical cirri analyzed in this work. These simulations show the great potential in the recovery of the cirri colors by means of this method, and the great precision of the colors recovered. We estimate the following photometric errors by using this methodology:  $\Delta(g-r) = 0.04 \text{ mag}$ ,  $\Delta(r-i) = 0.04 \text{ mag}$  and  $\Delta(i-z) = 0.11 \text{ mag}$ . We describe these simulations and further details of the method in the Appendix C.

Article number, page 12 of 23

Este documento incorpora firma electrónica, y es copia auténtica de un documento electrónico archivado por la ULL según la Ley 39/2015.  
 Su autenticidad puede ser contrastada en la siguiente dirección <https://sede.ull.es/validacion/>

Identificador del documento: 2260218 Código de verificación: Sm21pjYh

Firmado por: JAVIER ROMAN GARCIA  
 UNIVERSIDAD DE LA LAGUNA

Fecha: 02/11/2019 16:23:59

IGNACIO TRUJILLO CABRERA  
 UNIVERSIDAD DE LA LAGUNA

02/11/2019 17:39:19

Román et al.: Galactic cirri in deep optical imaging

In Fig. 9 we show this analysis applied to the Cirrus field (# = 5 in Table 2) described in the previous section. We plot the distribution for the  $g-r$ ,  $r-i$  and  $i-z$  colors in the right panels. Overplotted to the histograms are the fits to the Lorentzian + Gaussian functions (purple color) and the independent Lorentzian (red) and Gaussian (blue) functions as separated distributions. As can be observed, the color distributions are very well fitted with the defined function, with slight deviations in the case of the  $i-z$  color due to the shallower  $z$  band and its higher sky fluctuations. Alternatively, we show in the left panels the color vs. surface brightness distributions, plotting the color of each pixel as a point with a certain transparency. We plot the colors vs. the surface brightness of an independent band, avoiding biases. We represent with diamonds the average color values within bins of  $0.5 \text{ mag arcsec}^{-2}$  in surface brightness. A clear color trend is found from the central value of the Lorentzian function (dashed red line) to the central value of the Gaussian function (dashed blue line) as the signal to noise increases, which is interpreted as the transition from the average Poisson noise color to the underlying average dust color. However, this trend can not be appreciated in the  $g-r$  color as both the Poisson noise and the dust in this field share the same value ( $g-r \sim 0.5 \text{ mag}$ ). The convergence to the cirrus color is not reached immediately after exceeding the  $3\sigma$  threshold in surface brightness of the individual band (green dashed line in Fig. 9) but at brighter surface brightness values. This is expected, as the photometric error for a color is higher than that of an individual band at the same surface brightness. The calculated dust colors in this field are  $g-r = 0.57 \pm 0.04 \text{ mag}$ ,  $r-i = 0.06 \pm 0.04 \text{ mag}$  and  $i-z = 0.04 \pm 0.11 \text{ mag}$ . It should be noted that these colors agree in a general way with the two-dimensional color maps of this cirrus field shown in Appendix D and the trends observed in Fig 6. Finally, using the described method, we calculated the average dust colors of all the selected fields. In Table 2 we summarize the properties of these fields together with the calculated optical colors. The total analyzed area is  $26.5 \text{ square degrees}$ , which correspond roughly to 10% of the whole IAC Stripe82 Legacy Survey area.

#### 4.2. Optical color trends

In this section, we explore color trends of the Galactic Cirri. Using the IRAS  $100 \mu\text{m}$  intensity map, we calculate the average IR emission as a proxy of the dust column density in the selected fields. This average value is calculated taking into account the masked regions of the optical fields. The errors for the average color in the optical, as calculated in Appendix D are  $\Delta(g-r) = 0.04 \text{ mag}$ ,  $\Delta(r-i) = 0.04 \text{ mag}$  and  $\Delta(i-z) = 0.11 \text{ mag}$ . The error for the average value of the  $100 \mu\text{m}$  emission is negligible, due to the large number of pixels in the selected fields:  $\Delta(\langle S_{100\mu\text{m}} \rangle) = \sigma / \sqrt{N} \approx 0$ . We plot in Fig. 10 the correlation between the  $100 \mu\text{m}$  emission and the optical colors of the Galactic cirri. We find a clear correlation between the dust column density as traced by the far IR emission and the optical colors, being this correlation steeper for the bluer optical colors. We do not find any obvious trend between the far IR emission and the  $i-z$  color within the error bars. Additionally, we separate the different fields by coordinates. Fields with right ascension ranging between  $324 \text{ deg}$  to  $2.5 \text{ deg}$  (fields # 1 to 10) are plotted with a blue symbol. Fields with a right ascension ranging between  $54 \text{ deg}$  to  $60 \text{ deg}$  (fields # 11 to 16) are plotted with a red symbol. We do not find any obvious trend in this correlation as a function of the celestial coordinates. As an additional analysis, we plot in Fig. 11 the colors of the cirri vs. their celestial coordinates in right ascension and

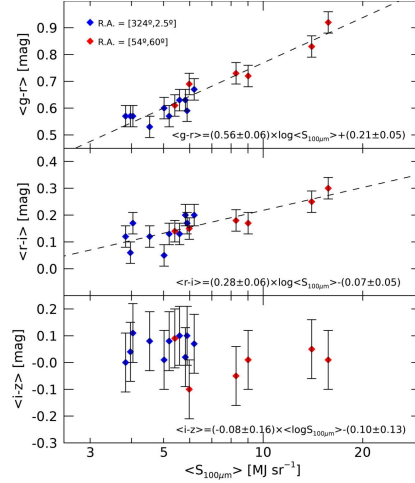


Fig. 10. Correlation between the average optical colors of the cirri and the average far IR emission in the  $100 \mu\text{m}$  IRAS band. The blue and red diamonds represent fields within different right ascension regions as described in the upper left corner. The error bars show the photometric uncertainty for the optical colors. The dashed lines are the best fits as indicated in the bottom equation of each panel.

galactic latitude and longitude. We did not conduct this analysis for the declination coordinates because the Stripe82 region is located between the declination of  $-2.5 \text{ deg}$  to  $2.5 \text{ deg}$ . For comparison, we also plot the average  $100 \mu\text{m}$  emission. We do not find any trend between the cirri colors and the celestial coordinates within the explored regions, being the color variations of the cirri equivalent to the emission in the  $100 \mu\text{m}$  IRAS band.

#### 4.3. Dust vs. extragalactic features colors

The goal of this work is to explore whether we can use the optical colors of the cirri to discern them from extragalactic sources. We address this issue in Fig. 12. We plot the cirri colors obtained in the previous analyzes. We also overplot E-MILES single stellar population models (Vazdekis et al. 2016) for different metallicities and different ages. We also include the colors of real extragalactic sources in the images. For this we use the dust-free Control field discussed in Section 3 and we select the colors of pixels belonging to galaxies (steliarity parameter less than 0.2) in the original images at pixel scale of  $0.396 \text{ arcseconds}$ . This is shown as contour regions in the color-color maps. We plot the  $1$  and  $2\sigma$  density contours. Note that the average colors of real extragalactic sources differ slightly from that of single stellar population models due to the different redshifts of the sources. Additionally, a relatively high dispersion is found due to the presence of multiple stellar populations in real galaxies, the direct photometry of  $0.396 \text{ arcsec}$  pixels (the cirri colors are obtained averaging its emission in large regions) and the redshift scatter.

Article number, page 13 of 23

Este documento incorpora firma electrónica, y es copia auténtica de un documento electrónico archivado por la ULL según la Ley 39/2015.  
 Su autenticidad puede ser contrastada en la siguiente dirección <https://sede.ull.es/validacion/>

Identificador del documento: 2260218

Código de verificación: Sm21pjYh

Firmado por: JAVIER ROMAN GARCIA  
 UNIVERSIDAD DE LA LAGUNA

Fecha: 02/11/2019 16:23:59

IGNACIO TRUJILLO CABRERA  
 UNIVERSIDAD DE LA LAGUNA

02/11/2019 17:39:19

A&A proofs: manuscript no. output

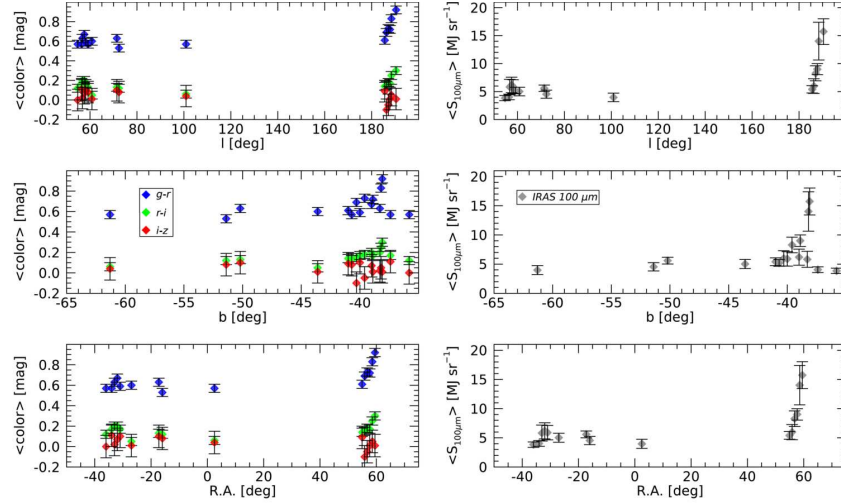


Fig. 11. Left panel: Optical colors of the cirri as a function of the location in the sky. Right panel: Same as in the left panel but showing the emission in the IRAS 100  $\mu\text{m}$  band as comparison.

While for the  $g-r$  vs  $i-z$  and  $r-i$  vs  $i-z$  maps the colors of the cirri overlap with the colors of the single stellar population models, for the  $g-r$  vs  $r-i$  the colors of the cirri are well differentiated from the colors of single stellar population models and also real extragalactic sources. It is worth mentioning the shallower depth of the  $z$ -band in relation to the other bands. This translates into the considerably greater uncertainty of the  $i-z$  color. To sum up, the  $g-r$  vs  $r-i$  map appears as an interesting tool to break a potential confusion between Galactic dust and extragalactic sources.

### 5. Conclusions and discussion

We have carried out a comprehensive study of the Galactic cirri within the Stripe82 region using data from the IAC Stripe82 Legacy Survey (Fliri & Trujillo 2016). We show that by means of a precise characterization of the PSF and techniques applied to deep optical data it is possible to study the optical diffuse emission of the interstellar dust, allowing a characterization of its optical colors. Both the subtraction of the scattered light from the stars and a correct masking of all the sources is a requirement for a correct analysis of the dust clouds. We analyzed a total area of 26.5 square degrees, finding a good match between the detected optical diffuse emission and the emission of the dust cold component as traced by the far IR bands of Herschel and IRAS.

The techniques developed in this work allow to accurately measure the average colors of the Galactic cirri in areas of few square degrees. We found a strong correlation between the average optical colors and the 100  $\mu\text{m}$  band average emission. This correlation is steeper for the  $g-r$  color than for the  $r-i$  color and inconclusive for the  $i-z$  color. The correlation between the cirri optical colors and the dust column density is a remarkable result

that has not been identified previously (see a summary of previous works by Ienaka et al. 2013, Table 3). The previous lack of detection of these correlations could be related with the presence of the scattered light by the stars. This source of contamination has been carefully subtracted in this work. However, as previously discussed, regions with high dust contamination are susceptible to larger uncertainties. We argue that it is difficult to understand this correlation as an artifact due to the uncertainties produced in highly contaminated regions by dust, existing several arguments that indicate that this reddening in optical wavelengths of the Galactic dust, as the column density increases, is real. First, the effects of over-subtraction in regions with a strong presence of diffuse emission should affect all bands similarly, so the colors should remain unaffected. Further, the spectrum of the diffuse Galactic light provided by Brandt & Draine (2012) matches our findings. This spectrum was calculated by averaging SDSS sky spectra in areas with  $S_{100\mu\text{m}} > 10 \text{ MJy sr}^{-1}$ . When convolving this spectrum with the SDSS filter response, we obtain the following colors:  $g-r = 0.84 \text{ mag}$  and  $r-i = 0.34 \text{ mag}$ , hence compatible with our findings (see Fig. 10). Assuming that the Galactic cirri colors in areas where the dust filaments are reliable, hence areas with a soft presence of dust and bluer, the trend towards red colors would be real. Given the fact that we are obtaining dust colors by averaging relatively large areas on the sky, the numerical parameters of the fitting for the correlation obtained in Fig. 10 should only be taken as an indication of its existence. Future deeper works and a better sky background reliability will provide these correlations at a smaller spatial resolution scale.

The explanation of the mechanisms capable of producing such reddening of the observed cirri colors as the dust column

Article number, page 14 of 23

Este documento incorpora firma electrónica, y es copia auténtica de un documento electrónico archivado por la ULL según la Ley 39/2015.  
 Su autenticidad puede ser contrastada en la siguiente dirección <https://sede.ull.es/validacion/>

Identificador del documento: 2260218 Código de verificación: Sm21pjYh

Firmado por: JAVIER ROMAN GARCIA  
 UNIVERSIDAD DE LA LAGUNA

Fecha: 02/11/2019 16:23:59

IGNACIO TRUJILLO CABRERA  
 UNIVERSIDAD DE LA LAGUNA

02/11/2019 17:39:19

Román et al.: Galactic cirri in deep optical imaging

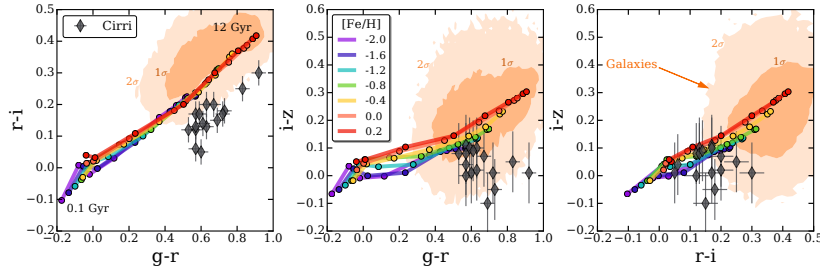


**Fig. 12.** Different color-color diagrams. Black/grey diamonds correspond to the cirri colors with their corresponding error bars. Overplotted are single stellar population models color-coded for different metallicities at each of the following ages: 0.1, 0.2, 0.5, 1, 2, 5, 10 and 12 Gyr. We also plot the color values of the pixels of real galaxies (see text). The light orange region encloses 95% ( $2\sigma$ ) of the pixels, while the dark orange encloses 68% ( $1\sigma$ ).

density increases is outside the scope of this work. Future works will be necessary to produce a theoretical framework capable of explaining these circumstances. Nevertheless, it might seem that it could be related with processes of self-extinction and scatter in the line of sight. A naive scenario is that the optical light from a given dust cloud must also suffer from extinction in case there is additional dust contamination between that cloud and us. Therefore in areas with a higher dust column density, the colors should also become redder. In fact, taking for example the extinction values of the field with a higher presence of dust analyzed in this work (Field # = 16), results in a reddening corresponding to  $A^c(g-r) = 0.43$  mag,  $A^c(r-i) = 0.25$  mag and  $A^c(i-z) = 0.18$  mag (Schlafly & Finkbeiner 2011). These values are of the same order but slightly higher than the difference in color between this field and the less contaminated fields analyzed in this work, as expected in this scenario. Additionally, the blue colors of the cirri found by Mihos et al. (2017) in the Virgo Cluster (where the dust contamination by cirri is moderate) and the redder colors found by Watkins et al. (2016) in a conspicuous and dense cloud nearby the M64 galaxy (where the dust contamination by cirri is severe) are in general terms, compatible with this scenario.

We show in Fig. 13 a field of great interest for this discussion. First, this field contains a conspicuous cloud with a high far IR emission (high column density) adjacent to a fairly clean area in which the sky can be referenced accurately. Taking into account that the colors of the cirri in this area are compatible with the correlation shown previously ( $S_{100\mu m} = 14.1$  MJy  $sr^{-1}$ ,  $g-r = 0.75$ ,  $r-i = 0.23$ ,  $i-z = 0.01$ ), it suggests the reliability of the colors obtained in other highly contaminated regions without a 0 flux sky reference. Additionally, we find a very peculiar circumstance in this field, and it is the presence of what looks like a star very close to the dust screen, illuminating it directly. This low-brightness nebulosity was previously cataloged as a low-surface-brightness galaxy by Impey et al. (1996) as the 0351-0019 galaxy, however, in our deeper data, it seems to be a reflection by the adjacent star. To obtain the colors of the light reflected by the star on the dust screen, we subtract the star using the PSF in a similar way to that described in previous sections. Additionally, this allows us to obtain the photometry of the star, which, being saturated, it is the only way to obtain it. The resulting colors of the star are  $g-r = 0.51$ ,  $r-i = 0.21$ ,  $i-z = 0.20$ . To obtain the color of the nebulosity we selected a small region,

avoiding the area where the internal reflection of the star is located which could affect the obtained colors. Due to the small angular size of this region we work with the original pixel scale of 0.396 arcsec. With this resolution, the signal to noise of the  $z$  band is low, therefore we discard this band. The resulting colors are  $g-r \approx 0.25$  and  $r-i \approx 0.10$ . The fact that the nebulosity has colors considerably bluer than the adjacent star suggests an albedo of the dust that causes a bluing of the reflected light. Additionally, the observed red dust colors in the surrounding field and the observed blue colors of the dust directly illuminated by the star supports the scenario of self extinction, in which the light directly reflected (without going through dust) is observed bluer and the light going through dense dust is absorbed/reflected more strongly in the blue bands, and therefore, observed redder. The scenario depicted here would be a simple and feasible explanation to the extended red emission found in some dense cirri regions (e.g. Witt et al. 2008).

It is also worth briefly discussing the potential of different optical surveys in the study of Galactic dust. In this work we have used data from the IAC Stripe82 Legacy Survey to study wide regions with presence of dust. The imminent arrival of the LSST could be extremely useful in the study of the photometric properties of the Galactic dust. The presence of six photometric bands ( $u, g, r, i, z$  and  $y$ ), the great depth of the final coadded data and the large explored area (30,000 square degrees of sky) are excellent characteristics for the detection of Galactic dust. However, an excellent reduction of the data preserving the lower surface brightness sources, and an exquisite characterization of the PSF at large radius allowing the modeling and subtraction of the scattered field by stars, will also be requirements. Assuming that the final data product meet the quality requirements for a correct study of the optical diffuse emission, it could be possible to conduct a systematic study of the Galactic dust using this superb optical dataset. The main advantage with respect to surveys in the far IR will be the much better spatial resolution and depth. This would allow to trace the dust and create extinction maps with an unprecedented quality. Note that the use of other wavelengths for the detection of dust with a higher resolution have already been proposed, for example by Boissier et al. (2015) using data in the UV, which could be complementary to the optical data of the LSST.

Article number, page 15 of 23

Este documento incorpora firma electrónica, y es copia auténtica de un documento electrónico archivado por la ULL según la Ley 39/2015.  
 Su autenticidad puede ser contrastada en la siguiente dirección <https://sede.ull.es/validacion/>

Identificador del documento: 2260218

Código de verificación: Sm21pjYh

Firmado por: JAVIER ROMAN GARCIA  
 UNIVERSIDAD DE LA LAGUNA

Fecha: 02/11/2019 16:23:59

IGNACIO TRUJILLO CABRERA  
 UNIVERSIDAD DE LA LAGUNA

02/11/2019 17:39:19

A&A proofs: manuscript no. output

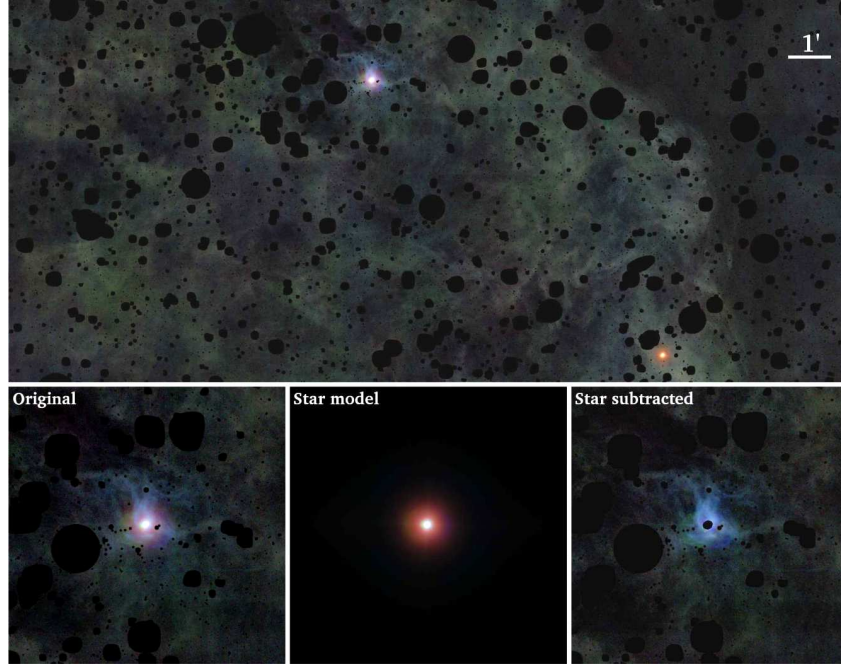


**Fig. 13.** Composite color image using  $g$   $r$  and  $i$  SDSS bands of the region  $RA = [58.158.8]$ ,  $Dec = [-0.4, -0.1]$  at a pixel scale of 0.396 arcsec. All the sources have been masked / subtracted except the star that appears directly illuminating the dust screen and a random star in the bottom right side illustrating the appearance of all the stars without this fact. In the lower panels a zoom of  $6.5 \times 6.5$  arcmin of the area of interest is shown with the result of the subtraction of the star, showing more clearly the reflected area.

**Acknowledgements.** The authors of this paper acknowledges support from grant AYA2016-77237-C3-1-P from the Spanish Ministry of Economy and Competitiveness (MINECO). We thank Timothy Brandt for sharing the spectrum of the diffuse galactic light with us. We thank Jorge Sánchez Almeida and David Valls-Gabaud for interesting discussions about the results. We thank Aaron Watkins for complementary analysis about the galactic dust colors and Juergen Fliri for his excellent work on the construction of the IAC Stripe82 Legacy Survey. We thank Lee Kelvin for sharing his code to compute beautiful color composed images. We also thank the participants of the workshop “Exploring the Ultra-Low Surface Brightness Universe” hosted in the ISSI headquarters, Bern, Switzerland on January 2017. Bern, Switzerland in which preliminary result were shown. JR thanks MINECO for financing his PhD through FPI grant. I.T. acknowledges financial support from the European Union’s Horizon 2020 research and innovation programme under Marie Skłodowska-Curie grant agreement No 721463 to the SUNDIAL ITN network. This research has been partly supported by the Spanish Ministry of Economy and Competitiveness (MINECO) under grants AYA2016-77237-C3-1-P.

#### References

Abraham, R. G., & van Dokkum, P. G. 2014, *PASP*, 126, 55  
 Abadi, M. G., Navarro, J. F., & Steinmetz, M. 2006, *MNRAS*, 365, 747  
 Abazajian, K. N., Adelman-McCarthy, J. K., Agüeros, M. A., et al. 2009, *ApJS*, 182, 543-558

Aihara, H., Arimoto, N., Armstrong, R., et al. 2018, *PASJ*, 70, S4  
 Akhlaghi, M., & Ichikawa, T. 2015, *ApJS*, 220, 1  
 Barrena, R., Streblyanska, A., Ferragamo, A., et al. 2018, *A&A*, 616, A42.  
 Bertin, E., & Arnouts, S. 1996, *A&AS*, 117, 393  
 Bertin, E., Mellier, Y., Radovich, M., et al. 2002, *Astronomical Data Analysis Software and Systems XI*, 281, 228  
 Bertin, E. 2011, *Astronomical Data Analysis Software and Systems XX*, 442, 435  
 Besta, G., Martínez-Delgado, D., van der Marel, R. P., et al. 2016, *ApJ*, 825, 20  
 Bilek, M., Cuillandre, J.-C., Gwyn, S., et al. 2016, *A&A*, 588, A77  
 Blanton, M. R., Lupton, R. H., Schlegel, D. J., et al. 2005, *ApJ*, 631, 208  
 Boissier, S., Boselli, A., Voyer, E., et al. 2015, *A&A*, 579, A29  
 Borlaff, A., Trujillo, I., Román, J., et al. 2019, *A&A*, 621, A133.  
 Brandt, T. D., & Draine, B. T. 2012, *ApJ*, 744, 129  
 Bullock, J. S., & Johnston, K. V. 2005, *ApJ*, 635, 931  
 Chiboucas, K., Karachentsev, I. D., & Tully, R. B. 2009, *AJ*, 137, 3009  
 Chiboucas, K., Jacobs, B. A., Tully, R. B., & Karachentsev, I. D. 2013, *AJ*, 146, 126  
 Cooper, A. P., Cole, S., Frenk, C. S., et al. 2010, *MNRAS*, 406, 744  
 Cooper, A. P., Gao, L., Guo, Q., et al. 2015, *MNRAS*, 451, 2703  
 Cortese, L., Bendo, G. J., Isaak, K. G., Davies, J. I., & Kent, B. R. 2010, *MNRAS*, 403, L26  
 Dalecanton, J. J., Spergel, D. N., Gunn, J. E., Schmidt, M., & Schneider, D. P. 1997, *AJ*, 114, 635  
 Dark Energy Survey Collaboration, Abbott, T., Abdalla, F. B., et al. 2016, *MNRAS*, 460, 1270

Article number, page 16 of 23

Este documento incorpora firma electrónica, y es copia auténtica de un documento electrónico archivado por la ULL según la Ley 39/2015.  
 Su autenticidad puede ser contrastada en la siguiente dirección <https://sede.ull.es/validacion/>

Identificador del documento: 2260218 Código de verificación: Sm21pYh

Firmado por: JAVIER ROMAN GARCIA  
 UNIVERSIDAD DE LA LAGUNA

Fecha: 02/11/2019 16:23:59

IGNACIO TRUJILLO CABRERA  
 UNIVERSIDAD DE LA LAGUNA

02/11/2019 17:39:19

Román et al.: Galactic cirri in deep optical imaging

- Das, S., Louis, T., Nolta, M. R., et al. 2014, *J. Cosmology Astropart. Phys.*, 4, 014
- Duc, P.-A., Cuillandre, J.-C., & Renaud, F. 2018, *MNRAS*, 475, L40.
- de Jong, R. S. 2008, *MNRAS*, 388, 1521
- de Vries, C. P., & Le Poole, R. S. 1985, *A&A*, 145, L7
- DeVore, J. G., Kristl, J. A., & Rappaport, S. A. 2013, *Journal of Geophysical Research (Atmospheres)*, 118, 5679
- Davies, J. L., Wilson, C. D., Auld, R., et al. 2010, *MNRAS*, 409, 102
- Duc, P.-A., Cuillandre, J.-C., Karabal, E., et al. 2015, *MNRAS*, 446, 120
- Elvey, C. T., & Roach, F. E. 1937, *ApJ*, 85, 213
- Erwin, P. 2015, *ApJ*, 799, 226
- Ferrarese, L., Côté, P., Cuillandre, J.-C., et al. 2012, *ApJS*, 200, 4
- Fliri, J., & Trujillo, I. 2016, *MNRAS*, 456, 1359
- Giallongo, E., Menci, N., Grazian, A., et al. 2014, *ApJ*, 781, 24
- Guhathakurta, P., & Tyson, J. A. 1989, *ApJ*, 346, 773
- Henvey, L. G., & Greenstein, J. L. 1941, *ApJ*, 93, 70
- Hodges-Klucik, E., & Bregman, J. N. 2014, *ApJ*, 789, 131
- Ibata, R., Mouhcine, M., & Rejkuba, M. 2009, *MNRAS*, 395, 126
- Ibata, R. A., Lewis, G. F., McConnachie, A. W., et al. 2014, *ApJ*, 780, 128
- Ienaka, N., Kawara, K., Matsuoka, Y., et al. 2013, *ApJ*, 767, 80
- Impey, C., Bothun, G., & Malin, D. 1988, *ApJ*, 330, 634
- Impey, C. D., Sprayberry, D., Irwin, M. J., & Bothun, G. D. 1996, *ApJS*, 105, 209
- Infante-Saiz, R., Trujillo I., Román J., 2019, in preparation.
- Javanmardi, B., Martínez-Delgado, D., Kroupa, P., et al. 2016, *A&A*, 588, A89
- Johnston, K. V., Bullock, J. S., Sharma, S., et al. 2008, *ApJ*, 689, 936-957
- Karabal, E., Duc, P.-A., Kuntschner, H., et al. 2017, *A&A*, 601, A86
- Klypin, A., Kravtsov, A. V., Valenzuela, O., & Prada, F. 1999, *ApJ*, 522, 82
- Lamarre, J. M., Puget, J. L., Bouchet, F., et al. 2003, *New A Rev.*, 47, 1017
- Laureijs, R. J., Maittala, K., & Schuur, G. 1987, *A&A*, 184, 269
- Levenson, L., Marsden, G., Zernov, M., et al. 2010, *MNRAS*, 409, 83
- Low, F. J., Young, E., Beintema, D. A., et al. 1984, *ApJ*, 278, L19
- Lu, T., Luo, W., Zhang, J., et al. 2018, *AJ*, 156, 14.
- LSST Science Collaboration, Abell, P. A., Allison, J., et al. 2009, arXiv:0912.0201
- Martin, N. F., Ibata, R. A., Rich, R. M., et al. 2014, *ApJ*, 787, 19
- Martínez-Delgado, D., Gabany, R. J., Crawford, K., et al. 2010, *AJ*, 140, 962
- Mattila, K. 1979, *A&A*, 78, 253
- McConnachie, A. W., Irwin, M. J., Ibata, R. A., et al. 2009, *Nature*, 461, 66
- McConnachie, A. W. 2012, *AJ*, 144, 4
- McConnachie, A. W., Ibata, R., Martin, N., et al. 2018, *ApJ*, 868, 55
- Mihos, J. C., Harding, P., Feldmeier, J., & Morrison, H. 2005, *ApJ*, 631, L41
- Mihos, J. C., Durrell, P. R., Ferrarese, L., et al. 2015, *ApJ*, 809, L21
- Mihos, J. C., Harding, P., Feldmeier, J. J., et al. 2017, *ApJ*, 834, 16
- Mihos, J. C., Carr, C. T., Watkins, A. E., Oosterloo, T., & Harding, P. 2018, *ApJ*, 863, L7
- Miville-Deschênes, M.-A., & Lagache, G. 2005, *ApJS*, 157, 302
- Monet, D. G., Levine, S. E., Canzian, B., et al. 2003, *AJ*, 125, 984
- Montes, M., & Trujillo, I. 2018, *MNRAS*, 474, 917
- Moore, B., Ghigna, S., Governato, F., et al. 1999, *ApJ*, 524, L19
- Muslimov, E., Valls-Gabaud, D., Lemaitre, G., et al. 2017, *ApJ*, 834, 56
- Pilbratt, G. L., Riedinger, J. R., Passvogel, T., et al. 2010, *A&A*, 518, L1
- Planck Collaboration, Ade, P. A. R., Aghanim, N., et al. 2011, *A&A*, 536, A19
- Peacock, M. B., Strader, J., Romanowsky, A. J., & Brodie, J. P. 2015, *ApJ*, 800, 13
- Ramírez-Moreta, P., Verdes-Montenegro, L., Blasco-Herrera, J., et al. 2018, *A&A*, 619, A163
- Román, J., & Trujillo, I. 2018, *Research Notes of the American Astronomical Society*, 2, 144
- Rudick, C. S., Mihos, J. C., Harding, P., et al. 2010, *ApJ*, 720, 569
- Sandage, A. 1976, *AJ*, 81, 954
- Sandage, A., & Binggeli, B. 1984, *AJ*, 89, 919
- Sandin, C. 2014, *A&A*, 567, A97
- Schlafly, E. F., & Finkbeiner, D. P. 2011, *ApJ*, 737, 103
- Slater, C. T., Harding, P., & Mihos, J. C. 2009, *PASP*, 121, 1267
- Sollima, A., Gil de Paz, A., Martínez-Delgado, D., et al. 2010, *A&A*, 516, A83
- Tanaka, M., Chiba, M., Komiyama, Y., Guhathakurta, P., & Kalirai, J. S. 2011, *ApJ*, 738, 150
- Thacker, C., Cooray, A., Smidt, J., et al. 2013, *ApJ*, 768, 58
- Trujillo, I., & Fliri, J. 2016, *ApJ*, 823, 123
- Uson, J. M., Boughe, S. P., & Kuhn, J. R. 1991, *ApJ*, 369, 46
- Valls-Gabaud, D., & MESSIER Collaboration 2017, *Formation and Evolution of Galaxy Outskirts*, 321, 199
- Vazdekis, A., Koleva, M., Ricciardelli, E., Röck, B., & Falcón-Barroso, J. 2016, *MNRAS*, 463, 3409
- Veneziani, M., Ade, P. A. R., Bock, J. J., et al. 2010, *ApJ*, 713, 959
- Viero, M. P., Wang, L., Zernov, M., et al. 2013, *ApJ*, 772, 77
- Viero, M. P., Asboth, V., Roseboom, I. G., et al. 2014, *ApJS*, 210, 22
- Watkins, A. E., Mihos, J. C., Harding, P., et al. 2014, *ApJ*, 791, 38.
- Watkins, A. E., Mihos, J. C., & Harding, P. 2015, *ApJ*, 800, L3.
- Watkins, A. E., Mihos, J. C., & Harding, P. 2016, *ApJ*, 826, 59
- Watkins, A. E., Mihos, J. C., & Harding, P. 2017, *ApJ*, 851, 51.
- Watkins, A. E., Mihos, J. C., Bershad, M., et al. 2018, *ApJ*, 858, L16.
- Willman, B. 2010, *Advances in Astronomy*, 2010, 285454
- Witt, A. N., Friedmann, B. C., & Sasseen, T. P. 1997, *ApJ*, 481, 809
- Witt, A. N., Mandel, S., Sell, P. H., Dixon, T., & Vijh, U. P. 2008, *ApJ*, 679, 497
- Zackrisson, E., de Jong, R. S., & Micheva, G. 2012, *MNRAS*, 421, 190

Article number, page 17 of 23

Este documento incorpora firma electrónica, y es copia auténtica de un documento electrónico archivado por la ULL según la Ley 39/2015.

Su autenticidad puede ser contrastada en la siguiente dirección <https://sede.ull.es/validacion/>

Identificador del documento: 2260218

Código de verificación: Sm21pjYh

Firmado por: JAVIER ROMAN GARCIA  
UNIVERSIDAD DE LA LAGUNA

Fecha: 02/11/2019 16:23:59

IGNACIO TRUJILLO CABRERA  
UNIVERSIDAD DE LA LAGUNA

02/11/2019 17:39:19

A&A proofs: manuscript no. output

#### Appendix A: Surface brightness limits of the data

We describe the process for obtaining the surface brightness limits of the data. In Fig. A.1 it is shown the histogram of counts of a masked image of the IAC Stripe 82 Legacy Survey for all the  $u$ ,  $g$ ,  $r$ ,  $i$  and  $z$  bands. As can be seen, the distributions follow an almost perfect gaussian shape as all the non masked pixels are dominated by the Poisson noise of the data. This Poisson noise is what limits the depth of the data. Fitting a gaussian function we obtain the standard deviation ( $\sigma$ ) of that Poisson noise. Therefore, the surface brightness limit at the  $3\sigma$  level in pixel to pixel variation can be defined as:

$$\mu_{lim}(3\sigma; pix \times pix) = -2.5 \times \log\left(\frac{3\sigma}{pix^2}\right) + Z_p$$

where  $pix$  is the pixel size in arcseconds and  $Z_p$  is the zero point of the data. This definition can be considered the detection threshold in surface brightness at  $3\sigma$  for a source with an angular size equivalent to that pixel size. However, the typical size of celestial sources is considerably larger. For this reason, the limiting surface brightness at the original pixel scale is not representative of the real detection threshold for extended sources. In addition, each particular survey has its own pixel scale, so this value is not comparable among different surveys or datasets. To obtain the surface brightness limit at any given angular scale, the above histograms of counts have to be obtained at the required angular scale. It could be done by rebinning the image and obtaining the standard deviation of this new distribution. However, the residuals of the masking process after the rebinning and the substantial reduction in the number of spatial elements make this option problematic, specially in images with high contamination or small area. Consequently, the practical way to obtain the surface brightness limit at a given angular scale is assuming that the flux follows a normal distribution. Then, the gaussian standard deviation will scale as:

$$\sigma(\Omega) = \sigma \sqrt{\frac{pix^2}{\Omega^2}}$$

where  $\Omega$  is the desired angular pixel scale of the new definition. With this, we can define the surface brightness limit for any angular scale as:

$$\mu_{lim}(3\sigma; \Omega \times \Omega) = -2.5 \times \log\left(\frac{3\sigma}{pix \times \Omega}\right) + Z_p$$

Traditionally, has been used an angular scale of  $10 \times 10$  arcseconds boxes as representative of the typical extended source. Using this definition, we obtain for the data used in this work:  $\mu(3\sigma; 10'' \times 10'') = 28.0, 29.1, 28.6, 28.2$  and  $26.6$  mag arcsec<sup>-2</sup> for the ( $u, g, r, i, z$ ) bands respectively. It is worth noting that the limiting depth is strongly dependent on the angular size or criteria to define it. For instance, the previous values in  $\mu_{lim}(3\sigma; 10'' \times 10'')$  would transform as  $\mu_{lim}(1\sigma; 10'' \times 10'') = 29.2, 30.3, 29.8, 29.4$  and  $27.8$  mag arcsec<sup>-2</sup> or  $\mu_{lim}(1\sigma; 60'' \times 60'') = 31.1, 32.3, 31.7, 31.3$  and  $29.8$  mag arcsec<sup>-2</sup> for the ( $u, g, r, i, z$ ) bands respectively.

#### Appendix B: PSF characterization

The quality of the modeling of the scattered light produced by the stars relies on the accuracy achieved in the characterization of the PSF and the subsequent accuracy at fitting this PSF model to the stars. Bearing this in mind, we have made

Article number, page 18 of 23

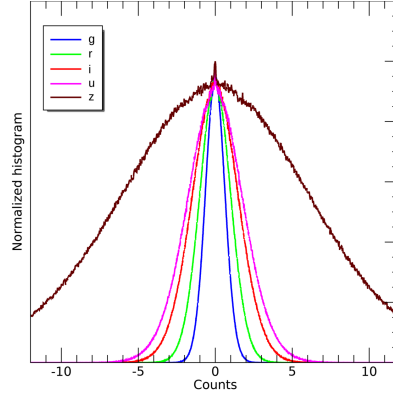


Fig. A.1. Distributions of counts for a  $0.5 \times 0.5$  degrees masked image at the original pixel size of  $0.396$  arcsec in the five SDSS bands. The histograms in each band follow a normal distribution with a gaussian shape. All bands own a similar zero point ( $Z_p$ ) of  $28.3291$  mag, as provided by the IAC Stripe 82 survey. Note the shallower  $z$  band evidenced by a wider distribution.

a characterization of the PSF taking into account possible adverse effects that can penalize a correct PSF model. The commonly used techniques, such as specific dedicated observation of a very bright star, can introduce systematic effects as it is based in unique observational conditions. This would translate in a different FWHM in the core of the PSF, and even fluctuations of the PSF wings at large radii (DeVore et al. 2013). Additionally, this kind of "external" characterization of the PSF is not feasible to perform in data from multiple coadded surveys. The reason is that the images of the survey are the coadd of several multi-epoch single exposures, so the PSF of a single exposure could be different of the PSF in the coadded survey. Consequently, a good alternative for obtaining a high quality and realistic PSF is to use the stars on the science images themselves.

In this section, we describe the process for obtaining the PSF model used in this work. This is done by stacking of masked stars which average will be considered the PSF model of the data. For the procedure described here we use data from the IAC Stripe 82 Legacy Survey, therefore, the PSF models produced here will be those of this survey. Nevertheless, this procedure is general and can be used for any dataset of similar characteristics.

#### Appendix B.1: PSF wings

Our aim is to obtain PSFs to explore the behavior of the scattered light at large distances from the source. In the present work, we have explored PSFs up to a radial distance of  $720$  arcseconds ( $12$  arcmin). Such large PSF radius imply that we will be able to characterize and remove the scattered light down to extremely faint surface brightness. In order to maximize the reliability of the PSFs, specially at large radius, we selected stars in a region with low contamination by Galactic cirri. The selected area is the Stripe82 region within the Hers82 survey (avoiding the cirri

Este documento incorpora firma electrónica, y es copia auténtica de un documento electrónico archivado por la ULL según la Ley 39/2015.  
 Su autenticidad puede ser contrastada en la siguiente dirección <https://sede.ull.es/validacion/>

Identificador del documento: 2260218

Código de verificación: Sm21pjYh

Firmado por: JAVIER ROMAN GARCIA  
 UNIVERSIDAD DE LA LAGUNA

Fecha: 02/11/2019 16:23:59

IGNACIO TRUJILLO CABRERA  
 UNIVERSIDAD DE LA LAGUNA

02/11/2019 17:39:19

Román et al.: Galactic cirri in deep optical imaging

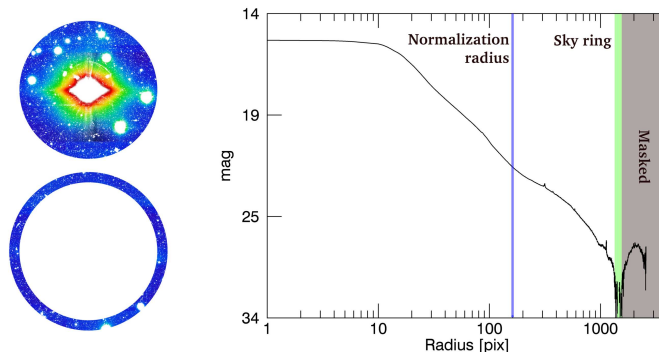


**Fig. B.1.** Schematic representation of the correction process in the case of oversubtraction around very bright stars. Left: images of an example star, showing the region of the star in an oversubtracted area (upper image) and the sky ring used to calibrate the sky that will be added to the star image (lower image). Right: Profile of the star showing the different regions.

clouds discussed in Section 3). Due to the precision required, accurate centering of the stars is necessary. The coordinates of bright saturated stars, provided by either SDSS or creating a catalog running SExtractor (Bertin & Arnouts 1996) do not have the desired precision. We use as coordinates those of the USNO-B catalog of stars (Monet et al. 2003) and we select stars that have null error in the coordinates according to the USNO-B catalogue at J2000 epoch. Stars matching this criteria in the selected area are many ( $\approx 1200$  stars with  $R < 12$  mag). However, stars with ( $R < 5$  mag) are few. It forces us to make the stacking of a large number of stars on a wide range of luminosity. The main problem of combining stars with different fluxes is normalization, so each normalized star shares a common flux or profile allowing for the stacking. The use of aperture photometry for the normalization of the individual stars is ruled out. The stars in this magnitude range are saturated in SDSS images, so the flux obtained by using a fixed aperture is not reliable. For this reason we make use of the profile of each star to perform the normalization. This precise measurement of the star fluxes would give us a better accuracy in the stacking process, crucial for a high quality PSF.

We proceed as follows. For each star of our pre-selected catalogue, we create a stamp for each band with an odd number of pixels<sup>3</sup> of 720 arcsec using the software SWarp (Bertin et al. 2002) centered in the coordinates of the star according to the USNO-B catalogue. We mask all external sources based on the detection map from SExtractor using the *r-deep* band (combination of *g*, *r* and *i* bands). Then we perform a visual inspection to discard unreliable stars. Circumstances for discarding a star are the presence of adjacent sources of similar luminosity, saturated rows and columns or any kind of artifact. Extremely bright stars are especially problematic, in fact, all stars with  $R < 5$  mag were discarded. A common problem in SDSS images is the presence of ghosts in fields adjacent to bright stars. Hence, we perform a manual masking of the ghosts for each star. From a pre-selection of 535 stars, we ended up with 399 stars in the

<sup>3</sup> We use an odd number of pixels to create the PSF in order to have a central reference pixel in the 2-D final image

magnitude range  $5.35 < R < 10.55$ , with 90% of the stars having  $R < 8$  mag and 75%  $R < 9$  mag. Then, we compute the profiles for all the stars. Another problem to handle is the oversubtraction of light around bright stars. To minimize this issue, we developed an automatic routine in which any possible oversubtraction is corrected/softened. This is made by detecting changes in the slope that could be indicative of oversubtraction. If oversubtraction is detected, we measure the sky value in a ring located farthest from the star in the the oversubtracted region and we add this value back to the whole stamp. The region of the star with radius larger than the selected oversubtracted area is masked (see Fig. B.1 for a visual example). Then, the whole 2-D image is normalized by a multiplicative factor obtained from the flux of the star in the profile within the segment between 40 and 60 arcseconds, so each normalized star has the same flux in this region. We choose this segment to avoid the central internal reflection of the star, located within the inner 40 arcseconds. We use a maximum radius of 60 arcseconds to avoid going too far in radius so the signal to noise ratio for the faintest selected stars in this region is reliable. Once all the stars are normalized in flux we proceed with the stacking. We obtain the combined PSF averaging the 2-D images of the stars, computing the mean of each pixel with an iterative rejection based on a gaussian distribution. We reject pixel values beyond the  $2\sigma$  value. Additionally, for the low signal regions (radius greater than  $\approx 300$  arcseconds for the *g*, *r* and *i* bands and radius larger than  $\approx 100$  arcseconds for the *u* and *z* bands) we forced a minimum rejection of the 15% of the maximum and 15% of the minimum pixel values. As all the stacked stars, the core region of this combined PSF appears saturated, therefore it is necessary to obtain a PSF of the innermost region using a similar procedure to complete the core region.

#### Appendix B.2: Core PSF

Building small PSFs is an usual procedure for performing photometry of stars. The usual technique for obtaining these small PSFs is the use of the PSFEX package (PSFEX; Bertin 2011). However, for the construction of the core of our PSFs, we use

Article number, page 19 of 23

Este documento incorpora firma electrónica, y es copia auténtica de un documento electrónico archivado por la ULL según la Ley 39/2015.  
 Su autenticidad puede ser contrastada en la siguiente dirección <https://sede.ull.es/validacion/>

Identificador del documento: 2260218

Código de verificación: Sm21pjYh

Firmado por: JAVIER ROMAN GARCIA  
 UNIVERSIDAD DE LA LAGUNA

Fecha: 02/11/2019 16:23:59

IGNACIO TRUJILLO CABRERA  
 UNIVERSIDAD DE LA LAGUNA

02/11/2019 17:39:19

A&A proofs: manuscript no. output

a technique similar to that of the wings, this is, the stacking of a large number of stars. We select an area of  $2.5^\circ \times 2.5^\circ$  centered at coordinates RA = 25.75, Dec. = 0. This region of the sky has a low contamination by Galactic dust, and importantly has a low number of very bright stars, therefore, low-luminosity stars are weakly influenced by the scattered light of external brighter stars. We selected sources in this region using SExtractor with stellarity factor greater than 0.8 and magnitude range between 15.5 and 16.5 mag according with the given band. With this selection, we guarantee selecting the range of brightest stars that are not saturated. The number of selected stars for the stacking depends on the band, being around 600 stars.

We proceed as follows. We created a stamp of 201 pixels ( $\approx 80$  arcsec) using SWarp centered at the coordinates retrieved from SExtractor of each star and we mask all other sources. As in the case of very bright stars for the construction of the wings, the exact coordinates of the stars is a crucial point and even more important in the case of the core. We discarded using coordinates from SDSS catalogs or SExtractor. To fine tune of the centering, we fit a Moffat function to each star using IMFIT (Erwin 2015) and we resample the stamp with the coordinates of the center of the Moffat best fit. We recalibrated the sky of each star in the region of the stamp with radius larger than 80 pixels. For the normalization in flux of the star we used the flux of the profile in a ring of 9 to 11 pixels ( $\approx 3.5$  to 4.5 arcsec). Finally we stacked all the stars using a resistant mean with a  $2\sigma$  rejection.

#### Appendix B.3: Final PSFs

To obtain the final PSFs we perform the junction of the cores with the wings. The main problem of this junction is the normalization and sky reference in the core PSF model. By definition, the measured sky in the core PSFs (region beyond 80 pixels) is not 0 but the value of the PSF wings in this region. However, the signal to noise ratio at that radius for the core PSF is not enough for a reliable sky level value. Because of this, we perform the junction of the PSF using the following normalization:

$$\begin{aligned} \text{Core}(R1) &= a \times \text{Wing}(R1) + b \\ \text{Core}(R2) &= a \times \text{Wing}(R2) + b \end{aligned}$$

Being R1 and R2 two different radial distances with enough signal to noise in both the wing and core PSFs. Hence, solving this equations will give us the normalization value (a) and sky level (b) to be applied to the core PSF for a perfect matching previous to the junction. We use different R1 and R2 radial distances for each band trying to avoid the internal reflection and reaching the best signal to noise as possible for the final PSFs (see Infante-Sainz et al. 2019 in prep., for further details). Finally, we assign the value of the Core PSF to the inner region (pixels less than R1 away from the center of the star) of the Wind PSF, producing the final PSF. We show the final PSF profiles for each band in Fig. B.2.

#### Appendix C: Simulation of diffuse emission photometry

In this Appendix we expand on the details on how the Galactic cirri colors are obtained and the method used. We also perform a set of simulations to quantify the uncertainties in this measurement.

Due to the Poisson nature of the noise of the images, the color distribution of this noise follows a Lorentzian distribution.

Article number, page 20 of 23

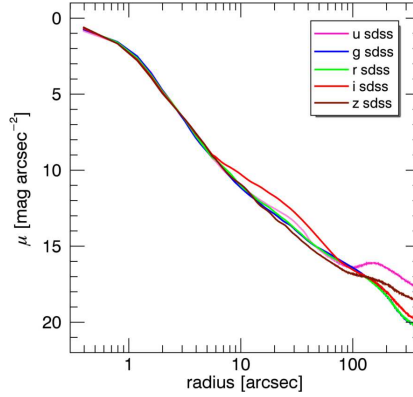


Fig. B.2. Radial profiles of the IAC Stripe82 PSFs obtained and applied in this work.

This Lorentzian distribution is the result of the convolution of the Gaussian distributions of the noise for each band at a given color, and it is centered approximately in the color corresponding to the Gaussian width difference, that is, the depth of the bands. For example, two photometric bands A and B with limiting depth of  $\mu_A = 25.5$  and  $\mu_B = 25.0$  mag arcsec $^{-2}$  will produce a Lorentzian distribution centered in the color A-B = 0.5 mag arcsec $^{-2}$ . Note that the Lorentzian distribution is due to the definition of magnitude in which only positive flux have physical sense, so for a given pixel to enter in the color distribution, both bands A and B in that pixel must have a positive intensity. Therefore, for pixels completely dominated by noise, only  $\frac{1}{4}$  of the pixels will enter in the color distribution (that pixel should have a positive value in both bands), being the average probability of this color given by the gaussian width difference between both bands. In Fig. C.1 left panel, we show the color distribution of pixels in the Control field (see Fig 6). Due to the absence of diffuse emission, the color distribution of the pixels in this field can be considered exclusively due to the noise of the image. We fit this distribution with a Lorentzian function. As can be seen, the fitting shows an excellent match with the observed color distribution. The centers of the Lorentzian distributions are  $x_L = 0.39, 0.52$  and  $1.06$  mag for the *g-r*, *r-i* and *i-z* colors respectively. While for the *g-r* and *r-i* colors the  $x_L$  values match with the depth differences of that bands, for *i-z* this value differs due to the high sky fluctuations in the *z* band.

The presence of any source of constant color will be added to the Lorentzian distribution. Assuming that this source does not cover the whole image but only a fraction of it, there will be a transition from the color of the noise to the color of the source as the signal or surface brightness of the source increases. For the fitting corresponding to the color of the source we use a Gaussian function. Note that although the color of the source would be constant, the expected color distribution produced is not a delta function but a Gaussian function due to photometric uncertainties introduced by the underlying sky background fluctuations. Therefore, the expected distributions are a Lorentzian plus a Gaussian functions, as it is described in the Section 4. In the

Este documento incorpora firma electrónica, y es copia auténtica de un documento electrónico archivado por la ULL según la Ley 39/2015.  
 Su autenticidad puede ser contrastada en la siguiente dirección <https://sede.ull.es/validacion/>

Identificador del documento: 2260218

Código de verificación: Sm21pjYh

Firmado por: JAVIER ROMAN GARCIA  
 UNIVERSIDAD DE LA LAGUNA

Fecha: 02/11/2019 16:23:59

IGNACIO TRUJILLO CABRERA  
 UNIVERSIDAD DE LA LAGUNA

02/11/2019 17:39:19

Román et al.: Galactic cirri in deep optical imaging

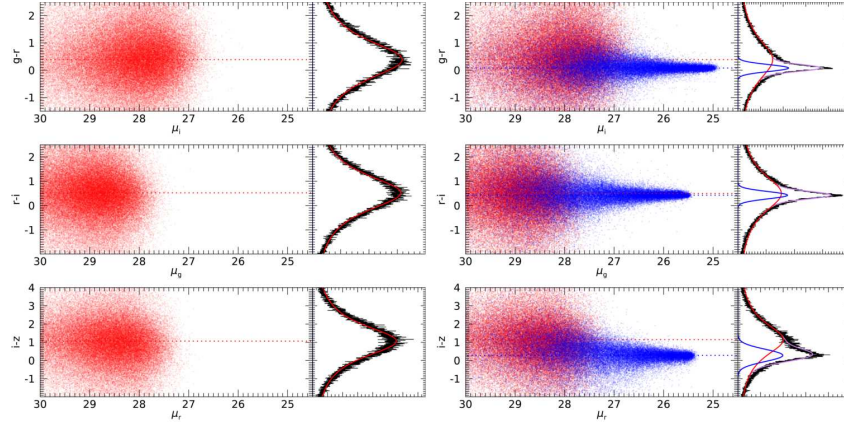


**Fig. C.1.** Color distribution of the noise in the Control Field and color distribution by adding an artificial constant color structure. Left panels: color vs. surface brightness values (red dots) of purely noise pixels and their distribution fitted by a Lorentzian function (red curve) in the right side of the plot. Right panel: same but adding a constant color structure (blue dots) fitted by a Gaussian function (blue curve). The purple curve is the fitted Lorentzian + Gaussian function. The horizontal dashed lines correspond to the calculated centers of the Lorentzian and Gaussian functions.

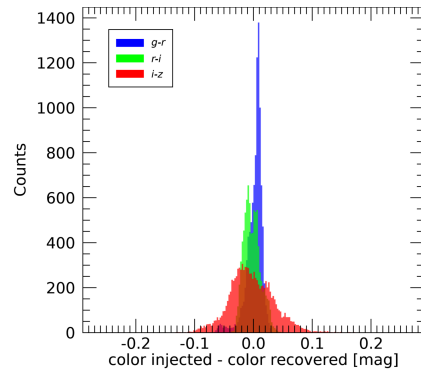


**Fig. C.2.** Distributions of the difference between the injected and recovered colors in the simulation.

right panel of Fig. C.1 we show the effect of adding a constant color artificial structure in the Control field with  $g$  band surface brightness ranging from 25 to 30 mag arcsec<sup>-2</sup>. The injected colors of that structure are  $g-r = 0.075$ ,  $r-i = 0.421$  and  $i-z = 0.267$ , while the recovered values are  $g-r = 0.080$ ,  $r-i = 0.428$  and  $i-z = 0.282$ .

To quantify the errors of our methodology at measuring the colors of the cirri, we perform a set of simulations injecting a constant color structure and recovering this color by the de-

scribed method. The injected structure has an area corresponding to approximately one fifth of the total area of the field and consists of a rectangle whose surface brightness decays along one axis. With these characteristics we simulate a structure with a wide range in surface brightness, similar to the scenario of the cirri. The maximum surface brightness is 25.5 mag arcsec<sup>-2</sup> and decreasing to approximately 30 mag arcsec<sup>-2</sup> in the  $g$  band. We perform a number of 10,000 injections / recoveries of the injected color. In each iteration we locate this artificial bias rectangle in random positions within the field, avoiding some bias that could be introduced in a certain area that could suffer from a given sky fluctuation. The colors of the structure are also random in each iteration, within the range [0,1] mag for the  $g-r$  color and [-0.5,0.5] mag for the  $r-i$  and  $i-z$  colors. In Fig. C.2 we plot the histogram of the difference between the injected and recovered  $g-r$ ,  $r-i$  and  $i-z$  colors. These follow an approximately Gaussian shape with slight deviations in their mean values with respect to 0 mag. These average values are -0.0066, -0.0115 and -0.0085 mag for the  $g-r$ ,  $r-i$  and  $i-z$  distributions respectively, therefore negligible. The  $3\sigma$  standard deviations of these distributions are: 0.04, 0.04 and 0.11 mag for the  $g-r$ ,  $r-i$  and  $i-z$  colors respectively. Therefore, we assume these values as uncertainties for the measurement of cirri colors by this method.

#### Appendix D: Photometric maps of the Cirrus field

A&A proofs: manuscript no. output

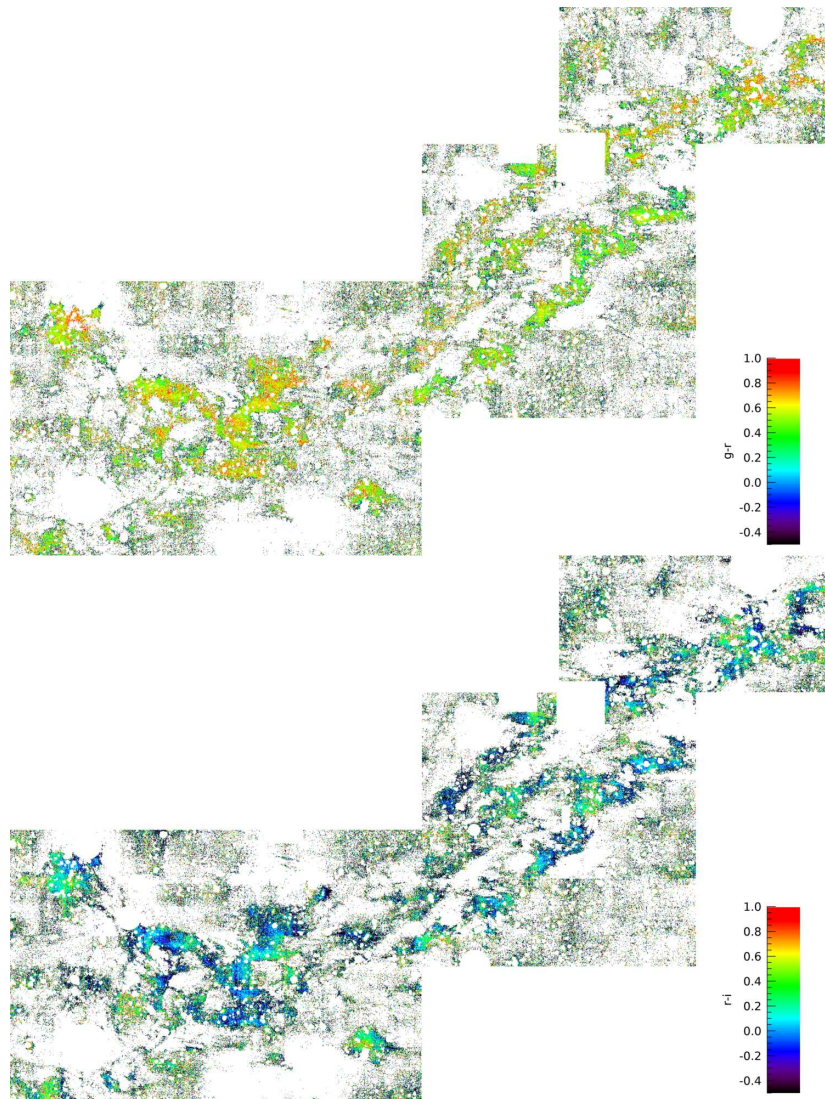


**Fig. D.1.**  $g-r$  and  $r-i$  color maps of the Cirrus Field.

Article number, page 22 of 23

Este documento incorpora firma electrónica, y es copia auténtica de un documento electrónico archivado por la ULL según la Ley 39/2015.  
Su autenticidad puede ser contrastada en la siguiente dirección <https://sede.ull.es/validacion/>

Identificador del documento: 2260218 Código de verificación: Sm21pYh

Firmado por: JAVIER ROMAN GARCIA  
UNIVERSIDAD DE LA LAGUNA

Fecha: 02/11/2019 16:23:59

IGNACIO TRUJILLO CABRERA  
UNIVERSIDAD DE LA LAGUNA

02/11/2019 17:39:19

Román et al.: Galactic cirri in deep optical imaging

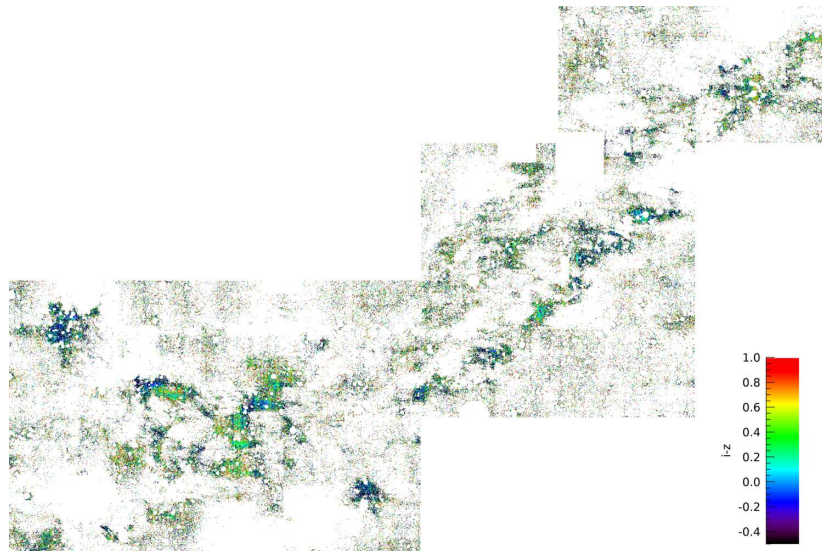


Fig. D.2.  $i-z$  color map of the Cirrus Field.

Article number, page 23 of 23

Este documento incorpora firma electrónica, y es copia auténtica de un documento electrónico archivado por la ULL según la Ley 39/2015.  
Su autenticidad puede ser contrastada en la siguiente dirección <https://sede.ull.es/validacion/>

Identificador del documento: 2260218 Código de verificación: Sm21pjYh

Firmado por: JAVIER ROMAN GARCIA  
UNIVERSIDAD DE LA LAGUNA

Fecha: 02/11/2019 16:23:59

IGNACIO TRUJILLO CABRERA  
UNIVERSIDAD DE LA LAGUNA

02/11/2019 17:39:19

## 4

### Additional results and ongoing work

#### 4.1 Testing the OGS telescope for low surface brightness science

During the months of May, June and July 2017, a total of 21 nights were granted for observations with the Optical Ground Station (OGS) telescope at the Izaña observatory in Tenerife (PI: Javier Román). The goal of the proposal was to test the capabilities of this telescope for low surface brightness science. The characteristics of this telescope are, in principle, optimal for deep observations of nearby targets: great availability, 1 meter aperture, 0.694" pixel scale, field of view of  $\approx 40$  arcmin, camera at a temperature of 160K with very low readout noise and located in relatively dark site at Izaña Observatory in Tenerife. However, this telescope has traditionally been used for other scientific issues such as the detection and monitoring of space debris, the detection of smaller bodies of the solar system or even quantum teleportation experiments using a laser beam installed in the telescope (see Figure 4.1). It allowed in 2012 to achieve the record of quantum teleportation distance of 143 km, the distance between the Izaña observatory and the Roque de los Muchachos observatory (Ma et al. 2012).

The possibility of being able to control all the steps, from the design of the observational strategy, the personal data acquisition in the telescope, the reduction of the data and the post-processing of the images makes it possible to minimize all the factors that create uncertainties such as the gradients present in the images. This is something not possible with the use of data from surveys, in which the data is already processed according to a given reduction criteria, being sometimes not optimal for low surface brightness studies. To conduct the observations made in the OGS telescope, specific observational strategies were designed that allowed great image quality and flat-fielding (see 2.2) together with the PSF characterization of this telescope through specific observations of bright stars and the subsequent subtraction of the scattered light by stars in the final coadded images (see Section 2.4).

The results of the observations made with the OGS telescope were very successful. It was possible to demonstrate the great reliability of this telescope in producing data of considerable low surface brightness. The most outstanding results obtained with this telescope are detailed below.

##### 4.1.1 IC 1101 the "largest galaxy in the Universe"

The IC 1101 galaxy is the dominant central galaxy of the Abell 2029 galaxy cluster. Its enormous size of 1 Mpc in diameter makes it the largest observed galaxy so far (Uson et al. 1991).

CXIX

Este documento incorpora firma electrónica, y es copia auténtica de un documento electrónico archivado por la ULL según la Ley 39/2015.  
Su autenticidad puede ser contrastada en la siguiente dirección <https://sede.ull.es/validacion/>

Identificador del documento: 2260218 Código de verificación: Sm21pjYh

Firmado por: JAVIER ROMAN GARCIA  
UNIVERSIDAD DE LA LAGUNA

Fecha: 02/11/2019 16:23:59

IGNACIO TRUJILLO CABRERA  
UNIVERSIDAD DE LA LAGUNA

02/11/2019 17:39:19



Figure 4.1: Image of the OGS telescope, located at Izaña Observatory, Tenerife, laser connected with Roque de los Muchachos Observatory in the island of La Palma.

This circumstance makes it an object of great interest. Its expected extreme accretion rate, explorable through the study of the cluster's luminosity function, the study of the morphological and photometric properties of its halo and the expected huge central supermassive black hole are the points to explore.

Observations were made with the OGS telescope in three photometric bands  $B$ ,  $V$  and  $R$ , with exposure times of 2.8, 3.9 and 3.8 hours respectively. The depth reached in the final coadded images is  $\mu_{lim}[3\sigma: 10'' \times 10''] = 29.3, 28.5$  and  $28.2$  mag arcsec $^{-2}$  in  $B$ ,  $V$  and  $R$  bands respectively. The work in progress with this data set is focused on obtaining precise photometry of the IC 1101 galaxy halo. This will require the elimination of the scattered light by the stars. The major limiting factor is the moderate presence of Galactic cirri in this field (see Figure 4.2). The results obtained in Section 3.6 are key in this regard. This will allow to discern if there is any diffuse emission in the environment of IC 1101 that may be due to foreground dust.

An additional result of great interest is the estimation of the mass of the central supermassive black hole of IC 1101. Given the known relationship between the mass of the central black hole and the stellar mass of the host galaxy (e.g. Bennert et al. 2011; Reines, & Volonteri 2015), it is expected that IC 1101 own the most massive black hole ever discovered, since this galaxy is the most massive ( $M^* \approx 10^{12} M_{\odot}$ ) galaxy ever observed. For this, MUSE data was obtained at the Very Large Telescope (PI: Fernando Buitrago). Observations were conducted using adaptive optics with a spatial resolution of approximately  $0.1''$ . The use of the photometric

Este documento incorpora firma electrónica, y es copia auténtica de un documento electrónico archivado por la ULL según la Ley 39/2015.  
 Su autenticidad puede ser contrastada en la siguiente dirección <https://sede.ull.es/validacion/>

Identificador del documento: 2260218 Código de verificación: Sm21pjYh

Firmado por: JAVIER ROMAN GARCIA  
 UNIVERSIDAD DE LA LAGUNA

Fecha: 02/11/2019 16:23:59

IGNACIO TRUJILLO CABRERA  
 UNIVERSIDAD DE LA LAGUNA

02/11/2019 17:39:19

4.1 Testing the OGS telescope for low surface brightness science CXXI

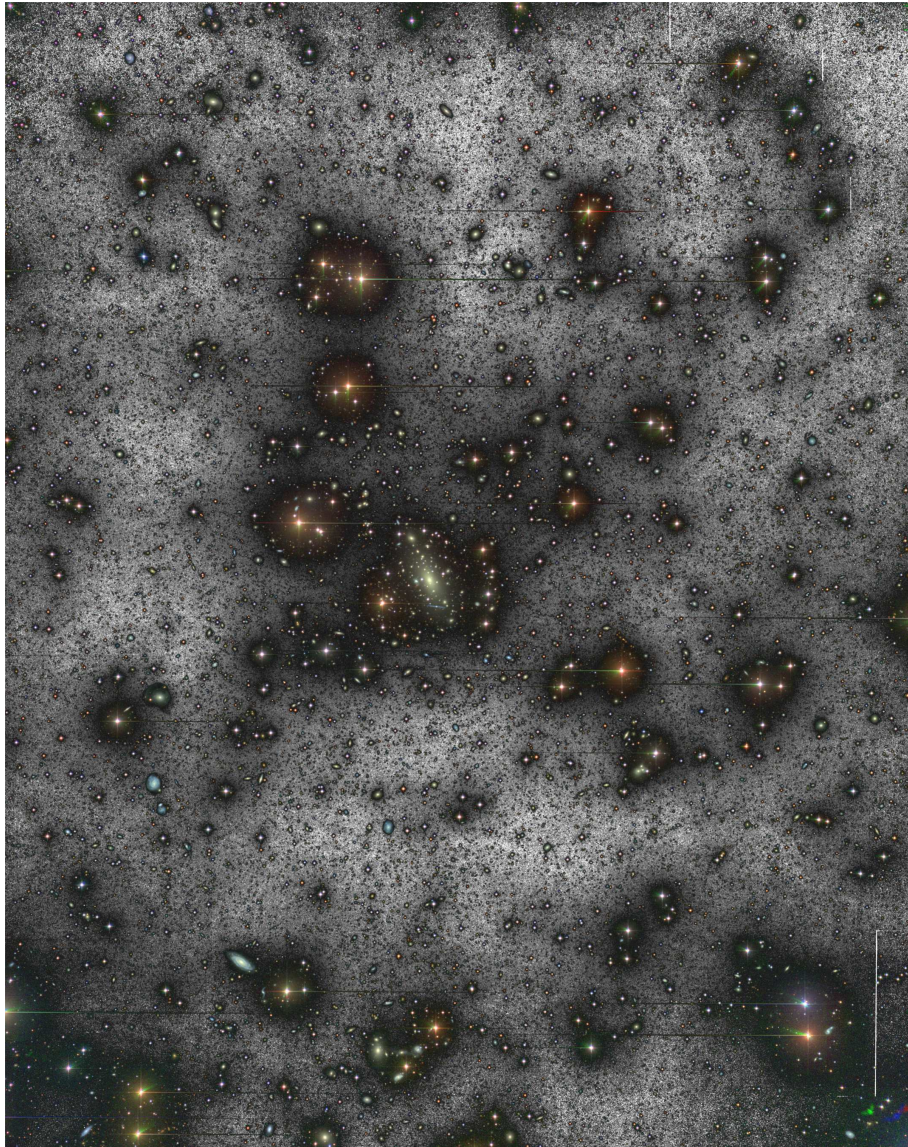


Figure 4.2: Color composite image using  $B$ ,  $V$  and  $R$  bands of the IC 1101 galaxy and its environment. The field-of-view is  $0.85 \times 1.05$  degrees. The black and white background map is constructed adding the  $B$ ,  $V$  and  $R$  bands.

Este documento incorpora firma electrónica, y es copia auténtica de un documento electrónico archivado por la ULL según la Ley 39/2015.  
Su autenticidad puede ser contrastada en la siguiente dirección <https://sede.ull.es/validacion/>

Identificador del documento: 2260218 Código de verificación: Sm21pjYh

Firmado por: JAVIER ROMAN GARCIA  
UNIVERSIDAD DE LA LAGUNA

Fecha: 02/11/2019 16:23:59

IGNACIO TRUJILLO CABRERA  
UNIVERSIDAD DE LA LAGUNA

02/11/2019 17:39:19

profiles obtained with the OGS telescope are crucial for this calculation. This analysis is work in progress and will be published after the presentation of this thesis.

#### 4.1.2 A new ultra-faint satellite candidate around the nearby NGC 4565 galaxy

The NGC 4565 galaxy is a well studied object located at a distance approximately of 12 Mpc (Radburn-Smith et al. 2011). Its edge-on projection and large apparent size makes it a perfect target for exploring its halo and the possible presence of tidal features. Additionally, due to the large field of view of the OGS camera, it is interesting to explore the presence of low surface brightness satellites. Multiband observations were carried out in three photometric bands with exposure times of 2.3, 1.25 and 2.3 hours in  $B$ ,  $V$  and  $R$  bands respectively. The depth reached is  $\mu_{lim}[3\sigma: 10'' \times 10''] = 28.8, 27.9$  y  $27.7$  mag arcsec<sup>-2</sup> in  $B$ ,  $V$  and  $R$  bands respectively.

In the final coadd, the scattered light by the stars was subtracted by the techniques described in Section 2.5 (see also Figure 2.8). No presence of tidal features was found around the galaxy at this depth. However, the presence of a very low surface brightness object located near the disc plane of the NGC 4565 galaxy was detected. With a mean surface brightness of  $\langle \mu_{eff} \rangle = 27.3$  mag arcsec<sup>-2</sup> in the  $B$  band and an effective radius of approximately 200 pc (assuming the distance to the NGC 4565 galaxy) is a clear candidate for being an ultra-faint satellite. Although there are observations of NGC 4565 with the Hubble space telescope by the GHOST survey (Seth et al. 2005), unfortunately the area in which the object is found is not observed by the footprint of this survey. It avoids being able to know with great precision the distance at which the object is. This object, together with the well-known satellites NGC 4562 and IC 3571, could be added to the list of satellites discovered for the NGC 4565 galaxy. Future deep spectroscopic observations will be necessary to obtain its radial velocity to confirm its association with the NGC 4565 galaxy.

#### 4.1.3 Identifying ultra-diffuse galaxies in the Coma cluster

In order to make observations of the Coma cluster intracluster light, preliminary images were obtained in the  $B$  and  $V$  bands with exposure time of 1 hour per band. After reduction of the data, creation of the coadd images and subtracting the stars from them, it was found that the internal reflections produced by the stars of high luminosity in the field did not allow to study the diffuse light of the Coma cluster. It should be noted that internal reflections are not part of the PSF, but residual light due to the telescope instrumentation. Due to this circumstance, the Coma intracluster light analysis was ruled out with this telescope and no more observations were taken.

Analyzing the images, it was found that the ultra-diffuse galaxies detected by Koda et al. (2015) were easily detected in the OGS images (see Figure 4.4). It is remarkable to detect these very low surface brightness galaxies with only one hour of exposure time per band in a 1 meter telescope as it is the OGS telescope, compared to the exposure time of 20 minutes with the 8 meter aperture Subaru telescope in the work by Koda et al. (2015).

The detection of these ultra diffuse galaxies and other non cataloged objects allowed to obtain structural and photometric parameters of the targets observed by Ruiz-Lara et al. (2018) on deep spectroscopic observations (20 hours of exposure time) with the GTC telescope using the OSIRIS instrument. For these low surface brightness objects an analysis of their stellar populations was performed.

Este documento incorpora firma electrónica, y es copia auténtica de un documento electrónico archivado por la ULL según la Ley 39/2015.  
 Su autenticidad puede ser contrastada en la siguiente dirección <https://sede.ull.es/validacion/>

Identificador del documento: 2260218 Código de verificación: Sm21pjYh

Firmado por: JAVIER ROMAN GARCIA  
 UNIVERSIDAD DE LA LAGUNA

Fecha: 02/11/2019 16:23:59

IGNACIO TRUJILLO CABRERA  
 UNIVERSIDAD DE LA LAGUNA

02/11/2019 17:39:19

4.1 Testing the OGS telescope for low surface brightness science CXXIII

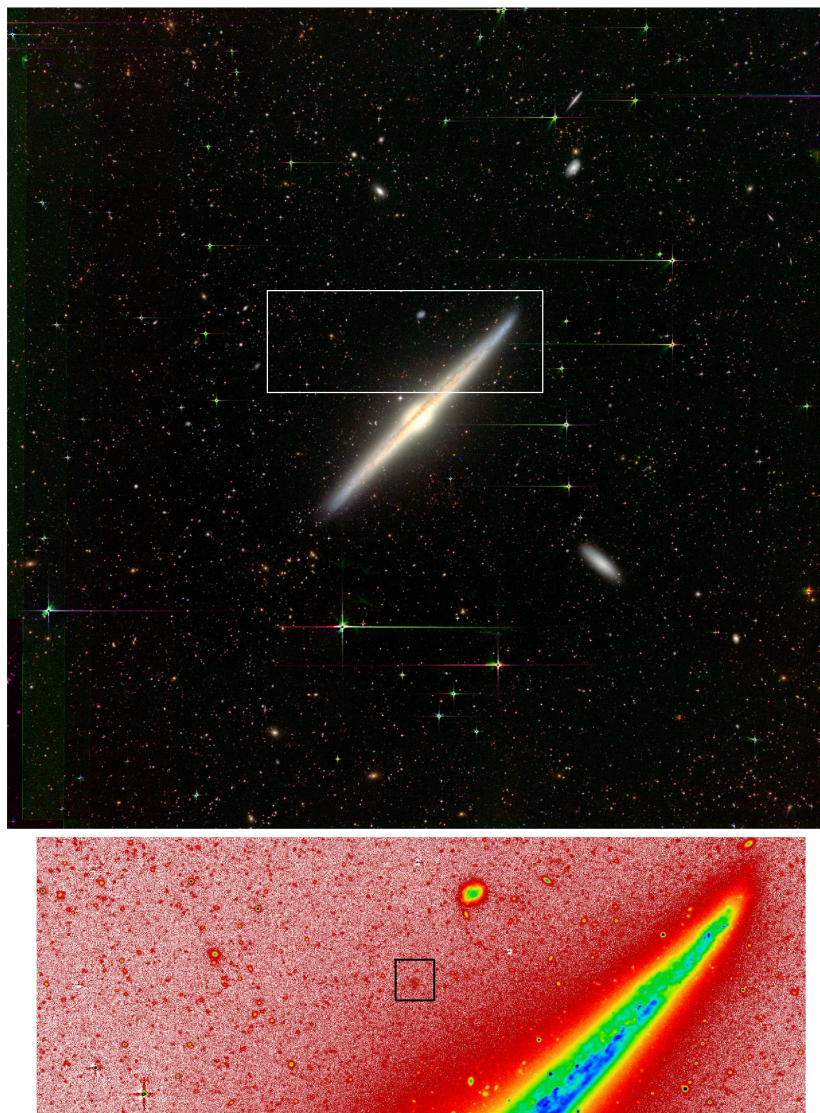


Figure 4.3: Upper panel: Color composite image of the NGC 4565 field using  $B$ ,  $V$  and  $R$  bands. Most of the stars in the field were removed. Bottom panel: Zoom-in field (see white rectangle in the upper panel) in the  $B$  band indicating the location of the new ultra-faint satellite with a black square.

Este documento incorpora firma electrónica, y es copia auténtica de un documento electrónico archivado por la ULL según la Ley 39/2015.  
Su autenticidad puede ser contrastada en la siguiente dirección <https://sede.ull.es/validacion/>

Identificador del documento: 2260218 Código de verificación: Sm21pjYh

Firmado por: JAVIER ROMAN GARCIA  
UNIVERSIDAD DE LA LAGUNA

Fecha: 02/11/2019 16:23:59

IGNACIO TRUJILLO CABRERA  
UNIVERSIDAD DE LA LAGUNA

02/11/2019 17:39:19

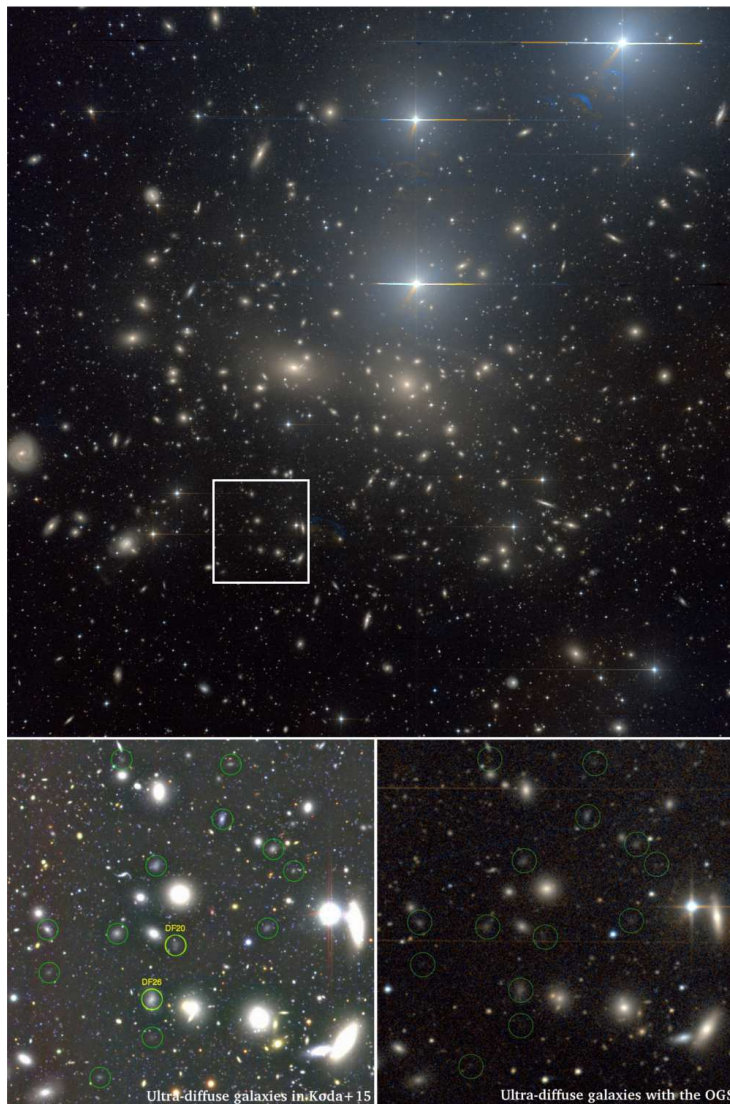


Figure 4.4: Top panel: A color composite image of the Coma cluster observed with the OGS using  $B$  and  $V$  bands. Bottom panels: Ultra-diffuse galaxies detected by Koda et al. (2015) are indicated with circles in the left panel and detected with the OGS telescope in the right panel.

Este documento incorpora firma electrónica, y es copia auténtica de un documento electrónico archivado por la ULL según la Ley 39/2015.  
Su autenticidad puede ser contrastada en la siguiente dirección <https://sede.ull.es/validacion/>

Identificador del documento: 2260218 Código de verificación: Sm21pjYh

Firmado por: JAVIER ROMAN GARCIA  
UNIVERSIDAD DE LA LAGUNA

Fecha: 02/11/2019 16:23:59

IGNACIO TRUJILLO CABRERA  
UNIVERSIDAD DE LA LAGUNA

02/11/2019 17:39:19

4.1 Testing the OGS telescope for low surface brightness science CXXV

4.1.4 Ultra-deep observations of the Abell 2199 galaxy cluster

In order to test the limits of the OGS telescope in ultra-deep observations, an observational campaign was carried out in the Abell 2199 galaxy cluster with a total integration time of 22 hours using a single band. This particular object was chosen because of its excellent characteristics for ultra-deep observations and the maximization of the science obtained. First, the presence of dust in this field is very low, with an extinction in  $g$  band of  $A_g = 0.035$  mag. It makes the presence of Galactic cirri unlikely, avoiding complications. Further, the central dominant galaxy of this cluster (NGC 6166) is a very well studied galaxy, with a large amount of ancillary data. Moreover, in the line of sight of this structure there are no structures in the background such as clusters or groups of galaxies, therefore any low surface brightness object detected in the field of view has a very high probability of belonging to the Abell 2199 structure. All these characteristics make it a perfect target in which to perform extremely deep observations.

22 hours of exposure time were carried out with an observational strategy focused on producing a high quality autoflat and minimizing the gradients by parasitic light. The data was subsequently reduced following the techniques detailed in Section 2.2. Additionally, for this particular coadd a specific pipeline was created for the elimination of the strong bleeding lines that the camera of the OGS telescope produces. The bleeding lines are clearly visible in Figures 4.2, 4.3 and 4.4. Removing the bleeding lines leaves only the spike lines of the secondary mirror structure on the image (see Figure 4.6). This bleeding correction is possible due to the characteristics of the camera having 4 independent chips. The bleeding lines range from the position of the stars to the central segment line where the reading of the camera is performed (see Figure 4.6). It causes that the bleeding line, depending on each individual exposure and due to the wide dithering of the observations, tends to be to the right or to the left depending on whether the star is on the CCD1 or CCD3 (bleeding to the right) or on CCD2 or CCD4 (bleeding to the left). By masking the bleeding line from the position in which the star is located to the center line, and taking into account the dithering patterns, it is possible to remove the strong bleeding lines in the final combined coadd by losing some signal to noise in these regions. Nevertheless, the bleeding lines have a small width of around 3 pixels and does not imply a great loss in the signal to noise of the final coadd, being the elimination of this bleeding much more advantageous.

The final coadded image is shown in the middle panel of Figure 4.5. As can be seen, the scattered light by the stars totally contaminates the field, making it impossible to identify structures with low surface brightness at first sight. After the modeling of the PSF and the subtraction of the stars with the developed pipelines, an image free of scattered light by the stars is obtained. This is shown in the lower panel of Figure 4.5. The depth of the final image has a surface brightness limit of  $\mu_{lim}[3\sigma: 10'' \times 10''] = 29.4$  mag arcsec<sup>-2</sup> in the  $R$  band. This image is one of the deepest images ever taken from the ground.

The final image of Abell 2199 reveals a gigantic halo of 300 kpc in diameter around NGC 6166. This halo contains a multitude of stellar streams and tidal debris of very low surface brightness, which is of great interest, showing a strong accretion activity. These extreme low surface brightness structures are similar, both in morphology and surface brightness, to those reported in the works by Mihos et al. (2005, 2017) in the Virgo Cluster. Some of these features are shown in great detail in Figure 4.7. The surface brightness of these features varies between  $\mu_R \approx 26.5$  mag arcsec<sup>-2</sup> of feature C up to  $\mu_R \approx 28.5$  mag arcsec<sup>-2</sup> of feature B. It should be noted that in the explored field there are also extremely faint halos belonging to the component galaxies

Este documento incorpora firma electrónica, y es copia auténtica de un documento electrónico archivado por la ULL según la Ley 39/2015.  
Su autenticidad puede ser contrastada en la siguiente dirección <https://sede.ull.es/validacion/>

Identificador del documento: 2260218 Código de verificación: Sm21pjYh

Firmado por: JAVIER ROMAN GARCIA  
UNIVERSIDAD DE LA LAGUNA

Fecha: 02/11/2019 16:23:59

IGNACIO TRUJILLO CABRERA  
UNIVERSIDAD DE LA LAGUNA

02/11/2019 17:39:19

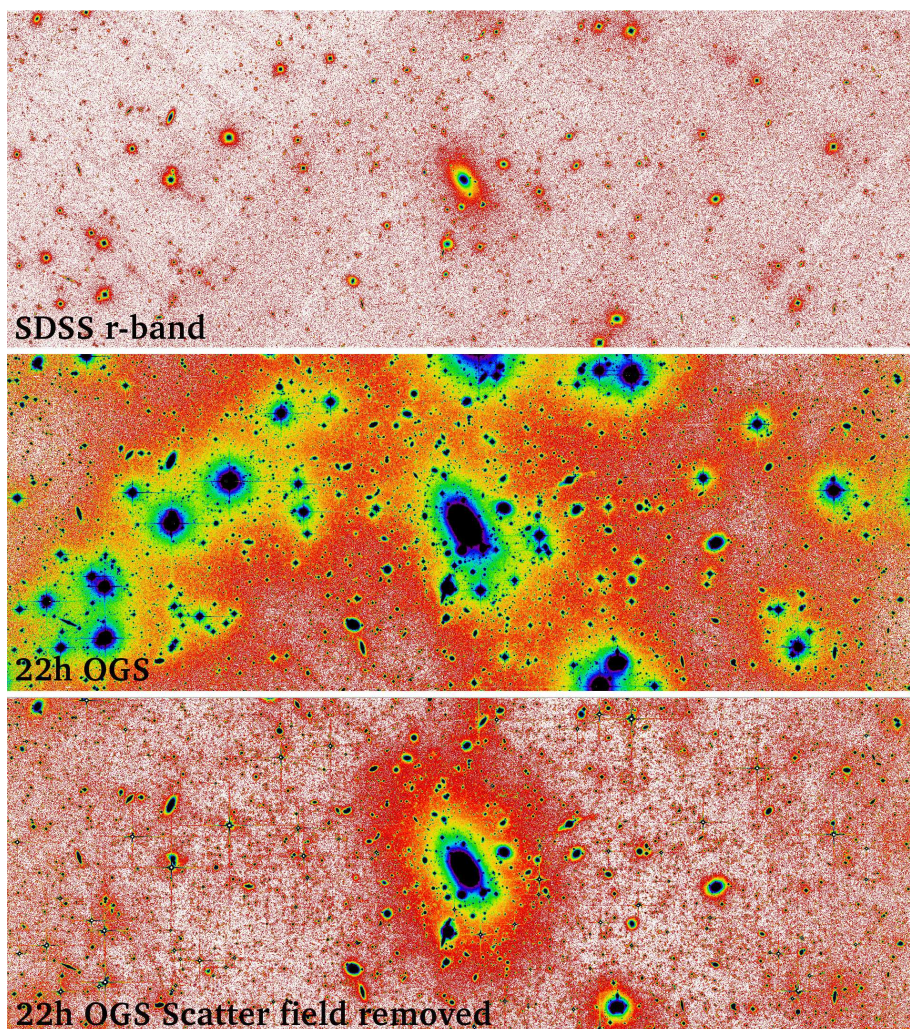


Figure 4.5: Images of the NGC 6166 galaxy, cD galaxy of the Galaxy Cluster Abell 2199. Top panel:  $r$  band image from SDSS. Medium panel: 22-hour coadd using the OGS telescope in the  $R$  band. Bottom panel: Similar to the previous one but having subtracted the brighter stars by careful characterization of the PSF. All images have a similar pixel scale. The OGS image has a depth of approximately  $3 \text{ mag arcsec}^{-2}$  deeper than that of SDSS.

Este documento incorpora firma electrónica, y es copia auténtica de un documento electrónico archivado por la ULL según la Ley 39/2015.  
Su autenticidad puede ser contrastada en la siguiente dirección <https://sede.ull.es/validacion/>

Identificador del documento: 2260218 Código de verificación: Sm21pjYh

Firmado por: JAVIER ROMAN GARCIA  
UNIVERSIDAD DE LA LAGUNA

Fecha: 02/11/2019 16:23:59

IGNACIO TRUJILLO CABRERA  
UNIVERSIDAD DE LA LAGUNA

02/11/2019 17:39:19

4.1 Testing the OGS telescope for low surface brightness science CXXVII

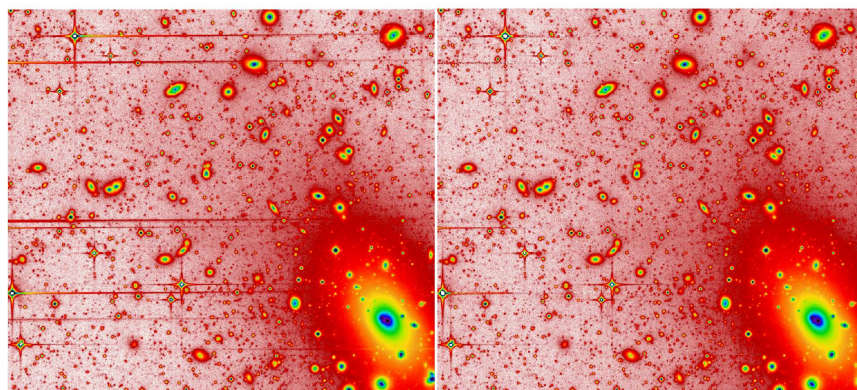
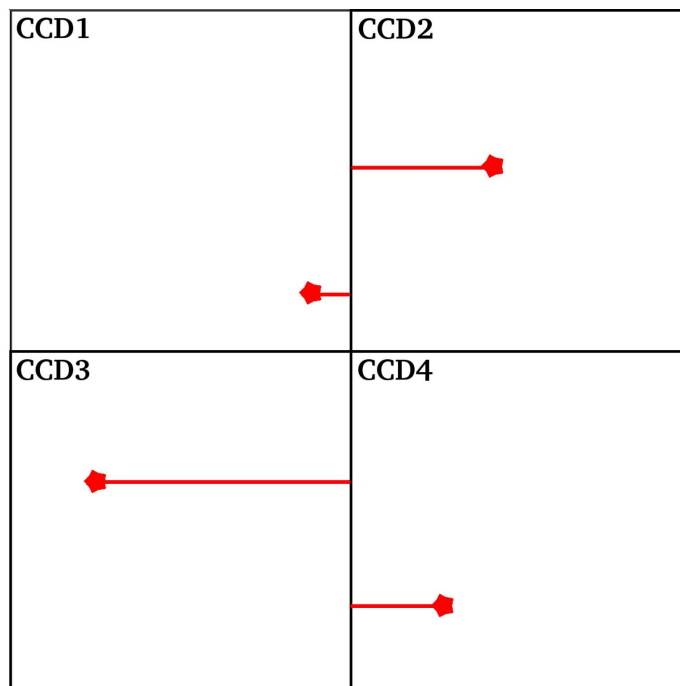


Figure 4.6: Correction of the bleeding lines of the OGS camera. In the upper panel a schematization of the camera is shown. The stars and red lines represent saturated stars and their corresponding bleeding lines. The image without correction by bleeding is shown in the lower left panel. The same image is shown on the right panel after bleeding correction.

Este documento incorpora firma electrónica, y es copia auténtica de un documento electrónico archivado por la ULL según la Ley 39/2015.  
 Su autenticidad puede ser contrastada en la siguiente dirección <https://sede.ull.es/validacion/>

Identificador del documento: 2260218 Código de verificación: Sm21pjYh

Firmado por: JAVIER ROMAN GARCIA  
 UNIVERSIDAD DE LA LAGUNA

Fecha: 02/11/2019 16:23:59

IGNACIO TRUJILLO CABRERA  
 UNIVERSIDAD DE LA LAGUNA

02/11/2019 17:39:19

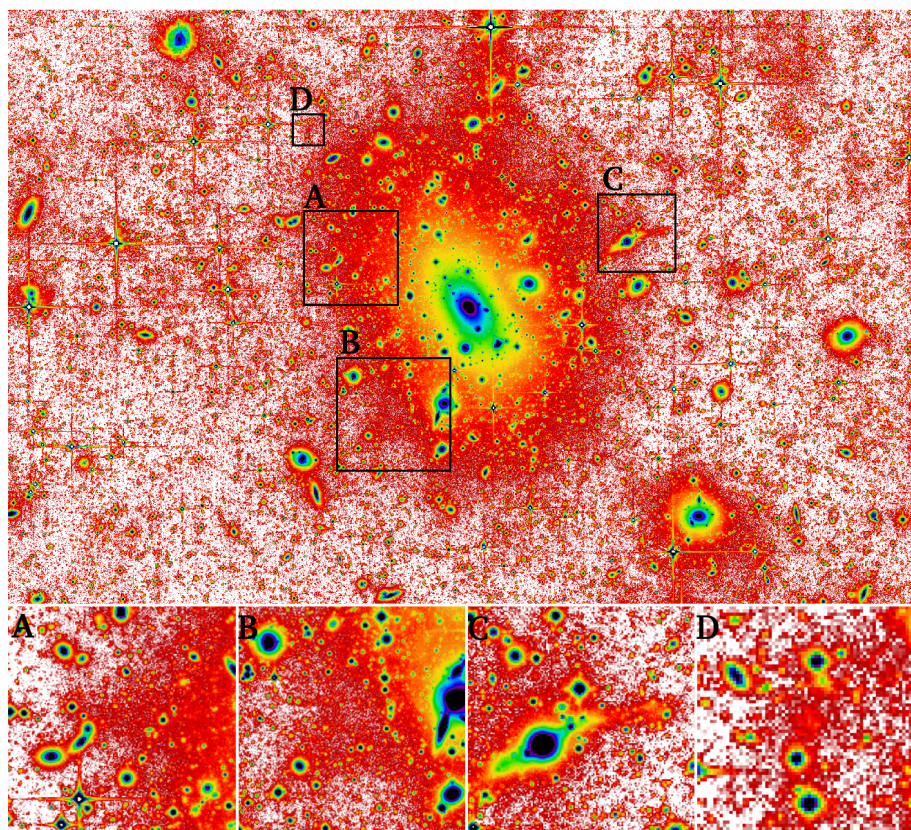


Figure 4.7: Extremely low surface brightness details in the Galaxy Cluster Abell 2199 observed by the OGS telescope. The top panel shows an overview of the NGC 6166 halo, located in the center of the image. Some galaxies belonging to the Galaxy Cluster Abell 2199 are also present. The lower panels show some zoom-in details of the areas corresponding to the rectangles marked in the top panel. Bottom panel A: Stellar stream due to galaxies in interaction with the central galaxy NGC 6166 ( $\mu_R \approx 27.5 \text{ mag arcsec}^{-2}$ ). Bottom panel B: Stellar stream in the form of a loop probably due to the galaxies interacting located on the right side of the panel ( $\mu_R \approx 28.5 \text{ mag arcsec}^{-2}$ ). Bottom panel C: Tidal galaxy debris in interaction with the central galaxy NGC 6166 ( $\mu_R \approx 26.5 \text{ mag arcsec}^{-2}$ ). Bottom panel D: Extremely low surface brightness satellite ( $\langle \mu_R \rangle > \approx 26.8 \text{ mag arcsec}^{-2}$  within the effective radius).

Este documento incorpora firma electrónica, y es copia auténtica de un documento electrónico archivado por la ULL según la Ley 39/2015.  
 Su autenticidad puede ser contrastada en la siguiente dirección <https://sede.ull.es/validacion/>

Identificador del documento: 2260218      Código de verificación: Sm21pjYh

Firmado por: JAVIER ROMAN GARCIA  
 UNIVERSIDAD DE LA LAGUNA

Fecha: 02/11/2019 16:23:59

IGNACIO TRUJILLO CABRERA  
 UNIVERSIDAD DE LA LAGUNA

02/11/2019 17:39:19

of the Abell 2199 cluster of galaxies, some of them also showing signs of interaction, something expected according to the cosmological model  $\Lambda$ -CDM at such depth in surface brightness.

Additionally, a large number of low surface brightness galaxies are detected. Due to the characteristics of this cluster in which no cluster or group of galaxies is located in the background of the structure, the vast majority of these objects are located at the distance of Abell 2199. The faintest low surface brightness satellite is shown in panel D of Figure 4.7. It has a surface brightness of  $\langle \mu_R \rangle = 26.8 \text{ mag arcsec}^{-2}$  with an effective radius of approximately 3 kpc. It is worth noting that although the image is deep enough to detect objects considerably fainter than this one, in our current analysis they are surprisingly not found. Having a considerable presence of ultra-diffuse galaxies (galaxies of very low surface brightness and effective radius greater than 1.5 kpc), an absence of objects with surface brightness  $\mu_R > 26.5 \text{ mag arcsec}^{-2}$  is found. This result could be very interesting and could impose a limit on surface brightness in which ultra-diffuse galaxies begin to be scarce, something not found in any previous analysis of UDGs in galaxy clusters.

## 4.2 Deep imaging with the Javalambre T80 telescope

The J80 telescope, located in the Javalambre Observatory, with its huge 1.7 degree field of view, 0.8 meter aperture, 0.55 "/pix pixel scale and state-of-the-art camera with high sensitivity, has excellent characteristics for its use in observations of objects with large apparent size that require deep observations. During this thesis different tests have been carried out with the T80 telescope to test its capabilities at low surface brightness.

First, a PSF model of the T80 telescope of the Javalambre observatory has been constructed. This PSF was built using dithered short exposures of very bright stars in the  $r$  band, these images being provided directly by the observatory staff. With these bright stars, a large PSF was built, reaching a radius of 40 arcmin. However, as discussed in Section 2.4, the center of this PSF model is saturated, and it is necessary to obtain a PSF core model to complete the central region of the PSF.

### 4.2.1 Ultra-deep observations of the M101 galaxy

In order to make ultra-deep observations of the M101 galaxy, a total of approximately 18 hours was obtained in the  $r$  band with the T80 telescope (PI: Dr Ignacio Trujillo). The goal of these observations is to explore the external regions of the M101 galaxy, of great interest due to its debated absence of halo (van Dokkum et al. 2014; Merritt et al. 2016), and in turn to achieve a great detection of galactic satellites or extreme low surface brightness objects in the field. The images are processed by the telescope reduction pipeline, including all steps, providing images ready for analysis. However, because the correction of flat-fielding is done through the use of twilight flats, the processed images contain some residual gradients. These gradients are very harmful in the case of ultra-deep observations, so they have to be corrected. Due to the complexity of the camera, data reduction from scratch was not possible. Due to this, a delta flat correction was performed (see Section 2.3). The result of the data processing through a delta flat correction was acceptable, efficiently eliminating the strong gradients present in the images. Using the coadd of the M101 image, stars were obtained for the construction of the PSF aureole and the PSF core models (see Section 2.4), allowing the construction of the global PSF model.

Este documento incorpora firma electrónica, y es copia auténtica de un documento electrónico archivado por la ULL según la Ley 39/2015.  
 Su autenticidad puede ser contrastada en la siguiente dirección <https://sede.ull.es/validacion/>

Identificador del documento: 2260218 Código de verificación: Sm21pjYh

Firmado por: JAVIER ROMAN GARCIA  
 UNIVERSIDAD DE LA LAGUNA

Fecha: 02/11/2019 16:23:59

IGNACIO TRUJILLO CABRERA  
 UNIVERSIDAD DE LA LAGUNA

02/11/2019 17:39:19

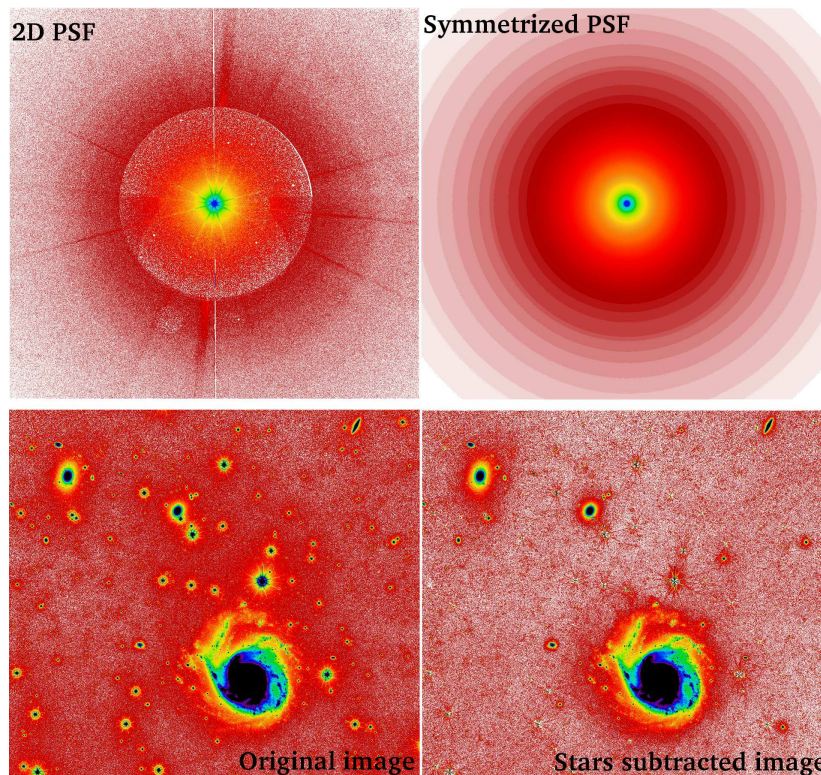


Figure 4.8: PSF model obtained from the T80 telescope (upper left panel) and its symmetry (upper right panel). In the lower panels the 18-hour coadd of the galaxy M101 (left panel) is shown and this image after the subtraction of the light scattered by the stars (right panel).

In Figure 4.8, upper panels show the PSF obtained. As can be seen in the two-dimensional PSF image, there are different visually differentiable regions. The appearance of these seemingly disconex areas is a visual artifact due to the large differences from signal to noise in different regions for the construction of the PSF, product of the masking. This can be easily seen by observing the symmetric PSF (Figure 4.8, right panel) in which the symmetric PSF model does not show distinct regions, having the PSF a smooth profile.

Using this PSF model, the removal of the scattered light by the stars in the coadd image of the M101 galaxy was carried out. The result is shown in the lower panel of the Figure 4.8. As can be seen, the presence of the scattered light by the stars makes it difficult to detect the structures of lower surface brightness, corresponding to the outermost regions of the galaxies present in this field. In the right panel, after the subtraction of the stars, these features are visible more easily. It is worth commenting that after the subtraction of the stars there are some

Este documento incorpora firma electrónica, y es copia auténtica de un documento electrónico archivado por la ULL según la Ley 39/2015.  
 Su autenticidad puede ser contrastada en la siguiente dirección <https://sede.ull.es/validacion/>

Identificador del documento: 2260218 Código de verificación: Sm21pjYh

Firmado por: JAVIER ROMAN GARCIA  
 UNIVERSIDAD DE LA LAGUNA

Fecha: 02/11/2019 16:23:59

IGNACIO TRUJILLO CABRERA  
 UNIVERSIDAD DE LA LAGUNA

02/11/2019 17:39:19

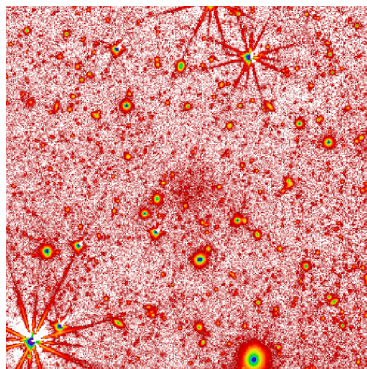


Figure 4.9: 6.5x6.5 arcmin stamp on the new M101 satellite candidate discovered with data from the Javalambre T80 telescope.

residuals corresponding to the internal reflections of the stars (not part of the PSF). However, these internal reflections have a considerably small apparent size, not significantly affecting the final image quality.

The preliminary results of this image show an extraordinary depth. This is evidenced by the visual detection, and with great signal to noise, of all the objects of extreme low surface brightness detected to date in the environment of the M101 galaxy (see the latest compilation by Bennet et al. 2017). Moreover, in our image, an object of extreme low surface brightness ( $\langle \mu_r \rangle \approx 28 \text{ mag arcsec}^{-2}$ ) and large extent (effective radius of 15 arcsec) is detected (see Figure 4.9), not having been previously cataloged. Due to its large apparent size, its association with the M101 galaxy is highly likely. If so, its effective radius would be 450 pc.

#### 4.2.2 Deep observations of the Perseus galaxy cluster

In order to study the intracluster light of the Perseus galaxy cluster, observations were made with an exposure time of 4 hours in the  $g$  and  $r$  bands (PI: Dr Mireia Montes). The processing of this data set consisted on using the already reduced images provided by the observatory and performing a gradient correction fitting with a smooth surface (see Section 2.3). This approach was sufficient to provide a high quality image with a minimal presence of gradients.

Although the presence of gradients in this image has been corrected significantly, the highest uncertainty comes from the high presence of Galactic cirri in the field of the Perseus galaxy cluster. This high dust contamination prevents the study of low surface brightness sources such as low brightness galaxies or the cluster's intracluster light easily. Figure 4.10 shows the presence of diffuse material throughout the entire field of view. Interestingly, only visually, a color differentiation of this diffuse material can be observed. While the intracluster light in the core of the cluster appears with more yellowish colors, the diffuse light in the outermost regions appears a more bluish or gray color. Using the techniques developed in Section 3.6, an approach using colors to discern between Galactic cirri and extragalactic sources will be possible.

The future analysis of this field will allow the analysis of low surface brightness galaxies,

Este documento incorpora firma electrónica, y es copia auténtica de un documento electrónico archivado por la ULL según la Ley 39/2015.  
 Su autenticidad puede ser contrastada en la siguiente dirección <https://sede.ull.es/validacion/>

Identificador del documento: 2260218 Código de verificación: Sm21pjYh

Firmado por: JAVIER ROMAN GARCIA  
 UNIVERSIDAD DE LA LAGUNA

Fecha: 02/11/2019 16:23:59

IGNACIO TRUJILLO CABRERA  
 UNIVERSIDAD DE LA LAGUNA

02/11/2019 17:39:19



Figure 4.10: Color composed image using  $g$  and  $r$  bands of the core of the Perseus cluster with the T80 Javalambre telescope.

expected very abundant due to the large virial mass of this cluster (the most massive in our vicinity). Additionally, through removal of the scattered light by the stars after modeling the PSF, it will be possible to obtain an estimate of the amount of intracluster material in the cluster.

### 4.3 Deep imaging with the Jeanne Rich telescope

The Jeanne Rich telescope is located at Polaris Observatory, California. Its characteristics are particularly good for the study of structures with low surface brightness. It has an aperture of 0.7 meter, field of view of approximately 1 degree and pixel scale of  $1,114''/\text{pix}$ . Its most notable feature is the quality of the optics in which internal reflections are virtually non-existent and excellent PSF quality, what makes it a highly competitive telescope in the study of galactic halos.

Este documento incorpora firma electrónica, y es copia auténtica de un documento electrónico archivado por la ULL según la Ley 39/2015.  
Su autenticidad puede ser contrastada en la siguiente dirección <https://sede.ull.es/validacion/>

Identificador del documento: 2260218 Código de verificación: Sm21pjYh

Firmado por: JAVIER ROMAN GARCIA  
UNIVERSIDAD DE LA LAGUNA

Fecha: 02/11/2019 16:23:59

IGNACIO TRUJILLO CABRERA  
UNIVERSIDAD DE LA LAGUNA

02/11/2019 17:39:19

#### 4.3.1 Detection of several stellar streams in the environment of the NGC 1052 galaxy

The proposed existence of two ultra-diffuse galaxies without dark matter (NGC 1052-DF2 and NGC 1052-DF4; van Dokkum et al. 2018, 2019) in the vicinity of the NGC 1052 galaxy aroused great attention from the community. This finding could be a challenge to theories of galaxy formation according to the current cosmological paradigm. However, as work by Trujillo et al. (2019) and Monelli & Trujillo (2019) revealed, the estimation of the distance to these galaxies has to be addressed carefully. In this sense, it is important to study the possible tidal streams present in galaxies to be able to guess association between them.

In order to explore the possible associations of these galaxies, an observational campaign was carried out with a total exposure time of 20 hours. A luminance filter was used because the goal was only the detection of faint structures, not requiring the use of a photometric band. However, the observations were taken with an observational strategy in which no dithering was conducted. This caused a strong presence of gradients that prevented obtaining a robust confirmation of the faintest features present in the coadd. A tidal interaction between NGC 1052 and NGC 1047 galaxies was found, confirming their physical association. Interestingly, no evidence for a recent tidal interaction for NGC 1052-DF2 and NGC 1052-DF4 was found, neither for the NGC 1042 galaxy. These results were published by Müller et al. (2019).

#### 4.3.2 Unveiling the intracluster light halo of the Coma galaxy cluster

Due to the special characteristics of the Jeanne Rich telescope, its use is optimal for studying the intracluster light in the Coma galaxy cluster. In section 4.1.3 it was discussed that the study of Coma intracluster light was not feasible with the OGS telescope due to the presence of strong internal reflections. With this goal, an observational campaign (PI: Javier Román) was carried out between April and June 2019 with a total integration time of 47 hours in the  $g$  band. The observations were taken with wide dithering offsets, optimizing the creation of a high quality autoflat. A specific reduction pipeline designed for this telescope was created. The general points of this pipeline follow the procedures discussed in Section 2.2 but being optimized specifically for the characteristics of the Jeanne Rich telescope's camera. Due to the broad dithering pattern, the integration time per pixel is less than that corresponding to the total 47 hour campaign. The average integration time per pixel is around 25 hours, with a maximum of about 35 hours for the central region of the final coadd, centered in the south west region of the Coma cluster.

In Figure 4.11, the final coadd image of Coma with the Jeanne Rich telescope is shown. The Coma image obtained by the Dragonfly telescope in the  $g$  band is also shown by comparison<sup>1</sup> (Abraham & van Dokkum 2014). It was the image used for the detection of ultra-diffuse galaxies in the Coma galaxy cluster (van Dokkum et al. 2015). The surface brightness limit is  $\mu_{im}[3\sigma, 10 \times 10 \text{ arcsec}] = 29.7 \text{ mag arcsec}^{-2}$ , which contrasts with the surface brightness limit of the Dragonfly image of  $\mu_{im}[3\sigma, 10 \times 10 \text{ arcsec}] = 28.7 \text{ mag arcsec}^{-2}$ . This difference in depth can be seen visually in Figure 4.11, which shows a greater extent of the halos and a clear better signal to noise. It is worth noting that the great depth achieved in the image of the Jeanne Rich telescope is due to the advanced reduction pipeline developed for this telescope. The use of a large number of images allowed to obtain a flat-fielding of exquisite quality. Another noteworthy point is the

<sup>1</sup>Image publicly available at: <https://www.dragonflytelescope.org/data-access.html>

Este documento incorpora firma electrónica, y es copia auténtica de un documento electrónico archivado por la ULL según la Ley 39/2015.  
 Su autenticidad puede ser contrastada en la siguiente dirección <https://sede.ull.es/validacion/>

Identificador del documento: 2260218      Código de verificación: Sm21pjYh

Firmado por: JAVIER ROMAN GARCIA  
 UNIVERSIDAD DE LA LAGUNA

Fecha: 02/11/2019 16:23:59

IGNACIO TRUJILLO CABRERA  
 UNIVERSIDAD DE LA LAGUNA

02/11/2019 17:39:19

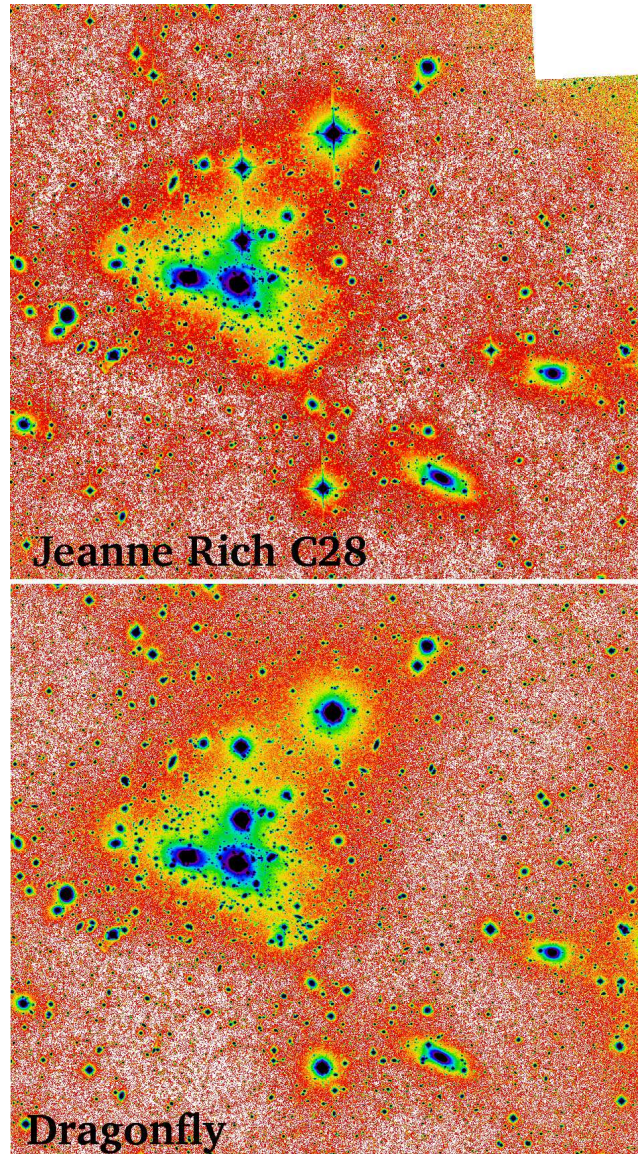


Figure 4.11: Image of the cluster of Coma galaxies obtained with the Jeanne Rich telescope (top panel) and the Dragonfly telephoto array (bottom panel), both in the  $g$  band. The field of view is  $1.5 \times 1.3$  degrees.

Este documento incorpora firma electrónica, y es copia auténtica de un documento electrónico archivado por la ULL según la Ley 39/2015.  
Su autenticidad puede ser contrastada en la siguiente dirección <https://sede.ull.es/validacion/>

Identificador del documento: 2260218 Código de verificación: Sm21pjYh

Firmado por: JAVIER ROMAN GARCIA  
UNIVERSIDAD DE LA LAGUNA

Fecha: 02/11/2019 16:23:59

IGNACIO TRUJILLO CABRERA  
UNIVERSIDAD DE LA LAGUNA

02/11/2019 17:39:19

4.3 Deep imaging with the Jeanne Rich telescope

CXXXV

excellent image quality of this telescope. Despite the presence of high luminosity stars adjacent to the core of the Coma cluster, no residual internal reflections are left in the final image, which contrasts with the strong internal reflections found in the Coma image obtained with the OGS telescope with just 1 hour of integration time compared to the 47 hours of integration time on the Jeanne Rich telescope.

The main goal in this ongoing analysis is the removal of the scattered light produced by the stars, allowing for the first time to reveal the true morphology of the intracluster light of the Coma cluster. At the date of presentation of this thesis, all the data have been taken, including the specific observations of the stars that will allow to obtain the PSF model of this telescope.

Este documento incorpora firma electrónica, y es copia auténtica de un documento electrónico archivado por la ULL según la Ley 39/2015.  
*Su autenticidad puede ser contrastada en la siguiente dirección <https://sede.ull.es/validacion/>*

Identificador del documento: 2260218 Código de verificación: Sm21pjYh

Firmado por: JAVIER ROMAN GARCIA  
UNIVERSIDAD DE LA LAGUNA

Fecha: 02/11/2019 16:23:59

IGNACIO TRUJILLO CABRERA  
UNIVERSIDAD DE LA LAGUNA

02/11/2019 17:39:19

## 5

### Summary and conclusions

In this thesis, an exhaustive study of the low surface brightness Universe has been carried out. Section 1.3 has shown the severe complications arising from the use of integrated photometry. For this reason, special emphasis has been placed on the study and correction of these important limitations in order to maximize the quality of astronomical data for its use in low surface brightness studies. In particular:

**Observational and processing of the data:** Reduction pipelines have been constructed for different astronomical facilities. These pipelines, along with specific observational strategies, have been applied to the OGS telescope at Izaña Observatory in Tenerife, T80 telescope at Javalambre Observatory in Teruel and Jeanne Rich telescope at Polaris Observatory in California. The results obtained through the application of the pipelines developed in this thesis have allowed to obtain high quality images by reducing the gradients in the images among other factors. It is worth commenting, that the images obtained from these telescopes, for example the Abell 2199 galaxy cluster coadd with the OGS telescope, the M101 galaxy coadd with the T80 telescope or the Coma galaxy cluster with the Jeanne Rich telescope, are the deepest images (in terms of surface brightness) obtained with these telescopes to date, and in turn, the deepest images of these objects by any previous work. In addition, data processing of the IAC Stripe82 Legacy Survey has been carried out, which has provided an improvement in the image quality of this data set.

**Point spread function:** Specific codes have been developed for obtaining PSF models. They have been successfully applied, obtaining PSF models for the 5 bands of the IAC Stripe Legacy Survey, for the *B*, *V* and *R* bands of the OGS telescope and for the *r* band of the T80 telescope. A very useful pipeline has also been developed to remove the scattered light produced by the stars in deep imaging automatically.

**Galactic cirri:** A comprehensive work has been carried out with the aim of performing a photometric characterization of the Galactic cirri. This work has revealed that the cirri colors in optical bands differ from the colors of extragalactic sources. The potential application of this result is very high. Currently, there is no approach to identify the presence of dust in ultra-deep images using optical data. If the results presented in this study are confirmed, it would be possible to use multiple optical bands for the detection and identification of cirri with much better resolution and depth than those provided by far IR data sets. This could have an important impact on future low surface brightness studies with the LSST.

CXXXVI

Este documento incorpora firma electrónica, y es copia auténtica de un documento electrónico archivado por la ULL según la Ley 39/2015.  
Su autenticidad puede ser contrastada en la siguiente dirección <https://sede.ull.es/validacion/>

Identificador del documento: 2260218 Código de verificación: Sm21pjYh

Firmado por: JAVIER ROMAN GARCIA  
UNIVERSIDAD DE LA LAGUNA

Fecha: 02/11/2019 16:23:59

IGNACIO TRUJILLO CABRERA  
UNIVERSIDAD DE LA LAGUNA

02/11/2019 17:39:19

Multiple tools have also been constructed for studying low surface brightness sources, including big data analysis for characterizing photometric and structural properties of extremely faint sources. They have been very effective for studying the so-called ultra-diffuse galaxies: galaxies with large effective radius ( $r_{eff} > 1.5$  kpc) and very low surface brightness ( $\mu_g(0) > 24$  mag arcsec<sup>-2</sup>). A summary of the results obtained in Section 3 for ultra-diffuse galaxies is:

- Detection of ultra-diffuse galaxies in large-scale structures. It resulted in the first evidence of the presence of ultra-diffuse galaxies outside galaxy clusters.
- By studying the spatial distribution of ultra-diffuse galaxies and their comparison with dwarf and MW-like galaxies, greater similarity was found in both spatial and color distribution with dwarf galaxies, suggesting the "dwarf nature" of ultra-diffuse galaxies.
- Analyzing a set of isolated groups, the presence of a population of blue ultra-diffuse galaxies with irregular morphology and young age was found. They are clear candidates for being progenitors of the red UDGs, which are older, with more roundish morphology and found in galaxy clusters. By extrapolating over time of the properties of these blue UDGs after quenching, the properties of the red UDGs were reproduced. It suggests a clear evolutionary path where environmental quenching plays a fundamental role.
- Extending the relationship suggested by van der Burg et al. (2016) between the host halo mass and the number of UDGs, showed that the correlation is slightly less than 1. It promotes the idea that UDGs are formed in low-density environments and are subsequently accreted to groups and clusters of galaxies hierarchically.
- The study of the nearby UGC 2162 galaxy allowed the first published detection of HI gas in ultra-diffuse galaxies. By using the width of the HI line it was possible to confirm that its total mass is typical of a dwarf galaxy, favoring the "dwarf nature" hypothesis for UDGs.
- By using the globular cluster luminosity function it was possible to estimate the distance to an ultra-diffuse galaxy. This galaxy is located in extremely low density environment. The distance was confirmed by deep spectroscopy from the GTC telescope and the reliability of this method was demonstrated for low surface brightness galaxies. This method has a huge potential in future ultra-deep surveys.

Multiple results have also been obtained using telescopes where we have got direct access, allowing to control all the steps, from the design of the observational strategy, the data acquisition and its reduction and final processing. Through the techniques developed in this thesis, great efficiency has been achieved in pushing the low surface brightness limits. The use of these telescopes has been crucial in providing a test field for applying the developed techniques. Some interesting results have been obtained, such as the detection of the extended light halos of the Coma galaxy cluster, the Abell 2199 galaxy cluster, the Perseus galaxy cluster and the IC1101 galaxy. These techniques have been also used to explore the galaxies in the line of sight of the NGC 1052 galaxy. It has also been detected what is likely the third satellite of the nearby NGC 4565 galaxy, a possible new satellite in the well studied M101 galaxy or the identification of ultra-diffuse galaxies in the Coma galaxy cluster, later explored by spectroscopic studies. Many of these results can be considered as future prospects and are expected to be published after the presentation of this thesis.

Este documento incorpora firma electrónica, y es copia auténtica de un documento electrónico archivado por la ULL según la Ley 39/2015.  
 Su autenticidad puede ser contrastada en la siguiente dirección <https://sede.ull.es/validacion/>

Identificador del documento: 2260218 Código de verificación: Sm21pjYh

Firmado por: JAVIER ROMAN GARCIA  
 UNIVERSIDAD DE LA LAGUNA

Fecha: 02/11/2019 16:23:59

IGNACIO TRUJILLO CABRERA  
 UNIVERSIDAD DE LA LAGUNA

02/11/2019 17:39:19

In conclusion, it can be said that this thesis has made significant contributions to the study of the low surface brightness Universe. All limitations in low surface brightness, such as the presence of gradients by the observational and reduction procedures of astronomical data, uncertainties due to PSF, the presence of Galactic cirri in deep observations and other aspects such as big data analysis or the problem of estimating distances, have been confronted in this thesis with significant improvements. We can conclude by saying that the work developed in this thesis has helped to push the surface brightness limits of optical integrated photometry.

Este documento incorpora firma electrónica, y es copia auténtica de un documento electrónico archivado por la ULL según la Ley 39/2015.  
*Su autenticidad puede ser contrastada en la siguiente dirección <https://sede.ull.es/validacion/>*

Identificador del documento: 2260218 Código de verificación: Sm21pjYh

Firmado por: JAVIER ROMAN GARCIA  
UNIVERSIDAD DE LA LAGUNA

Fecha: 02/11/2019 16:23:59

IGNACIO TRUJILLO CABRERA  
UNIVERSIDAD DE LA LAGUNA

02/11/2019 17:39:19

## Bibliography

- Abadi, M. G., Navarro, J. F., & Steinmetz, M. 2006, MNRAS, 365, 747
- Abazajian, K. N., Adelman-McCarthy, J. K., Agüeros, M. A., et al. 2009, ApJS, 182, 543-558
- Abraham, R. G., & van Dokkum, P. G. 2014, PASP, 126, 55
- Adelman-McCarthy, J. K., Agüeros, M. A., Allam, S. S., et al. 2007, ApJS, 172, 634
- Aihara, H., Arimoto, N., Armstrong, R., et al. 2018, PASJ, 70, S4
- Aihara, H., AlSayyad, Y., Ando, M., et al. 2019, arXiv e-prints, arXiv:1905.12221
- Akhlaghi, M., & Ichikawa, T. 2015, ApJS, 220, 1
- Alabi, A., Ferré-Mateu, A., Romanowsky, A. J., et al. 2018, MNRAS, 479, 3308
- Amorisco, N. C., & Loeb, A. 2016, MNRAS, 459, L51
- Amorisco, N. C., Monachesi, A., Agnello, A., et al. 2018, MNRAS, 475, 4235
- Annis, J., Soares-Santos, M., Strauss, M. A., et al. 2014, ApJ, 794, 120
- Arp, H. 1965, Science, 148, 363
- Arp, H., & Bertola, F. 1969, Astrophysical Letters, 4, 23.
- Arp, H., & Bertola, F. 1971, ApJ, 163, 195.
- Ashman, K. M., Conti, A., & Zepf, S. E. 1995, AJ, 110, 1164
- Barker, M. K., Ferguson, A. M. N., Irwin, M., et al. 2009, AJ, 138, 1469
- Barrena, R., Streblyanska, A., Ferragamo, A., et al. 2018, A&A, 616, A42.
- Beasley, M. A., Romanowsky, A. J., Pota, V., et al. 2016, ApJ, 819, L20
- Beasley, M. A., & Trujillo, I. 2016, ApJ, 830, 23
- Bechtol, K., Drlica-Wagner, A., Balbinot, E., et al. 2015, ApJ, 807, 50
- Bell, E. F., McIntosh, D. H., Katz, N., & Weinberg, M. D. 2003, ApJS, 149, 289
- Bellazzini, M., Belokurov, V., Magrini, L., et al. 2017, MNRAS, 467, 3751

CXXXIX

Este documento incorpora firma electrónica, y es copia auténtica de un documento electrónico archivado por la ULL según la Ley 39/2015.  
Su autenticidad puede ser contrastada en la siguiente dirección <https://sede.ull.es/validacion/>

Identificador del documento: 2260218 Código de verificación: Sm21pjYh

Firmado por: JAVIER ROMAN GARCIA  
UNIVERSIDAD DE LA LAGUNA

Fecha: 02/11/2019 16:23:59

IGNACIO TRUJILLO CABRERA  
UNIVERSIDAD DE LA LAGUNA

02/11/2019 17:39:19

CXL

BIBLIOGRAPHY

- Bennert, V. N., Auger, M. W., Treu, T., et al. 2011, ApJ, 742, 107
- Bennet, P., Sand, D. J., Crnojević, D., et al. 2017, ApJ, 850, 109
- Bertelli, G., Bressan, A., Chiosi, C., Fagotto, F., & Nasi, E. 1994, A&A, 106,
- Bertin, E., & Arnouts, S. 1996, AAPS, 117, 393
- Bertin, E., Mellier, Y., Radovich, M., et al. 2002, Astronomical Data Analysis Software and Systems XI, 281, 228
- Bertin, E. 2011, Astronomical Data Analysis Software and Systems XX, 442, 435
- Besla, G., Martínez-Delgado, D., van der Marel, R. P., et al. 2016, ApJ, 825, 20
- Bílek, M., Cuillandre, J.-C., Gwyn, S., et al. 2016, A&A, 588, A77
- Blanton, M. R., Lupton, R. H., Schlegel, D. J., et al. 2005, ApJ, 631, 208
- Boissier, S., Boselli, A., Voyer, E., et al. 2015, A&A, 579, A29
- Borlaff, A., Trujillo, I., Román, J., et al. 2019, A&A, 621, A133
- Bothun, G. D., Impey, C. D., Malin, D. F., et al. 1987, AJ, 94, 23.
- Bothun, G. D., Impey, C. D., & Malin, D. F. 1991, ApJ, 376, 404
- Brandt, T. D., & Draine, B. T. 2012, ApJ, 744, 129
- Bullock, J. S., & Johnston, K. V. 2005, ApJ, 635, 931
- Burkert, A., & Forbes, D. 2019, arXiv e-prints , arXiv:1901.00900.
- Burkholder, V., Impey, C., & Sprayberry, D. 2001, AJ, 122, 2318
- Buote, D. A. 2002, Merging Processes in Galaxy Clusters, 272, 79
- Cappellari, M. 2017, MNRAS, 466, 798
- Carleton, T., Errani, R., Cooper, M., et al. 2019, MNRAS, 485, 382
- Carlsten, S. G., Beaton, R. L., Greco, J. P., et al. 2019, ApJ, 879, 13
- Carlsten, S. G., Beaton, R. L., Greco, J. P., et al. 2019, ApJL, 878, L16
- Cebrián, M., & Trujillo, I. 2014, MNRAS, 444, 682
- Chan, T. K., Kereš, D., Wetzel, A., et al. 2018, MNRAS, 478, 906
- Chiboucas, K., Karachentsev, I. D., & Tully, R. B. 2009, AJ, 137, 3009
- Chiboucas, K., Jacobs, B. A., Tully, R. B., & Karachentsev, I. D. 2013, AJ, 146, 126
- Chilingarian, Igor V.; Melchior, Anne-Laure; Zolotukhin, Ivan Yu. 2010, MNRAS, 405, 1409

Este documento incorpora firma electrónica, y es copia auténtica de un documento electrónico archivado por la ULL según la Ley 39/2015.  
Su autenticidad puede ser contrastada en la siguiente dirección <https://sede.ull.es/validacion/>

Identificador del documento: 2260218 Código de verificación: Sm21pjYh

Firmado por: JAVIER ROMAN GARCIA  
UNIVERSIDAD DE LA LAGUNA

Fecha: 02/11/2019 16:23:59

IGNACIO TRUJILLO CABRERA  
UNIVERSIDAD DE LA LAGUNA

02/11/2019 17:39:19

BIBLIOGRAPHY

CXLI

- Cid Fernandes, R., Mateus, A., Sodr , L., Stasińska, G., & Gomes, J. M. 2005, MNRAS, 358, 363
- Comer n, S., Salo, H., & Knapen, J. H. 2018, A&A, 610, A5
- Conselice, C. J., Gallagher, J. S., III, & Wyse, R. F. G. 2003, AJ, 125, 66
- Cooper, A. P., Cole, S., Frenk, C. S., et al. 2010, MNRAS, 406, 744
- Cooper, A. P., Gao, L., Guo, Q., et al. 2015, MNRAS, 451, 2703
- Cortese, L., Bendo, G. J., Isaak, K. G., Davies, J. I., & Kent, B. R. 2010, MNRAS, 403, L26
- Crnojević, D., Sand, D. J., Caldwell, N., et al. 2014, ApJl, 795, L35
- Dalcanton, J. J., Spergel, D. N., Gunn, J. E., Schmidt, M., & Schneider, D. P. 1997, AJ, 114, 635
- Dark Energy Survey Collaboration, Abbott, T., Abdalla, F. B., et al. 2016, MNRAS, 460, 1270
- Davidge, T. J. 2009, ApJ, 697, 1439
- Davies, J. I., Wilson, C. D., Auld, R., et al. 2010, MNRAS, 409, 102
- de Jong, R. S. 2008, MNRAS, 388, 1521
- de Vaucouleurs, G. 1969, Astrophysical Letters, 4, 17.
- de Vries, C. P., & Le Poole, R. S. 1985, A&A, 145, L7
- de Mello, D. F., Smith, L. J., Sabbi, E., et al. 2008, AJ, 135, 548
- Da Rocha, C., & Mendes de Oliveira, C. 2005, MNRAS, 364, 1069
- Da Rocha, C., Ziegler, B. L., & Mendes de Oliveira, C. 2008, MNRAS, 388, 1433
- Das, S., Louis, T., Nolta, M. R., et al. 2014, JCAP, 4, 014
- Davies, J. I., Davies, L. J. M., & Keenan, O. C. 2016, MNRAS, 456, 1607
- Dekel, A., & Silk, J. 1986, ApJ, 303, 39
- DeVore, J. G., Kristl, J. A., & Rappaport, S. A. 2013, Journal of Geophysical Research (Atmospheres), 118, 5679
- Di Cintio, A., Brook, C. B., Dutton, A. A., et al. 2017, MNRAS, 466, L1
- Disney, M. J. 1976, Nature, 263, 573.
- D’Onghia, E., Besla, G., Cox, T. J., et al. 2009, NAT, 460, 605.
- Drlica-Wagner, A., Bechtol, K., Rykoff, E. S., et al. 2015, ApJ, 813, 109
- Drinkwater, M. J., Gregg, M. D., & Colless, M. 2001, ApJl, 548, L139

Este documento incorpora firma electr nica, y es copia aut ntica de un documento electr nico archivado por la ULL seg n la Ley 39/2015.  
Su autenticidad puede ser contrastada en la siguiente direcci n <https://sede.ull.es/validacion/>

Identificador del documento: 2260218 C digo de verificaci n: Sm21pjYh

Firmado por: JAVIER ROMAN GARCIA  
UNIVERSIDAD DE LA LAGUNA

Fecha: 02/11/2019 16:23:59

IGNACIO TRUJILLO CABRERA  
UNIVERSIDAD DE LA LAGUNA

02/11/2019 17:39:19

- Duc, P.-A., Cuillandre, J.-C., Karabal, E., et al. 2015, MNRAS, 446, 120
- Duc, P.-A., Cuillandre, J.-C., & Renaud, F. 2018, MNRAS, 475, L40.
- Durrell, P. R., Côté, P., Peng, E. W., et al. 2014, ApJ, 794, 103
- Elvey, C. T., & Roach, F. E. 1937, ApJ, 85, 213
- Erwin, P. 2015, ApJ, 799, 226
- Fakhouri, O., Ma, C.-P., & Boylan-Kolchin, M. 2010, MNRAS, 406, 2267
- Falcón-Barroso, J., Sánchez-Blázquez, P., Vazdekis, A., et al. 2011, A&A, 532, A95
- Fall, S. M., & Efstathiou, G. 1980, MNRAS, 193, 189
- Fensch, J., van der Burg, R. F. J., Jeřábková, T., et al. 2019, A&A, 625, A77
- Ferguson, H. C., & Sandage, A. 1988, AJ, 96, 1520
- Ferrarese, L., Ford, H. C., Huchra, J., et al. 2000, ApJs, 128, 431
- Ferrarese, L., Côté, P., Cuillandre, J.-C., et al. 2012, ApJS, 200, 4
- Ferré-Mateu, A., Alabi, A., Forbes, D. A., et al. 2018, MNRAS, 479, 4891
- Fliri, J., & Trujillo, I. 2016, MNRAS, 456, 1359
- Forbes, D. A. 2017, MNRAS, 472, L104
- Fuse, C., Marcum, P., & Fanelli, M. 2012, AJ, 144, 57
- Galaz, G., Herrera-Camus, R., Garcia-Lambas, D., & Padilla, N. 2011, ApJ, 728, 74
- Georgiev, I. Y., Puzia, T. H., Hilker, M., & Goudfrooij, P. 2009, MNRAS, 392, 879
- Gu, M., Conroy, C., Law, D., et al. 2018, ApJ, 859, 37
- Giallongo, E., Menci, N., Grazian, A., et al. 2014, ApJ, 781, 24
- Girardi, M., Biviano, A., Giuricin, G., Mardirossian, F., & Mezzetti, M. 1993, ApJ, 404, 38
- Girardi, M., & Biviano, A. 2002, Merging Processes in Galaxy Clusters, 272, 39
- Greco, J. P., Greene, J. E., Strauss, M. A., et al. 2018, ApJ, 857, 104
- Greco, J. P., Goulding, A. D., Greene, J. E., et al. 2018, ApJ, 866, 112
- Guhathakurta, P., & Tyson, J. A. 1989, ApJ, 346, 773
- Hanes, D. A. 1977, MNRAS, 180, 309
- Harris, W. E. 1996, AJ, 112, 1487
- Heney, L. G., & Greenstein, J. L. 1941, ApJ, 93, 70

Este documento incorpora firma electrónica, y es copia auténtica de un documento electrónico archivado por la ULL según la Ley 39/2015.  
Su autenticidad puede ser contrastada en la siguiente dirección <https://sede.ull.es/validacion/>

Identificador del documento: 2260218 Código de verificación: Sm21pjYh

Firmado por: JAVIER ROMAN GARCIA  
UNIVERSIDAD DE LA LAGUNA

Fecha: 02/11/2019 16:23:59

IGNACIO TRUJILLO CABRERA  
UNIVERSIDAD DE LA LAGUNA

02/11/2019 17:39:19

BIBLIOGRAPHY

CXLIII

- Hess, K. M., Cluver, M. E., Yahya, S., et al. 2017, MNRAS, 464, 957
- Hickson, P. 1982, ApJ, 255, 382
- Hickson, P., Mendes de Oliveira, C., Huchra, J. P., & Palumbo, G. G. 1992, ApJ, 399, 353
- Hodges-Kluck, E., & Bregman, J. N. 2014, ApJ, 789, 131
- Homma, D., Chiba, M., Okamoto, S., et al. 2016, ApJ, 832, 21
- Homma, D., Chiba, M., Okamoto, S., et al. 2018, PASJ, 70, S18
- Homma, D., Chiba, M., Komiyama, Y., et al. 2019, arXiv e-prints, arXiv:1906.07332
- Ibata, R., Martin, N. F., Irwin, M., et al. 2007, ApJ, 671, 1591
- Ibata, R., Mouhcine, M., & Rejkuba, M. 2009, MNRAS, 395, 126
- Ibata, R. A., Lewis, G. F., McConnachie, A. W., et al. 2014, ApJ, 780, 128
- Ienaka, N., Kawara, K., Matsuoka, Y., et al. 2013, ApJ, 767, 80
- Impey, C., Bothun, G., & Malin, D. 1988, ApJ, 330, 634
- Infante-Saiz, R., Trujillo I., Román J., 2019, in preparation.
- Jacoby, G. H., Branch, D., Ciardullo, R., et al. 1992, PASP, 104, 599
- Javanmardi, B., Martinez-Delgado, D., Kroupa, P., et al. 2016, A&A, 588, A89
- Jiang, L., Fan, X., Annis, J., et al. 2008, AJ, 135, 1057
- Jiang, L., Fan, X., Bian, F., et al. 2014, ApJS, 213, 12
- Jiang, F., Dekel, A., Freundlich, J., et al. 2019, MNRAS, 1490
- Johnston, K. V., Bullock, J. S., Sharma, S., et al. 2008, ApJ, 689, 936-957
- Jones, M. G., Papastergis, E., Pandya, V., et al. 2018, A&A, 614, A21.
- Jordán, A., McLaughlin, D. E., Côté, P., et al. 2007, ApJs, 171, 101
- Kadowaki, J., Zaritsky, D., & Donnerstein, R. L. 2017, ApJL, 838, L21
- Karabal, E., Duc, P.-A., Kuntschner, H., et al. 2017, A&A, 601, A86
- Kazantzidis, S., Łokas, E. L., Callegari, S., Mayer, L., & Moustakas, L. A. 2011, ApJ, 726, 98
- Kelson, D. D. 2003, PASP, 115, 688
- Kim, D., Jerjen, H., Milone, A. P., et al. 2015, ApJ, 803, 63
- Kim, D., & Jerjen, H. 2015, ApJL, 808, L39

Este documento incorpora firma electrónica, y es copia auténtica de un documento electrónico archivado por la ULL según la Ley 39/2015.  
Su autenticidad puede ser contrastada en la siguiente dirección <https://sede.ull.es/validacion/>

Identificador del documento: 2260218 Código de verificación: Sm21pjYh

Firmado por: JAVIER ROMAN GARCIA  
UNIVERSIDAD DE LA LAGUNA

Fecha: 02/11/2019 16:23:59

IGNACIO TRUJILLO CABRERA  
UNIVERSIDAD DE LA LAGUNA

02/11/2019 17:39:19

- Kim, S., Peter, A., & Hargis, J. 2019, American Astronomical Society Meeting Abstracts #233  
233, 439.02
- Klypin, A., Kravtsov, A. V., Valenzuela, O., & Prada, F. 1999, ApJ, 522, 82
- Koda, J., Yagi, M., Yamanoi, H., et al. 2015, ApJL, 807, L2
- Koposov, S. E., Belokurov, V., Torrealba, G., et al. 2015, ApJ, 805, 130
- Kormendy, J., & Bahcall, J. N. 1974, AJ, 79, 671.
- Kroupa, Pavel. 2001, MNRAS,322,231
- Laevens, B. P. M., Martin, N. F., Sesar, B., et al. 2014, ApJL, 786, L3
- Laevens, B. P. M., Martin, N. F., Bernard, E. J., et al. 2015, ApJ, 813, 44
- Laevens, B. P. M., Martin, N. F., Ibata, R. A., et al. 2015, ApJL, 802, L18
- Lagattuta, D. J., Mould, J. R., Staveley-Smith, L., et al. 2013, ApJ, 771, 88
- Lamarre, J. M., Puget, J. L., Bouchet, F., et al. 2003, NAR, 47, 1017
- Laureijs, R. J., Mattila, K., & Schmur, G. 1987, A&A, 184, 269
- Lee, M. G., Freedman, W. L., & Madore, B. F. 1993, ApJ, 417, 553
- Lee, M. G., Kang, J., Lee, J. H., & Jang, I. S. 2017, ApJ, 844, 157
- Leisman, L., Haynes, M. P., Janowiecki, S., et al. 2017, ApJ, 842, 133
- Levenson, L., Marsden, G., Zmcov, M., et al. 2010, MNRAS, 409, 83
- Lim, S., Peng, E. W., Côté, P., et al. 2018, ApJ, 862, 82
- Liu, C., Peng, E. W., Côté, P., et al. 2015, ApJ, 812, 34
- Liao, S., Gao, L., Frenk, C. S., et al. 2019, arXiv e-prints, arXiv:1904.06356
- Lopes de Oliveira, R.; Carrasco, E. R.; Mendes de Oliveira, C.; Bortoletto, D. R.; Cypriano, E.;  
Sodr, L., Jr.; Lima Neto, G. B. 2010, ApJ,139,L216
- Low, F. J., Young, E., Beintema, D. A., et al. 1984, ApJL, 278, L19
- LSST Science Collaboration, Abell, P. A., Allison, J., et al. 2009, arXiv:0912.0201
- Lu, T., Luo, W., Zhang, J., et al. 2018, AJ, 156, 14.
- Ma, X.-. song ., Herbst, T., Scheidl, T., et al. 2012, arXiv e-prints, arXiv:1205.3909
- Madau, P., Diemand, J., & Kuhlen, M. 2008, ApJ, 679, 1260-1271
- Makarova, L. N., Grebel, E. K., Karachentsev, I. D., et al. 2002, A&A, 396, 473

Este documento incorpora firma electrónica, y es copia auténtica de un documento electrónico archivado por la ULL según la Ley 39/2015.  
Su autenticidad puede ser contrastada en la siguiente dirección <https://sede.ull.es/validacion/>

Identificador del documento: 2260218 Código de verificación: Sm21pjYh

Firmado por: JAVIER ROMAN GARCIA  
UNIVERSIDAD DE LA LAGUNA

Fecha: 02/11/2019 16:23:59

IGNACIO TRUJILLO CABRERA  
UNIVERSIDAD DE LA LAGUNA

02/11/2019 17:39:19

BIBLIOGRAPHY

CXLV

- Mancera Piña, P. E., Peletier, R. F., Aguerri, J. A. L., et al. 2018, MNRAS, 481, 4381  
Mancera Piña, P. E., Aguerri, J. A. L., Peletier, R. F., et al. 2019, MNRAS, 241.  
Martin, N. F., Ibata, R. A., Irwin, M. J., et al. 2006, MNRAS, 371, 1983  
Martin, N. F., Ibata, R. A., Rich, R. M., et al. 2014, ApJ, 787, 19  
Martín-Navarro, I., Romanowsky, A. J., Brodie, J. P., et al. 2019, MNRAS, 484, 3425.  
Martínez-Delgado, D., Peñarrubia, J., Gabany, R. J., et al. 2008, ApJ, 689, 184  
Martínez-Delgado, D., Gabany, R. J., Crawford, K., et al. 2010, AJ, 140, 962  
Martínez-Delgado, D., Läsker, R., Sharina, M., et al. 2016, AJ, 151, 96  
Martínez-Delgado, D., Grebel, E. K., Javanmardi, B., et al. 2018, A&A, 620, A126  
Mattila, K. 1979, A&A, 78, 253  
McGaugh, S. S., & Bothun, G. D. 1994, AJ, 107, 530  
McConnachie, A. W., Huxor, A., Martin, N. F., et al. 2008, ApJ, 688, 1009  
McConnachie, A. W., Irwin, M. J., Ibata, R. A., et al. 2009, NAT, 461, 66  
McConnachie, A. W. 2012, AJ, 144, 4  
McConnachie, A. W., Ibata, R., Martin, N., et al. 2018, ApJ, 868, 55  
McMonigal, B., Bate, N. F., Conn, A. R., et al. 2016, MNRAS, 456, 405  
Merritt, A., van Dokkum, P., Danieli, S., et al. 2016, ApJ, 833, 168  
Merritt, A., van Dokkum, P., Abraham, R., et al. 2016, ApJ, 830, 62  
Mihos, C. 2003, arXiv:astro-ph/0305512  
Mihos, J. C., Harding, P., Feldmeier, J., & Morrison, H. 2005, ApJL, 631, L41  
Mihos, J. C., Durrell, P. R., Ferrarese, L., et al. 2015, ApJ, 809, L21  
Mihos, J. C., Harding, P., Feldmeier, J. J., et al. 2017, ApJ, 834, 16  
Mihos, J. C., Carr, C. T., Watkins, A. E., Oosterloo, T., & Harding, P. 2018, ApJL, 863, L7  
Miville-Deschênes, M.-A., & Lagache, G. 2005, ApJS, 157, 302  
Mo, H. J., Mao, S., & White, S. D. M. 1998, MNRAS, 295, 319  
Monelli, M., & Trujillo, I. 2019, ApJL, 880, L11  
Monet, D. G., Levine, S. E., Canzian, B., et al. 2003, AJ, 125, 984  
Montes, M., & Trujillo, I. 2014, ApJ, 794, 137.

Este documento incorpora firma electrónica, y es copia auténtica de un documento electrónico archivado por la ULL según la Ley 39/2015.  
Su autenticidad puede ser contrastada en la siguiente dirección <https://sede.ull.es/validacion/>

Identificador del documento: 2260218 Código de verificación: Sm21pjYh

Firmado por: JAVIER ROMAN GARCIA  
UNIVERSIDAD DE LA LAGUNA

Fecha: 02/11/2019 16:23:59

IGNACIO TRUJILLO CABRERA  
UNIVERSIDAD DE LA LAGUNA

02/11/2019 17:39:19

- Montes, M., & Trujillo, I. 2018, MNRAS, 474, 917
- Moore, B., Ghigna, S., Governato, F., et al. 1999, ApJL, 524, L19
- Müller, O., Rich, R. M., Román, J., et al. 2019, A&A, 624, L6
- Munari, E., Biviano, A., Borgani, S., Murante, G., & Fabjan, D. 2013, MNRAS, 430, 2638
- Muñoz, R. P., Eigenthaler, P., Puzia, T. H., et al. 2015, ApJL, 813, L15
- Muñoz, R. R., Côté, P., Santana, F. A., et al. 2018, ApJ, 860, 66
- Müller, O., Jerjen, H., & Binggeli, B. 2017, A&A, 597, A7
- Muslimov, E., Valls-Gabaud, D., Lemaître, G., et al. 2017, AO, 56,
- Nishiura, S., Murayama, T., Shimada, M., et al. 2000, AJ, 120, 2355
- Ocvirk, P., Pichon, C., Lançon, A., & Thiébaud, E. 2006, MNRAS, 365, 74
- Okamoto, S., Arimoto, N., Ferguson, A. M. N., et al. 2015, ApJL, 809, L1
- Ordenes-Briceño, Y., Taylor, M. A., Puzia, T. H., et al. 2016, MNRAS, 463, 1284
- Pan, D. C., Vogeley, M. S., Hoyle, F., Choi, Y.-Y., & Park, C. 2012, MNRAS, 421, 926
- Pandya, V., Romanowsky, A. J., Laine, S., et al. 2018, ApJ, 858, 29
- Papastergis, E., Adams, E. A. K., & Romanowsky, A. J. 2017, A&A, 601, L10
- Peacock, M. B., Strader, J., Romanowsky, A. J., & Brodie, J. P. 2015, ApJ, 800, 13
- Peng, E. W., & Lim, S. 2016, ApJ, 822, L31
- Penny, S. J., Brown, M. J. I., Pimblet, K. A., et al. 2015, MNRAS, 453, 3519
- Pilbratt, G. L., Riedinger, J. R., Passvogel, T., et al. 2010, A&A, 518, L1
- Planck Collaboration, Ade, P. A. R., Aghanim, N., et al. 2011, A&A, 536, A19
- Prole, D. J., Davies, J. I., Keenan, O. C., et al. 2018, MNRAS, 478, 667
- Prole, D. J., van der Burg, R. F. J., Hilker, M., et al. 2019, MNRAS, 488, 2143
- Pompei, E., & Iovino, A. 2012, A&A, 539, A106
- Ponman, T. J., Bourner, P. D. J., Ebeling, H., & Böhringer, H. 1996, MNRAS, 283, 690
- Racine, R. 1968, JARSC, 62, 367
- Radburn-Smith, D. J., de Jong, R. S., Seth, A. C., et al. 2011, ApJS, 195, 18
- Ramírez-Moreta, P., Verdes-Montenegro, L., Blasco-Herrera, J., et al. 2018, A&A, 619, A163.
- Read, J. I., & Erkal, D. 2019, MNRAS, 1615

Este documento incorpora firma electrónica, y es copia auténtica de un documento electrónico archivado por la ULL según la Ley 39/2015.  
Su autenticidad puede ser contrastada en la siguiente dirección <https://sede.ull.es/validacion/>

Identificador del documento: 2260218 Código de verificación: Sm21pjYh

Firmado por: JAVIER ROMAN GARCIA  
UNIVERSIDAD DE LA LAGUNA

Fecha: 02/11/2019 16:23:59

IGNACIO TRUJILLO CABRERA  
UNIVERSIDAD DE LA LAGUNA

02/11/2019 17:39:19

BIBLIOGRAPHY

CXLVII

- Reines, A. E., & Volonteri, M. 2015, ApJ, 813, 82  
Reis, Ribamar R. R. et al. 2012, 2012ApJ...747...59R  
Rejkuba, M. 2012, A&A, 341, 195  
Richtler, T. 2003, Stellar Candles for the Extragalactic Distance Scale, 635, 281  
Roediger, J. C., & Courteau, S. 2015, MNRAS, 452, 3209  
Román, J., & Trujillo, I. 2017, MNRAS, 468, 703  
Román, J., & Trujillo, I. 2017, MNRAS, 468, 4039  
Román, J., & Trujillo, I. 2018, Research Notes of the American Astronomical Society, 2, 144  
Rosenbaum, S. D., Krusch, E., Bomans, D. J., & Dettmar, R.-J. 2009, A&A, 504, 807  
Rudick, C. S., Mihos, J. C., Harding, P., et al. 2010, ApJ, 720, 569  
Ruiz-Lara, T., Beasley, M. A., Falcón-Barroso, J., et al. 2018, MNRAS, 478, 2034  
Ruiz-Lara, T., Gallart, C., Beasley, M., et al. 2018, A&A, 617, A18  
Sánchez Almeida, J., Olmo-García, A., Elmegreen, B. G., et al. 2018, ApJ, 869, 40  
Sánchez-Janssen, R., Ferrarese, L., MacArthur, L. A., et al. 2016, ApJ, 820, 69  
Sand, D. J., Crnojević, D., Strader, J., et al. 2014, ApJL, 793, L7  
Sandage, A. 1968, ApJL, 152, L149  
Sandage, A. 1976, AJ, 81, 954  
Sandage, A., & Binggeli, B. 1984, AJ, 89, 919.  
Sandin, C. 2014, A&A, 567, A97  
Sandin, C. 2015, A&A, 577, A106  
Schlafly, E. F., & Finkbeiner, D. P. 2011, ApJ, 737, 103  
Schombert, J. M., & Bothun, G. D. 1988, AJ, 95, 1389.  
Sersic, J. L. 1968, Cordoba, Argentina: Observatorio Astronomico, 1968  
Seth, A. C., Dalcanton, J. J., & de Jong, R. S. 2005, AJ, 130, 1574  
Sifón, C., Hoekstra, H., Cacciato, M., et al. 2015, A&A, 575, A48  
Slater, C. T., Harding, P., & Mihos, J. C. 2009, PASP, 121, 1267  
Smith, R., Davies, J. I., & Nelson, A. H. 2010, MNRAS, 405, 1723  
Smith, R., Sánchez-Janssen, R., Beasley, M. A., et al. 2015, MNRAS, 454, 2502

Este documento incorpora firma electrónica, y es copia auténtica de un documento electrónico archivado por la ULL según la Ley 39/2015.  
Su autenticidad puede ser contrastada en la siguiente dirección <https://sede.ull.es/validacion/>

Identificador del documento: 2260218 Código de verificación: Sm21pjYh

Firmado por: JAVIER ROMAN GARCIA  
UNIVERSIDAD DE LA LAGUNA

Fecha: 02/11/2019 16:23:59

IGNACIO TRUJILLO CABRERA  
UNIVERSIDAD DE LA LAGUNA

02/11/2019 17:39:19

- Smith Castelli, A. V., Faifer, F. R., & Escudero, C. G. 2016, A&A, 596, A23
- Sollima, A., Gil de Paz, A., Martínez-Delgado, D., et al. 2010, A&A, 516, A83
- Spekkens, K., & Karunakaran, A. 2018, ApJ, 855, 28
- Springel, V., Wang, J., Vogelsberger, M., et al. 2008, MNRAS, 391, 1685
- Springob, C. M., Magoulas, C., Colless, M., et al. 2014, MNRAS, 445, 2677
- Struble, M. F., & Rood, H. J. 1991, ApJs, 77, 363
- Tammann, G. A., & Sandage, A. 1999, Harmonizing Cosmic Distance Scales in a Post-HIPPARCOS Era, 167, 204
- Tanaka, M., Chiba, M., Komiyama, Y., Guhathakurta, P., & Kalirai, J. S. 2011, ApJ, 738, 150
- Thacker, C., Cooray, A., Smidt, J., et al. 2013, ApJ, 768, 58
- Toloba, E., Lim, S., Peng, E., et al. 2018, ApJl, 856, L31
- Tonry, J., & Davis, M. 1979, AJ, 84, 1511
- Torrealba, G., Kozlov, S. E., Belokurov, V., et al. 2016, MNRAS, 463, 712
- Torrealba, G., Belokurov, V., Kozlov, S. E., et al. 2018, MNRAS, 475, 5085
- Tovmassian, H., Plionis, M., & Torres-Papaqui, J. P. 2006, A&A, 456, 839
- Trujillo, I., & Fliri, J. 2016, ApJ, 823, 123
- Trujillo, I., Roman, J., Filho, M., et al. 2017, ApJ, 836, 191
- Trujillo, I., Beasley, M. A., Borlaff, A., et al. 2019, MNRAS, 486, 1192
- Tully, R. B., Courtois, H. M., & Sorce, J. G. 2016, AJ, 152, 50.
- Uson, J. M., Boughn, S. P., & Kuhn, J. R. 1991, ApJ, 369, 46
- van den Bergh, S., Pritchet, C., & Grillmair, C. 1985, AJ, 90, 595
- van der Burg, R. F. J., Muzzin, A., & Hoekstra, H. 2016, A&A, 590, A20
- van Dokkum, P. G., Abraham, R., & Merritt, A. 2014, ApJL, 782, L24
- van Dokkum, P. G., Abraham, R., Merritt, A., et al. 2015, ApJL, 798, L45
- van Dokkum, P. G.; Romanowsky, A. J.; Abraham, R.; Brodie, J. P.; Conroy, C.; Geha, M.; Merritt, A.; Villaume, A.; Zhang, J. 2015, ApJ, 804, L26
- van Dokkum, P., Abraham, R., Brodie, J., et al. 2016, ApJl, 828, L6
- van Dokkum, P., Abraham, R., Romanowsky, A. J., et al. 2017, ApJl, 844, L11

Este documento incorpora firma electrónica, y es copia auténtica de un documento electrónico archivado por la ULL según la Ley 39/2015.  
Su autenticidad puede ser contrastada en la siguiente dirección <https://sede.ull.es/validacion/>

Identificador del documento: 2260218 Código de verificación: Sm21pjYh

Firmado por: JAVIER ROMAN GARCIA  
UNIVERSIDAD DE LA LAGUNA

Fecha: 02/11/2019 16:23:59

IGNACIO TRUJILLO CABRERA  
UNIVERSIDAD DE LA LAGUNA

02/11/2019 17:39:19

BIBLIOGRAPHY

CXLIX

- van Dokkum, P., Danieli, S., Cohen, Y., et al. 2018, NAT, 555, 629
- van Dokkum, P., Danieli, S., Abraham, R., et al. 2019, ApJL, 874, L5
- Valls-Gabaud, D., & MESSIER Collaboration 2017, Formation and Evolution of Galaxy Outskirts, 321, 199
- Vazdekis, A., Casuso, E., Peletier, R. F., & Beckman, J. E. 1996, ApJS, 106, 307
- Vazdekis, A., Sánchez-Blázquez, P., Falcón-Barroso, J., et al. 2010, MNRAS, 404, 1639
- Vazdekis, A., Coelho, P., Cassisi, S., et al. 2015, MNRAS, 449, 1177
- Vazdekis, A., Koleva, M., Ricciardelli, E., Röck, B., & Falcón-Barroso, J. 2016, MNRAS, 463, 3409
- Veneziani, M., Ade, P. A. R., Bock, J. J., et al. 2010, ApJ, 713, 959
- Venhola, A., Peletier, R., Laurikainen, E., et al. 2017, A&A, 608, A142
- Viero, M. P., Wang, L., Zemcov, M., et al. 2013, ApJ, 772, 77
- Viero, M. P., Asboth, V., Roseboom, I. G., et al. 2014, ApJS, 210, 22
- Villegas, D., Jordán, A., Peng, E. W., et al. 2010, ApJ, 717, 603
- Vollmer, B., Perret, B., Petremand, M., et al. 2013, AJ, 145, 36
- Watkins, A. E., Mihos, J. C., Harding, P., et al. 2014, ApJ, 791, 38.
- Watkins, A. E., Mihos, J. C., & Harding, P. 2015, ApJ, 800, L3.
- Watkins, A. E., Mihos, J. C., & Harding, P. 2016, ApJ, 826, 59
- Watkins, A. E., Mihos, J. C., & Harding, P. 2017, ApJ, 851, 51.
- Watkins, A. E., Mihos, J. C., Bershady, M., et al. 2018, ApJ, 858, L16.
- Weinmann, S. M., van den Bosch, F. C., Yang, X., & Mo, H. J. 2006, MNRAS, 366, 2
- White, P. M., Bothun, G., Guerrero, M. A., West, M. J., & Barkhouse, W. A. 2003, ApJ, 585, 739
- Willman, B. 2010, Advances in Astronomy, 2010, 285454
- Whitmore, B. C. 1997, in "The extragalactic distance scale", M. Livio, M. Donahue and N. Panagia (eds) (Cambridge: Cambridge University Press), p. 254
- Witt, A. N., Friedmann, B. C., & Sasseeen, T. P. 1997, ApJ, 481, 809
- Witt, A. N., Mandel, S., Sell, P. H., Dixon, T., & Vijh, U. P. 2008, ApJ, 679, 497
- Yang, Y., Zhou, X., Yuan, Q., et al. 2004, ApJ, 600, 141

Este documento incorpora firma electrónica, y es copia auténtica de un documento electrónico archivado por la ULL según la Ley 39/2015.  
Su autenticidad puede ser contrastada en la siguiente dirección <https://sede.ull.es/validacion/>

Identificador del documento: 2260218 Código de verificación: Sm21pjYh

Firmado por: JAVIER ROMAN GARCIA  
UNIVERSIDAD DE LA LAGUNA

Fecha: 02/11/2019 16:23:59

IGNACIO TRUJILLO CABRERA  
UNIVERSIDAD DE LA LAGUNA

02/11/2019 17:39:19

CL

BIBLIOGRAPHY

- York, D. G., Adelman, J., Anderson, J. E., et al. 2000, AJ, 120, 1579
- Yozin, C., & Bekki, K. 2015, MNRAS, 452, 937
- Yozin, C., & Bekki, K. 2015, MNRAS, 453, 14
- Zackrisson, E., de Jong, R. S., & Micheva, G. 2012, MNRAS, 421, 190
- Zaritsky, D. 2017, MNRAS, 464, L110
- Zaritsky, D., Donnerstein, R., Dey, A., et al. 2019, ApJS, 240, 1
- Zhang, H.-X., Peng, E. W., Côté, P., et al. 2015, ApJ, 802, 30

Este documento incorpora firma electrónica, y es copia auténtica de un documento electrónico archivado por la ULL según la Ley 39/2015.  
Su autenticidad puede ser contrastada en la siguiente dirección <https://sede.ull.es/validacion/>

Identificador del documento: 2260218 Código de verificación: Sm21pjYh

Firmado por: JAVIER ROMAN GARCIA  
UNIVERSIDAD DE LA LAGUNA

Fecha: 02/11/2019 16:23:59

IGNACIO TRUJILLO CABRERA  
UNIVERSIDAD DE LA LAGUNA

02/11/2019 17:39:19

# A

## Publications during this thesis

1. The Sloan Digital Sky Survey extended Point Spread Functions. Infante-Saiz, R.; Román, J.; Trujillo, I. Submitted at thesis presentation date.
2. Galactic cirri in deep optical imaging. Román, Javier; Trujillo, Ignacio; Montes, Mireia. arXiv:1907.00978. Submitted to MNRAS.
3. Stellar content, planetary nebulae, and globular clusters of [KKS2000]04 (NGC1052-DF2). Ruiz-Lara, T.; Trujillo, I.; Beasley, M. A. et al. 2019MNRAS.486.5670R
4. Discovery of a red ultra-diffuse galaxy in a nearby void based on its globular cluster luminosity function. Román, J.; Beasley, M. A.; Valls-Gabaud D.; Ruiz-Lara, T. 2019, MNRAS, 486, 823R
5. A tidal tale: detection of several stellar streams in the environment of NGC 1052. Müller, O., Rich, R. M., Román, J., et al. A&A, 624 (2019) L6
6. A distance of 13 Mpc resolves the claimed anomalies of the galaxy lacking dark matter. Trujillo, I., Beasley, M. A., Borlaff, A., et al. 2019, MNRAS, 733
7. The missing light of the Hubble Ultra Deep Field. Borlaff, a.; Trujillo, I. ; Román, J.; et al. 2019 A&A, 621A, 133B
8. A headless tadpole galaxy: the high gas-phase metallicity of the ultra-diffuse galaxy UGC 2162. Sánchez Almeida, J., Olmo-García, A., Elmegreen, B. G., et al. ApJ, 869, 40S (2018)
9. The IAC Stripe82 Legacy Survey: Improved Sky-rectified Images. Román, Javier & Trujillo, Ignacio. 2018, Research Notes of the American Astronomical Society, 2, 144
10. Spectroscopic characterisation of the stellar content of ultra diffuse galaxies. Ruiz-Lara, T.; Beasley, M. A.; Falcón-Barroso, J.; Román, J; et al. MNRAS, 478, 2034R (2018)
11. The nearest ultra diffuse galaxy. Trujillo, Ignacio; Román, Javier; Filho, Mercedes & Sánchez Almeida, Jorge. ApJ, 836, 191 (2017)
12. Ultra diffuse galaxies outside clusters: clues to their formation and evolution. Román, Javier & Trujillo, Ignacio. MNRAS, 468, 4039 (2017)

CLI

Este documento incorpora firma electrónica, y es copia auténtica de un documento electrónico archivado por la ULL según la Ley 39/2015.  
Su autenticidad puede ser contrastada en la siguiente dirección <https://sede.ull.es/validacion/>

Identificador del documento: 2260218 Código de verificación: Sm21pjYh

Firmado por: JAVIER ROMAN GARCIA  
UNIVERSIDAD DE LA LAGUNA

Fecha: 02/11/2019 16:23:59

IGNACIO TRUJILLO CABRERA  
UNIVERSIDAD DE LA LAGUNA

02/11/2019 17:39:19

CLII

Chapter A. Publications during this thesis

13. Spatial distribution of ultra-diffuse galaxies within large-scale structures. Román, Javier & Trujillo, Ignacio. MNRAS, 468, 703 (2017)

Este documento incorpora firma electrónica, y es copia auténtica de un documento electrónico archivado por la ULL según la Ley 39/2015.  
*Su autenticidad puede ser contrastada en la siguiente dirección <https://sede.ull.es/validacion/>*

Identificador del documento: 2260218 Código de verificación: Sm21pjYh

Firmado por: JAVIER ROMAN GARCIA  
UNIVERSIDAD DE LA LAGUNA

Fecha: 02/11/2019 16:23:59

IGNACIO TRUJILLO CABRERA  
UNIVERSIDAD DE LA LAGUNA

02/11/2019 17:39:19

## B

### Oral contributions in conferences during this thesis

1. **Contributed talk.** Román, J., Trujillo, I. & Montes M. "Galactic cirri in deep optical imaging". IAU Symposium 355: The Realm of the Low Surface Brightness Universe. July 2019, Tenerife, Spain.
2. **Contributed talk.** Román, Javier & Borlaff, Alejandro. "The ultra-low surface brightness Universe as counterpart to SKA detections". Spain in SKA!. June 2019, Granada, Spain.
3. **Contributed talk.** Román, Javier. "A possible link between irregular blue dwarfs and UDGs. (And distances to UDGs)". The Bewildering Nature of Ultra-diffuse Galaxies. August 2018, Leiden, Holland.
4. **Contributed talk.** Román, Javier. "Pushing the low surface brightness limits: PSF and dust characterization". Stellar Halos across the Cosmos. July 2018, Heidelberg, Germany.
5. **Invited review.** Román, Javier. "What do we know about ultra-diffuse galaxies?". Invited review at European Week of Astronomy and Space Science (EWASS) 2018. 3rd April 2018, Liverpool, England.
6. **Contributed talk.** Román, Javier. "Exploring low surface brightness with a space debris dedicated telescope". Exploring the Ultra-Low Surface Brightness Universe, Second meeting. ISSI International Team led by David Valls-Gabaud. November 2017, Bern, Switzerland.
7. **Contributed talk.** Román, Javier. "Pushing the surface brightness limits: PSF and dust characterization". Exploring the Ultra-Low Surface Brightness Universe, First meeting. ISSI International Team led by David Valls-Gabaud. January 2017, Bern, Switzerland.

CLIII

Este documento incorpora firma electrónica, y es copia auténtica de un documento electrónico archivado por la ULL según la Ley 39/2015.  
Su autenticidad puede ser contrastada en la siguiente dirección <https://sede.ull.es/validacion/>

Identificador del documento: 2260218 Código de verificación: Sm21pjYh

Firmado por: JAVIER ROMAN GARCIA  
UNIVERSIDAD DE LA LAGUNA

Fecha: 02/11/2019 16:23:59

IGNACIO TRUJILLO CABRERA  
UNIVERSIDAD DE LA LAGUNA

02/11/2019 17:39:19

# C

## Proceedings during this thesis

1. Galactic cirri in deep optical imaging. Román, Javier; Trujillo, Ignacio; Montes, Mireia. IAU Symposium 355: The Realm of the Low Surface Brightness Universe. In press.
2. The IAC stripe82 legacy project. Román, J., Fliri, J., & Trujillo, I. 2017, Formation and Evolution of Galaxy Outskirts, 266

CLIV

Este documento incorpora firma electrónica, y es copia auténtica de un documento electrónico archivado por la ULL según la Ley 39/2015.  
Su autenticidad puede ser contrastada en la siguiente dirección <https://sede.ull.es/validacion/>

Identificador del documento: 2260218 Código de verificación: Sm21pjYh

Firmado por: JAVIER ROMAN GARCIA  
UNIVERSIDAD DE LA LAGUNA

Fecha: 02/11/2019 16:23:59

IGNACIO TRUJILLO CABRERA  
UNIVERSIDAD DE LA LAGUNA

02/11/2019 17:39:19

## D

### Acknowledgments

Pudiera parecer un tópico, pero realmente esta tesis no hubiera sido posible sin la ayuda y esfuerzo de un gran número de excelentes profesionales además de grandes personas. En primer lugar tengo que agradecer a mi jefe, Ignacio Trujillo. Ha sido increíble la cantidad de cosas que he aprendido contigo, algo que voy a guardar siempre. También tengo que agradecer al fantástico grupo en el que he trabajado, para mí no hay otro grupo igual en el mundo, tanto por calidad profesional como humana. Especiales agradecimientos a Mike Beasley, Jesús Falcón, Tomás Ruiz Lara y Alejandro Vazdekis. En el Instituto de Astrofísica de Canarias (IAC) agradezco a: Mohammad Akhlaghi, John Beckman, Miguel Cerviño, Johan Knapen, Jorge Sánchez Almeida y Juan Usón. También a mis compañeros de faena diaria, los que nos peleamos con los datos todos los días: Alejandro Borlaff, Nushkia Chamba y Raúl Infante, sois unos cracks. Quiero agradecer también a Mireia Montes por su ayuda y cobijo en Yale, a David Valls-Gabaud por permitirme ser parte de los meetings de Messier y por su impagable ayuda en muchos aspectos y a Michael Rich por su ayuda y por confiar en mí permitiendome acceso al fantástico telescopio Jeanne Rich con el que tan buena ciencia estamos haciendo. También agradezco enormemente a Lourdes Verdes-Montenegro por darme la oportunidad de trabajar en su fantástico grupo en el Instituto de Astrofísica de Andalucía, desde el que escribo estas palabras.

Desde el punto de vista institucional quiero agradecer al Instituto de Astrofísica de Canarias y a todo su personal. Agradezco al Ministerio de Economía y Competitividad (MINECO) por financiar mi formación predoctoral y mi estancia en la Universidad de Yale. Agradezco a la fundación Alfred P. Sloan por el Sloan Digital Sky Survey, fundamental en mi tesis y en la comunidad astrofísica en general. Agradezco al personal de los observatorios de Izaña y del Roque de los Muchachos por su excelente trabajo. También al personal de Centro de Estudios de Física del Cosmos de Aragón.

CLV

Este documento incorpora firma electrónica, y es copia auténtica de un documento electrónico archivado por la ULL según la Ley 39/2015.  
Su autenticidad puede ser contrastada en la siguiente dirección <https://sede.ull.es/validacion/>

Identificador del documento: 2260218 Código de verificación: Sm21pjYh

Firmado por: JAVIER ROMAN GARCIA  
UNIVERSIDAD DE LA LAGUNA

Fecha: 02/11/2019 16:23:59

IGNACIO TRUJILLO CABRERA  
UNIVERSIDAD DE LA LAGUNA

02/11/2019 17:39:19